EMBEDDED REFERENCE ELECTRODES FOR CORROSION POTENTIAL MONITORING, ELECTROCHEMICAL CHARACTERIZATION, AND CONTROLLED-POTENTIAL CATHODIC PROTECTION

A Dissertation
Submitted to the Graduate Faculty
of the
North Dakota State University
of Agriculture and Applied Science

By

Bobbi Jo Elizabeth Merten

In Partial Fulfillment of the Requirements
for the Degree of
DOCTOR OF PHILOSOPHY

Major Department:
Coatings and Polymeric Material

December 2011

Fargo, North Dakota

North Dakota State University
Graduate School

Title

Embedded Reference Electrodes for Corrosion Potential Monitoring,

Electrochemical Characterization and Controlled-Potential Cathodic Protection

By

Bobbi Jo Elizabeth Merten

The Supervisory Committee certifies that this ***disquisition*** complies with North Dakota State University's regulations and meets the accepted standards for the degree of

DOCTOR OF PHILOSOPHY

SUPERVISORY COMMITTEE:

Gordon Bierwagen

Chair

Stuart Croll

Dante Battocchi

Kalpana Katti

Approved by Department Chair:

1-19-2012
Date

Stuart Croll
Signature

ABSTRACT

A thin wire Ag/AgCl reference electrode was prepared using 50 μm Ag wire in dilute $FeCl_3$. The wire was embedded beneath the polyurethane topcoat of two sacrificial coating systems to monitor their corrosion potential. This is the first report of a reference electrode embedded between organic coating layers to monitor substrate health.

The embedded reference electrode (ERE) successfully monitored the corrosion potential of Mg primer on AA 2024-T3 for 800 days of constant immersion in dilute Harrison's solution. Zn primer on steel had low accuracy in comparison. This is in part due to short circuiting by Zn oxidation products, which are much more conductive than Mg corrosion products. Data interpretation was improved through statistical analysis. On average, ERE corrosion potentials are 0.1 to 0.2 V and 0.2 to 0.3 V more positive than a saturated calomel electrode (SCE) in solution for AA 2024-T3 and steel coating systems, respectively. Further research may confirm that ERE obtains corrosion potential information not possible by an exterior, conventional reference electrode.

The ERE is stable under polarization. AA 2024-T3 was polarized to -0.95 V vs ERE to emulate controlled potential cathodic protection (CPCP) applications. Polarizations of -0.75 V vs ERE are recommended for future experiments to minimize cathodic delamination.

The ERE was utilized to analyze coating mixtures of lithium carbonate, magnesium nitrate, and Mg metal on AA2024-T3. Corrosion potential, low frequency impedance by electrochemical impedance spectroscopy (EIS), and noise resistance by electrochemical noise method (ENM) were reported. Coating performance ranking is consistent with standard electrochemical characterization and visual analyses. The results suggest anti-

corrosion resistance superior to a standard Mg primer following 1600 hours of B117 salt spray. Both lithium carbonate and magnesium nitrate are necessary to achieve corrosion protection. Unique corrosion protective coatings for aluminum could be designed through continued mixture optimization.

The Ag wire ERE has been utilized for the characterization and ranking of experimental coatings on metal substrates. Structural health monitoring and corrosion potential feedback of cathodic protection systems are additional uses. There is some indication that CPCP may be applied by ERE to control the substrate polarization for an organic coating system.

ACKNOWLEDGEMENTS

There is a diverse, loving group of persons whom deserve acknowledgment for their part in this chapter of my life.

First and foremost, I would like to begin by thanking the wonderful community at NDSU's Department of Coatings and Polymeric Materials. The staff, students, and faculty have played a significant role in my growth as a graduate student and individual. Thank you Prof. Kalpana Katti, Prof. Stuart Croll, and Dr. Dante Battocchi for serving as my committee members and mentors. I am also thankful to Prof. Gordon Bierwagen for his guidance and the particularly tedious duty of serving as my major advisor. A special thanks Stacy Sommer for her role as peer and friend.

The city of Fargo has provided me with numerous recreational opportunities to improve my team skills and meet inspiring people. Thank you Team Happy Teeth, the Net Devils, Agassiz Underground (2010 National Champs), and the hard-working women of the Fargo Moorhead Derby Girls.

Thank you to the Pride Network, FM Pride, and other area diversity initiatives for working to create a welcoming space for LGBTQ-identified individuals at NDSU and across Fargo-Moorhead. It has been a privilege to develop meaningful relationships with the courageous women and men I've met through this community.

Last but not least, I am especially grateful for the infinite wisdom, love, and patience of Samantha Larson. I could not be more excited to begin the next chapter of my life with such a beautiful person.

DEDICATION

I dedicate the completion of this dissertation to my parents, Sandy and Paul Merten. Their lifetime of hard-work and devotion to their children has allowed me the opportunity and great privilege of achieving this Doctorate of Philosophy.

LIST OF TABLES

LIST OF FIGURES

TABLE OF CONTENTS

CHAPTER 1. INTRODUCTION

Tremendous investments have been made throughout developed nations for civil and industrial infrastructure. Though strong and durable, regular maintenance and corrosion mitigation practices are necessary to detect and prevent catastrophic deterioration of these structures. A recent instance is the August 2007 collapse of the 40 year-old I-35W Bridge in Minneapolis, MN. Approximately 170,000 private and commercial vehicles used the I-35W Bridge daily to cross the Mississippi River into the Minneapolis metropolitan area [1]. Aside from safety considerations, these failures interrupt complex air and land travel infrastructure in the United States. The end result is severe inconvenience and economic loss.

Vast research efforts are underway to increase the quality control of infrastructure in service. Examples include various sensor-based and remote measurement techniques to determine corrosion rate, changes in mechanical properties, or other vital characteristics. This field is recognized as structural health monitoring (SHM). Previous work by Bierwagen and co-workers [2-10] at NDSU has demonstrated the use of embedded Pt films for electrochemical analysis of aircraft and industrial organic coating cathodic protection systems. Electrochemical impedance spectroscopy (EIS) and electrochemical noise method (ENM) are the standard methods of evaluation in these experiments.

Concrete research and development includes extensive work on embedded materials for SHM. Ahmad [11] used an external $Cu/CuSO_4$ reference electrode, electrically connected through a wet sponge, to measure the corrosion rate of reinforcement bar (rebar) within concrete. Linear polarization and other measurements such as corrosion potential

and chloride ion concentration are often combined to improve the accuracy of the analysis. Duffó [12-13] utilized metal-metal oxide, graphite, and Ag/AgCl materials for rebar health monitoring in concrete systems. Cella [14] measured electrical resistance changes to embedded thin steel wires as an indirect method of monitoring the steel rebar. Lu [15] and Pereira [16] have also contributed to assessing the service condition of concrete structures. Muralidharan [17-19] has explored novel reference electrode materials such as MnO_2 and $NiFe_2O_4$ for this application. This technology has been applied to additional structures including underground pipelines and storage containers [20-21], and the grounding grid corrosion of power plants, substations, and power transmission lines [22]. The review by Song [23] contains general information on the use of electrochemical and non-destructive corrosion assessment techniques as well as specific details for embedded corrosion sensors. Kumar [24] has described the need and prospective for online corrosion monitoring systems.

The corrosion lab at NDSU has provided many contributions to the field of coating health monitoring and characterization by embedded Pt sensors. The purpose of this research is to prepare a thin wire silver-silver chloride embedded reference electrode (ERE) for corrosion potential monitoring of sacrificial coating systems. This is a known and effective method of detecting cathodic protection in a metal-rich coating system [25]. The Ag wire ERE is the first use of a reference electrode, embedded between a primer and topcoat, to make electrochemical measurements. The 50 micron wire is also utilized for electrochemical impedance spectroscopy (EIS) and the electrochemical noise method (ENM). The research has been expanded to the areas of controlled-potential cathodic protection (CPCP) and the development of novel sacrificial coating systems.

1.1. References

[1] H. Stambaugh and H. Cohen, I-35W Bridge Collapse and Response, in: Technical Report Series, U.S. Fire Administration, 2007, pp. 1-60.
[2] Q. Su, K.N. Allahar and G.P. Bierwagen, In situ embedded sensor monitoring of a United States Air Force primer beneath a topcoat exposed to atmospheric humidity and thermal conditions, Corrosion, 66 (2010) 1-12.
[3] Q. Su, K. Allahar and G. Bierwagen, Embedded electrode electrochemical noise monitoring of the corrosion beneath organic coatings induced by ac–dc–ac conditions, Electrochimica Acta, 53 (2008) 2825–2830.
[4] G.P. Bierwagen, X. Wang and D.E. Tallman, In situ study of coatings using embedded electrodes for ENM measurements, Progress in Organic Coatings, 46 (2003) 163–175.
[5] K.N. Allahar, Q. Su, G.P. Bierwagen, D. Battocchi, V.J. Gelling and D. Tallman, Examination of the feasibility of the use of in-situ corrosion sensors in army vehicles, in: Tri-Service Corrosion Conference, 2005, pp. 1-11.
[6] K.N. Allahar, V. Upadhyay, G.P. Bierwagen and V.J. Gelling, Monitoring of a military vehicle coating under Prohesion exposure by embedded sensors, Progress in Organic Coatings, 65 (2009) 142–151.
[7] G.P. Bierwagen, K.N. Allahar, Q. Su and V.J. Gelling, Electrochemically characterizing the ac–dc–ac accelerated test method using embedded electrodes, Corrosion Science, 51 (2008) 95–101.
[8] K.N. Allahar, Q. Su, G.P. Bierwagen and D.-H. Lee, Monitoring of the AC-DC-AC degradation of organic coatings using embedded electrodes, Corrosion, 64 (2008) 773-787.
[9] K.N. Allahar, Q. Su and G.P. Bierwagen, Electrochemical noise monitoring of the cathodic protection of Mg-rich primers, Corrosion, 66 (2010) 1-12.
[10] X. Wang, R. Bennett, K. Spenningsby and G. Bierwagen, Use of electrochemical noise methods for in situ corrosion monitoring, in: D.R.A. Mantz and D.P.C. Trulove (Eds.) Tri-Service Corrosion Conference, San Antonio, TX, 2002, pp. 18.
[11] S. Ahmad and B. Bhattacharjee, A simple arrangement and procedure for in-situ measurement of corrosion rate of rebar embedded in concrete, Corrosion Science, 37 (1995) 781-791.
[12] G.S. Duffó, S.B. Farina and C.M. Giordano, Characterization of solid embeddable reference electrodes for corrosion monitoring in reinforced concrete structures, Electrochimica Acta, 54 (2009) 1010-1020.
[13] G.S. Duffó and S.B. Farina, Development of an embeddable sensor to monitor the corrosion process of new and existing reinforced concrete structures, Construction and Building Materials, 23 (2009) 2746–2751.
[14] P.A. Cella and S.R. Taylor, Electrical resistance changes as an alternate method for monitoring the corrosion of steel in concrete and mortar, Corrosion, 56 (2000) 951-959.
[15] S. Lu and H.-J. Ba, Corrosion sensor for monitoring the service condition of chloride-contaminated cement mortar, Sensors, 10 (2010) 4145-4158.
[16] E.V. Pereira, R.B. Figueira, M.M.L. Salta and I.T.E.d. Fonseca, A galvanic sensor for monitoring the corrosion condition of the concrete reinforcing steel: Relationship between the galvanic and the corrosion currents, Sensors, 9 (2009) 8391-8398.

[17] S. Muralidharan, T.-H. Haa, J.-H. Baea, Y.-C. Haa, H.-G. Lee, K.-W. Park and D.-K. Kim, Electrochemical studies on the performance characteristics of solid metal–metal oxide reference sensor for concrete environments, Sensors and Actuators B, 113 (2006) 187–193.
[18] S. Muralidharan, V. Saraswathy, L.J. Berchmans, K. Thangavel and K.Y. Ann, Nickel ferrite ($NiFe_2O_4$): A possible candidate material as reference electrode for corrosion monitoring of steel in concrete environments, Sensors and Actuators B, 145 (2010) 225–231.
[19] S. Muralidharan, V. Saraswathy, K. Thangavel and N. Palaniswamy, Electrochemical studies on the performance characteristics of alkaline solid embeddable sensor for concrete environments, Sensors and Actuators B, 130 (2008) 864–870.
[20] F.M. Song, S. Brossia, D. Dunn and N. Sridhar, New permanent reference electrode for protection of underground pipelines and storage tanks, Corrosion Engineering, Science and Technology, 40 (2005) 262-269.
[21] Y.-S. Choi, J.-G. Kim and S.J. Yang, A galvanic sensor for monitoring the corrosion damage of buried pipelines: Part 2—Correlation of sensor output to actual corrosion damage of pipeline in soil and tap water environments, Corrosion, 62 (2006) 522-532.
[22] X.-L. Zhang, X.-H. Zhao, Y.-G. Wang and N. Mo, Development of an electrochemical in situ detection sensor for grounding grid corrosion, Corrosion, 66 (2010) 1-7.
[23] H.-W. Song and V. Saraswathy, Corrosion monitoring of reinforced concrete structures - A review, International Journal of Electrochemical Science, 2 (2007) 1-28.
[24] K. Kumar, C.S.U. Nair, H.T. Jegadish, S. Muralidharan, A.K. Parande, M.S. Karthikeyan and N. Palaniswamy, Online corrosion and force monitoring for inner containment concrete structures, Sensors & Transducers Journal, 92 (2008) 108-121.
[25] S. Felix, R. Barajas, J.M. Bastidas, M. Morcillo and S. Feliu, Study of protections mechanism of zinc-rich paints by electrochemical impedance spectroscopy, in: J.R. Scully, D.C. Silverman and M. Kendig (Eds.) Electrochemical Impedance Spectroscopy, ASTM STP 1188, American Society of Testing and Materials (ASTM), Philadelphia, PA, 1993, pp. 438–449.

CHAPTER 2. A SENSOR FOR CORROSION PROTECTION AND STRUCTURAL HEALTH MONITORING - A REVIEW

2.1. Introduction

2.1.1. The function of organic coatings and the effects of time

Organic coatings have gained extensive use over the last century to prolong the service lifetime of metallic infrastructure. The films are applied with thicknesses ranging from nanometers to hundreds of microns (micrometers), depending on the intended use. Additionally, the material is engineered to meet hardness, flexibility, permeability, and other requirements as demanded by the end-use application. Intact coatings inhibit the corrosion of metallic structures by serving as a barrier to ions, oxygen, and water [1]. Additionally, they have very high electrical resistance, impeding charge flow between the anode and cathode [2-3].

Coating defects greatly reduce the effective service life for a coating system. These may result from impurities present during the curing process. Multi-layer coatings systems lessen the probability of a defect extending from the exterior of the coating system to the substrate [4-5]. They are generally formulated so that the basecoat, or primer, provides adhesion between the two layers while the topcoat serves as a barrier to the surrounding environment [6]. The basecoat may also contain passivating or active species to aid in corrosion mitigation. Physical damages also occur to a coating during its service lifetime. This type of coating defect is impossible to predict or prevent. Simple examples include the vehicular vandalism that results in a shiny scratch down the length of one's car, the incidental collision of avian species with in-flight aircraft, and the careless operation of

heavy machinery in near proximity to bridges or pipelines. Regardless of the origin of a coating defect, it is imperative that the coating be repaired to sequester active corrosion at exposed metal surface and restore the system's corrosion protection.

Adhesion is crucial to a coating's ability to protect a substrate. Coating atoms at the metal surface must be in intimate contact with the substrate, acting through mechanisms such as chemical bonds and mechanical interlocking [3]. These bonds must remain intact in dry as well as saturated, known as wet adhesion, environmental conditions. Pooling of water at the metal/coating interface occurs during corrosion as a result of strong osmotic forces. Funke [7] estimated that osmotic pressure is in the range of 2500-3000 kPa, whereas most coatings deform at 6-40 kPa. This and hydrogen evolution disbondment are the most aggressive causes of adhesive failure.

Defect-free, strongly adhered coatings are not exempt from degradation by environmental elements. Rather, coating degradation occurs on a slow timescale as the permeation of water, ions, and other corrosive species into the coating, leading to the development of physical pathways. As the degradation progresses, water and ions are able to diffuse with greater ease and eventually arrive at the metal surface. Here, electrochemical cells initiate and propagate along the metal/coating interface, disrupting adhesion and further reducing the protective capabilities of the system. The metal corrodes freely as long as the reductive and oxidative reactants continue to be replenished. Generic anode and cathode metal corrosion reactions are shown in Equations 2.1 and 2.2, respectively [8] with the number of electrons transferred given by n.

$$M \rightarrow M^{n+} + ne^- \tag{2.1}$$

$$2H^+ + 2e^- \rightarrow H_2 \tag{2.2}$$

The environments experienced by modern infrastructural coatings have been categorized according to Figure 2.1 [9]. Outdoor corrosion prevention applications can be qualified by one of the below categories. Immersion-based exposures range from buried pipelines (most often in soil) to fresh water holding tanks to offshore drilling equipment or ship hulls. Atmospheric exposure conditions range from marine conditions at coastlines to industrial conditions experienced in urban and manufacturing centers to rural areas. Splash zones refer to coatings designed to protect the area above a waterline Unique challenges are presented by the environments and special considerations must be made for each.

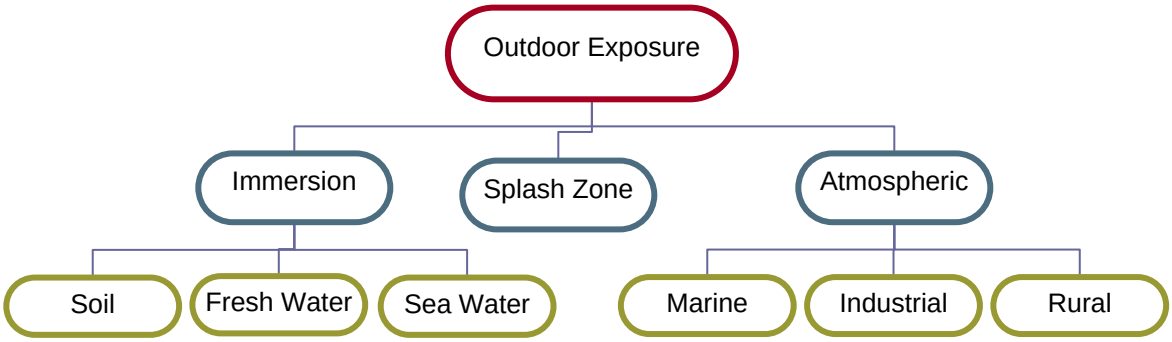

Figure 2.1. Categorical framework for the environments experienced by coatings for corrosion control. Figure redrawn from Reference [9].

To aid in protection, coatings are often equipped with supplemental corrosion prevention technology. Cathodic protection can be used to protect a substrate by formulating sacrificial pigments into the organic coating. Zinc-rich coatings have been used to protect steel in this fashion [10-12]. This may also be achieved by electrical connection to an external sacrificial anode. Zinc or magnesium anodes have been used on steel ship hulls for this purpose. Impressed current cathodic protection (ICCP) methods assist organic coatings by depressing oxidative reactions at the coating/metal interface through a rectified

current source. The most common use of ICCP is to supplement fusion bonded epoxy (FBE) coatings on steel pipelines.

The effective service lifetime of many coated systems has been extended significantly through application of these cathodic protection methods. However, generally-speaking, coatings do not outlive the structure in which they are protecting, and processes for removing and/or recoating must be considered prior to application. The consequences of unrepaired coatings include catastrophic failure of the infrastructure as well as substantial economic loss.

2.1.2. Present practices of organic coating health monitoring and lifetime prediction

Coatings must be stripped and reapplied once they no longer serve to protect their substrate. However, it can be difficult to identify a failed coating system while it is in service. Although some structural health monitoring (SHM) techniques are being experimented with in the field, most coating reapplication and maintenance procedures are performed routinely and coupled with scheduled visual inspections. For aerospace structures, the inspections generally require gaining access to difficult regions only to find that no corrosion is detected [13]. Moreover, the inspections often compromise the existing controls, consequently adding undesirable cost to corrosion-detection method. These practices have proved to be costly and inefficient and estimates indicate that maintenance and repairs represent one quarter of total operating costs [14]. A variety of SHM solutions have been proposed to improve safety and cost efficiency, those applicable to with a focus on embedded sensors for field measurement. Applications to aerospace vehicles, reinforced concrete, pipelines, nuclear power plants, and others are presented in this paper to identify the technologies used across these fields.

It is desirable to be able to predict the service lifetime of a coating based on the deterioration of one or more measureable properties [15]. An end point or a point of failure for the coating property must be established, and the data is extrapolated to make a prediction. Impedance measurements taken at low frequency (~0.1 Hz) have been utilized in lifetime prediction attempts [16-17].

In order to apply lifetime prediction for health monitoring, one would take measurements in the field and insert them into an analytical model to estimate the systems remaining effective service life. Long time constraints for coating failure have complicated the ability to compare experimental lifetime prediction data with field-weathered coatings. Additionally, insufficient understanding of complex coating degradation mechanisms reduces the confidence of the results. The strong dependency on temperature, humidity, and concentration of ionic species for both the coating and corrosion of the underlying metal further complicates the process since these environmental variables are difficult to measure. Active, metal-rich coatings require further considerations.

Structural health monitoring (SHM) refers to any technique which characterizes a material during its service lifetime. This is through systematic measurement of select properties, classified as either passive or active. Passive properties include measurement of operational parameters such as air speed or vibration levels. These are used to determine an aircraft's remaining useful life based on design algorithms. Active SHM assesses structural health by directly measuring the presence and extent of corrosion, cracks, and impact damages [14, 18]. Successful application of SHM requires extensive research and modeling as well as comprehensive understanding of the coating system.

2.1.2.1. Motive for introducing embedded sensors to organic coatings

Embedded sensors used in coatings research and development have been instrumental in characterizing coating properties. Additionally, they present the possibility of in situ laboratory measurements or in-service SHM. Embedding a sensor below a coating layer or topcoat offers the following advantages: 1) protection from surface environmental attack; 2) enhanced separation/isolation between sensors; 3) improved adhesion to the underlying film; 4) improved measurement for small ENM samples; 5) increased sensitivity to changes in coating impedance and the potential to monitor impedance changes between coating layers during different exposure conditions as well as study corrosion/degradation mechanisms; 6) potential to design novel accelerated testing protocols for improved simulation and faster ranking [19]. Measurements may be configured for certain layers and not for others as in the case of multilayer coatings systems.

The present paper reviews the use of embedded sensors in organic coatings research. Special interest is paid to the configurations used for embedded sensor electrochemical analysis of coatings. Sensors used in other SHM fields such as bridges, concrete, or other infrastructure will be briefly discussed for completeness. Finally, potential applications for sensors in electrochemical SHM of aerospace structures will be considered.

2.2. Sensor materials

In order for a material to be considered for use as an embedded sensor, it must satisfy certain requirements and possess useful properties. This is dictated by the sensor's end-use application. Various sensor materials have been organized within this section

based on their type and end-use. The list is not comprehensive but instead meant to shed light on the broad range of materials examined for embedded sensor applications. Embedded reference and pseudo reference electrode materials are examined first. The second section presents examples of the recent emergence of active metal and metal alloy corrosion sensors. Wire beam electrodes (WBE), traditionally used for theoretical electrochemistry, are explored in the subsequent section. Electroconductive inks and inductor-capacitor (LC) sensors are reviewed in the subsequent sections. The final section discusses smart materials, namely piezoelectric wafer active sensors (PWAS).

2.2.1. Reference and pseudo reference electrodes

Materials chosen to be used as embedded reference or pseudo-reference electrodes must be conductive, stable under chemical and thermal environmental changes, and durable for field use as well as the manufacture's processing. Noble metals such as platinum, gold, nickel, and silver are among the most common electrodes. They are extremely stable in the metallic state, allowing for extended use applications and minimal side reactions. Additionally, they pass current with little or no charge and have, therefore, been used as pseudo reference electrodes. As a result these materials have found broad use in the electrochemical analysis of organic coatings. Kittel et al. [20] and Bierwagen and co-workers [21-25] used a platinum foil leaf for embedded sensor experiments. The thinness of the leaf was less than a micron. Thin, platinum wire was also used [19, 26-27]. Merten [28] used silver wire to form silver/silver chloride reference electrodes for embedding in coatings. The aforementioned electrodes required little or no metal preparation prior to embedding within a coating system.

Earlier published work on sensors included intricate fabrication techniques such as electron-beam-deposition [29-30] or physical vapor deposition [31] to form thin inert metal deposits on a coating surface. These sensors were left uncoated, not embedded, to make in situ electrochemical measurements.

Reference and pseudo reference electrodes have gained much interest for SHM of concrete systems, specifically to measure the corrosion of steel reinforcement bars (rebar). Common materials include silver/silver-chloride and copper/copper-sulfate. Muralidharan et al. [32-33] have explored Manganese oxide, metal-metal oxide (MMO) mixtures, nickel ferrite, and graphite as reference electrodes. Song et al. developed a tungsten/tungsten oxide microelectrode using 0.1 mm diameter wire [34]. Linear polarization techniques are often performed and pH, O_2, and Cl^- sensors may accompany the commercial, self-contained sensors which have been in use for some time now [35-37]. Though these materials often satisfy requirements for embedding in concrete, most have yet to be miniaturized and examined for application in organic coatings. The advantages, short-comings, and/or drawbacks of these materials as well as the general challenges facing implementation of embedded sensors for concrete research will not be discussed here. Interested readers can find such information in the recent review article by Martínez [38].

2.2.2. Metal alloy sensors

Active metals have been explored recently as methods to examine corrosion degradation. Wilson and Muscat [13] used insulated thin AA 2024 wires as corrosion sensors for AA 2024 substrate. The use of similar substrate and sensor materials is optimal since dissimilar metals develop an electrochemical potential, stimulating unwanted corrosion and noise. The sensor is expected to have great long term stability compared the

substrate it is monitoring. In their experiment, small strips of the insulating material were removed from the wires and they were subsequently positioned directly to the surface of the conducting substrate. A coating system was applied it was assured that the exposed wire sections are not in intimate contact with the substrate. Corrosion is monitored by measuring the conductance of the embedded wire from one end to the other as well as to the substrate. Initially, and wire to substrate conductance is low but increases as water and ions advance through the system. End-to-end wire conductance begins high; eventually, an open circuit is realized, indicating that the wire has corroded through. It is assumed that substrate has begun to corrode at this point and recoating is desired. A series of Ohm's Law-based matrix equations assist in the data analysis for this novel corrosion degradation sensor.

Li et al. prepared [39] thin film electrical resistance (TFER) sensors by DC magnetron sputtering of carbon steel. The sensor was used in conjunction with impressed current cathodic protection (ICCP) for a steel pipeline to monitor and evaluate the protection afforded. Electrical resistivity measurements can be correlated to the intrinsic resistivity and geometry to calculate the corrosion rate from the measure of metal loss. Steel TFER sensors require good temperature control for implementation due to electrical resistivity changes of iron with the change in temperature.

2.2.3. Wire beam electrodes

Wire beam electrodes (WBE) have been used for the study of localized corrosion processes. Tan [40] fabricated a WBE from 100 mild steel electrodes (figure) to study this material. The electrode acts as a both a sensor and substrate. The development of this technique is highlighted in the review by Tan [41]. The combination of the WBE with

ENM measurement is suggested for noise resistance mapping. The scanning vibrating electrode technique (SVET) has also been utilized for measurements [42-44].

Chiang et al. [45-46] and Thu et al. [47] investigated micro-electrode arrays for high temperature and marine cathodic protection sensor applications, respectively. The WBE technique has also been used for biochemical and environmental electro-analyses [48].

2.2.4. Electroconductive ink sensors

Electroconductive ink sensors offer several advantages over the metal wire or foil sensors discussed above, including facile preparation. The surface area and thinness is easily adjusted for any application and it is not limited by "flat" surfaces. The ink sensor can be painted directly to a masked area on the primer surface. Additionally, the adhesion between the two coating layers is improved [49]. Davis et al. [50-51] painted gold, silver, nickel, and carbon sensors onto the surface of the coating to make in situ corrosion measurements via electrochemical impedance spectroscopy. The sensor was not embedded. The gold sensor had the drawback of high cost while least expensive ink, carbon, had the lowest electrical conductivity. On the other hand, nickel possesses better corrosion resistance than the highly conductive silver.

2.2.5. Inductor-capacitor (LC) sensors

Ong et al. [52] used ingle-sided printed circuit board (PCB) to prepare an embedded inductor-capacitor (LC) resonant circuit for monitoring water content in various civil engineering materials such as asphalt pavements or concrete bridges. The resonant frequency decreased as water content increased. The technology capitalizes on the disparity between the dielectric constant of water, approximately 80, to that of most coatings, 1 to 5.

LC sensors are low cost, passive, and flexible. Furthermore, their simple design is an improvement over other failure-prone, passive sensors used with radio-frequency identification (RFID) technology [52]. A limitation of this method is that the measurements are restricted the location of the sensor. Therefore, the sensor is unable to detect localized damages at other locations, minimizing its applicability to aerospace SHM.

2.2.6. Smart materials

Piezoelectric wafer active sensors (PWAS), consisting of lead zirconate titantate (PZT) or other materials, have generated much interest for active SHM applications on aerospace structures [14, 53-54]. Piezoelectric materials are unique in that a mechanical stress on the material leads to the generation of an electric field [14, 55]. Alternatively, they have a mechanical strain response to an imposed electric field. The former property is a sensing property and the latter is actuating and therefore, the material can act as both sensor and actuator for coatings applications. PWAS are ideal for embedded applications because they are inexpensive, small, lightweight, and manufactured to various geometries [14]. Chang and co-workers [56-57] applied embedded PWAS to various aircraft damage-detection schemes for areas such as lap and bolt joints.

PZT has been researched as a suitable piezoelectric material due to its high electromechanical coupling coefficient [53]. Zhao et al. [53] used a 0.254 mm thick and 6.3 mm diameter PZT ceramic disk with silver electrodes on both sides. The discs were bonded to the aircraft wing surface to test their novel analysis technique: reconstruction algorithm for probabilistic inspection of defects (RAPID). The search for an effective algorithm to accurately process PZT data for the complex aircraft structure is ongoing and one of the greater challenges of implementing PWAS [53].

Kang et al. [58] developed piezoresistive strain sensors using carbon nanotube (CNT) polymeric materials for passive SHM applications A simple, low cost, and lightweight biomimetic artificial neuron sensor was achieved by extending the sensor length. CNTs are unique in that their superior strength and super-elasticity make them suitable to add structural function as well.

Fiber optic sensors are also a promising smart material for health monitoring and have the added benefit electromagnetic interference immunity [59].

2.3. Electrochemical analysis of organic coatings

Various electrochemical methods are available to characterize the dielectric or corrosion-resistant properties of a material. The focus is limited to Electrochemical impedance spectroscopy (EIS) and electrochemical noise measurements (ENM) but other pertinent methods are included where necessary. Both methods are versatile in their ability to provide material characteristics. Open circuit potential (OCP) or corrosion potential is understood inherently by these methods to be the potential, relative to an established reference electrode, at which the anodic and cathodic currents of a metal surface are in dynamic equilibrium.

EIS and ENM have traditionally been used in a laboratory setting to assist in the research and development new coatings systems. The data is used to extract coating dielectric properties such as resistance and capacitance. These experiments were previously limited to laboratory bench tops due to an inherent requirement for a separated electrode within an electrolyte solution. Literature results have since shown that the electrodes can be placed within the coating system and used for electrochemical measurement without altering the experimental outcomes [31]. This development has allowed the introduction of

new laboratory techniques as well as the possibility for direct use in field application. The latter is the topic of discussion in a later section of this paper. EIS and ENM characterization methods are briefly described and the modified experimental configurations for embedded electrodes are presented. Corrosion potential measurements are also described. A number of sensors can be used as reference or pseudo reference electrodes to assess the corrosion potential of metal substrates within a desired accuracy.

2.3.1. Electrochemical impedance spectroscopy (EIS)

2.3.1.1. EIS measurements and presentation of the data

The EIS method, standardized by ASTM G106, analyzes frequency-dependent dielectric properties of a coating of interest by applying small, sinusoidal perturbations across a broad frequency range. Common measurement parameters are 10 mV and 10^{6} to 10^{-2} Hz, respectively. A simple potentiostat is required for the analysis and it is recommended that a Faraday cage is used to eliminate outside noise. For further description and discussion on the electrical components of this instrumentation see Loveday et al.[60].

Utilizing Ohm's Law, the instrument calculates the impedance (Z) values by measuring the current response to voltage perturbations made on the coating system. The impedance is equivalent to resistance since the perturbations consist of alternating electrical current.

$$Z = V / I \tag{1.3}$$

There are two common methods of graphical representation for the resulting data. The Nyquist plot depicts each measurement as its real vs. imaginary impedance components. The corresponding measurement frequencies are not easily discernable, however, limiting its value for the making of frequency-dependent observations. The

second type is the Bode plot, which portrays both impedance magnitude ($|Z|$) and phase angle (θ) vs. frequency. It is used often by coating scientists because it clearly displays the frequency of a given measurement [61].

Equivalent circuit models can be used to describe the data obtained by EIS [62-63]. Various electrical components, such as resistors and capacitors, are applied to model the resistive and capacitive nature of the coating system. A Randle's circuit is shown in Figure 2.2 (a). This simple, three component circuit is used as a first approximation for most coatings systems. As coating degradation progresses and corrosion initiates at the metal/coating interface, the complexity of the model increases as shown in Figure 2.2 (b) [20, 64]. See Loveday et al [60, 64] for further information on circuit modeling of organic coatings on metal substrates and EIS theory.

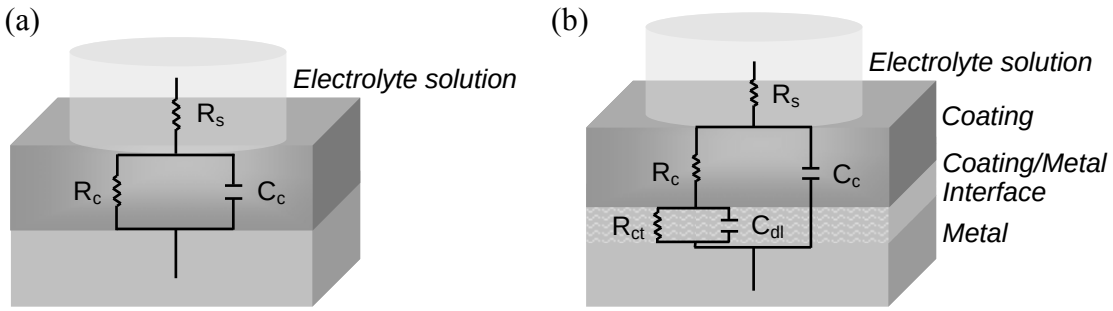

Figure 2.2. (a) Randle's circuit, (b) circuit including metal/coating interface.

2.3.1.2. Analyzing frequency-dependent properties of organic coatings

At low frequencies, such as $|Z|_{0.01\ Hz}$, the data from a Nyquist or Bode plot corresponds to the total impedance of the coating system, since a capacitor has near infinite impedance here [60]. The coating/metal interface resistance contributes to a majority of this impedance value. Additionally, it is at low frequencies in which the coating's resistance to ionic transport is discovered, providing an indication of barrier or protective properties

[20]. Therefore, $|Z|_{0.01\ \mathrm{Hz}}$, is often monitored over time to describe the health of a coating system. High values ($10^9\ \Omega/\mathrm{cm}^2$) result from a strong barrier coating with intimate bonding at the coating/metal interface and a defect-free, continuous bulk coating. This minimizes the contact of water and ionic species with the substrate, effectively reducing corrosion initiation and propagation. The advancement of water through a bulk coating system degrades the integrity of the material. As degradation progresses, the coating/metal interface deteriorates and $|Z|_{0.01\ \mathrm{Hz}}$ decreases rapidly. The coating protection is generally considered to be minimally effective below $10^7\ \Omega/\mathrm{cm}^2$ [65] .

EIS data can also be used to monitor the capacitance of a coating over time. Higher or mid-frequency data, such as 5 kHz, is used to calculate coating capacitance (C_c) by

$$C_c = \omega\sqrt{|Z|}\sin\theta^{-1} \tag{1.4}$$

where ω is angular frequency [24]. At such frequencies, the impedance of a capacitor becomes very small and it can be assumed that all of the current flows through it and none through the resistive element [60].

Consequently, high frequency EIS data can be used to calculate the volume percent of water within the coating, first derived by Brasher and Kingsbury [66].

$$\phi = \frac{\log(C_c / C_0)}{\log \varepsilon_w} \tag{1.5}$$

Here, ϕ is the volume fraction and C_0 is the coating capacitance prior to exposure, and ε_w is the dielectric constant of water. The premise is based on the evolving dielectric constant of a coating system, itself a very low dielectric material. The penetration of water, a very high dielectric material, into the coating causes a shift in the average value. The measurable increase in coating capacitance is proportional to the increased concentration of water. This

phenomenon occurs naturally, as a result of exposure to environmental humidity or immersion conditions.

In regard to the use of EIS for analysis of organic coatings, the reviews by Amirudin and Thierry [30] should be obtained for a thorough explanation of the fundamentals and instrumentation. Bierwagen et al [67] and Loveday et al [68] describe the application of EIS to accelerated exposure testing.

2.3.1.3. Traditional EIS method

When making electrochemical measurements via the EIS method, a three-electrode set-up has traditionally been used. This includes an electrolyte immersion cell, a reference electrode (RE), a counter electrode (CE), and a working electrode (WE). This setup is demonstrated in Figure 2.3.

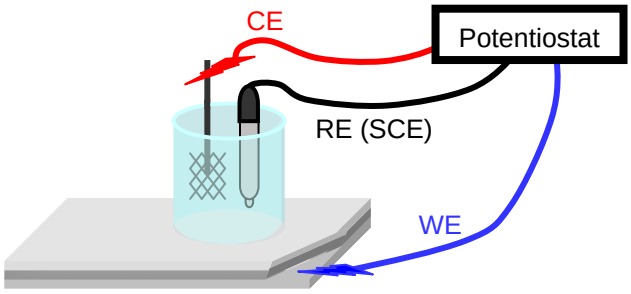

Figure 2.3. Traditional three electrode EIS.

These requirements are generally fulfilled using a laboratory RE, a platinum mesh CE, and the metal substrate as the WE. It is also possible to perform measurements using a two-electrode EIS (2E-EIS) set-up [29] in which the platinum mesh or similar material is the both the RE and the CE, denoted RE/CE as demonstrated in Figure 2.4.

When a metal substrate is not available, the experiment must be configured in a way in which current flows between the CE and WE, located on opposite sides of the coating. In

the laboratory, one can use a free coating film and attach electrolyte immersion cells at both sides to measure coating properties. However, this is not applicable a coated substrate. A non-substrate 2E-EIS configuration is desirable in the field where electrical connection to the substrate is not feasible

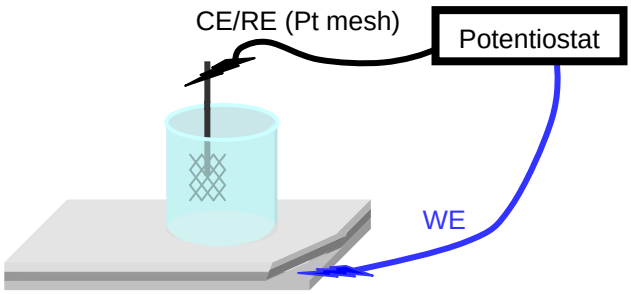

Figure 2.4. Configuration for 2E-EIS.

Davis and co-workers [51, 69-72] fastened sensors to a material surface for in-situ EIS measurement. The configuration provided health monitoring without requirement for electrolyte

2.3.1.4. EIS measurements by embedded electrodes

Miszczyk and Shauer [49] utilized non-substrate 2E-EIS for a coating system with two embedded platinum electrodes. One serves as the RE/CE and the other as the WE as shown in Figure 2.5. The examination characterized the effect of moisture on topcoat/primer interlayer, or interface, adhesion by measuring the impedance of polyurethane-polyacrylate basecoat/polyurethane topcoat/steel coatings systems at different values of relative humidity [49].

Their results suggest showed a considerable decrease in impedance at high relative humidity. Allahar et al [6] performed a similar experiment on a polyurethane topcoat/epoxy primer/AA 2024-T3 coating system to model water transport between the coating layers. Ultimately, the assumptions in the model were inadequate in characterizing the

topcoat/primer interface and lacked a proper fit to the experimental results. Further analysis may show that the data acquired by the embedded electrodes may have been describing the regions below each electrode rather than across the interface.

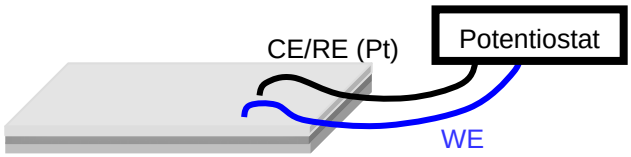

Figure 2.5. Non-substrate 2E-EIS via embedded electrodes.

Nogueira et al. [27] analyzed the electric field distribution of Pt embedded electrode 2E-EIS experiments for coatings under various wet and dry conditions using finite-element simulations as well as experimental measurements on an alkyd topcoat/alkyd primer/carbon steel coating system. They found the current short circuits through a metal substrate under most conditions, especially at high frequencies, $|Z|_{100\ \mathrm{Hz}}$. The exception was found in the case of a wet coating with a dry metal/coating interface. At low frequencies, $|Z|_{0.1\ \mathrm{Hz}}$, 58% of the current passed directly through the coating to the opposite electrode. This suggests that the metal/substrate interface is more resistive than other coating components, lending a greater contribution to the $|Z|_{0.01\ \mathrm{Hz}}$.

Careful experimentation of alkyd primer/alkyd topcoat/steel and epoxy primer/polyurethane topcoat/steel coatings by Allahar et al. [25] have shown non-substrate 2E-EIS to include current passage across the electrode/coating interface, coating, and coating/substrate interface for the area directly below each electrode. The results had a value of impedance approximately twice that obtained by a single Pt embedded

electrode/substrate 2E-EIS experimental control. Figure 2.6 highlights this hypothesized route of current.

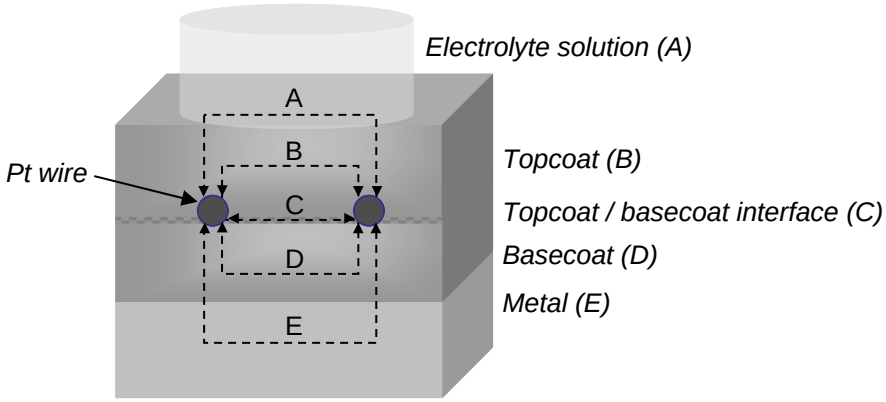

Figure 2.6. Hypothesized routes of current for non-substrate 2E-EIS.

However, the alkyd coating system reached a degree of saturation or degradation around 50 days in which current flow across coating, directly between the two embedded electrodes, became the path of least resistance. This was marked by a sudden decrease in total impedance, as shown in Figure 2.7. This behavior is analogous to that suggested by Miszczyk and Schauer [49]. The reports have shown non-substrate 2E-EIS may be more applicable to epoxy coatings systems than alkyds. See the paper by Allahar et al. [25] for a simple experimental setup to determine the applicability to other coatings systems.

Recent patents [50, 73-74] demonstrate the desire to utilize embedded sensors for health monitoring applications through the use of EIS measurements. Additionally, these analyses are advancing the research and development of coatings systems. Su et al. [75] utilized EIS results to develop contour maps for United States Air Force primer barrier performance as a function of temperature and humidity. Furthermore, Allahar et al. [24, 76] suggested that coating ranking can be achieved at earlier times through the use of

embedded sensors, which monitored the primer / metal system more closely than an exterior reference electrode.

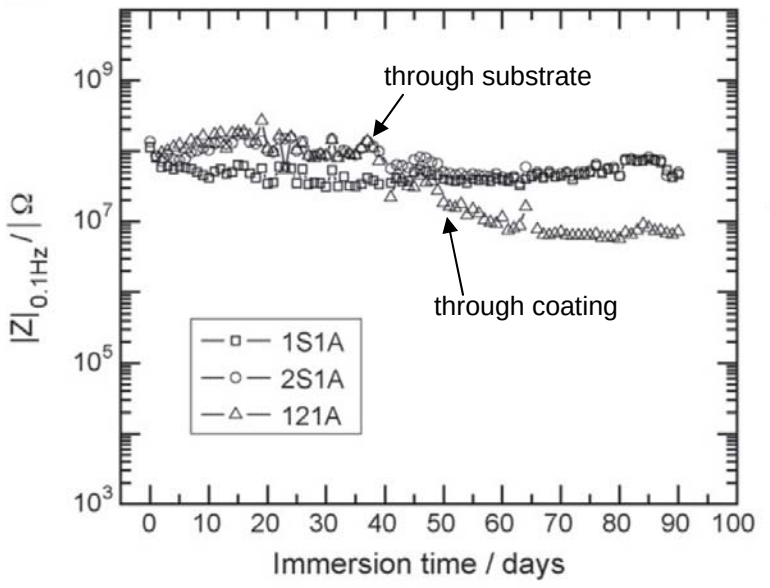

Figure 2.7. Impedance decreases as passage of current through coating becomes path of least resistance. Retrieved from Reference [25].

2.3.2. Electrochemical noise measurement (ENM)

2.3.2.1. Introduction to ENM

The resistive dielectric properties of coatings systems have also been monitored by ENM which also characterizes the type and rate of corrosion processes occurring at the metal/coating interface. When compared to EIS, a number of advantages/disadvantages are often noted. An advantage of ENM is that a sinusoidal perturbation is not required, suggesting that it is less intrusive, or destructive, when compared to EIS [19]. Also, measurements can be made with greater accuracy on active coating systems; non-erroneous low frequency EIS measurements can be difficult or impossible to acquire when the system

does not have a stable corrosion potential. Disadvantages of using ENM include that the electrochemical information obtained for a given system has statistically greater variance [77] as well as less extensive and theoretically more complex data [19].

2.3.2.2. ENM theory

Iverson [78] first noted a correlation between electrode potential fluctuations and corrosion processes. Eden and Skerry [79] first applied the technique to coated metals. Goellner et al. [80] demonstrated that comparable results can be obtained provided suitable equipment and correct procedures are used via an experiment across 17 participating institutions and organizations

The ENM technique consists of recording the voltage (V) and current (I) fluctuations, otherwise described as noise, between two nominally identical samples. The most common representation of this data is the noise resistance, R_n. It is calculated by dividing the standard deviation of the voltage noise by the standard deviation of current noise [81].

$$R_n = \sigma_V(t) / \sigma_I(t) \tag{1.6}$$

Experimentally, R_n is equivalent to low frequency impedance, $|Z|_{0.01\ Hz}$ and polarization resistance, R_p, taken from EIS and linear polarization methods, respectively [82-83]. And like EIS, a decrease in R_n is indicative of increased the coating degradation, a result of the advancement of water, ion, and other destructive species into the coating system

The types of corrosion processes are often characterized by coatings scientists using the localization index (LI):

$$LI = \sigma_I(t) / RMS_I \tag{1.7}$$

where (RMS_I) is the root mean square of the current noise. It is generally accepted that *LI* values between 0.001 and 0.01 correspond to uniform corrosion processes occurring at the substrate of a coating system. This is desired to ensure long effective lifetimes and to preserve the structural integrity of materials. Larger *LI* values, 0.01 to 0.1, indicate a mixture of uniform and localized corrosion processes. Values higher than this, up to 1.0, identify strong localized corrosion processes and a failed coatings system. These values are shown in Table 2.1.

Table 2.1. Localized index values and corresponding corrosion processes.

Type of corrosion processes	Localization index (LI)
Uniform	0.001 to 0.01
Uniform and Localized	0.01 to 0.1
Localized	0.1 to 1.0

Polynomial detrending is required to remove the drift in ENM data [84]. For more complex drifting, a moving average method should be used [85].

Fast Fourier transform (FFT) and maximum entropy method (MEM) can be used to calculate spectral noise resistance (R_{sn}) for ENM [61, 82-83, 86-87]. The techniques allow for frequency-dependent analysis of ENM data, similarly to EIS. The advantage of MEM over FFT is that is can be performed with shorter time periods and it is smoother. However, MEM must be used with caution in non-stationary systems [19]. Aballe [88] studied the effect of asymmetric configurations.

See the review by Cottis [89] for a detailed description of the sources of noise in addition to explanations of shot noise theory and spectral analysis methods. Tan [40-41] reviews ENM advancements and demonstrates the importance of performing the method

with WBEs for localized corrosion research. References [84, 88, 90] contain additional noteworthy papers on ENM theory.

2.3.2.3. ENM by the traditional method

The traditional experimental setup for organic coating noise measurements includes two similar samples with electrolyte immersion cells attached, shown in Figure 2.8.

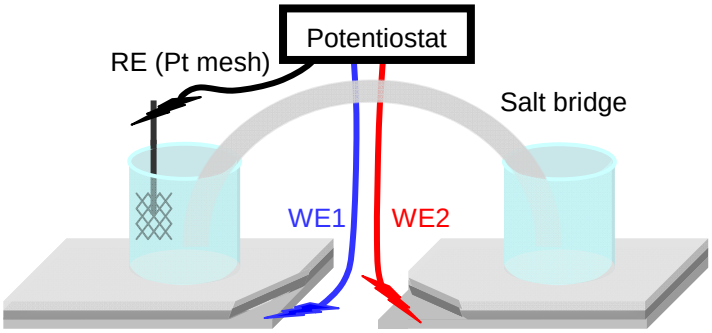

Figure 2.8. Traditional ENM arrangement.

A salt bridge connects the immersion cells and for the current to flow freely between the two samples. A laboratory RE is placed in one of the immersion cells. Each substrate acts as a working electrode by connecting the CE lead to one substrate and the WE lead to the other. A zero resistance ammeter (ZRA) holds the potential difference at zero as the measurements are made.

2.3.2.4. Development of the configuration for ENM

Early ENM measurements utilized a double reference electrode set-up with a single substrate. Hladky and Dawson [91-92] replaced the second reference electrode with a second, nominally identical working electrode finding no significant change to potential noise data.

Mabbutt and Mills [93] re-introduced the double reference electrode experimental set-up, opening the door to embedded electrode techniques. As shown in Figure 2.9 (a), a single substrate/sample is used with two electrolyte immersion cells. The substrate is connected to the RE lead and laboratory reference electrodes replace the previous WEs. Notice, the requirement for a salt bridge has been eliminated. Essentially, all electrical components have been reversed, making the expression "reverse configuration" quite appropriate for this set-up. Mills et al [94] applied the single substrate method in the field using electrolyte-soaked filter paper in place of the electrolyte immersion cell. A copper foil pseudo reference electrode was set on the filter paper and taped across to hold in place. ENM measurements are made by connection to this electrode and achieved suitable results. A subsequent reverse ENM experiment by Mabbutt et al. [95] required no connection to the substrate; three laboratory electrodes are electrically isolated by electrolyte immersion cells, as shown in Figure 2.9 (b).

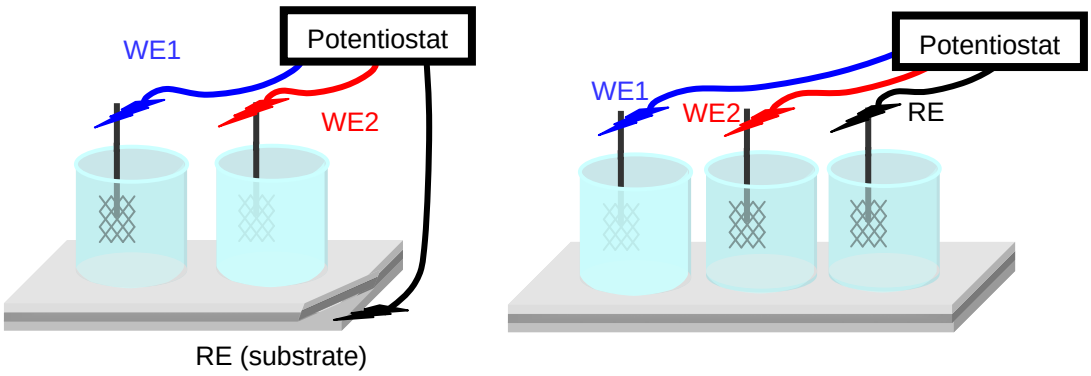

(a) (b)

Figure 2.9. (a) Reverse ENM using a single substrate and no salt bridge and (b) Reverse, non-substrate ENM.

Various coatings systems and reference/pseudo reference electrodes were used to demonstrate the validity of the measurement. This increases the applicability of ENM to in situ examinations where connection to the substrate is difficult or impossible.

2.3.2.5. ENM by embedded electrodes

Embedded electrode ENM was realized soon after Pt mesh electrodes were used in place of the laboratory reference electrodes in the reverse configuration. Thereafter, Wang et al. [26] place Pt wire electrodes within the coating and successfully applied ENM characterization of organic coatings (Figure 2.10). The paper by Wang [96] shows agreement between these three ENM configurations. Continuous measurements may be made using this in situ ENM as long as the humidity satisfies conductivity requirements to allow accurate resistance measurements [19].

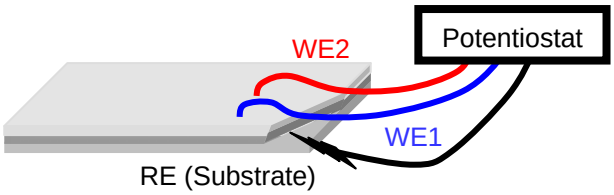

Figure 2.10. Reverse ENM using embedded electrodes.

Bierwagen et al. [19] first applied embedded electrode ENM to coated metal systems for analysis of corrosion. Prohesion® cycle results show that the corrosion rate goes through a maximum at the end of the dry cycle. The authors further postulated that, for aircraft, this corresponds to the morning dry-out which occurs after the evening dew cycle.

Su et al. [21] examined embedded Pt foil leaf electrodes for ENM and shot noise during accelerated weathering of aircraft and industrial coatings by the AC-DC-AC

method. The embedded systems were exposed to thermal cycling [24] and Prohesion [23] in subsequent experiments. EIS measurements were used in addition to reverse configuration ENM.

Kittel et al. [31] used embedded gold sensors to measure the inner and outer impedance for substrates supported by coatings as well as for free films. Further analysis showed that the primer substrate adhesion is a major contributor to a coating system's protective properties [20]. Simpson et al. [29] also used the set-up to measure the dielectric response of a coating via a sensor on glass

2.4. Structural health monitoring

Structural health monitoring (SHM) aims to remotely detect the presence and location of coating or infrastructure damage while the vehicle is in service as well as during inspections. This would allow for as needed, or condition-based, maintenance (CBM). Presently, the aerospace coatings systems undergo visual inspection and scheduled maintenance, which is ineffective, costly, and unreliable. An ideal health monitoring system could be applied to the existing to safely and reliably extend their useful lifetime as well as to the design plans of future infrastructure. This would mean that future air fleets, pipelines, bridges, and other infrastructure can expect greatly reduced life cycle costs and relaxed inspections efforts. A great deal of SHM research focuses on both of these issues. The present paper reviews health monitoring techniques for aerospace, concrete, and other infrastructural applications.

2.4.1. Aerospace vehicles

Aerospace vehicles are subjected to a variety of environmental stresses during their flight cycle. This includes significant changes in humidity, temperature, pressure, and

speed [53]. Stresses have both electrochemical and mechanical implications on the structural integrity of the aircraft. For coated metals, the organic coating system is in direct contact with the environment and is responsible for minimizing the effect of these changes on the underlying structure. Nonetheless, these stresses wear at the coating, leading to coating degradation and the eventual development of cracks, delamination, and corrosion. Impact damages also present a significant risk to the integrity of aerospace vehicles. Bierwagen and Tallman [67] describe key coating properties and measurements for aircraft coating systems; the information is summarized in Table 2.2. For recent reviews and detailed descriptions of aerospace health monitoring, see References [54, 97-99].

Table 2.2. Aircraft coating system key properties and measurement techniques.

Key coating properties		Measurement techniques
Property	**Source**	
Corrosion protection	Topcoat, primer	EIS, ENM, potentiodynamic, hydrothermal
Optical	Topcoat	Gloss, color
Mechanical, solvent resistance	Topcoat, primer	DMA*, DSC†, solvent resistance
Exterior durability	Topcoat	Spectroscopy (FTIR‡, Raman), contact angle
Film thickness	Topcoat, primer	Film thickness

Composite materials, such as carbon-fiber reinforced (CFR), were introduced as a replacement for various aircraft components [100]. High strength and strength at low weight lead to wide use and large-scale structural responsibilities for CFR composites over the past decades [101]. They are especially susceptible to low-velocity impacts and the damages range from matrix cracking to ply delamination to broken fibers [100, 102].

* Dynamic mechanical analysis (DMA)
† Differential scanning calorimetry (DSC)
‡ Fourier transform infrared (FTIR)

Traditional non-destructive SHM methods for aerospace vehicles have included visual inspection by the "naked eye" as well as and optical methods to detect changes in the material properties [54]. Acoustic emission methods detect the movement or growth of aerospace defects rather than the geometry, which requires stressing the material. However, the technique is susceptible to external noise. Vibration-based, radiographic, and thermographic inspection methods are time consuming, expensive, and often require removal of the material for testing. Lamb waves propagate for long distances in plates or thin-walled structures and are superior in many ways to the previously mentioned techniques. They are capable of testing inaccessible and complex aircraft components to detect and determine geometrical flaw information quickly at low cost [53, 103]. A present goal for aerospace health monitoring is to combine the Lamb wave method with piezoelectric sensor/actuators in order to develop an embeddable, active SHM sensor [14].

Brossia et al [74] developed an embedded electrode array for active SHM, based on aerospace coatings systems. The method utilizes EIS measurements at three discrete frequencies to determine the effectiveness of a coating, by monitoring *N'*, the product of impedance magnitude and phase angle, during exposure. The invention consisted of pins embedded into and electrically isolated from the substrate. The assembly is similar to that of WBEs. These electrodes are hard-wired to the integrated circuit and power source on the reverse side of the substrate. An alternative design utilizes MEMs technology by embedding the self-contained microspheres directly into the coating. The size of this system is greatly reduced compared to the first, and it operates through radio-frequency telemetry. However, its placement within the coating limits its analysis to coating degradation whereas the first monitors the condition of the coating and the substrate.

Lin and Chang [101] prepared thin flexible PZT layers using a printed circuit technique for aerospace CFR composites SHM. The PZT sensors are versatile, active sensing devices in that they produce ultrasonic signals by actuator and receive them by sensor. The technique was also used to detect complete cure of the composite material during manufacturing [101]. PZT sensors were used by Ihn and Chang [56] to detect fatigue growth and Park et al. [104] to apply high frequency structural mechanical impedance as a monitoring method.

Fiber optic acoustic sensors, such as fiber Bragg Grating (FBG), are also proposed as a promising candidate for aircraft SHM sensor networks [105].

Cole and co-workers [106-107] developed a dual-approach, intelligent sensing network to monitor damage to hidden areas. Cluster of sensors measure temperature, surface wetness, conductivity of surface moisture, humidity, a galvanic corrosion sensor composed of Al and Cu strips, etc., to monitor microclimates. Additionally, health of simple geometries is monitored by a Rayleigh wave method to provide a "calibration point" and predict corrosion rates at places in which no sensors can be placed.

2.4.2. Reinforced concrete

Concrete slab reinforced by steel bar is the most commonly used infrastructural building material in civil engineering applications. The system is unique in that a very high pH, approximately 12 to 13.5, exists within the concrete during curing which is passivating to the steel rebar. Additionally, the strength of concrete continues to increase over service time.

Cured reinforced concrete can be treated similarly to a coated metal system with capacitive and resistive properties. This has allowed for the implementation of rebar health

monitoring via electrochemical methods, utilizing concrete as an effective electrolyte solution. Concrete resistance is dependent on environmental conditions and the concentration of ionic species within the system. A gradient of resistance develops within the system as water and ions enter the concrete cover. Sufficiently high resistance at the steel surface serves to impede current flow between steel anodes and cathodes, preventing corrosion reactions.

Distinct stages of concrete structural deterioration have been established. This includes the diffusion of Cl^- and CO_2 to the rebar/concrete interface, corrosion initiation, and concrete cracking due to internal pressures formed by the conversion of dense iron metal to less dense iron oxide [108]. Catastrophic failure follows once the structural integrity of the rebar is reduced beyond a critical level. See the paper by Song [109] for an extensive review of electrochemical and non-destructive techniques for concrete/rebar health monitoring.

Bertolini et al. [110] studied reinforced concrete with permanent Ti mesh anodes. Impressed current cathodic protection was applied by the anodes, which acted as a cathode and conductive pathway for reinforcement corrosion when the CP was not active. Concrete is similar to polymers/coatings in the sense that it is a highly resistive material containing water and electrolytes. Therefore, a critical resistance can be reached in which current flow can be prevented between anode and cathode.

Cella and Taylor [111] embedded thin steel wires in concrete to monitor the corrosion of rebar by the electrical resistance method. Results were more sensitive and definitive on steel than traditional electrochemical methods. Pereira et al. [108] developed a similar embedded galvanic corrosion sensor for monitoring rebar.

Lau et al. [112] reviewed composites and optical fiber sensors for repair and SHM of concrete structures. Leung et al. [113] prepared the cut end of an optical fiber with a thin steel film to measure rebar corrosion by the reduction of reflectivity in the fiber. Similarly, Gaon et al. [114] coupled a fiber optic sensor with two steel rebar elements as a corrosion sensing device.

Kumar et al. [115] developed a system for monitoring corrosion and strain within concrete containments.

Nieves-Mendoza et al. [116] attempted to use ENM as a monitoring method for reinforced concrete. The concrete cover acted as the electrolyte in this set-up. Yu et al. [117] proposed harvesting electrochemical current noise from corrosion processes as a power supply for SHM networks. Lu and Ba [118] used an embedded reference electrode to measure polarization resistance, R_p, of rebar by linear polarization and cement mortar resistance, R_s, by high frequency EIS; a linear correlation was observed between ln (R_p) and R_s. A high R_p is associated with high corrosion resistance and R_s increases with penetration of water and ions into the cover mortar. The electrochemical analysis and modeling commonly used for coated metals is well-established for reinforced concrete health monitoring [119-121].

Rajibipour and Weiss [122] found pore fluid composition, moisture content, temperature, and concrete microstructure to be significant variables in field conditions. Additionally, they suggest that pore fluid conductivity must be incorporated into ASTM C1202 measurements for accurate evaluation of concrete quality. Multi-sensor approaches are a promising health monitoring technique; however, sensor “calibration” is crucial to avoid misleading results in field conditions [122].

2.4.3. Pipeline, bridge, power station, nuclear plant, and other infrastructure

Pipeline health monitoring methods are a common area of interest for SHM. The structures are usually coated with one or more layers and then applied with impressed current cathodic protection (ICCP) to mitigate corrosion at coating defects or holidays. Often the current passes through multiple soil layers, this has created numerous design challenges due to temperature and conductivity variations. Seasonal transitions make buried pipelines susceptible to high-pH stress corrosion cracking [123]. Numerous efforts have been applied to advance cathodic protection models for pipelines [124] oil well casings [125] and Zn sacrificial anode-protected steel storage tanks [126]. The recent papers by Sun [127] and Glaser [128] review SHM techniques for the broad field of civil engineering.

Impressed currents limit the SHM methods which can be useful. The permanent reference electrode by Song et al. [34] is applicable to both underground pipelines and storage tanks. More recently, Choi et al. [129] developed a galvanic corrosion sensor and Li et al. [39] an electrical resistance sensor for health monitoring of buried pipeline.

Mabbutt et al. [130] utilized ENM as a method of monitoring corrosion in accelerated corrosion conditions, such as combustion plants. Chiang and co-workers [45-46] developed high-temperature resistant WBEs for use as sensing electrodes in applications such as nuclear power plants. Zhang et al. [131] monitored grounding grid corrosion utilizing it as a working electrode in a polarization resistance measurement. The technology may be applicable to substations, power plants, and power transmission lines.

2.5. Summary

There is great interest in using embedded electrodes for implementation of active SHM. Ideally, the proposed technology would be applicable to existing structures as well as new manufacturing. The transition from the laboratory to the field presents a number of challenges such as miniaturization of components and refining measurement procedures without causing any harm to surrounding coating system.

ENM and EIS are respected electrochemical techniques for measuring the dielectric properties of organic coatings. Unique measurement configurations were presented and reviewed for the non-substrate 2E-EIS and reverse ENM implementation via embedded electrodes. The 2E-EIS technique would be applicable for active SHM as long as current passage remains through the metal, or more specifically the coating/substrate interface. Combined, total impedance/coating resistance and coating capacitance could provide direct in situ health monitoring of coated metal systems. Here, it is suggested that $|Z|_{0.01\ \mathrm{Hz}}$ and $C_{5\ \mathrm{kHz}}$ are monitored over time. Recent work has shown that this may be applied through the use of embedded sensors without requiring connection to the substrate [25].

Although the embedded sensor electrochemical methods have been shown to be durable under a range of environmental conditions, moisture is needed to conduct the experiment. If the electrical pathway between the embedded electrodes is too resistive a measurement can not be made. Normally, the required moisture content is satisfied by ambient air humidity. The concept is counterintuitive, however, because as long as moisture is too low to make a noise measurement via embedded electrodes, a user can have confidence that the water content within a coating is sufficiently low to prevent coating degradation as well as metal corrosion at the substrate.

An intelligent sensing system is under development for aircraft health monitoring [106-107]. A variety of sensors are utilized to obtain local experimental variable such as temperature, humidity and surface conductivity. The information, when properly calibrated, is coupled with a galvanic corrosion sensor to model aircraft degradation. The goal is to provide useful and accurate health monitoring for the entire aircraft, especially for inaccessible areas. A similar multi-parameter design is in progress for reinforced concrete [122].

PZT sensors are a promising candidate for aircraft health monitoring while optical fibers are proving useful for a broader range of infrastructural applications. The WBE is gaining more interest as a health monitoring sensor and has unique corrosion monitoring capabilities. It is likely to find greater application as its full capabilities are further realized.

2.6. Additional comments

2.6.1. Projected needs and uses for embedded sensors

An embedded sensor is needed for the measurement and control of the corrosion potential at metal infrastructural surfaces for impressed cathodic protection systems. The ohmic drop between the anode and substrate must be accounted for to provide adequate protection. The placement of a reference electrode very near to the substrate as a feedback device for controlled-pontential cathodic protection could minimize ohmic drop. Presently, this method is only used for marine applications and the conductive sea medium is utilized to assure negligible ohmic drop. The implementation of an embedded reference electrode for controlled-potential cathodic protection of coated metals is very desirable for civil engineering applications.

2.6.2. Future work on the retrieving information from sensors

A serious challenge to the implementation of embedded sensors for health monitoring is answering the question: How do you get the signal out in a useful way? Pipelines are buried, making them difficult to monitor. Additionally, one must also determine if the health monitoring system requires continuous, intermittent, or situational operation.

Energy sources have been a limiting factor for health monitoring systems. Therefore, it is necessary to operate/power a system as minimally as possibly without impacting the significance of the information. This question can also be asked for protection methods. For instance, it has been suggested that minimal electrochemical damages occur to aircraft in flight. The protection is needed between flights when the aircraft in on the ground and exposed to high to moderate temperatures and humidity conditions. A situational cathodic protection system, suspended during flight, would present a cost-effective approach for protection of aerospace vehicles. A multi-purpose sensor is desirable to provide cathodic protection to coated metals as well as to serve as a health monitoring system.

2.6.3. Remarks on energy sources for electrochemical SHM

The progression of active sensors requires wireless technology. Batteries were explored as a first approximation energy source for wireless sensor networks (WSNs). However, their efficiency is drastically reduced at high altitudes where the air temperature reaches -60 °C. The battery also creates a potential hazard during radical temperature changes. Additionally, the lifetime is limited by the amount of energy the battery can store.

Energy harvesting refers to the capture of a continuous energy source. Energy

scavenging is used when the source is intermittent. A rechargeable power storage device is which can be connected to an energy capturing energy conversion transducer is desired. Ideally, the system could conserve the energy and only use it as required.

Mechanisms of energy capture are under vast exploration. Possible sources for energy harvesting/scavenging have included: solar energy, pressure variations during flight, thermal gradients, mechanical vibrations, and acoustic noise as well as others [18]. Additionally, Yu et al. [117] has proposed harvesting the electrochemical noise currents which are released during the oxidation of metals. See Park et al. [132] and Dilhac et al [18] for recent reviews on recent energy harvesting methods and application to structural health monitoring.

2.7. References

[1] R.A. Dickie and A.G. Smith, How paint arrests rust, Chemtech, 10 (1980) 31.
[2] D.A. Jones, Principles and Prevention of Corrosion, 2nd ed., Prentice Hall, Upper Saddle River, NJ, 1996.
[3] A. Forsgren, Corrosion Control Through Organic Coatings, Taylor & Francis Group, Boca Raton, 2006.
[4] V.B. Miskovic-Stankovic, D.M. Drazic and M.J. Teodorovic, Electrolyte penetration through epoxy coatings electrodeposited on steel, Corrosion Science, 37 (1995) 241-252.
[5] P. Moongkhamklang and S.R. Taylor, The delineation of ionic pathways in organic coatings using a molecular probe technique, Progress in Organic Coatings, 46 (2003) 259–265.
[6] K.N. Allahar, B.R. Hinderliter, D.E. Tallman and G.P. Bierwagen, Water transport in multilayer organic coatings, Journal of the Electrochemical Society, 155 (2008) F201-F208.
[7] W. Funke, Corrosion tests for organic coatings: A review of their usefulness and limitations, Journal of the Oil and Colour Chemist's Association, 62 (1979) 63-67.
[8] Z.W. Wicks, F.N. Jones and S.P. Pappas, Organic Coatings Science and Technology, 2nd ed., Wiley-Interscience, Hoboken, NJ, 1999.
[9] P.A. Sørensen, S. Kiil, K. Dam-Johansen and C.E. Weinell, Anticorrosive coatings: A review, Journal of Coatings Technology Research, 6 (2009) 135–176.
[10] S. Feliu, R. Barajas, J.M. Bastidas and M. Morcillo, Mechanism of cathodic protection of zinc-rich paints by electrochemical impedance spectroscopy. 1. Galvanic stage, Journal of Coatings Technology, 61 (1989) 63-69.

[11] S. Feliu, R. Barajas, J.M. Bastidas and M. Morcillo, Mechanism of cathodic protection s zinc-rich paints by electrochemical impedance spectroscopy. 2. Barrier stage., Journal of Coatings Technology, 61 (1989) 71-76.
[12] S. Bohm, R.J. Holness, H.N. McMurray and D.A. Worsley, Charge percolation and sacrificial protection in zinc-rich organic coatings, in: Eurocorr 2000, Queen Mary and Westfield College, London, 2000.
[13] A.R. Wilson and R.F. Muscat, Novel thin wire paint and sealant degradation sensor, Sensors and Actuators A, (2010).
[14] V. Giurgiutiu, Structural Health Monitoring with Piezoelectric Wafer Active Sensors, Academic Press, Burlington, MA, 2008.
[15] S.G. Croll and B.R. Hinderliter, Estimating service lifetimes in weathering: an optimistic view, Journal of Coatings Technology Research, 4 (2007) 217–230.
[16] J.R. Scully and S.T. Hensley, Lifetime prediction for organic coatings on steel and a magnesium alloy using electrochemical impedance methods, Corrosion, 50 (1994) 705-716.
[17] G. Bierwagen, D. Tallman, J. Li, L. He and C. Jeffcoate, EIS studies of coated metals in accelerated exposure, Progress in Organic Coatings, 46 (2003) 148–157.
[18] J.M. Dilhac, M. Bafleur, J.Y. Fourniols, C. Escriba, R. Plana, D. Dragomirescu, L. Assouère, P. Pons, H. Aubert and C. Buchheit, Crossfunctional design of wireless sensor networks applied to aircraft health monitoring, in: International Workshop on Structural Health Monitoring, Stanford, United States, 2009.
[19] G.P. Bierwagen, X. Wang and D.E. Tallman, In situ study of coatings using embedded electrodes for ENM measurements, Progress in Organic Coatings, 46 (2003) 163–175.
[20] J. Kittel, N. Celati, M. Keddam and H. Takenouti, Influence of the coating–substrate interactions on the corrosion protection: characterisation by impedance spectroscopy of the inner and outer parts of a coating, Progress in Organic Coatings, 46 (2003) 135–147.
[21] Q. Su, K. Allahar and G. Bierwagen, Embedded electrode electrochemical noise monitoring of the corrosion beneath organic coatings induced by ac–dc–ac conditions, Electrochimica Acta, 53 (2008) 2825–2830.
[22] G.P. Bierwagen, K.N. Allahar, Q. Su and V.J. Gelling, Electrochemically characterizing the ac–dc–ac accelerated test method using embedded electrodes, Corrosion Science, 51 (2008) 95–101.
[23] K.N. Allahar, V. Upadhyay, G.P. Bierwagen and V.J. Gelling, Monitoring of a military vehicle coating under Prohesion exposure by embedded sensors, Progress in Organic Coatings, 65 (2009) 142–151.
[24] K.N. Allahar, Q. Su, G.P. Bierwagen, D. Battocchi, V.J. Gelling and D. Tallman, Examination of the feasibility of the use of in-situ corrosion sensors in army vehicles, in: Tri-Service Corrosion Conference, 2005, pp. 1-11.
[25] K. Allahar, Q. Su and G. Bierwagen, Non-substrate EIS monitoring of organic coatings with embedded electrodes, Progress in Organic Coatings, 67 (2010) 180–187.
[26] X. Wang, R. Bennett, K. Spenningsby and G. Bierwagen, Use of electrochemical noise methods for in situ corrosion monitoring, in: D.R.A. Mantz and D.P.C. Trulove (Eds.) Tri-Service Corrosion Conference, San Antonio, TX, 2002, pp. 18.
[27] A. Nogueira, X.R. Novoa and C. Perez, On the possibility of using embedded electrodes for the measurement of dielectric properties in organic coatings, Progress in Organic Coatings, 59 (2007) 186–191.

[28] B.E. Merten, D. Battocchi, D.E. Tallman and G.P. Bierwagen, Embedded reference electrode for potential-monitoring of cathodic protective systems, Journal of the Electrochemical Society, 157 (2010) C244-C247.
[29] T.C. Simpson, P.J. Moran, W.C. Moshier, G.D. Davis, B.A. Shaw, C.O. Arah and K.L. Zankel, An electrochemical monitor for the detection of coating degradation in atmosphere, Journal of the Electrochemical Society, 136 (1989) 2761-2762.
[30] A. Amirudin and D. Thierry, Application of electrochemical impedance spectroscopy to study the degradation of polymer-coated metals, Progress in Organic Coatings, 26 (1995) 1-28.
[31] J. Kittel, N. Celati, M. Keddam and H. Takenouti, New methods for the study of organic coatings by EIS - New insights into attached and free films, Progress in Organic Coatings, 41 (2001) 93–98.
[32] S. Muralidharan, V. Saraswathy, A. Madhavamayandi, K. Thangavel and N. Palaniswamy, Evaluation of embeddable potential sensor for corrosion monitoring in concrete structures, Electrochimica Acta, 53 (2008) 7248–7254.
[33] S. Muralidharan, V. Saraswathy, L.J. Berchmans, K. Thangavel and K.Y. Ann, Nickel ferrite ($NiFe_2O_4$): A possible candidate material as reference electrode for corrosion monitoring of steel in concrete environments, Sensors and Actuators B, 145 (2010) 225–231.
[34] F.M. Song, S. Brossia, D. Dunn and N. Sridhar, New permanent reference electrode for protection of underground pipelines and storage tanks, Corrosion Engineering, Science and Technology, 40 (2005) 262-269.
[35] P.S. Marsh and D.M. Frangopol, Lifetime multiobjective optimization of cost and spacing of corrosion rate sensors embedded in a deteriorating reinforced concrete bridge deck, Journal of Structural Engineering, 133 (2007) 777-787.
[36] G.S. Duffó, S.B. Farina and C.M. Giordano, Characterization of solid embeddable reference electrodes for corrosion monitoring in reinforced concrete structures, Electrochimica Acta, 54 (2009) 1010-1020.
[37] M.F. Montemor, J.H. Alves, A.M. Simoes, J.C.S. Fernandes, Z. Lourenco, A.J.S. Costa, A.J. Appleton and M.G.S. Ferreira, Multiprobe chloride sensor for in situ monitoring of reinforced concrete structures, Cement & Concrete Composites, 28 (2006) 233–236.
[38] I. Martínez and C. Andrade, Examples of reinforcement corrosion monitoring by embedded sensors in concrete structures, Cement & Concrete Composites, 31 (2009) 545–554.
[39] S. Li, Y.-G. Kima, S. Jung, H.-S. Songa and S.-M. Lee, Application of steel thin film electrical resistance sensor for in situ corrosion monitoring, Sensors and Actuators B, 120 (2007) 368–377.
[40] Y. Tan, Monitoring localized corrosion processes and estimating localized corrosion rates using a wire-beam electrode, Corrosion, 54 (1998) 403-413.
[41] Y. Tan, Sensing localised corrosion by means of electrochemical noise detection and analysis, Sensors and Actuators B, 139 (2009) 688–698.
[42] A.M. Simoes, D. Battocchi, D.E. Tallman and G.P. Bierwagen, SVET and SECM imaging of cathodic protection of aluminium by a Mg-rich coating, Corrosion Science, 49 (2007) 3838–3849.

[43] G. Bierwagen, D. Battocchi, A. Simoes, A. Stamness and D. Tallman, The use of multiple electrochemical techniques to characterize Mg-rich primers for Al alloys, Progress in Organic Coatings, 59 (2007) 172–178.
[44] A. Simoes, D. Battocchi, D. Tallman and G. Bierwagen, Assessment of the corrosion protection of aluminium substrates by a Mg-rich primer: EIS, SVET and SECM study, Progress in Organic Coatings, 63 (2008) 260–266.
[45] K.T. Chiang, L. Yang, R. Wei and K. Coulter, Development of diamond-like carbon-coated electrodes for corrosion sensor applications at high temperatures, Thin Solid Films, 517 (2008) 1120–1124.
[46] K.T. Chiang and L. Yang, High-temperature electrochemical sensor for online corrosion monitoring, Corrosion, 66 (2010) 1-8.
[47] Q.L. Thu, G. Bonnet, C. Compere, H.L. Trong and S. Touzain, Modified wire beam electrode: A useful tool to evaluate compatibility between organic coatings and cathodic protection, Progress in Organic Coatings, 52 (2005) 118–125.
[48] J. Orozco, C. Fernández-Sánchez and C. Jiménez-Jorquera, Ultramicroelectrode array based sensors: A promising analytical tool for environmental monitoring, Sensors, 10 (2010) 475-490.
[49] A. Miszczyk and T. Schauer, Electrochemical approach to evaluate the interlayer adhesion of organic coatings, Progress in Organic Coatings, 52 (2005) 298–305.
[50] G.D. Davis and C.M. Dacres, Electrochemical sensors for evaluating corrosion and adhesion on painted metal structures, in: U.S. Patent 5,859,537, 1999, pp. 1-19.
[51] G.D. Davis, L.A. Krebs and C.M. Dacres, Coating evaluation and validation of accelerated test conditions using an in-situ corrosion sensor, Journal of Coatings Technology, 74 (2002) 69-74.
[52] J.B. Ong, Z. You, J. Mills-Beale, E.L. Tan, B.D. Pereles and K.G. Ong, A wireless, passive embedded sensor for real-time monitoring of water content in civil engineering materials, IEEE Sensors Journal, 8 (2008) 2053-2058.
[53] X. Zhao, H. Gao, G. Zhang, B. Ayhan, F. Yan, C. Kwan and J.L. Rose, Active health monitoring of an aircraft wing with embedded piezoelectric sensor/actuator network: I. Defect detection, localization and growth monitoring, Smart Materials and Structures, 16 (2007) 1208-1217.
[54] K. Diamanti and C. Soutis, Structural health monitoring techniques for aircraft composite structures, Progress in Aerospace Sciences, 46 (2010) 342–352.
[55] S. Egusay and N. Iwasawaz, Piezoelectric paints as one approach to smart structural materials with health-monitoring capabilities, Smart Materials and Structures, 7 (1998) 438-445.
[56] J.-B. Ihn and F.-K. Chang, Detection and monitoring of hidden fatigue crack growth using a built-in piezoelectric sensor/actuator network: II. Validation using riveted joints and repair patches, Smart Materials and Structures, 13 (2004) 621–630.
[57] X.P. Qing, S.J. Beard, A. Kumar, T.K. Ooi and F.-K. Chang, Built-in sensor network for structural health monitoring of composite structure, Journal of Intelligent Materials and Structures, 18 (2007) 39-49.
[58] I. Kang, M.J. Schulz, J.H. Kim, V. Shanov and D. Shi, A carbon nanotube strain sensor for structural health monitoring, Smart Materials and Structures, 15 (2006) 737–748.

[59] H. Murayama, K. Kageyama, T. Kamita and H. Igawa, Structural health monitoring of a full-scale composite structure with fiber-optic sensors, Advance Composite Materials, 11 (2003) 287–297.
[60] D. Loveday, P. Peterson and B. Rodgers, Evaluation of organic coatings with electrochemical Impedance Spectroscopy Part 1: Fundamentals of electrochemical impedance spectroscopy, in: JCT Coatings Tech, www.coatingstech.org, 2004, pp. 46-52.
[61] F. Mansfeld, L.T. Han and C.C. Lee, Analysis of electrochemical noise data for polymer coated steel in the time and frequency domains, Journal of the Electrochemical Society, 143 (1996) L286-L289.
[62] G.W. Walter, The review of impedance plot methods used for corrosion performance analysis of painted metals, Corrosion Science, 26 (1986) 681-703.
[63] J.G.N. Thomas, The use of AC impedance spectroscopy for the study of coated metals; A review, Paint Research Association, Princeton, NJ, 1990.
[64] D. Loveday, P. Peterson and B. Rodgers, Evaluation of organic coatings with electrochemical impedance spectroscopy Part 2: Application of EIS to coatings, in: JCT Coatings Tech, www.coatingstech.org, 2004, pp. 88-93.
[65] S. Shreepathi, P. Bajaj and B.P. Mallik, Electrochemical impedance spectroscopy investigations of epoxy zinc rich coatings: Role of Zn content on corrosion protection mechanism, Electrochimica Acta, 55 (2010) 5129–5134.
[66] D.M. Brasher and A.H. Kingsbury, Electrical measurements in the study of immersed paint coatings on metal. I. Comparison between capacitance and gravimetric methods of estimating water-uptake, Journal of Applied Chemistry, 4 (1954) 62-72.
[67] G.P. Bierwagen and D.E. Tallman, Choice and measurement of crucial aircraft coatings system properties, Progress in Organic Coatings, 41 (2001) 201–216.
[68] D. Loveday, P. Peterson and B. Rodgers, Evaluation of organic coatings with electrochemical impedance spectroscopy Part 3: Protocols for testing coatings with EIS, in: JCT Coatings Tech, www.coatingstech.org, 2005, pp. 22-27.
[69] G.D. Davis, K. Thayer, M.J. Rich and L.T. Drzal, Inspection of composite and metal adhesive bonds with an electrochemical sensor, Journal of Adhesion Science and Technology, 16 (2002) 1307–1326.
[70] G.D. Davis, T.G. Vargo, A.W. Dalgleish and D. Deason, Corrosion protection and condition monitoring using 'Smart' appliqués, in: Materials Performance, Materials Performance, 2004, pp. 32-36.
[71] G.D. Davis, Electrochemical impedance evaluation of aluminum/boron–epoxy composite bonds, Journal of Adhesion Science and Technology, 19 (2005) 1397–1408.
[72] G.D. Davis, R.A. Pethrick and J. Doyle, Detection of moisture in adhesive bonds using electrochemical impedance and dielectric spectroscopies, Journal of Adhesion Science and Technology, 23 (2009) 507–528.
[73] T. Bos, S. Buter and C.P.G. Schrauwen, Mountable electrode, in: E.P. Office (Ed.) EP 2 177 894 A1, 2010.
[74] C.S. Brossia and D.S. Dunn, Apparatus and method for detecting the degradation of a coating using embedded sensors, in: U.S.P. Office (Ed.) U.S. Patent 6,911,828 B1, 2005.
[75] Q. Su, K.N. Allahar and G.P. Bierwagen, In situ embedded sensor monitoring of a United States Air Force primer beneath a topcoat exposed to atmospheric humidity and thermal conditions, Corrosion, 66 (2010) 1-12.

[76] K.N. Allahar, Q. Su, G.P. Bierwagen and D.-H. Lee, Monitoring of the AC-DC-AC degradation of organic coatings using embedded electrodes, Corrosion, 64 (2008) 773-787.
[77] R.L. De Rosa, D.A. Earl and G.P. Bierwagen, Statistical evaluation of EIS and ENM data collected for monitoring corrosion barrier properties of organic coatings on Al-2024-T3, Corrosion Science, 44 (2002) 1607-1620.
[78] W.P. Iverson, Transient voltage changes produced in corroding metals and alloys, Journal of the Electrochemical Society, 115 (1968) 617-618.
[79] B.S. Skerry and D.A. Eden, Characterisation of coatings performance using electrochemical noise analysis, Progress in Organic Coatings, 19 (1991) 379-396.
[80] J. Goellner, A. Burkert, A. Heyn and J. Hickling, Using electrochemical noise to detect corrosion: Evaluation of a round-robin experiment, Corrosion, 55 (1999) 476-492.
[81] G.P. Bierwagen, Calculation of noise resistance from simultaneous electrochemical voltage and current noise data, Journal of the Electrochemical Society, 141 (1994) L155-L157.
[82] U. Bertocci, C. Gabrielli, F. Huet and M. Keddam, Noise resistance applied to corrosion measurements I. Theoretical analysis, Journal of the Electrochemical Society, 144 (1997) 31-37.
[83] U. Bertocci, C. Gabrielli, F. Huet, M. Keddam and P. Rousseau, Noise resistance applied to corrosion measurements II. Experimental tests, Journal of the Electrochemical Society, 144 (1997) 37-43.
[84] U. Bertocci, F. Huet, R.P. Nogueira and P. Rousseau, Drift removal procedures in the analysis of electrochemical noise, Corrosion, 58 (2002) 337-347.
[85] Y.J. Tan, The monitoring of the formation and destruction of corrosion inhibitor films using electrochemical noise analysis (ENA), Corrosion Science, 38 (1996) 1681-1695.
[86] T. Schauer, H. Greisiger and L. Dulog, Details on MEM analysis of electrochemical noise data and correlation with impedance measurements for organic coatings on metals, Electrochimica Acta, 43 (1998) 2423-2433.
[87] F. Mansfeld, L.T. Han, C.C. Lee and G. Zhang, Evaluation of corrosion protection by polymer coatings using electrochemical impedance spectroscopy and noise analysis, Electrochimica Acta, 43 (1998) 2933-2945.
[88] A. Aballe, A. Bautista, U. Bertocci and F. Huet, Measurement of the noise resistance for corrosion applications, Corrosion, 57 (2001) 35-42.
[89] R.A. Cottis, Sources of electrochemical noise in corroding systems, Russian Journal of Electrochemistry, 42 (2006) 497–505.
[90] R.A. Cottis and S. Turgoose, Electrochemical noise measurements - a theoretical basis, Materials Science Forum, 192-194 (1995) 663-672.
[91] K. Hladky and J.L. Dawson, The measurement of localized corrosion using electrochemical noise, Corrosion Science, 21 (1981) 317-322.
[92] K. Hladky and J.L. Dawson, The measurement of corrosion using electrochemcial 1/f noise, Corrosion Science, 22 (1982) 231-237.
[93] S.J. Mabbutt and D.J. Mills, Novel configurations for electrochemical noise measurements, British Corrosion Journal, 33 (1998) 158-160.
[94] D.J. Mills, M. Broster and I. Razaq, Continuing work to enable electrochemical methods to be used to monitor the performance of organic coatings in the field, Progress in Organic Coatings, 63 (2008) 267–271.

[95] S. Mabbutt, D.J. Mills and C.P. Woodcock, Developments of the electrochemical noise method (ENM) for more practical assessment of anti-corrosion coatings, Progress in Organic Coatings, 59 (2007) 192–196.
[96] X. Wang, G. Bierwagen and D. Tallman, Electrode configurations for in situ electrochemical impedance measurements on coated metal systems, in: The 197th Meeting of the Electrochemical Society, Toronto, Canada, 2000.
[97] Health Monitoring of Aerospace Structures - Smart Sensor Technologies and Signal Processing, John Wiley & Sons, Ltd, Munich, Germany, 2004.
[98] P.G. Venâncio, R.A. Cottis, R. Narayanaswamy and J.C.S. Fernandes, Corrosion sensors for aircraft aging, Corrosion Protective Materials, 28 (2009) 78-86.
[99] C. Boller, Ways and options for aircraft structural health management, Smart Materials and Structures, 10 (2001) 432–440.
[100] C. Soutis, Carbon fiber reinforced plastics in aircraft construction, Materials Science and Engineering A, 412 (2005) 171–176.
[101] M. Lin and F.-K. Chang, The manufacture of composite structures with a built-in network of piezoceramics, Composites Science and Technology, 62 (2002) 919–939.
[102] M. Kashtalyan and C. Soutis, Stiffness and fracture analysis of laminated composites with off-axis ply matrix cracking, Composites Part A, 38 (2007) 1262–1269.
[103] Y.H. Teo, W.K. Chiu, F.K. Chang and N. Rajic, Optimal placement of sensors for sub-surface fatigue crack monitoring, Theoretical Mechanics A, 52 (2009) 40–49.
[104] G. Park, H.H. Cudney and D.J. Inman, Impedance-based health monitoring of civil structural components, Journal of infrastructure systems, (2000) 153-160.
[105] J.-R. Lee, S.Y. Chong, C.-Y. Yun and D.-J. Yoon, A lasing wavelength stabilized simultaneous multipoint acoustic sensing system using pressure-coupled fiber Bragg gratings, Optics and Lasers in Engineering, 49 (2011) 110–120.
[106] I.S. Cole, P.A. Corrigan, G.C. Edwards, D. Followell, S. Galea, W. Ganther, B.R. Hinton, T. Ho, C.J. Lewis, T.H. Muster, D. Paterson, D.C. Price, D.A. Scott and P. Trathen, A sensor-based learning approach to prognostics in intelligent vehicle health monitoring, Materials Forum, 33 (2009) 27-35.
[107] D.A. Scott, D.C. Price, G.C. Edwards, A.B. Batten, J. Kolmeder, T.H. Muster, P. Corrigan and I.S. Cole, Development of a corrosion sensor for an aircraft vehicle health monitoring system, in: D.O. Thompson and D.E. Chimenti (Eds.) American Institute of Physics, American Institute of Physics, 2010, pp. 1005-1012.
[108] E.V. Pereira, R.B. Figueira, M.M.L. Salta and I.T.E.d. Fonseca, A galvanic sensor for monitoring the corrosion condition of the concrete reinforcing steel: Relationship between the galvanic and the corrosion currents, Sensors, 9 (2009) 8391-8398.
[109] H.-W. Song and V. Saraswathy, Corrosion monitoring of reinforced concrete structures - A review, International Journal of Electrochemical Science, 2 (2007) 1-28.
[110] L. Bertolini, P. Pedeferri, T. Pastore, B. Bazzoni and L. Lazzari, Macrocell effects on potential measurements in concrete cathodic protection systems, Corrosion, 52 (1996) 552-557.
[111] P.A. Cella and S.R. Taylor, Electrical resistance changes as an alternate method for monitoring the corrosion of steel in concrete and mortar, Corrosion, 56 (2000) 951-959.
[112] K.-T. Lau, L.-M. Zhou, P.-C. Tse and L.-B. Yuan, Applications of composites, optical fibre sensors and smart composites for concrete rehabilitation: An overview, Applied Composite Materials, 9 (2002) 221-247.

[113] C.K.Y. Leung, K.T. Wan and L. Chen, A novel optical fiber sensor for steel corrosion in concrete structures, Sensors, 8 (2008) 17.
[114] J.W. Junqi Gaon, Jun Li, Xinming Zhao, Monitoring of corrosion in reinforced concrete structure using Bragg grating sensing, NDT & E International, 44 (2011) 202-205.
[115] K. Kumar, C.S.U. Nair, H.T. Jegadish, S. Muralidharan, A.K. Parande, M.S. Karthikeyan and N. Palaniswamy, Online corrosion and force monitoring for inner containment concrete structures, Sensors & Transducers Journal, 92 (2008) 108-121.
[116] D. Nieves-Mendoza, F. Almeraya-Calderón, J. Uruchurtu-Chavarin, A. Martínez-Villafañe, J. Chacón-Nava, M. Baltazar-Zamora, C. Gaona-Tiburcio and J.L. Menchaca, Evaluation of reinforced concrete structures by means of a novel electrochemical noise corrosion sensor, Corrosion, 64 (2008) 920-928.
[117] Y. Yu, G. Qiao and J. Ou, Self-powered wireless corrosion monitoring sensors and networks, IEEE Sensors Journal, 10 (2010) 1901-1902.
[118] S. Lu and H.-J. Ba, Corrosion sensor for monitoring the service condition of chloride-contaminated cement mortar, Sensors, 10 (2010) 4145-4158.
[119] S. Ahmad and B. Bhattacharjee, A simple arrangement and procedure for in-situ measurement of corrosion rate of rebar embedded in concrete, Corrosion Science, 37 (1995) 781-791.
[120] F. Pruckner, J. Theiner, J. Eric and G.E. Nauer, In-situ monitoring of the efficiency of the cathodic protection of reinforced concrete by electrochemical impedance spectroscopy, Electrochimica Acta, 41 (1996) 1233-1238.
[121] J.P. Broomfield, K. Davies and K. Hladky, The use of permanent corrosion monitoring in new and existing reinforced concrete structures, Cement & Concrete Composites, 24 (2002) 27–34.
[122] F. Rajabipour and J. Weiss, Parameters affecting the measurements of embedded electrical sensors for concrete health monitoring applications, in: J.S. Popovics (Ed.) Health monitoring systems and sensors for assessing concrete, Curran Associates, Inc., Los Angeles, CA, 2008, pp. 7-22.
[123] F.M. Song, Predicting the effect of soil seasonal change on stress corrosion cracking susceptibility of buried pipelines at high pH, Corrosion, 66 (2010) 1-14.
[124] K.N. Allahar and M.E. Orazem, On the extension of CP models to address cathodic protection under a delaminated coating, Corrosion Science, 51 (2009) 962–970.
[125] M.H. Parsa, S.R. Allahkaram and A.H. Ghobadi, Simulation of cathodic protection potential distributions on oil well casings, Journal of Petroleum Science and Engineering, 72 (2010) 215–219.
[126] O. Abootalebi, A. Kermanpur, M.R. Shishesaz and M.A. Golozar, Optimizing the electrode position in sacrificial anode cathodic protection systems using boundary element method, Corrosion Science, 52 (2010) 678–687.
[127] M. Sun, W.J. Staszewski and R.N. Swamy, Smart sensing technologies for structural health monitoring of civil engineering structures, Advances in Civil Engineering, (2010).
[128] S.D. Glaser, H. Li, M.L. Wang, J. Ou and J. Lynch, Sensor technology innovation for the advancement of structural health monitoring: a strategic program of US-China research for the next decade, Smart Structures and Systems, 3 (2007) 221-244.
[129] Y.-S. Choi, J.-G. Kim and S.J. Yang, A galvanic sensor for monitoring the corrosion damage of buried pipelines: Part 2—Correlation of sensor output to actual corrosion damage of pipeline in soil and tap water environments, Corrosion, 62 (2006) 522-532.

[130] S. Mabbutt, N. Simms and J. Oakey, High temperature corrosion monitoring by electrochemical noise techniques, Corrosion Engineering, Science and Technology, 44 (2009) 186-195.
[131] X.-L. Zhang, X.-H. Zhao, Y.-G. Wang and N. Mo, Development of an electrochemical in situ detection sensor for grounding grid corrosion, Corrosion, 66 (2010) 1-7.
[132] G. Park, T. Rosing, M.D. Todd, C.R. Farrar and W. Hodgkiss, Energy harvesting for structural health monitoring sensor networks, Journal of Infrastructure Systems, 14 (2008) 64-79.

CHAPTER 3. DEVELOPMENT OF EMBEDDABLE WIRE REFERENCE ELECTRODE FOR CORROSION POTENTIAL MONITORING: CONSTANT IMMERSION STUDY USING SACRIFICIAL COATING SYSTEMS

3.1. Introduction

United States corrosion related costs have been estimated at $276 billion annually, or roughly 3.1% of the gross domestic product (GDP). This value takes into account the wide-ranging areas that are dependent on metals or alloys including utilities, infrastructure, transportation, and industry [1]. There is a desire to reduce these costs through the improvement structural maintenance procedures. Various sensors have been developed and incorporated into both new and existing structures to allow for *in-situ* examination of the structural health [2-6]. Cost-effective, needs-based maintenance procedures are emerging through the advancement of these structural health monitoring (SHM) methods [7-13].

Cathodic protection methods are essential techniques for preserving the performance of structural metals or alloys which succeed by forcing corrodible metal surfaces to be the cathodes in electrochemical corrosion cells [14]. Imposed cathodic protection utilizes an external power source to polarize the material; common in pipelines, rectifiers are positioned along the length of the structure to apply a small, constant and controllable current [15]. While galvanostatic applications are more facile and less expensive, in this case, non-uniform polarization is an ongoing concern. Similarly, potentiostatic methods also exist, but it is difficult to control the system's potential and

they require a conductive medium. Alternatively, sacrificial protection is attained by coupling the metal substrate with a second metal that is more electrochemically active; the latter will corrode preferentially, thus protecting the former. Large sacrificial anodes of magnesium, zinc, or aluminum are commonly used by installing them on offshore drilling platforms or burying them near pipelines [14]. Metal-rich primers and galvanized metals are also common forms of sacrificial protection.

The corrosion potential or open circuit potential of any sacrificial cathodic protection system provides measure of the protection's effectiveness at any time given the substrate corrosion potential is known. Cathodic protection is active when the mixed corrosion potential is more negative than the substrate corrosion potential, generally by at least 0.1 V.

An embeddable reference electrode can be used to monitor the mixed corrosion potential for cathodic protection systems. True reference electrodes pass small currents without polarization and maintain a stable, known reduction/oxidation potential to within ±0.001 V [16]. By measuring the corrosion potential versus a known reference electrode, the half-cell potential of the substrate can be calculated. The accuracy required for cathodic protection applications is on the order of tens of millivolts which allows for the use of pseudo reference electrodes.

Reinforced concrete research is an active area of interest for new embedded electrode or sensor technologies. The condition reinforcement bar (rebar) within the concrete is the major indicator of the health of the structure. Pipeline health is another sector which benefits from corrosion potential sensors. Numerous electrode materials, including $Cu/CuSO_4$, Ag/AgCl, W/WO_2, MnO_2, MoO_2, Luggin probes, titanium activated

with mixed metal-metal oxides, and graphite rods have been explored for health monitoring in these systems [17-21]. Duffó et al. [22-23] developed an intricate multi-sensor to monitor the structural health of rebar by the measurement of corrosion rate, concrete electrical resistivity, oxygen transport, and temperature. Furthermore, the multi-sensor is applicable to both new and existing structures. Figure 3.1 gives an example for concrete.

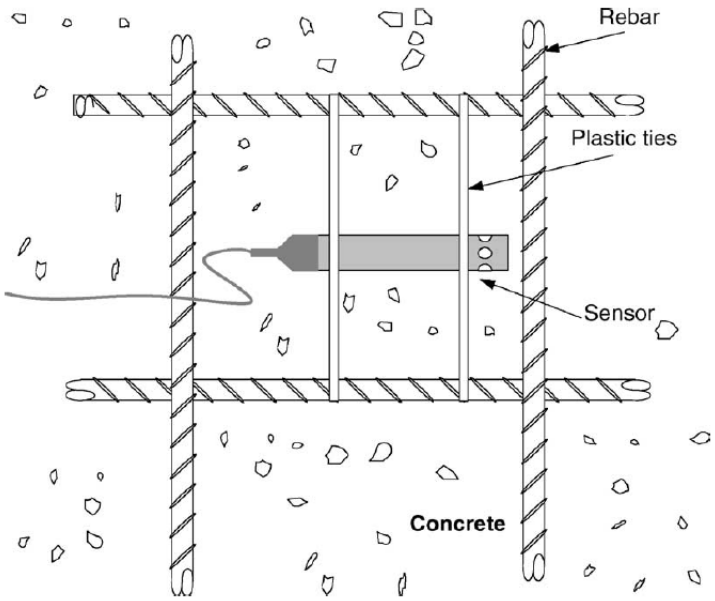

Figure 3.1. Reference electrode within reinforced concrete structure. Reproduced from Reference [17].

Researchers at NDSU have embedded thin metal foil and wire sensors for the characterization of organic coating systems (Figure 3.2) [24-35]. Long-term reliability and stability is a key requirement for an embedded reference electrode (ERE). In this research, experimental EREs have been applied to a Mg-rich primer coating system on AA 2024-T3 substrate [36]. This technology was developed as a chromate-free replacement for aerospace alloys [37]. The experimental ERE is also examined using Zn-rich primer on steel substrate. This a commonly used sacrificial metal-rich coating system [38-39].

(a) (b)

Figure 3.2. Example for a platinum sensor developed at NDSU with (a) primed substrate plus sensor and (b) topcoated system. Reproduced from Ref [25].

3.1.1. Choice of reference electrode

A robust reference electrode is required for successful implementation of an ERE for health monitoring of cathodic protection systems. Our lab positions the electrode between the primer and topcoat layers of a polymeric system. Embedding the electrode between a topcoat and primer protects it from environmental elements such as UV radiation. Additionally, it places the reference electrode at micron-range distance from the substrate which reduces IR drop and creates a slow, diffusion-controlled environment for measurement stability.

The initial step for this research is to determine a suitable material to use as the ERE. Various established reference electrode are available to choose from. Table 3.1 gives commonly used reference electrodes and their reduction/oxidation (redox) potential.

Table 3.1. Common reference electrodes.

Name	Half-Cell Reaction	Potential (V vs SHE)
Standard Hydrogen Electrode (SHE)	$H^+ + 2e^- = H_2$	+0.000
Silver-Silver Chloride (Ag/AgCl)	$AgCl + e^- = Ag + Cl^-$	+0.222
Saturated Calomel Electrode (SCE)	$Hg_2Cl_2 + 2e^- = 2Hg + 2Cl^-$	+0.268
Copper-Copper Sulfate (Cu/$CuSO_4$)	$CuSO_4 + 2e^- = Cu + SO_4^{2-}$	+0.318

Three key requirements have been established for a reference electrode to be appropriate for this study (Figure 3.3). First, it must pass small currents without polarization which is the definition of a reference electrode [14, 16]. Considerations must also be made for processing of the reference electrode at production scales. It should be robust under manufacturing conditions and tolerant of minor mishandling. Furthermore, an inexpensive reference electrode is most desired to improve marketability. The third requirement is that the reference electrode must remain functional under service conditions. This includes chemical and thermal stability as well as maintaining an operational lifetime which is greater than the structure being monitored.

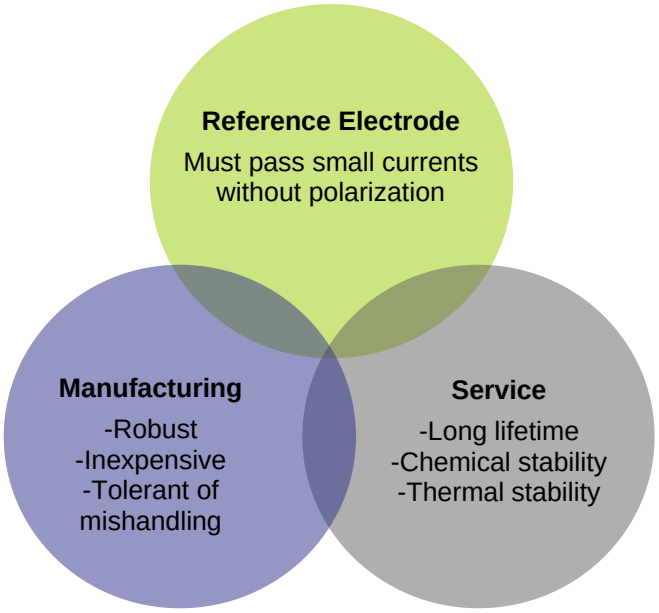

Figure 3.3. Three components required for a suitable embedded reference electrode.

The silver-silver chloride electrode is environmentally benign and has recognized advantages of temperature stability, low expense, and ease of construction, [40-41]. It has been proposed that thin Ag wires may be embedded between coating layers without

introducing detrimental effects to the protective properties of the coatings. Embedded noble metals such as gold, nickel, and platinum have been used for the analysis of dielectric properties and interlayer adhesion in organic coating systems [28, 34, 42-45]. These materials may also be considered pseudo reference electrodes for corrosion potential measurements [16].

3.1.2. Methods for developing Ag/AgCl reference electrodes

3.1.2.1. Chemical oxidation

Two basic methods exist for making Ag/AgCl reference electrodes. The first is the use of chemical oxidation. Dilute $FeCl_3$ is commonly used. In the presence of a silver wire, a galvanic electrochemical reaction occurs. The Ag oxidizes, freeing an electron.

$$Ag = Ag^+ + e^- \quad (3.1)$$

The $FeCl_3$ consumes the free electron, reducing Fe^{3+} to Fe^{2+} and freeing a chloride ion.

$$FeCl_3 + e^- = FeCl_2 + Cl^- \quad (3.2)$$

The final step is the combination of the anion and cation to AgCl.

$$Ag^+ + Cl^- \leftrightarrow AgCl \quad (3.3)$$

The AgCl precipitates on the surface of the silver wire. Theoretically, a stable potential develops between the Ag metal atoms and the AgCl, establishing the reference electrode function.

3.1.2.2. Electrochemical anodization

The second method is electrochemical anodization. The general electrochemistry does not change compared to chemical oxidation, but the solution does. In this method, a small current is applied to the wire over specified amount of time. The wire becomes the anode as the current polarizes the Ag wire to a potential in which Ag atoms at the wire

surface oxidize (Equation 3.1). A simple battery or a potentiostat with galvanostatic capabilities can be used to conduct this anodization. The anodizing potential can also be achieved directly using a potentiostatic method.

The electrochemical anodization is staged in a solution which contains the desired anion. For Ag/AgCl reference electrodes, HCl is generally used in the oxidation step [46]. In addition to the Ag wire, a counter electrode such as platinum mesh is also immersed in the solution. The reduction reaction occurs on the surface of this counter electrode, consuming liberated electrons to produce hydrogen and chloride ions.

$$2HCl + 2e^- = H_2 + 2Cl^- \quad (3.4)$$

Again, the anion and cation combine on the surface of the Ag wire to form the reference electrode (Equation 3.3).

3.2. Experimental methods

3.2.1. Procedure for developing wire Ag/AgCl reference electrode

Silver wires of 50 μm ±10% and 25 μm ±10% diameter were supplied by Goodfellow Corporation (Huntingdon, England). The purity was 99.99% for both sizes. Wires were cut to a length of 4 cm. A 0.75 cm X 1.5 cm strip of conductive tape was folded over one end of the wire for handling. In addition, the conductive tape will later serve as a contact point between the embedded reference electrode and external equipment for measurements to be made. The wires were cleaned by first rinsing with distilled (DI) water, hexane, and DI water again.

3.2.1.1. Chemically oxidized Ag wire

Dilute $FeCl_3$ was used for the chemical oxidation of Ag wire. Concentrations of 0.06 M $FeCl_3$ and 0.03 M $FeCl_3$ were examined. The method proceeded by submerging the

clean Ag wire in one the two solutions for a period of time: 30 seconds for the former, 60 seconds for the latter. Approximately 0.5 cm at the junction of the conductive tape was left clear of the solution. Figure 3.4 illustrates the set-up for this method.

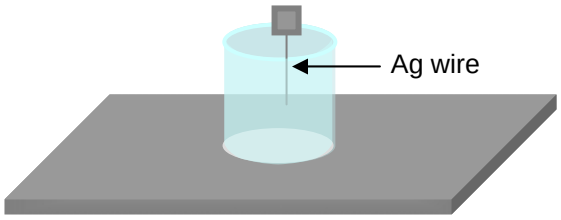

Figure 3.4. Illustration is given for the chemical oxidation of Ag wire.

.

The chemical oxidation proceeds according to the reactions described in this chapter's introduction. Equation 3.5 combines the Equations 3.1, 3.2, and 3.3, giving the overall reaction for the chemical oxidation method.

$$Ag + FeCl_3 = AgCl + FeCl_2 \quad (3.5)$$

The Ag/AgCl wires were rinsed with water and stored in a saturated AgCl solution for one day. The solution assists in finalizing the development of a stable AgCl layer.

3.2.1.2. Electrochemically anodized Ag wire

Clean wires were placed in a 1 M HCl solution and connected to the working and counter electrode (WE/CE) leads of a Gamry PCI4/300 potentiostat/galvanostat with dedicated EIS 300 software, supplied by Gamry Instruments, Inc. (Warminster, PA). Approximately 0.5 cm at the junction of the conductive tape was left clear of the solution. A laboratory-grade SCE was used as the reference electrode (RE). The instrumental set-up is given in Figure 3.5.

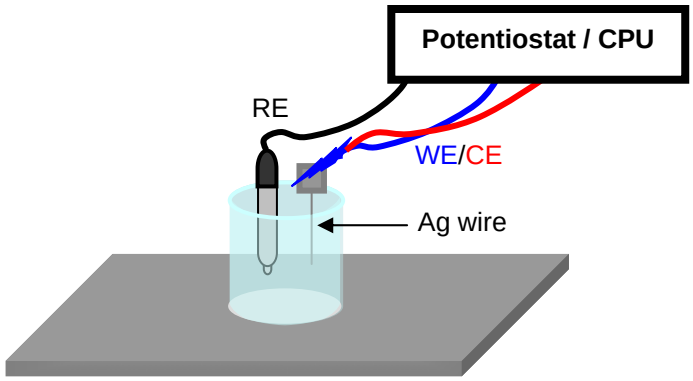

Figure 3.5. Instrumental set-up is given for electrochemical anodization of Ag wire.

A potential of 1.2 V vs SCE applied using a potentiostatic method for a period of 20 seconds. A galvanostatic current was then applied at -30 mA for 20 seconds. Finally, the potentiostatic method was repeated for a period of 300 seconds. Equation 3.6 combines the Equations 3.1, 3.3, and 3.4, giving the overall reaction for the electrochemical anodization method.

$$2Ag + 2HCl = 2AgCl + H_2 \quad (3.6)$$

The electrochemically anodized Ag/AgCl wire reference electrodes were stored in the same manner as above.

3.2.2. Experimental coating systems

Table 3.2 demonstrates the coatings systems used and the sets of wire reference electrodes prepared via each method.

3.2.2.1. Mg-rich coating system

Aluminum alloy (AA) 2024-T3 panels (12 cm x 5 cm x 0.3 cm), supplied by Q Panel Lab Products (Cleveland, OH), were pretreated by sandblasting, rinsing and wiping with hexane, wiping with Turco® solution (diluted to 10%) from Akzo Nobel. The panels were then rinsed with 18 MΩ·cm water and forced dry with an air nozzle. They were

subsequently coated with Mg-rich primer, supplied by Akzo Nobel Aerospace Coatings (Waukegan, IL), and prepared according to the manufacturer's instructions. The two-component coating included products XP406 and XP391 as well as the thinner XP374. Coatings were applied by air spray to target thickness 50 μm and cured under ambient conditions for 2 days.

Table 3.2. Experimental design is given for the electrodes and coating systems used.

Coating System (Primer / Substrate)	Experimental Reference Electrode			
	Preparation	Size (μm)	Solution	Replicates
Mg-rich / AA2024-T3	Chemical	25.4	0.06 M $FeCl_3$	4
			0.03 M $FeCl_3$	4
		50.8	0.06 M $FeCl_3$	4
			0.03 M $FeCl_3$	4
	Electrochemical	25.4	1 M HCl	2
		50.8	1 M HCl	2
Zn-rich / Steel	Chemical	25.4	0.06 M $FeCl_3$	4
			0.03 M $FeCl_3$	4
		50.8	0.06 M $FeCl_3$	4
			0.03 M $FeCl_3$	4
	Electrochemical	25.4	1 M HCl	2
		50.8	1 M HCl	2

3.2.2.2. Zn-rich coating system

Cold-rolled steel panels (12 cm x 5 cm x 0.3 cm), supplied by Q Panel Lab Products (Cleveland, OH), were pretreated by hand-sanding and rinsing and wiping with hexane to remove oils. The panels were then rinsed with 18 MΩ·cm water and forced dry with an air nozzle. They were subsequently coated with Zinc Clad® IV, supplied by Sherwin-Williams (Cleveland, OH), prepared according to the manufacturer's instructions. Coatings were applied by air spray to target thickness 50 μm and cured under ambient conditions for 2 days.

3.2.3. Placement of reference electrode within coating system

The corrosion potential was measured for each wire reference electrode prior to embedding within in the coating system. A small beaker was filled with dilute Harrison's solution (DHS), 0.5% NaCl and 0.35% $NaSO_4$. The wire reference electrode was removed from storage, rinsed with distilled water, and clamped with an alligator clip to the conductive tab. The clip is connected to the RE lead of the Gamry potentiostat (Figure 3.6). A laboratory SCE is used as the WE to provide a stable, reference potential.

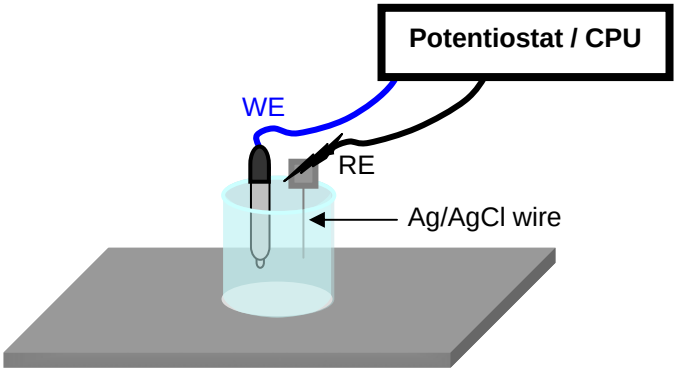

Figure 3.6. Instrumental set-up is given for corrosion potential measurement using the Ag/AgCl wire reference electrode.

A thin strip of commercial rapid cure epoxy was used to secure the reference electrode to the surface of the primer. A piece of conductive tape was carefully applied over the first and to the substrate. The tape serves as an electrical lead for experimental procedures. In order to preserve connectivity, masking tape was placed over the external part to prevent it from being coated in the next step.

The high solids polyurethane gloss enamel 646-58-7925 and X-501 curing solution were prepared according to manufacturer's instructions for use as the topcoat, supplied by Akzo Nobel (Waukegan, IL). It was air sprayed at target thickness of 50 μm for both

coating systems. The panels were cured at ambient conditions for one week. Figure 3.7 gives this set-up using (a) an illustrated cross-section and (b) photographed samples midway and upon completion of panel preparation.

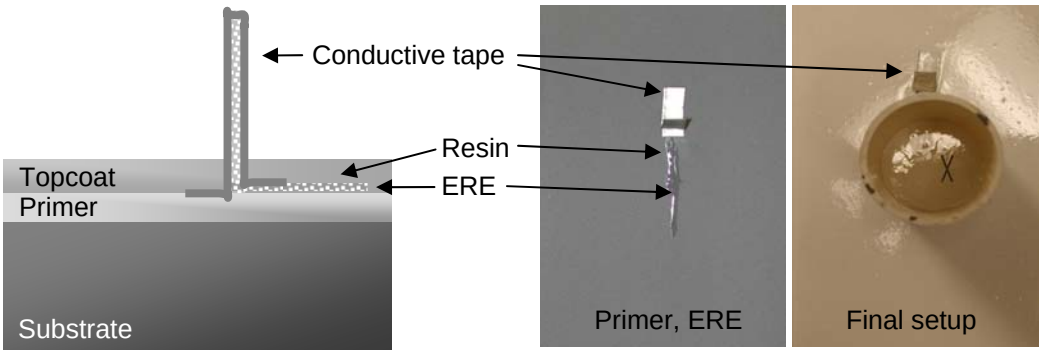

Figure 3.7. The coating system is shown for (a) an illustrated cross-section and (b) photographed primer plus reference electrode before and after the top-coat, electrolyte cell, and scribe are applied.

A small scribe was placed approximately 1 cm from the ERE and in the shape of an "X" for all panels. An 8 cm tall cylindrical cell, cut from a 3.8 cm diameter PVC pipe, was fastened to the panel as shown using commercial Marine Goop®.

3.2.4. Experimental analysis methods

3.2.4.1. Scanning electron microscopy

Samples of the Ag wire, as received, and Ag/AgCl wire reference electrode were mounted and examined via scanning electron microscopy (SEM). Energy dispersive x-ray spectroscopy (EDX) was used to analyze the chemical composition. Sample cross-sections of the experimental ERE were also characterized.

3.2.4.2. Corrosion potential measurement

The cylindrical cell for each sample was filled to approximately two-thirds full using 5% NaCl. The solution concentration was maintained regularly using additions of distilled water to the two-thirds full point.

A Gamry PCI4/300 potentiostat/galvanostat with dedicated EIS 300 software and multiplexor were used for electrochemical experiments. A JEOL JSM-6490LV Scanning Electron Microscope (SEM) (Peabody, MA) was used to obtain electron micrographs and perform chemical analysis.

Figure 3.8 gives the instrumental set-up for the corrosion potential analysis. Two multiplexor channels were utilized for each panel. The illustration demonstrates a panel connected to Channels 1 & 2. The experimental ERE test is performed on odd-numbered channels and SCE standard on even ones. Each is connected to the respective RE lead on the multiplexor. The substrate is fastened to the WE lead for all channels.

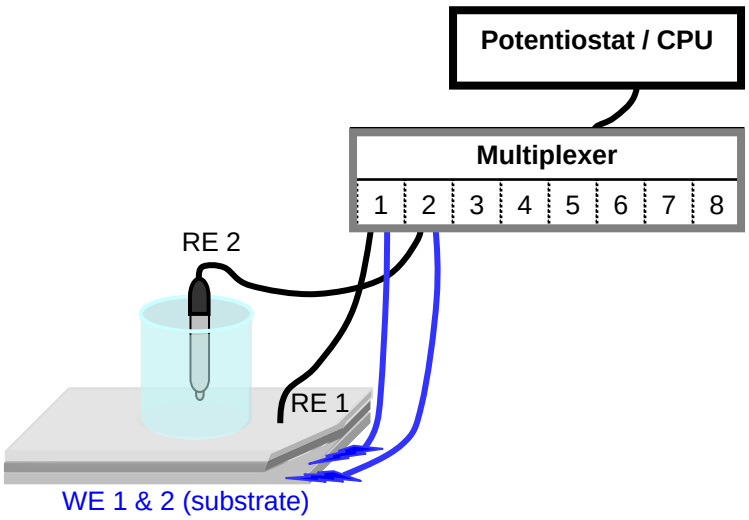

Figure 3.8. Instrumental set-up for corrosion potential measurements using a potentiostat and 8 channel multiplexor.

The OCP was recorded for one hour at 0.5 measurements per minute. The multiplexer measures one data point at the active channel and switches to the next, cycling through the 8 channels over the course of the experiment. Consequently, the measurements are within a few seconds of simultaneity and allow the conventional SCE standard to be used as a practical comparison for the experimental ERE.

3.2.4.3. Potentiodynamic sweep

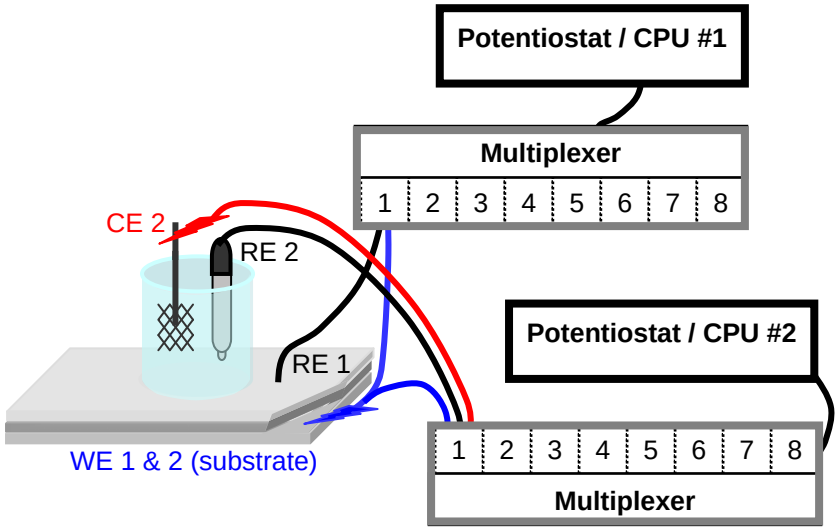

Figure 3.9. Instrumental set-up for potentiodynamic sweep (SCE standard) and corrosion potential measurements (experimental ERE). Two potentiostats and 8 channel multiplexors are used.

A dynamic potential was applied to the coating system using a second potentiostat. A laboratory SCE served as the RE, the substrate as the WE, and a platinum mesh as the counter electrode (CE). The scan rate was 0.005 V/s and the potential range -1.5 to 1.5 V versus SCE. The corrosion potential was measured concurrently according to Section 3.2.4.1. The ERE served as the RE and the substrate as the WE. This experimental set-up is utilized to measure the ERE response to a known, controlled potential environment. Any

time lag or instability in the ERE will also be realized. The instrumental setup is given in Figure 3.9.

3.3. Results

3.3.1. Scanning electron microscopy (SEM)

The appearance of the Ag wire, as received, was observed by SEM. Figures 3.10 (a) and (b) show the 2 mil Ag wire at two different magnifications. The surface is smooth and uniform. A few small streaks appear, parallel to the length of the wire. These are likely a result of the drawn manufacturing process and are not considered to be a concern for the desired application.

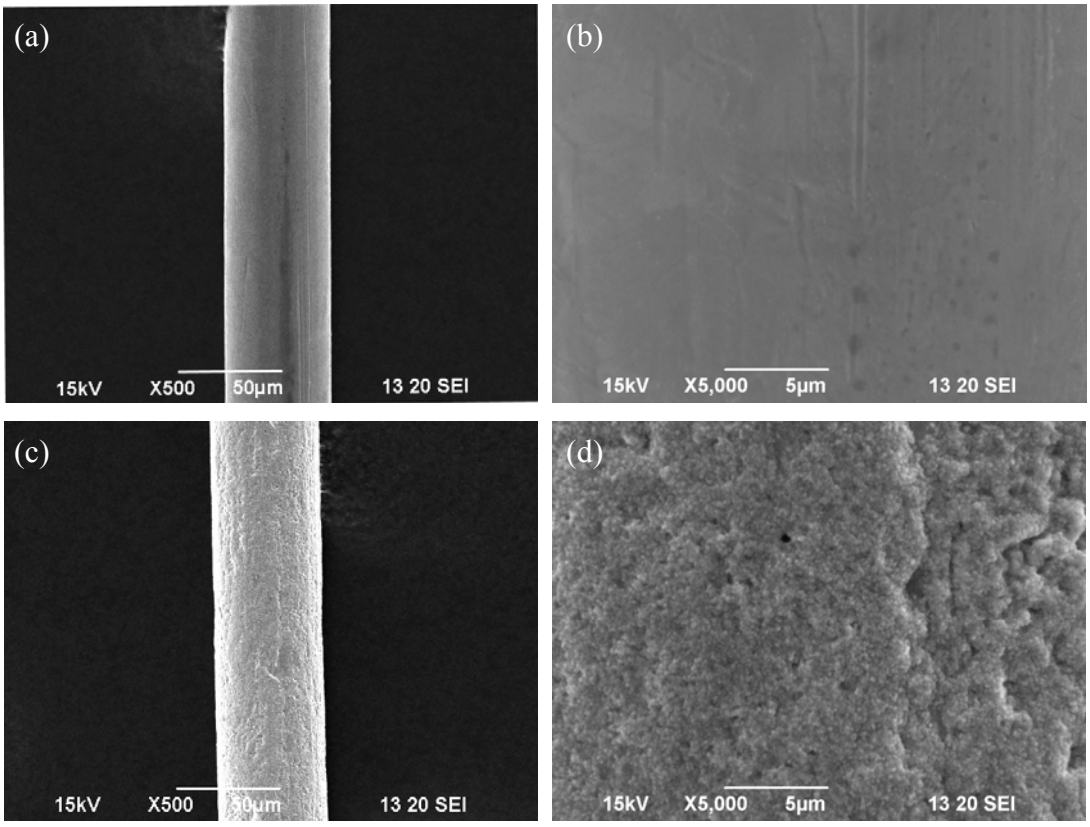

Figure 3.10 SEM micrographs for 2 mil Ag wire as received at (a) X500 and (b) X5,000 magnification as well as following chemical oxidation in 0.03 M $FeCl_3$ for 60 seconds at (c) X500 and (d) X5,000 magnification.

Subsequent SEM micrographs were obtained to observe the effects of AgCl deposition. Figure 3.10 (d) shows an obvious change to the surface structure which is quite uniform, but imperfect. The diameter has increased by roughly 1 μm (not shown). This suggests that the change in appearance is due to the growth of the AgCl crystalline layer.

The composition of the crystalline layer was determined using EDX. The maps in Figure 3.11 show the net counts for Cl (a) and Ag (b) with increasing color saturation. The presence of both elements confirms that the crystalline layer is AgCl. Figure 3.11 (c) shows a map of the two elements combined. There is a vertical strip approximately 1/3 the distance from the right edge of the wire. It can be concluded from the three micrographs that the AgCl layer is absent. The defect may have been acquired during SEM preparation.

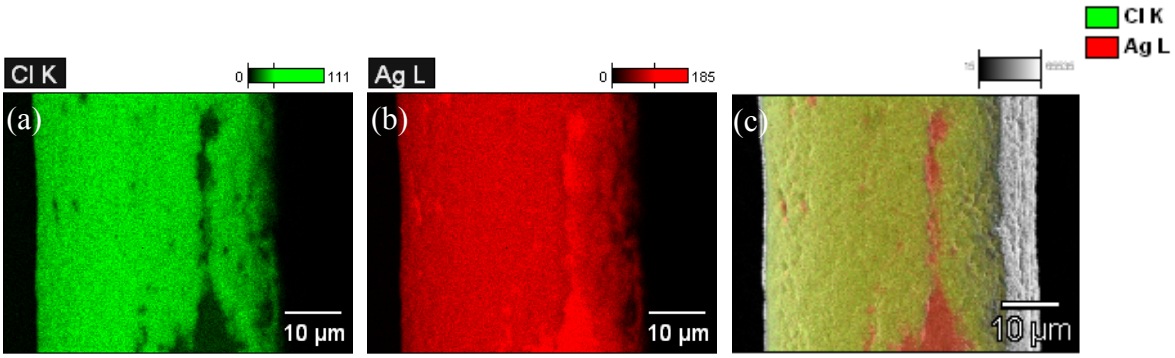

Figure 3.11 EDX maps of Ag wire RE formed by chemical oxidation in 0.03 M $FeCl_3$ for 60 seconds showing (a) Cl, (b) Ag, and (c) Cl and Ag.

Figure 3.12 presents SEM and EDX cross-section data. Figure 3.12 (a) shows a thin, uniform AgCl layer (gray) and the Ag wire (light). The scale bar suggests that the size of the layer is on the order of 1 μm, which supports the SEM data described above.

An EDX map is shown in Figure 3.12 (b), using the same magnification and accelerating voltage as Figure 3.12 (a). The plots in Figure 3.12 (c) and (d) show the EDX

scan for the crystalline layer and Ag wire, respectively. These parts are labeled as 1 and 2 in Figure 3.12 (b).

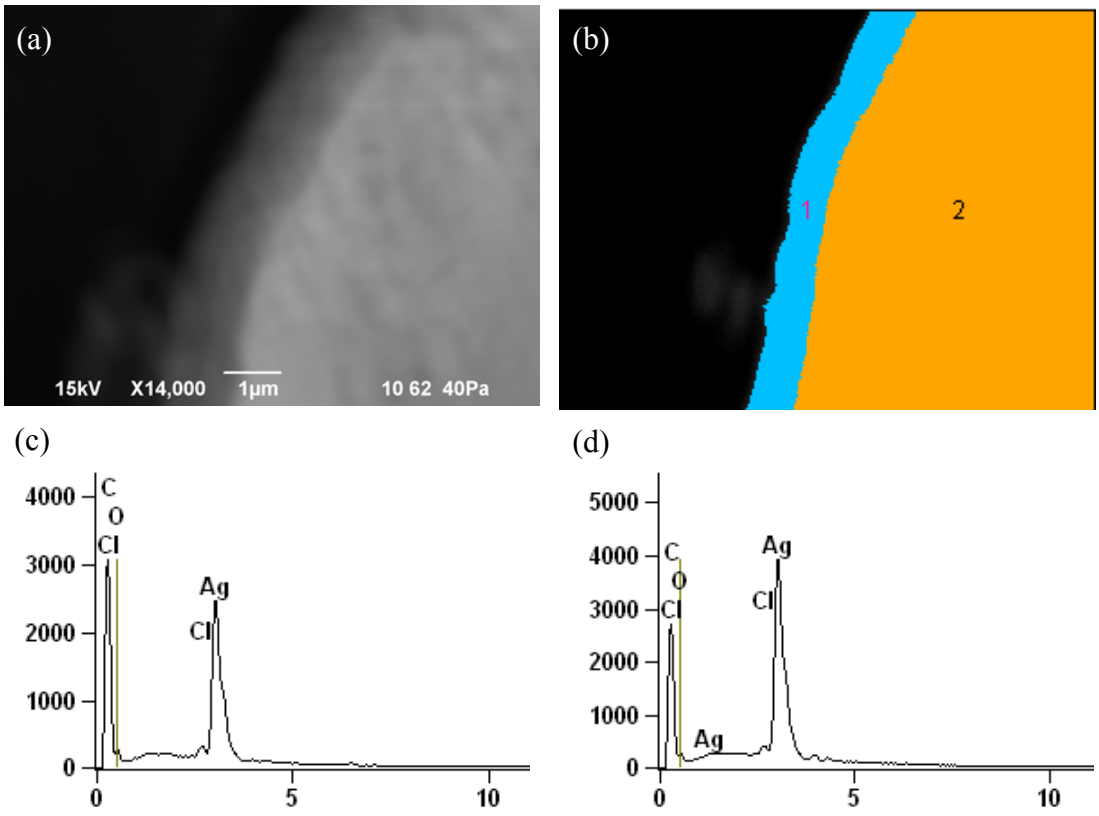

Figure 3.12 Cross-section of Ag wire RE for (a) SEM, (b) EDX map, (c) EDX scan area #1, and (d) EDX scan area #2.

Table 3.3. Results for EDX scan of crystalline layer (1) and Ag wire (2).

Measure	(#)	C-K	O-K	Cl-K	Fe-K	Ag-L
Net Counts	1	29869	-	757	299	62844
	2	26099	596	441	-	96732
Weight %	1	58.10 (1.06)	-	0.29 (0.15)	0.46 (0.38)	41.16 (1.64)
(±3 Sigma)	2	44.69 (0.87)	1.58 (0.76)	0.14 (0.14)	-	53.58 (1.71)

The net count and weight % results for the EDX scans are listed in Table 3.3. Ag was observed in both scan areas. A higher weight % was observed for Cl in the crystalline layer, confirming the presence of AgCl. The Cl in the Ag wire is trivial due to the high

sigma value. It is also noted that a small percentage of Fe was observed in the crystalline layer as well as O in the Ag wire.

3.3.2. Corrosion potential measurements

The experimental coating systems were exposed to 5% NaCl constant immersion. Corrosion potential measurements were performed regularly to examine the experimental ERE. A laboratory SCE served as the standard measurement. The two reference electrode measurements were performed concurrently. For each data set, the mean, $\bar{x}$, and standard deviation, σ, were calculated for the respective reference electrodes.

$$\bar{x} = \frac{1}{n}\sum_{i=1}^{n} x_i \tag{3.7}$$

$$\sigma = \frac{1}{N-1}\sum_{i=1}^{N} (x_i - \bar{x})^2 \tag{3.8}$$

The standard deviation characterized the amount of scatter that occurs in the data during the measurement for each reference electrode. These values are plotted versus immersion time. The experimental ERE replicate with the most consistent results is presented in the following sections for each sample set. In cases where large variance occurred between the replicates, this is noted.

3.3.2.1 Mg-rich coating system

3.3.2.1.1. Chemically oxidized EREs

Figure 3.13 gives corrosion potential as a function of immersion time for the chemically oxidized 1 mil and 2 mil Ag wire EREs. Each point on the graph is the mean corrosion potential and standard deviation for a single test. The standard deviations are very low for SCE measurements, and the mean is between -0.7 and -0.8 V vs SCE for the first 600 days. These values are consistent with active cathodic protection by a Mg-rich

primer over AA 2024-T3 [47]. The experimental ERE standard deviations are small for most measurements, and they are approximately 0.1 to 0.2 V positive of the SCE standard. This is an expected value for the ERE, compared to the SCE.

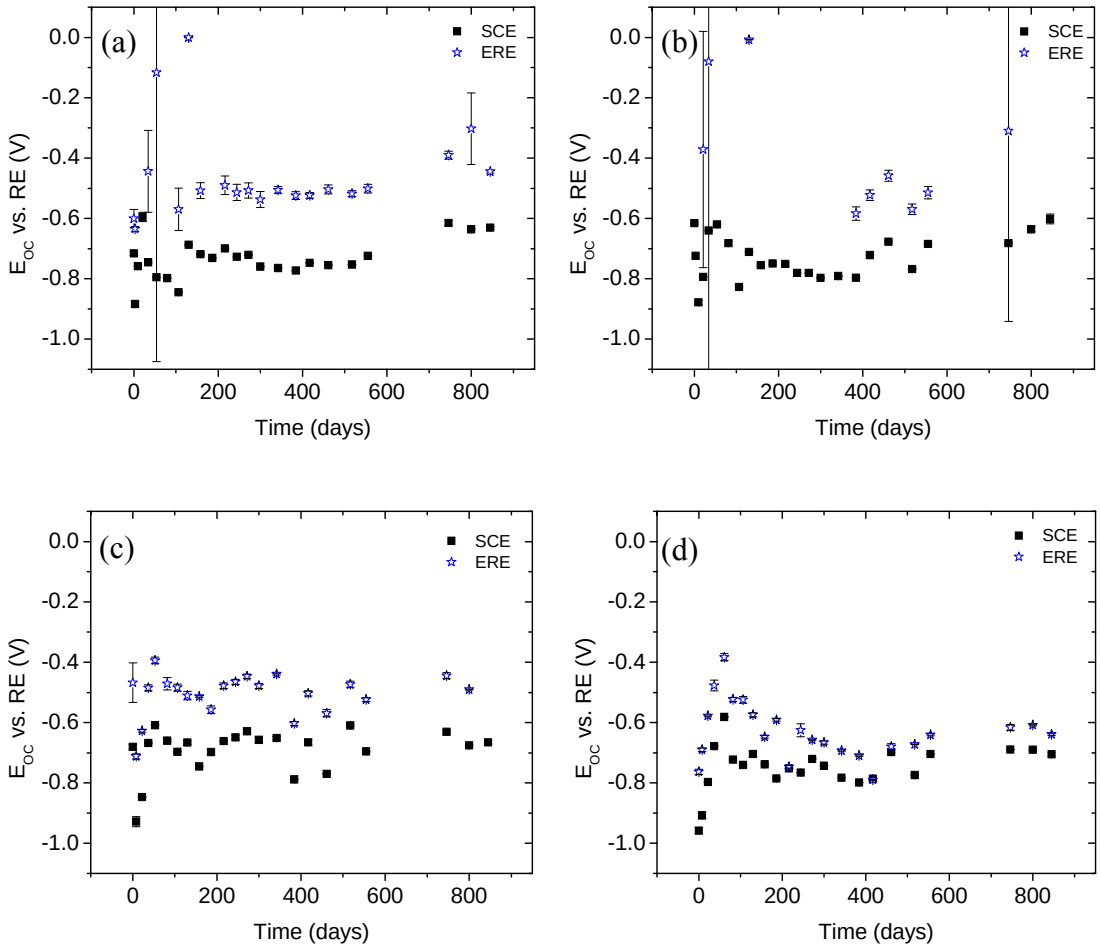

Figure 3.13. Mg primer / AA 2024-T3 mean corrosion potential data for chemically oxidized Ag wires (a) 1 mil, 0.06 M $FeCl_3$, (b) 1 mil, 0.03 M $FeCl_3$, (c) 2 mil, 0.06 M $FeCl_3$, and (d) 2 mil, 0.03 M $FeCl_3$.

The 1 mil Ag wires oxidized with 0.06 M $FeCl_3$ gave better results than the 0.03 $FeCl_3$. More than half of the data points in Figure 3.13 (b) are not shown here because they lie outside the plotted range, generally at a value of 5.0 V vs ERE.

Excellent results were observed for the 2 mil Ag wire EREs, prepared by chemical oxidation. Both 0.06 M $FeCl_3$ and 0.03 M $FeCl_3$ show very small standard deviations in Figures 13 (c) and (d). Additionally, the mean corrosion potential is approximately 0.2 V positive of the corresponding SCE standard data point. In Figure 3.13 (d), this distance narrows to 0.15 to 0.10 V as the experiment progresses beyond 200 days.

The experimental ERE corrosion potential measurements are expected to fall within -0.2 to -0.8 V vs ERE for a Mg-rich primer / AA 2024-T3 coating system, depending on the chloride ion concentration at the ERE. Standard deviations greater than 0.05 V negate the experimental significance in the corrosion potential analysis and are not desired. The experimental outliers and the effect of chloride ion concentration are discussed within Section 3.4.2.2.1.

Very good results were observed for all replicates in the 2 mil Ag wire set prepared by chemical oxidation in 0.03 M $FeCl_3$. The replicates in the 1 mil Ag wire set were less consistent.

3.3.2.1.2. Electrochemically anodized EREs

The results for the electrochemically anodized 1 mil and 2 mil Ag wire are shown in Figure 3.14. Approximately half of the data points were 0.1 to 0.2 V positive of the SCE standard for the 1 mil wire. The other half of the data points either lie outside of the plotted range or have large standard deviations. The data for the 2 mil Ag wire was also not favorable, and the potential difference between the experimental ERE and the SCE standard was unpredictable.

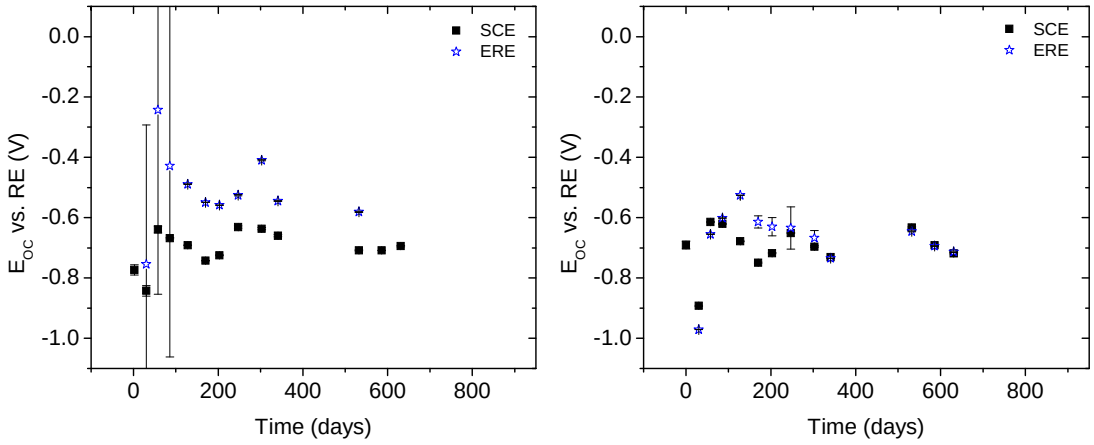

Figure 3.14. Mg primer / AA 2024-T3 mean corrosion potential data for electrochemically anodized Ag wires (a) 1 mil and (b) 2 mil.

3.3.2.3. Zn-rich coating system

3.3.2.3.1. Chemically oxidized EREs

Poor corrosion potential results were obtained from the 1 mil Ag wires prepared by chemical oxidation (Figure 3.15). The most obvious feature in the figure is the occurrence of ERE data points at 0.0 V vs RE. This value is not an accurate representation of the electrode's electrochemical environment and is regarded as an outlier, to be discussed in Section 3.4.3.2.2. The ERE data points which are not at 0.0 V vs ERE have large standard deviations, indicating that the measurements were not stable over the course of the acquisition period. The SCE standard data in Figure 3.15 is in the range of -0.65 to -0.85 V vs SCE as expected for a Zn-rich primer [38].

The 2 mil Ag wire experimental ERE results are also poor for both $FeCl_3$ solutions. Nearly all data points in Figure 3.15 (c) are 0.0 V vs ERE. Figure 3.15 (d) shows the ERE data approximately 0.3 V positive to the SCE standard for the first 50 days of immersion, followed by many data points at 0.0 V vs ERE.

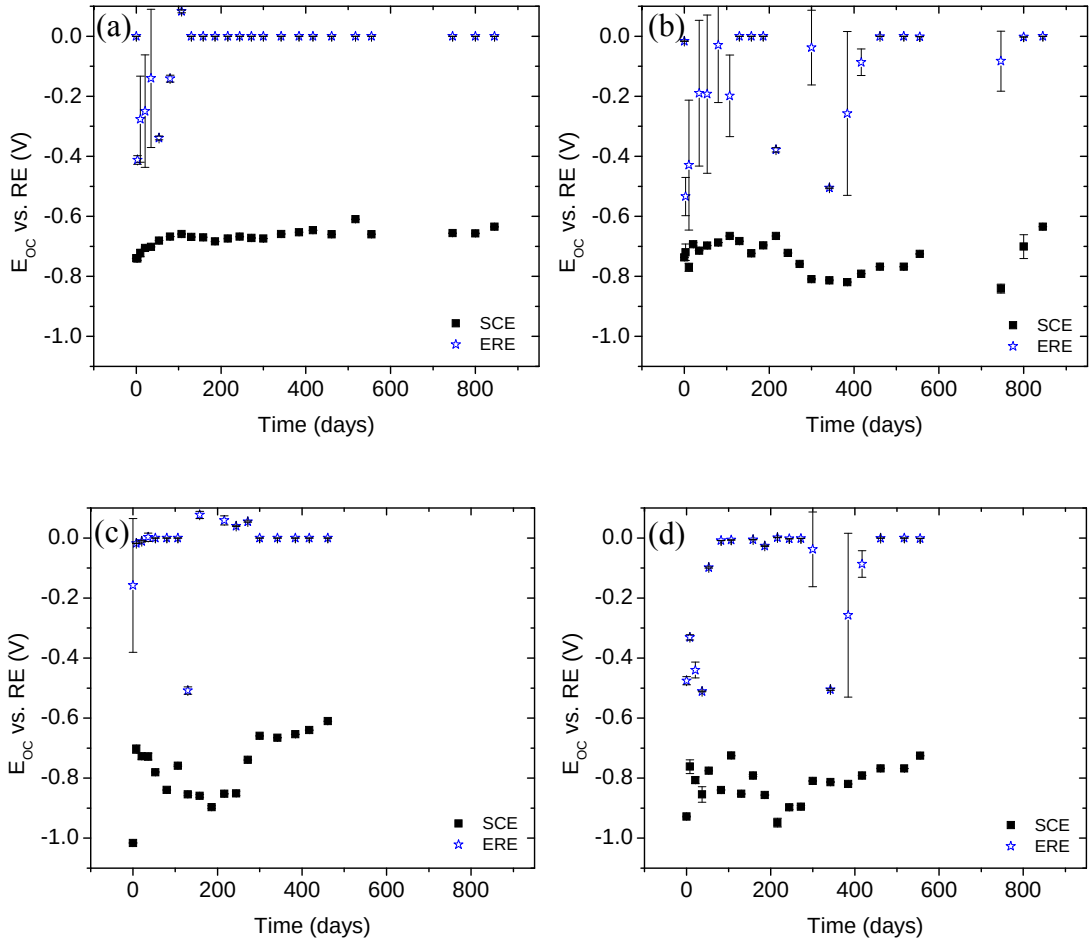

Figure 3.15. Zn primer / steel mean corrosion potential data for chemically oxidized Ag wires (a) 1 mil, 0.06 M $FeCl_3$, (b) 1 mil, 0.03 M $FeCl_3$, (c) 2 mil, 0.06 M $FeCl_3$, and (d) 2 mil, 0.03 M $FeCl_3$.

The chemically oxidized EREs were not successful in obtaining consistent, useful corrosion potential information within a Zn-rich primer.

3.3.2.3.2. Electrochemically anodized EREs

The mean and standard deviation corrosion potential results are given in Figure 3.16 for the electrochemically anodized Ag wires in Zn-rich primer. Poor results were observed by the 1 mil Ag wire. However, somewhat favorable results were observed by the

2 mil wire. A corrosion potential 0.2 to 0.3 V positive to the standard SCE was recorded for a significant portion of the experiment.

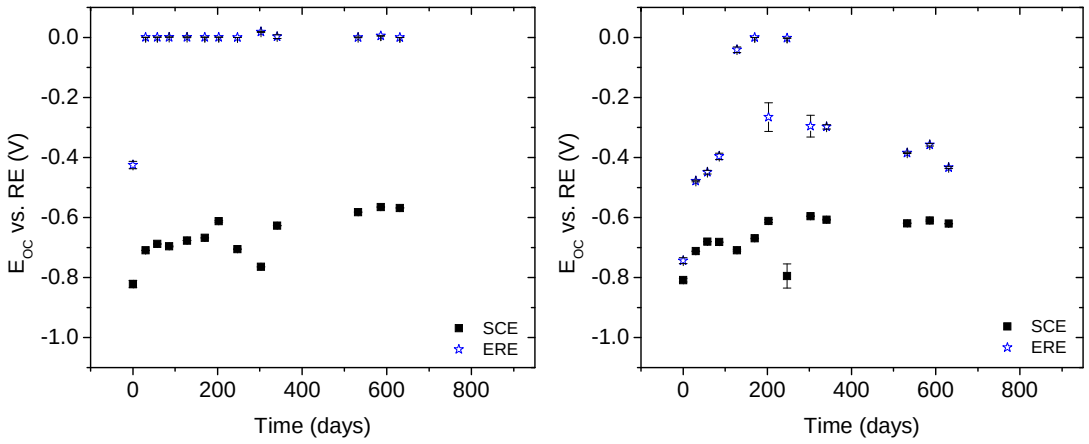

Figure 3.16. Zn primer / steel mean corrosion potential data for electrochemically anodized Ag wires (a) 1 mil and (b) 2 mil.

3.3.3. Potentiodynamic testing

A potentiodynamic experiment was utilized to examine the response of the ERE to an electrode with an externally applied potential. Four replicate experiments were performed using the Mg-rich primer sample set with an ERE prepared by chemical oxidation of 2 mil Ag wire in 0.03 M $FeCl_3$. This set was chosen based on the high reproducibility and stability observed by the ERE corrosion potential measurements.

Excellent results were observed by all four samples for the potential range examined. Figure 3.17 presents one of these samples. The horizontal data points are the rest potentials. The scan data is at the center of the plot with a high positive slope.

The measured corrosion potential is very stable throughout the applied potential scan. It is also noted that there is a slight shift in the potential measurement before and after the scan. This is attributed to a change in the corrosion potential of the substrate, a result of

the polarization that occurs during a potentiodynamic scan [16]. The system returns to steady-state over a time period greater than 2000 seconds.

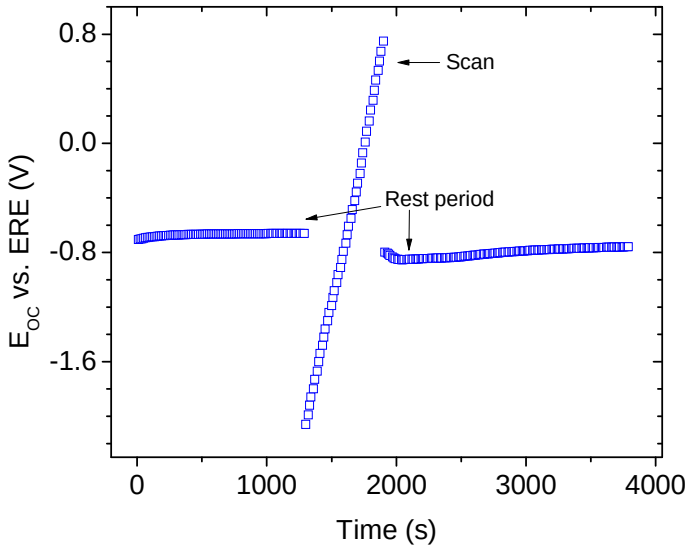

Figure 3.17. Corrosion potential results for 0.005 V/s scan rate.

3.4. Discussion

3.4.1. Analysis of Ag wire morphology and chemical composition

SEM analysis was performed to characterize the change in surface structure before and after the formation of a Ag/AgCl reference electrode. The photomicrographs indicated that a smooth Ag wire surface structure was replaced by a rough, crystalline material. A slight increase in the measured diameter was observed, indicating that material is deposited on the surface. The approximate thickness of the layer is 1 μm.

EDX was performed to chemically analyze the results of this process. The Ag and Cl maps in Section 3.3.1 confirm that the composition of the deposited layer is AgCl.

A series of experiments was performed using the 0.03 M $FeCl_3$ chemical oxidation process. Ag wire (2 mil) electrodes were formed with immersion times of < 1, 30, 60, 90,

and 120 seconds. The results are not shown here. An obvious change occurred to the surface of the Ag wire after the < 1 second experiment. Additionally, no significant further changes were observed for 90 and 120 seconds, compared to 60 seconds. For this reason, the 60 second immersion time was maintained for chemical oxidation in 0.03 M $FeCl_3$.

3.4.2. Corrosion potential monitoring

An experimental ERE was evaluated for corrosion potential measurement using two sacrificial coating systems and a SCE standard reference electrode for comparison. Coating degradation was accelerated using continuous immersion in 5% NaCl salt solution. The feasibility of the experimental ERE was determined under these conditions.

Two criteria must be satisfied to consider the experimental ERE a viable potential monitoring device. First, the measured values must be logical with respect to the Ag/AgCl redox potential under prescribed environmental conditions as well as the respective coating system's metal-rich primer/substrate mixed potential. Second, they must show stability in their measurement. This is justified by a consistent measurement with respect to the SCE standard.

3.4.2.1. Uncoated Ag/AgCl wire reference electrode

Prior to embedding the Ag wire reference electrode in a coating system, corrosion potential measurements were performed to screen each electrode. Reference electrodes with unsatisfactory measurements were not used in the ERE data sets presented here. On a few occurrences, Ag wires with unsatisfactory results were re-oxidized/anodized and retested until a stable reference potential formed.

The impact of [Cl^-] on the measured corrosion potential is demonstrated in Figure 3.18. A Mg-rich coating system on AA 2024-T3 was measured for its corrosion potential.

The potential was recorded using a standard saturated Ag/AgCl reference electrode and the Ag wire reference electrode. The standard Ag/AgCl RE is encased in saturated KCl solution. The Ag wire RE is exposed to the 5% NaCl immersion solution.

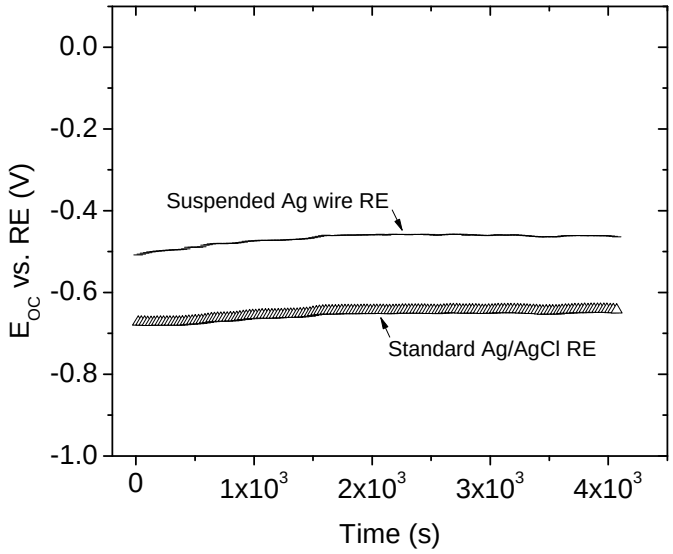

Figure 3.18. Ag/AgCl Corrosion potential for as suspended wire and standard RE.

Figure 3.18 shows the measured potential is 0.18 V positive of the standard Ag/AgCl. This is a result of a lower [Cl^-]. The Ag wire corrosion potential data in Figure 3.18 also represents satisfactory measurement by the experimental reference electrode. The values are both logical and marked by a stable potential difference with respect to the standard Ag/AgCl reference electrode. The example was taken from the set of 2 mil Ag wires chemically oxidized in 0.03 M $FeCl_3$.

Screening of the Ag wire reference electrodes was performed using a SCE as a stable potential reference. The corrosion potential was measured versus each experimental Ag wire reference electrode. Figure 3.19 gives the results for the electrochemically

oxidized data sets. The average for the 1 mil wire was 0.106 V vs ERE while the 2 mil wire was 0.102 V vs ERE, as represented by solid lines.

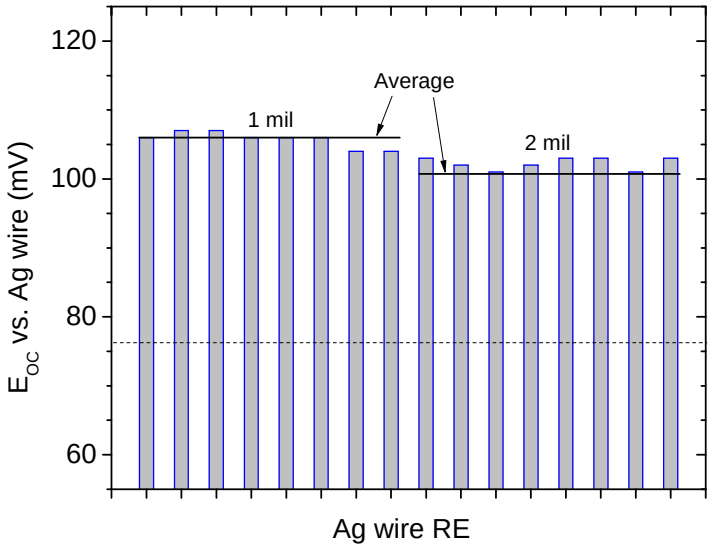

Figure 3.19. Electrochemically anodized RE potential for screening of 1 and 2 mil Ag wire.

The theoretical potential of a reference electrode due to the concentration of species in a redox couple is determined by the Nernst equation.

$$E = E^{0}_{Ag\,/\,AgCl} - 2.303\frac{RT}{nF}\log[Cl^{-}] \tag{3.9}$$

E is the theoretical potential, $E°$ is the standard state potential for the Ag/AgCl redox reaction, R is the universal gas constant, T is temperature, n is the number of electrons transferred in the reaction, F is Faraday's constant, and C_{Cl^-} is the chloride ion concentration [16]. While a number of experimental variables exist, this is reduced to

$$E = -0.046 - 0.059\log[Cl^{-}] \tag{3.10}$$

at 298° K vs. SCE.

The solution was DHS for the potential measurements represented in Figure 3.19. This has a [Cl^-] equal to 8.6 x 10^{-3} M which gives a theoretical value of E = 0.076 V vs RE from Equation 3.10**.** The dotted line denotes this value in Figure 3.19.

The values for the Ag wires are slightly more positive than the theoretical value with the 1 mil Ag wire slightly higher than the 2 mil (Figure 3.19). The source of this difference is likely of geometrical origin since curvature effects on surface potentials usually occur at smaller radii of curvature [48]**.** The disparity between the two wire sizes is less than 0.010 V vs RE and is well within the accuracies desired for the intended applications of the Ag wire reference electrode. One important parameter, [Cl^-], is unknown at the surface of the ERE. The equation produces a 0.059 V shift per order of magnitude decrease in [Cl^-]. The Ag/AgCl electrode has been utilized for [Cl^-] sensors for pipeline and concrete structures through the relationship in Equation 3.10 [20, 22-23, 40-41, 49-51]. A supplemental reference electrode (SCE in its present form) is used to measure E, and the equation is solved for [Cl^-]. The Ag wire reference electrode examined in this paper could also be used a [Cl^-] sensor although it is not the intended application. The relationship between [Cl^-] and the corrosion potential measured by ERE vs SCE is presented graphically in Section 3.4.2.2.1.

3.4.2.2. Embedded Ag/AgCl wire reference electrode

Corrosion potential measurements were measured for 1 mil and 2 mil Ag wire embedded reference electrodes, formed under chemical oxidation and electrochemical anodization methods. The purpose of the multi-method approach is to determine which treatment gave the most favorable results. The Ag wires were embedded in two sacrificial coating systems and examined over time as corrosion potential monitoring devices.

Polymers greatly reduce the rates of diffusion for water, oxygen, and ions within a coating system [52]. It is assumed, to a first approximation, that $[Cl^-]$ at the surface of the ERE is sufficiently stable to meet the accuracy requirements for a corrosion potential monitoring device. Though the requirements have not been established, it is anticipated to be tens of millivolts for sacrificial protection applications.

The sacrificial coating is observed under constant immersion conditions. Wet-dry cycling occurs during most natural exposure conditions but was not examined here. Shi [53] has characterized the time dependence of moisture transportation to find that drying occurs on a slow timescale below the coating's T_g—approximately 30 wt.% of the water is retained after 12 hours of drying for a saturated epoxy. Water content was not estimated for the coatings tested in this experiment, and it was assumed to be saturated. During Ag wire ERE operation in natural exposure conditions it would be especially useful to estimate the water content. An estimate could be obtained using relative humidity and temperature, modeling for the specific coating system.

As a result of the unknown $[Cl^-]$ at the surface of the ERE, much attention was given to defining satisfactory corrosion potential measurements for the experimental ERE in the sample coatings. The stable potential difference with respect to the SCE standard was used to verify the assumed constant $[Cl^-]$.

Dramatic differences were observed between the unsatisfactory corrosion potential measurements for Mg-rich and Zn-rich primers. No significant differences were observed for satisfactory measurements, however.

This initial step in defining the satisfactory corrosion potentials is to understand the corrosion behavior of the sacrificial coating system. Table 3.4 gives the corrosion potential

for the metals and alloys within these coating systems. The primer pigment and substrate couple to produce a mixed corrosion potential. This value is intermediate of the independent corrosion potentials and not necessarily their mean.

Table 3.4 Corrosion potentials, measured in flowing seawater, for metals and alloys used in this experiment.

Name	Potential (V vs SCE)
Steel	-0.60 to -0.70
Aluminum Alloys	-0.70 to -0.90
Zinc	-0.98 to -1.03
Magnesium	-1.60 to -1.63

During active corrosion protection a mixed corrosion potential is observed. However, sacrificial protection is finite and dependent on the electrical connectivity of the primer pigment and substrate. Once the electrical resistance between these materials surpasses a critical value, the substrate becomes the lone circuit component and the corrosion potential shifts to the substrate value. The sacrificial protection is exhausted and the substrate must be stripped and recoated in order to preserve its structural integrity. The purpose of the experimental ERE is to monitor the corrosion potential and to identify the point at which sacrificial protection is exhausted. Therefore, the ERE requires an accuracy which allows the operator to make this distinction with 95% confidence or greater.

3.4.2.2.1. Mg-rich coating system

Mg-rich primer was used in this experiment as a sacrificial coating for AA 2024-T3 panels. Localized corrosion is the most susceptible form of corrosion for this substrate [27]. Sacrificial protection occurs when a mixed corrosion potential is observed. Battocchi [54] has measured the Mg pigment corrosion potential to be -1.6 V vs SCE in 0.1% NaCl while the AA 2024-T3 is -0.5 V vs SCE in the same solution. The mixed potential for Mg primer

/ AA 2024-T3 is approximately 0.35 V negative of the corrosion potential for the bare substrate [47].

During the activation of sacrificial protection, the corrosion potential quickly moves from the substrate value to as high as -1.1 V or -1.2 V vs SCE and then to -0.8 to -0.9 V vs SCE. The corrosion potential often stabilizes in this range for long periods. Subsequently, it slowly drifts in the positive direction. Sacrificial protection is no longer available once the value for the bare substrate is reached. Practical requirements for field use are to maintain a value 0.15 V negative of the free corrosion potential to ensure complete protection [55-56].

The laboratory SCE was used as a standard in these experiments to measure the Mg primer / AA 2024-T3 corrosion potential. The present objective does not require that the sacrificial protection be active, but that its status is distinguished by the experimental ERE monitoring device.

Mixed results were observed for the experimental ERE in a Mg-rich primer coating system. The 2 mil Ag wires performed better than the 1 mil Ag wire. It is suggested that the 1 mil Ag is too brittle. No improvement was observed in electrochemical anodization over the chemical method, and the Ag wires formed in 0.03 M $FeCl_3$ outperformed those in 0.06 M $FeCl_3$.

The chemical oxidation of 2 mil Ag wire in 0.03 M $FeCl_3$ produced favorable results for all four replicates. Linear fitting and smoothing were applied to the data for two samples in Figure 3.20. Similar treatment has been given to EIS data for the application of lifetime prediction [57-58]. A linear fit is given in Figure 3.20 (a) beyond 100 days of exposure. The coating system experiences stable sacrificial protection in this region. The slight positive slope implies a steady decline of this protection. The 95% confidence limit

is illustrated by the dotted lines. Equipment operators or maintenance personnel can expect the mean corrosion potential to fall within this range.

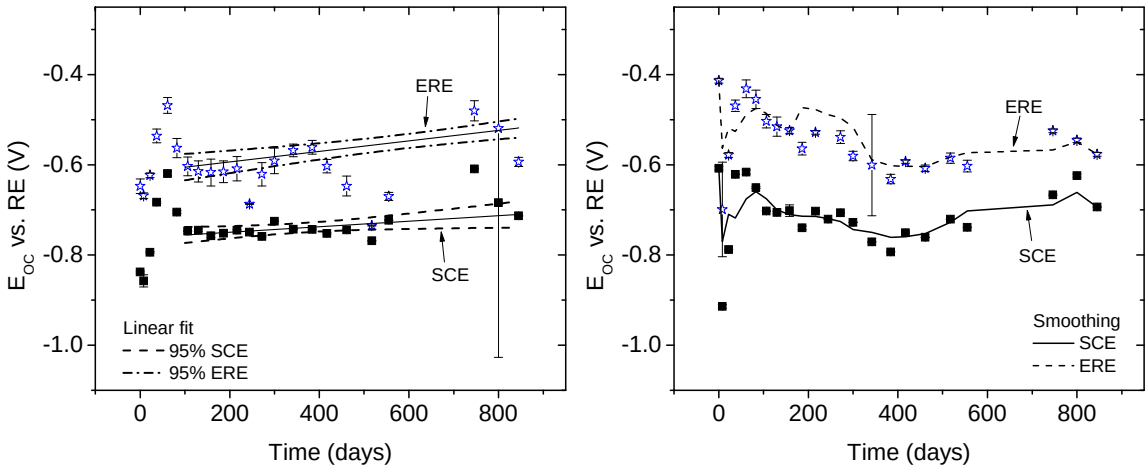

Figure 3.20. Statistical analysis is performed on mean corrosion potential data to show a (a) linear fit with 95% confidence bands and (b) smoothed trend line.

Figure 3.20 (b) shows a smoothed trend line for the entire experiment. This assists the viewer in gauging the stability of the experimental ERE mean data with respect to the SCE standard. The trend lines are very similar which suggests excellent correlation between the experimental ERE and the SCE standard values. The trend line was obtained by an adjacent-averaging method. All plots have been prepared using Origin Lab (Northampton, MA) software, version 8.1.

All data in Figure 3.20 is experimentally significant for the experimental ERE with the exception of the 800 hours data point in Figure 3.20 (a). A few noticeable standard deviations are observed between 100 and 300 hours but they are all within 0.05 V which is estimated as an acceptable, confident range for an operator.

The experimental corrosion potential is 0.1 to 0.2 V positive of the SCE standard based on the linear fitting and smoothing in Figure 3.20. This is consistent with other

sample sets examined. The correlation between experimental ERE corrosion potential and SCE standard is given in Figure 3.21 to estimate [Cl^-]. The solid trend line is Equation 3.10. Common Cl^- solutions are also included on the figure. The observed values are shaded, and the [Cl^-] is estimated to be on the order of 10^{-3} to 10^{-4} M within the Mg primer coating system. This is roughly one to two orders of magnitude less than DHS.

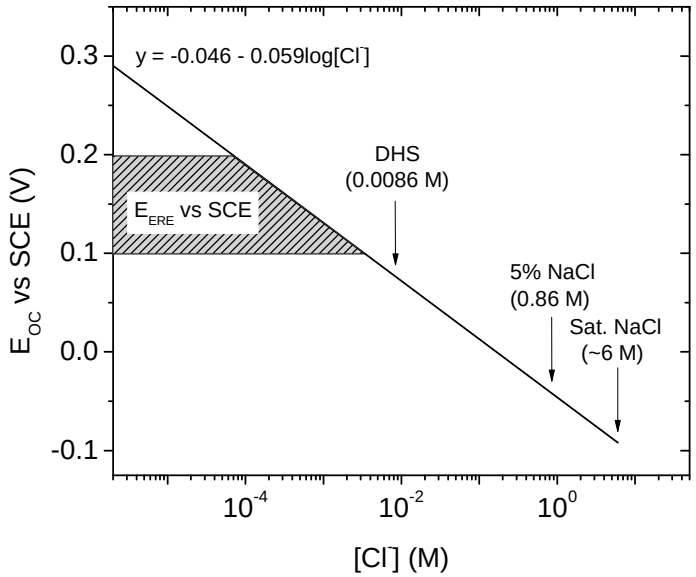

Figure 3.21. Corrosion potential versus [Cl^-].

An ERE may be used for constant data acquisition/corrosion potential monitoring or intermittent, scheduled monitoring. The previous experiments utilize the mean corrosion potential, which is an example of the latter. An additional experiment was performed for a long time period to provide an example of the former.

The raw corrosion potential data for 2 mil Ag wire formed by chemical oxidation is shown in Figure 3.22. It is plotted from -1.0 to 5.5 V vs RE to show all data. The test period was greater than 6 days. This figure presents the information that an operator or maintenance personnel would be tasked with understanding and using to form decisions.

The data also highlights the disparity between accurate corrosion potential measurements and experimental outliers. A new, uncoated Ag wire formed by the same conditions was suspended in the solution and used as a standard for the measurement. Corrosion potentials more negative than -0.2 V vs RE are experimentally significant. The values at 5.0 V vs RE are the result of an instrumental limitation. And all values in between are the result of charging or high resistance, leading to the instrumental limitation value.

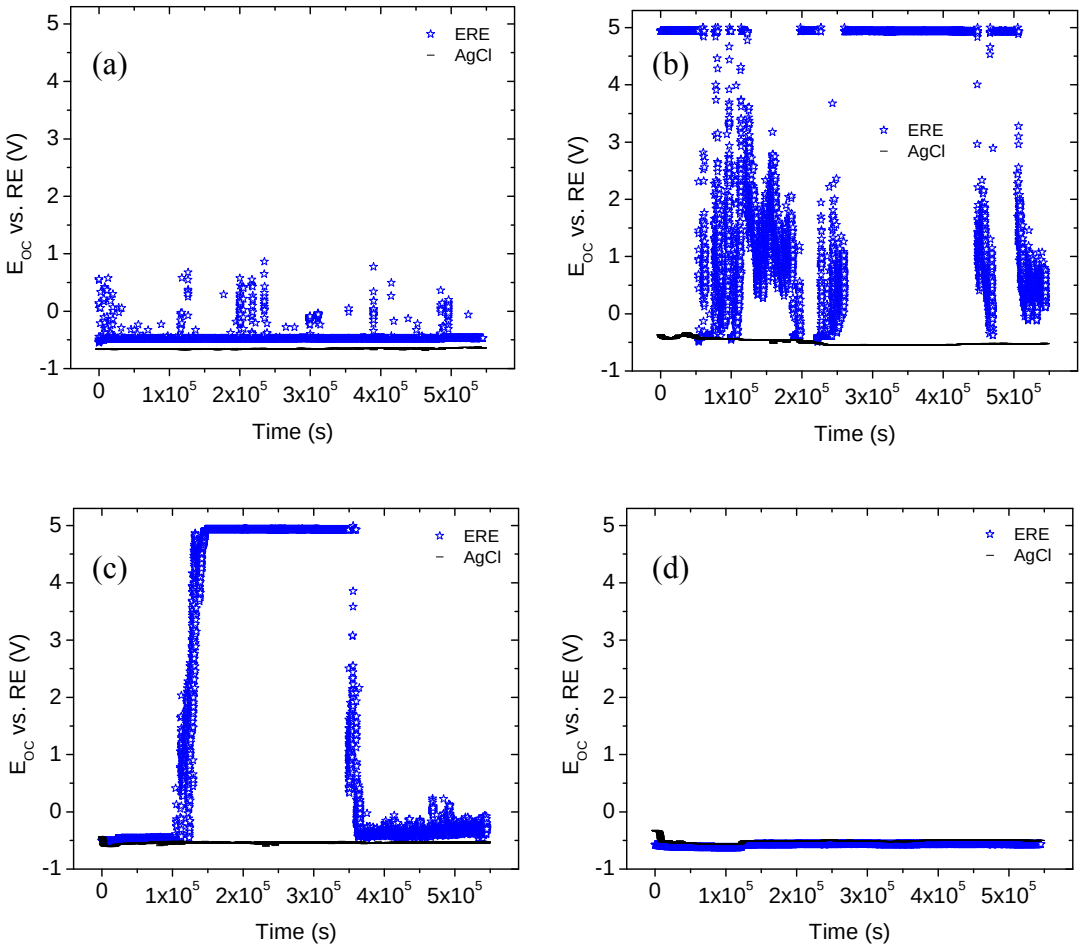

Figure 3.22. Raw corrosion potential measurements for suspended wire Ag/AgCl and ERE, chemically oxidized in (a) 1 mil, 0.06 M $FeCl_3$, (b) 1 mil, 0.03 M $FeCl_3$, (c) 2 mil, 0.06 M $FeCl_3$, and (d) 2 mil, 0.03 M $FeCl_3$.

Listed in descending order, Figure 3.22 (d), (a), (c), and (b) provide the most useful information as a corrosion potential monitoring device. The x-axis for Figure 3.22 (d) has been expanded in Figure 3.23 to show experimental detail. It is here that the electrode will allow inferences on the status of the sacrificial protection. The ERE corrosion potential could be measured periodically versus a standard reference electrode to estimate [Cl^-]. This could be applied to field use of a constant corrosion potential monitoring device as a calibration of the ERE for the operator.

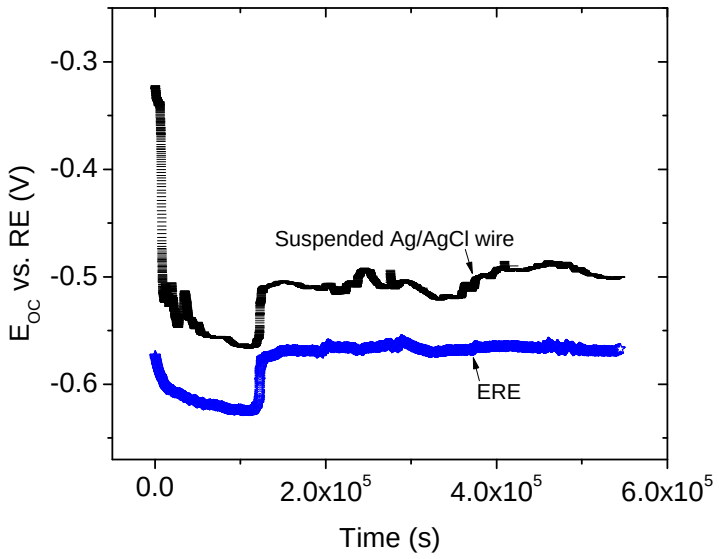

Figure 3.23. The x-axis is expanded to show the detail from Figure 3.22 (d).

A positive shift was observed at the beginning of many Mg primer / AA 204-T3 corrosion potential experiments. This can be used to describe the slightly higher standard deviation observed for many ERE mean corrosion potentials, compared to the SCE. It is suggested that this transient is a result of a decrease in [Cl^-] which persists until a stable redox potential is reached. An experiment was performed to observe the effect of this transient. Two corrosion potential measurements were carried out in succession with a 45

minute rest period in between. The 2 mil Ag wire ERE chemically oxidized by 0.03 M $FeCl_3$ was utilized to guarantee practical data. Figure 3.24 gives the results of this experiment.

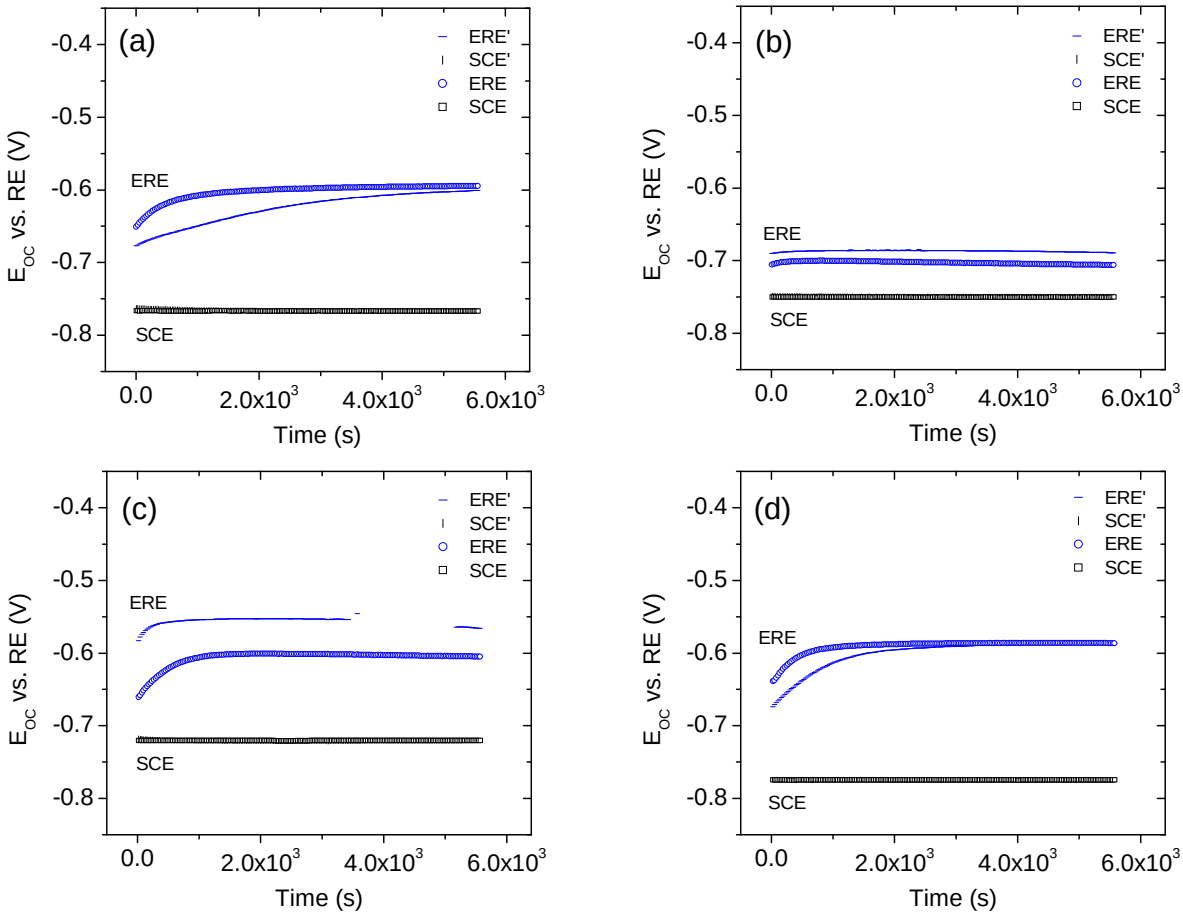

Figure 3.24. Measurements taken at two times, separated by a 45 minute rest period. Full set of aluminum samples for EREs prepared by chemical oxidation of 2 mil Ag wire with 0.03 M $FeCl_3$.

A transient decay to a more positive corrosion potential is observed for the initial measurement (ERE' and SCE') in all samples, although it is very small in Figure 3.24 (b). The same is true for the second measurement (ERE and SCE). For Figure 3.24 (a) and (d), the same value is reached for both measurements, despite the transient, which suggests that the steady-state corrosion potential environment has not changed. In Figure 3.24 (a) the

initial transient occurs over a period of 1.5 hours while the second is 0.5 hours. And in Figure 3.24 (d) they are 1 hour and 0.3 hours, respectively. In both cases steady-state is reached more quickly during the second corrosion potential measurement.

In descending order, the most useful data for this experiment is Figure 3.24 (d), (a), (b), and (c). Figure 3.24 (c) has an inconsistency between 3.5 x 10^{-4} and 5.0 x 10^{-4} seconds. Values of 5.0 V vs RE were recorded in this window, which reduce the confidence for the entire measurement. Figures 3.24 (a), (c), and (d) have [Cl^-] between 10^{-3} and 10^{-4} M. This is consistent with most above calculations. However, Figure 3.24 (b) is closer to 10^{-2} M according to Figure 3.21.

3.4.2.2.2. Zn-rich coating system

Zn-rich primer was used in this experiment as a sacrificial coating for steel. The Zn pigment corrosion potential is -1.0 V vs SCE while the steel is -0.6 to -0.7 vs SCE, both measured in artificial seawater. Sacrificial protection occurs when a mixed potential is observed, generally at least 0.15 V negative of the free corrosion potential for the bare substrate [56].

The corrosion potential behavior for Zn primer / steel is similar to that described in Section 3.4.2.2.1 and will not be repeated here. The main difference is that the corrosion potential range for the activation period is less extreme. References [38, 58-59] also describe Zn primer / steel sacrificial protection.

Poor results were observed for the ERE in a Zn-rich primer in all sample sets. The 2 mil Ag wire results were generally more favorable than the 1 mil results. The 2 mil Ag wire formed in 0.03 M $FeCl_3$ was superior to all other chemical oxidation sample sets. It was common for the experimental ERE to show satisfactory measurements at the beginning of

exposure to DHS. The mean corrosion potential became more positive to the SCE standard with each subsequent measurement. The value rested at 0.0 V vs RE. This unsatisfactory measurement was reached within 100 days of exposure. The possibility of Zn or Fe experimental ERE poisoning in the Zn primer / steel system is examined in Chapter 4.

One of the 2 mil Ag wire reference electrodes formed by electrochemical anodization contained only a few unsatisfactory measurements during the course of the examination. Fitting and smoothing are applied to this sample (Figure 3.25). Third order polynomial fitting was used in Figure 3.25 (a). This fit is applied to the entire range as a result of the smooth activation period at the beginning of the exposure. The three data points near 0.0 V vs RE are not an accurate representation of the corrosion potential and were excluded from the fit. The dotted lines represent the 95% confidence limits.

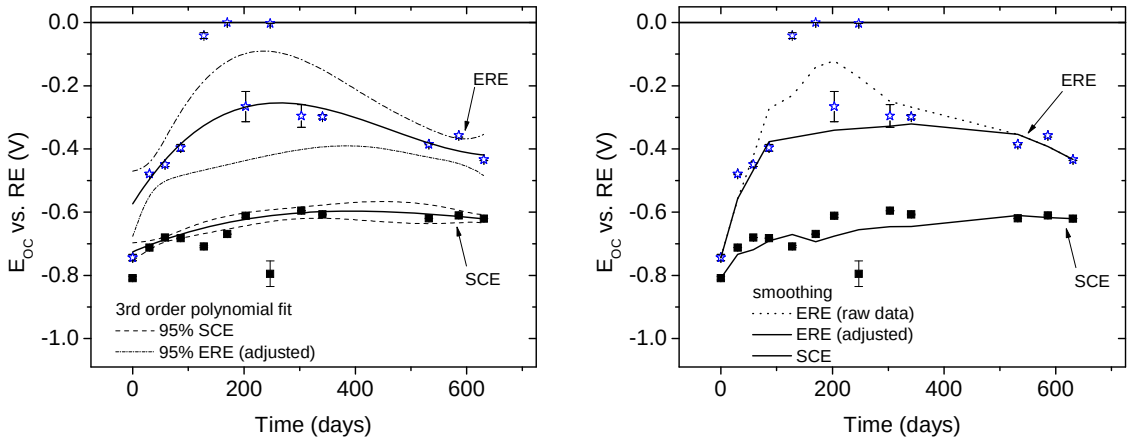

Figure 3.25. Statistical analysis is performed on Zn primer / steel mean corrosion potential data to show a (a) third order polynomial fit with 95% confidence bands and (b) smoothed trend line.

Figure 3.25 (b) was given a smoothed trend line. Two trend lines were given for the experimental ERE. The dotted line includes all mean corrosion potential data while the solid line excludes the three unsatisfactory data points near 0.0 V vs RE.

Figures 3.25 (a) and (b) are the same data set and good correlation is seen between the statistical analysis methods in each. The confidence limits for the experimental ERE data must be narrower to consider it as a potential monitoring device. The present fitting would be much improved if the two data points with significant standard deviations are removed; however, the overall objective is to improve the precision of the measurements.

From Figure 3.25 and those in Section 3.3.1.3, the unsatisfactory measurements for Zn primer / steel appear at 0.0 V vs RE and were discarded during the statistical analysis. This is an instrumental limitation and likely represents an insufficient resistance to make a measurement, i.e., a short circuit. Murray [60] describes a short circuit to occur when the coating impedance is within two orders of magnitude of the measuring device. The cause is not well understood, and as discussed in Section 3.4.2.2.1, the opposite effect—5.0 V vs RE—was observed for the Mg primer / AA 2024-T3 system.

The measurements below -0.2 V vs RE are defined as experimentally significant for the experimental ERE. A potential difference of -0.2 V to -0.3 V is observed in the Zn primer / steel system. The $[Cl^-]$ is 10^{-4} to 10^{-5} M according to Figure 3.21. This is lower than that observed for the Mg primer system. However, a higher volume of Zn primer / steel corrosion potential data is required to determine experimental significance. The effect of Zn pigments on experimental ERE measurements is examined further in Chapter 4.

3.4.3. Potentiodynamic studies of the ERE

Potentiodynamic experiments were performed to gauge the stability of the experimental ERE to externally applied potentials. This potential range was -1.5 to 1.5 V vs RE. This is more extreme than would be experienced during regular corrosion potential

monitoring, even for the most active system. Additionally, the measurement provided an indication of the accuracy of the experimental ERE data.

Excellent results were obtained and the experimental ERE showed quick response and electrode stability over a wide range of electrochemical potentials. Figure 3.26 provides a statistical analysis for one of these samples. A dashed line is used to show the experimental rate applied to the coating system. All data points fall very close to this line. A solid line is used to show the calculated rate of the experimental ERE data. The value for this is 0.0046 V/s which is comparable to the applied 0.005 V/s. The intended applications of the experimental ERE are well-within the range of this inaccuracy.

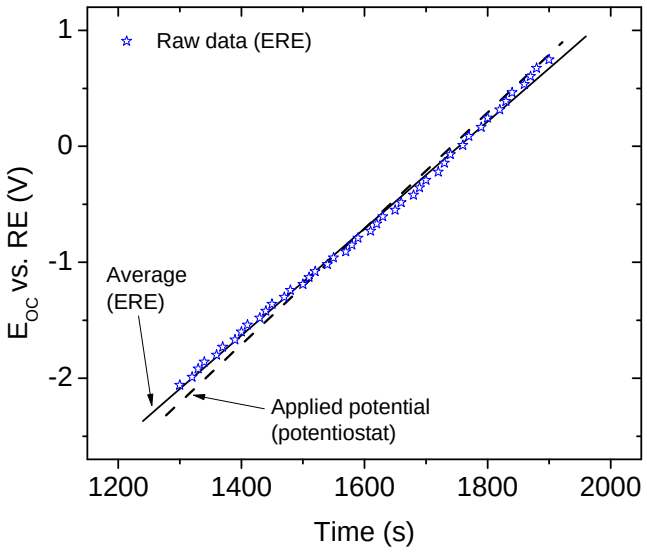

Figure 3.26. Potentiodynamic corrosion potential data and the calculated mean for a scan rate of 0.005 V/s.

The instrumental setup for this experiment is similar to an impressed cathodic protection system with an ERE for corrosion potential feedback near the substrate. This is demonstrated by potentiostat # 2 and #1, respectively, in Figure 3.9 (Section 3.2.4.3). The

effectiveness of the impressed protection is measured by the experimental ERE results for substrate corrosion potential. This represents an additional possibility for application of the ERE. A related application is examined in Section 6.

3.5. Conclusions

A Ag/AgCl reference electrode was developed using 25 and 50 micron Ag wire. SEM and EDX confirmed that a thin, 1 to 2 μm AgCl deposition formed on the Ag wire reference electrodes. The experimental reference electrodes were embedded within Mg-rich primer / AA 2024-T3 and Zn-rich primer / steel coating systems to examine their feasibility as a corrosion potential monitoring device. This is the first use of a reference electrode, embedded between a primer and topcoat, for electrochemical analysis of organic coatings.

Good results were obtained from the Mg primer / AA 2024-T3 coating system. Reference electrodes formed by chemical oxidation in 0.03 M $FeCl_3$ of 2 mil Ag wire gave consistent results for all samples in the set. This was observed by testing for more than 800 days of coating exposure to DHS by constant immersion. The results for corrosion potential monitoring of a Zn primer / steel were inconsistent. Unrealistic measurements at 0.0 V vs ERE were of recorded. The cause for this is explored in Chapter 4.

Based on the corrosion potential results in this Chapter, it is estimated that the ERE within a Mg-rich prime on AA 2024-T3 is, on average, approximately 0.1 to 0.2 V more positive than a measurement made by SCE. Despite the poor Zn-rich primer results, is estimated that the corrosion potential 0.2 to 0.3 V more positive than the SCE standard.

The $[Cl^-]$ is an uncontrolled parameter; however, it appears that the concentration is sufficiently stable within a coating system. The ERE can be used as a $[Cl^-]$ sensor if the corrosion potential is known. The experimental ERE and standard SCE were applied to the

Nernst Equation. The [Cl^-] was estimated at 10^{-3} to 10^{-4} M (and occasionally as high as 10^{-2} M) for the Mg primer / AA 2024-T3 coating system.

Potentiodynamic experiments were performed to gauge the stability of the experimental ERE under an applied potential. Excellent results were observed and experimental scan rate of 0.0046 V/s was calculated. This is in good correlation with the applied 0.005 V/s. The potentiodynamic results suggest that ERE can be used as a corrosion potential measuring device for control of impressed cathodic protection systems. A related application is examined in Chapter 6.

3.5. References

[1] G.H. Koch, M.P.H. Brongers, M.G. Thompson, Y.P. Virmani and J.H. Prayer, Corrosion Costs and Preventive Strategies in the United States, in, Federal Highway Administration, Office of Infrastructure Research and Development, McLean, VA, 2001, pp. 62.

[2] X. Zhao, H. Gao, G. Zhang, B. Ayhan, F. Yan, C. Kwan and J.L. Rose, Active health monitoring of an aircraft wing with embedded piezoelectric sensor/actuator network: I. Defect detection, localization and growth monitoring, Smart Materials and Structures, 16 (2007) 1208-1217.

[3] A.R. Wilson and R.F. Muscat, Novel thin wire paint and sealant degradation sensor, Sensors and Actuators A, (2010).

[4] J.B. Ong, Z. You, J. Mills-Beale, E.L. Tan, B.D. Pereles and K.G. Ong, A wireless, passive embedded sensor for real-time monitoring of water content in civil engineering materials, IEEE Sensors Journal, 8 (2008) 2053-2058.

[5] F. Pruckner, J. Theiner, J. Eric and G.E. Nauer, In-situ monitoring of the efficiency of the cathodic protection of reinforced concrete by electrochemical impedance spectroscopy, Electrochimica Acta, 41 (1996) 1233-1238.

[6] J.P. Broomfield, K. Davies and K. Hladky, The use of permanent corrosion monitoring in new and existing reinforced concrete structures, Cement & Concrete Composites, 24 (2002) 27–34.

[7] V. Giurgiutiu, Structural Health Monitoring with Piezoelectric Wafer Active Sensors, Academic Press, Burlington, MA, 2008.

[8] Health Monitoring of Aerospace Structures - Smart Sensor Technologies and Signal Processing, John Wiley & Sons, Ltd, Munich, Germany, 2004.

[9] J.M. Dilhac, M. Bafleur, J.Y. Fourniols, C. Escriba, R. Plana, D. Dragomirescu, L. Assouère, P. Pons, H. Aubert and C. Buchheit, Crossfunctional design of wireless sensor networks applied to aircraft health monitoring, in: International Workshop on Structural Health Monitoring, Stanford, United States, 2009.

[10] K. Diamanti and C. Soutis, Structural health monitoring techniques for aircraft composite structures, Progress in Aerospace Sciences, 46 (2010) 342–352.
[11] P.S. Marsh and D.M. Frangopol, Lifetime multiobjective optimization of cost and spacing of corrosion rate sensors embedded in a deteriorating reinforced concrete bridge deck, Journal of Structural Engineering, 133 (2007) 777-787.
[12] S.D. Glaser, H. Li, M.L. Wang, J. Ou and J. Lynch, Sensor technology innovation for the advancement of structural health monitoring: a strategic program of US-China research for the next decade, Smart Structures and Systems, 3 (2007) 221-244.
[13] G. Park, T. Rosing, M.D. Todd, C.R. Farrar and W. Hodgkiss, Energy harvesting for structural health monitoring sensor networks, Journal of Infrastructure Systems, 14 (2008) 64-79.
[14] D.A. Jones, Principles and Prevention of Corrosion, 2nd ed., Prentice Hall, Upper Saddle River, NJ, 1996.
[15] C. Christodoulou, G. Glass, J. Webb, S. Austin and C. Goodier, Assessing the long term benefits of impressed current cathodic protection, Corrosion Science, 52 (2010) 2671–2679.
[16] K.B. Oldham and J.C. Myland, Fundamentals of Electrochemical Science, Academic Principles, Inc., San Diego, CA, 1994.
[17] S. Muralidharan, T.-H. Haa, J.-H. Baea, Y.-C. Haa, H.-G. Lee, K.-W. Park and D.-K. Kim, Electrochemical studies on the performance characteristics of solid metal–metal oxide reference sensor for concrete environments, Sensors and Actuators B, 113 (2006) 187–193.
[18] S. Muralidharan, V. Saraswathy, K. Thangavel and N. Palaniswamy, Electrochemical studies on the performance characteristics of alkaline solid embeddable sensor for concrete environments, Sensors and Actuators B, 130 (2008) 864–870.
[19] S. Muralidharan, V. Saraswathy, A. Madhavamayandi, K. Thangavel and N. Palaniswamy, Evaluation of embeddable potential sensor for corrosion monitoring in concrete structures, Electrochimica Acta, 53 (2008) 7248–7254.
[20] F.M. Song, S. Brossia, D. Dunn and N. Sridhar, New permanent reference electrode for protection of underground pipelines and storage tanks, Corrosion Engineering, Science and Technology, 40 (2005) 262-269.
[21] M.C. Yan, J.Q. Wang, E.H. Han and W. Ke, Electrochemical measurements using combination microelectrode in crevice simulating disbonded of pipeline coatings under cathodic protection, Corrosion Engineering, Science and Technology, 42 (2007) 42-49.
[22] G.S. Duffó and S.B. Farina, Development of an embeddable sensor to monitor the corrosion process of new and existing reinforced concrete structures, Construction and Building Materials, 23 (2009) 2746–2751.
[23] G.S. Duffó, S.B. Farina and C.M. Giordano, Characterization of solid embeddable reference electrodes for corrosion monitoring in reinforced concrete structures, Electrochimica Acta, 54 (2009) 1010-1020.
[24] G.P. Bierwagen, X. Wang and D.E. Tallman, In situ study of coatings using embedded electrodes for ENM measurements, Progress in Organic Coatings, 46 (2003) 163–175.
[25] K.N. Allahar, Q. Su, G.P. Bierwagen, D. Battocchi, V.J. Gelling and D. Tallman, Examination of the feasibility of the use of in-situ corrosion sensors in army vehicles, in: Tri-Service Corrosion Conference, 2005, pp. 1-11.

[26] Q. Su, The application of embedded sensors for in-situ monitoring of protective coatings on metal substrates, in: Coatings and Polymeric Materials, North Dakota State University, Fargo, ND, 2008, pp. 259.
[27] Q. Su, K. Allahar and G. Bierwagen, Embedded electrode electrochemical noise monitoring of the corrosion beneath organic coatings induced by ac–dc–ac conditions, Electrochimica Acta, 53 (2008) 2825–2830.
[28] K.N. Allahar, Q. Su, G.P. Bierwagen and D.-H. Lee, Monitoring of the AC-DC-AC degradation of organic coatings using embedded electrodes, Corrosion, 64 (2008) 773-787.
[29] K.N. Allahar, B.R. Hinderliter, D.E. Tallman and G.P. Bierwagen, Water transport in multilayer organic coatings, Journal of the Electrochemical Society, 155 (2008) F201-F208.
[30] G.P. Bierwagen, K.N. Allahar, Q. Su and V.J. Gelling, Electrochemically characterizing the ac–dc–ac accelerated test method using embedded electrodes, Corrosion Science, 51 (2008) 95–101.
[31] K.N. Allahar, V. Upadhyay, G.P. Bierwagen and V.J. Gelling, Monitoring of a military vehicle coating under Prohesion exposure by embedded sensors, Progress in Organic Coatings, 65 (2009) 142–151.
[32] Q. Su, K.N. Allahar and G.P. Bierwagen, In situ embedded sensor monitoring of a United States Air Force primer beneath a topcoat exposed to atmospheric humidity and thermal conditions, Corrosion, 66 (2010) 1-12.
[33] D. Wang, D. Battocchi, K.N. Allahar, S. Balbyshev and G.P. Bierwagen, In situ monitoring of a Mg-rich primer beneath a topcoat exposed to Prohesion conditions, Corrosion Science, 52 (2010) 441–448.
[34] K. Allahar, Q. Su and G. Bierwagen, Non-substrate EIS monitoring of organic coatings with embedded electrodes, Progress in Organic Coatings, 67 (2010) 180–187.
[35] K.N. Allahar, Q. Su and G.P. Bierwagen, Electrochemical noise monitoring of the cathodic protection of Mg-rich primers, Corrosion, 66 (2010) 1-12.
[36] B.E. Merten, D. Battocchi, D.E. Tallman and G.P. Bierwagen, Embedded reference electrode for potential-monitoring of cathodic protective systems, Journal of the Electrochemical Society, 157 (2010) C244-C247.
[37] M.E. Nanna and G.P. Bierwagen, Mg-rich coatings: a new paradigm for Cr-free corrosion protection of Al aerospace alloys, Journal of Coatings Technology Research, 1 (2004) 69-80.
[38] S. Felix, R. Barajas, J.M. Bastidas, M. Morcillo and S. Feliu, Study of protections mechanism of zinc-rich paints by electrochemical impedance spectroscopy, in: J.R. Scully, D.C. Silverman and M. Kendig (Eds.) Electrochemical Impedance Spectroscopy, ASTM STP 1188, American Society of Testing and Materials (ASTM), Philadelphia, PA, 1993, pp. 438–449.
[39] C. Hare, Uhlig's Corrosion Handbook, 2nd ed., John Wiley & Sons, New York, 2000.
[40] R.-G. Du, R.-G. Hu, R.-S. Huang and C.-J. Lin, In situ measurement of Cl^- concentrations and pH at the reinforcing steel/concrete interface by combination sensors, Analytical Chemistry, 78 (2006) 3179-3185.
[41] C.P. Atkins, M.A. Carter and J.D. Scantlebury, Sources of error in using silver/silver chloride electrodes to monitor chloride activity in concrete, Cement and Concrete Research, 31 (2001) 1207– 1211.

[42] J. Kittel, N. Celati, M. Keddam and H. Takenouti, New methods for the study of organic coatings by EIS - New insights into attached and free films, Progress in Organic Coatings, 41 (2001) 93–98.
[43] J. Kittel, N. Celati, M. Keddam and H. Takenouti, Influence of the coating–substrate interactions on the corrosion protection: characterisation by impedance spectroscopy of the inner and outer parts of a coating, Progress in Organic Coatings, 46 (2003) 135–147.
[44] A. Nogueira, X.R. Novoa and C. Perez, On the possibility of using embedded electrodes for the measurement of dielectric properties in organic coatings, Progress in Organic Coatings, 59 (2007) 186–191.
[45] A. Miszczyk and T. Schauer, Electrochemical approach to evaluate the interlayer adhesion of organic coatings, Progress in Organic Coatings, 52 (2005) 298–305.
[46] B. Galuszka-Muga, M.L. Muga and R.J. Hanrahan, The effect of gamma radiation on the stability of miniature reference electrodes, Radiation Physics and Chemistry, 75 (2006) 927–931.
[47] D. Battocchi, A.M. Simoes, D.E. Tallman and G.P. Bierwagen, Electrochemical behaviour of a Mg-rich primer in the protection of Al alloys, Corrosion Science, 48 (2006) 1292–1306.
[48] R.J. Stokes and D.F. Evans, Fundamentals of Interfacial Engineering, Wiley-VCH, New York, 1997.
[49] M.A. Climent-Llorca, E. Viqueira-PCrez and M.M. Lopez-Atalaya, Embeddable Ag/AgCl sensor for in-situ monitoring chloride contents in concrete, Cement and Concrete Research, 26 (1996) 1157-I 1161.
[50] M.F. Montemor, J.H. Alves, A.M. Simoes, J.C.S. Fernandes, Z. Lourenco, A.J.S. Costa, A.J. Appleton and M.G.S. Ferreira, Multiprobe chloride sensor for in situ monitoring of reinforced concrete structures, Cement & Concrete Composites, 28 (2006) 233–236.
[51] C.P. Atkins, J.D. Scantlebury, P.J. Nedwell and S.P. Blatch, Monitoring chloride concentrations in hardened cement pastes using ion selective electrodes, Cement and Concrete Research, 26 (1996) 319-324.
[52] R.A. Dickie and A.G. Smith, How paint arrests rust, Chemtech, 10 (1980) 31-35.
[53] X. Shi, B.R. Hinderliter and S.G. Croll, Environmental and time dependence of moisture transportation in an epoxy coating and its significance for accelerated weathering, in: CoatingsTech Conference, Journal of Coatings Technology Research, Indianapolis, IN, 2009.
[54] D. Battocchi, A.M. Simoes, D.E. Tallman and G.P. Bierwagen, Comparison of testing solutions on the protection of Al-alloys using a Mg-rich primer, Corrosion Science, 48 (2006) 2226–2240.
[55] J.M. Leeds, Cathodic protection, coatings, and the NACE external corrosion direct assessment (ECDA) RP 0502-2002, Journal of Corrosion Science and Engineering, 9 (2004).
[56] J. Zhang, K. Sun, X. Huang, J. Yin and S. Peng, Cathodic protection of aluminum hull ship, Chinese Journal of Oceanology and Limnology, 8 (1990) 257-262.
[57] G. Bierwagen, D. Tallman, J. Li, L. He and C. Jeffcoate, EIS studies of coated metals in accelerated exposure, Progress in Organic Coatings, 46 (2003) 148–157.

[58] S. Shreepathi, P. Bajaj and B.P. Mallik, Electrochemical impedance spectroscopy investigations of epoxy zinc rich coatings: Role of Zn content on corrosion protection mechanism, Electrochimica Acta, 55 (2010) 5129–5134.
[59] A. Kalendová, Effects of particle sizes and shapes of zinc metal on the properties of anticorrosive coatings, Progress in Organic Coatings, 46 (2003) 324–332.
[60] J.N. Murray, Electrochemical test methods for evaluating organic coatings on metals: an update. Part II: single test parameter measurements, Progress in Organic Coatings, 31 (1997) 255–264.

CHAPTER 4. ANALYSIS OF EMBEDDED REFERENCE ELECTRODE: *IN-SITU* SALT SPRAY STUDIES AND THE EFFECT OF REPLICATES, PRIMER THICKNESS, AND Zn PIGMENT ON CORROSION POTENTIAL

4.1. Introduction

ASTM B117 is an accelerated weathering method widely used in the coatings industry. The purpose is to accelerate corrosion and coating degradation within a coating system without changing the mechanisms involved. The test condition is constant salt fog (5% NaCl) at 35 °C. Salt spray cabinets are available which maintain these conditions with little maintenance. Other accelerated weathering cabinets can be used to cycle wet and dry corrosive conditions or to introduce ultraviolet rays. They usually provide enhanced and more realistic acceleration of coating degradation than the ASTM B117 exposure protocol but are unnecessary for this preliminary study of the experimental ERE in accelerated weathering conditions.

Sacrificial coating systems are used for the examination of the experimental ERE. The cathodic protection afforded to the substrate can be monitored by measuring the corrosion potential with any reference electrode. Laboratory grade reference electrodes are immersed in a well-defined electrolyte solution, encapsulated by Pyrex™ or some glass containers [1]. This creates a stable electrochemistry to serve as a reference point for corrosion potential measurements [2].

The Ag wire experimental ERE is fabricated at minimal cost and process time. The stable, encapsulated electrolyte solution is replaced with a thin layer of commercial rapid cure epoxy resin. The absence of very controlled permeability boundaries for the Ag ERE electrochemical reaction introduces the risk of electrode poisoning. The metallic pigments in the sacrificial primer are of tens of microns from the presumed electrochemically stable surface of the Ag ERE. Additionally, a well-defined electrolyte solution is not present. It is assumed that the thin layer of epoxy provides a stable anion concentration for the ERE.

The feasibility of Ag wire ERE was reported in Chapter 3. Excellent results were observed for corrosion potential monitoring of the Mg primer / AA 2024-T3 coating system by the 2 mil Ag wire chemically oxidized in 0.03 M $FeCl_3$ [3]. The measurements were performed in excess of 800 days in 5% NaCl constant immersion condition. This prototype was utilized in the subsequent ERE experiments.

A number of variables are examined in this chapter for their effect on measurement of the corrosion potential as recorded by the ERE under varying conditions. The first experiment was the monitoring of corrosion potential *in-situ*, from within the salt spray cabinet. The measurement is made without interruption to the salt spray and provides results for corrosion potential measurements performed during exposure at 35 °C and in a constant, 5% NaCl fog.

The second experiment was performed using three EREs within each coating system. Corrosion potential measurements by the EREs are performed concurrently along with a SCE standard to examine statistical effects. The electrochemical potential of a sacrificial coating system can be locally fast-changing which presents a challenge for interpreting data for small sample sets.

The primer thickness is the variable of interest in the third set of experiments examined here. A topcoat is also applied but is not a variable. The study is performed to determine if there is a correlation between the thickness of the primer and the corrosion potential measured by the ERE. In order to successfully implement such an ERE, this variable must be well understood in order to observe and interpret corrosion potential data with the greatest accuracy. The thicknesses ranged from 80 to 250 μm which is relatively medium to very thick for sacrificial coating systems.

Finally, an experiment was prepared to examine the effects of Zn pigment on corrosion potential measurements by the ERE. Poor results were observed for the Zn primer / steel substrate in Chapter 3. The most likely cause of this failure is an insufficiently resistive electrical pathway between the substrate and ERE, i.e. a short circuit. It is suggested this is an effect of the Zn or Zn oxidation products and by-products since it is not observed in the Mg primer / AA 2024-T3 coating system. The Zn metal pigment oxidization causes a decrease in density for the material and an increase in density occurs when Mg metal pigments oxidize, so swelling of the Zn / ZnO particles may also be part of the problem. The Mg primer / AA 2024-T3 coating system is used as a standard in this experiment due to its consistent results by ERE corrosion potential measurement. Experimental Zn / Mg primers were prepared at various low to medium Zn:Mg ratio.

4.2. Experimental methods

4.2.1. Ag/AgCl wire reference electrode preparation

Reference electrodes were prepared using 50 μm silver wire, supplied by Goodfellow Corporation (Huntingdon, England). A chemical oxidation method was performed to create the reference electrode using a 0.03 M $FeCl_3$ solution and a 60 second

immersion period. This method is described in detail in Section 3.2.1 and will not be explained further here.

4.2.2. Placement of reference electrode within coating system

The corrosion potential of each Ag wire reference electrode was measured versus a standard reference electrode to ensure that the stable electrochemical potential has developed. It is then secured to the primer surface using a small amount of commercial rapid cure epoxy. A piece of conductive tape tab is also applied to use as a lead for electrochemical measurement via the ERE. This tab is covered with masking tape, and the topcoat is applied. See Figure 4.1 and Section 3.2.3 for more details.

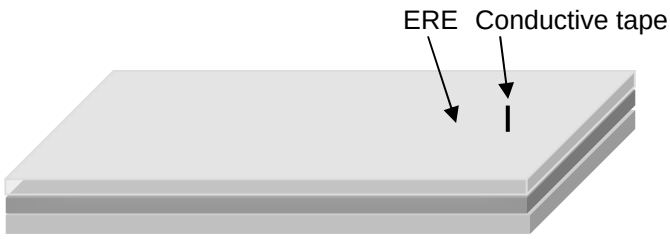

Figure 4.1. The coating system is illustrated to show the embedded reference electrode and conductive tape lead.

4.2.3. Experimental studies

4.2.3.1. *In-situ* corrosion potential monitoring

Coating systems equipped with an ERE were prepared for *in-situ* corrosion potential monitoring within a salt spray cabinet. Mg primer / AA 2024-T3 and Zn primer / steel sacrificial coating systems were utilized. Table 4.1 presents the coating systems. An epoxy polyamide was used as the primer binder. Polyurethane was used as the topcoat. All coating layers were applied by air spray gun at a target thickness of 50 μm. The materials and methods for this primer and topcoat are given in Section 3.2.2.

Table 4.1. Coating systems for the *in-situ* corrosion potential monitoring experiment.

Experiment	Primer	Substrate	Electrode	Replicates
Mg primer / AA 2024-T3	Mg	AA 2024-T3	Ag ERE	7
Zn primer / steel	Zn	Steel	Ag ERE	7

An electrical grade insulated wire was obtained and cut into eight foot long sections. Each was secured to the conductive tape of the ERE using a generous amount of commercial rapid cure epoxy. A second wire was secured to the substrate using the same epoxy. The ERE / coating system replicates were then placed in an ASTM B117 salt spray cabinet. The electrical wires were carefully moved to the exterior of the cabinet as it was closed and latched (Figure 4.2).

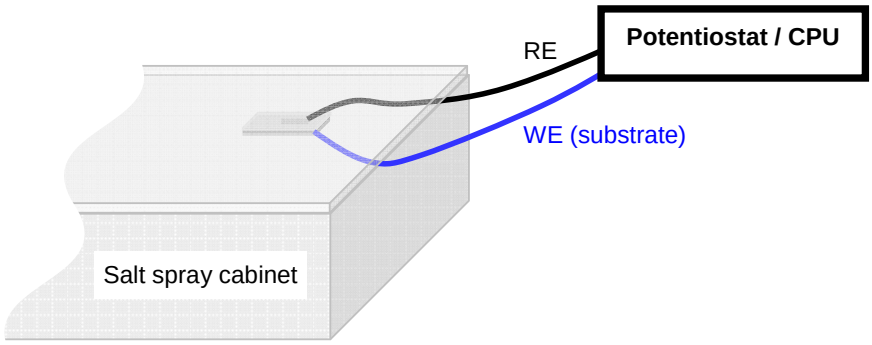

Figure 4.2. Instrumental set-up for *in-situ* corrosion potential monitoring experiment.

Corrosion potential measurements were made at regular intervals without interruption to the constant salt fog of the salt spray cabinet. A Gamry PCI4/300 potentiostat/galvanostat with dedicated EIS 300 software, supplied by Gamry Instruments, Inc. (Warminster, PA), was utilized for the measurements. One electrical wire serves to connect the ERE / coating system to the RE lead of the potentiostat. The second wire is used to connect the substrate / coating system to the WE lead of the potentiostat. A ten

minute data acquisition period is used at a frequency of 0.5 measurements per minute. Following the accelerated weathering experiment the ERE / coating system was examined using a JEOL JSM-6490LV SEM (Peabody, MA).

4.2.3.2. ERE replicates experiment

An experiment was prepared to examine multiple experimental EREs within a coating system. An epoxy polyamide primer was formulated at 45 % Mg PVC using Mg 3820 pigment from Ecka-Granules of America (Louisville, KY), Epon 828 binder, and Epikure 3164 curing agent, both from Hexion Specialty Products (Stafford, TX). It was air sprayed to AA 2024-T3 at a dry film thickness of 50 μm. Three experimental EREs were secured to the primer surface in a parallel manner as shown in Figure 4.3. The three EREs represent a replicate measurement to a higher degree than those observed between separate samples.

Figure 4.3. Illustration of three ERE set-up for replicate experiment.

The conductive tabs were masked. A high solids polyurethane gloss enamel 646-58-7925 and X-501 curing solution were prepared according to manufacturer's instructions for use as the topcoat, supplied by Akzo Nobel (Waukegan, IL). It was applied at a dry film thickness of 50 μm. A total of 5 replicate coating systems were prepared. They were exposed to accelerated weathering according to ASTM B117 in a salt spray cabinet and removed regularly to make corrosion potential measurements. A large solution cell was

attached and a Gamry PCI4/300 potentiostat/galvanostat with dedicated EIS 300 software was utilized for the measurements. Four multiplexor channels are used for each sample. DHS is the electrolyte used. The EREs and a laboratory SCE standard are connected to the RE lead while the substrate serves as the WE (Figure 4.4). The measurements are made within seconds of each other and assumed to be concurrent.

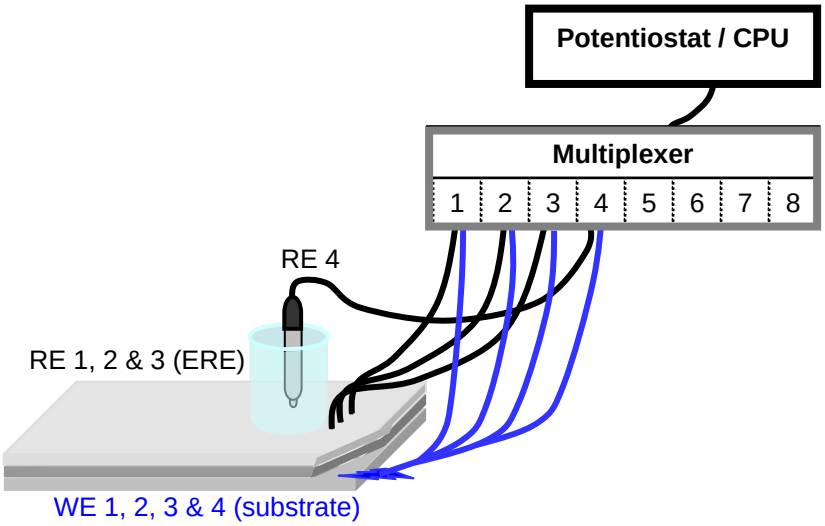

Figure 4.4. Experimental set-up is shown for the three ERE replicate experiment.

4.2.3.3. Examination of the effects of primer thickness

An experiment was designed to examine the effect of primer thickness on the corrosion potential measurement of the experimental ERE. A 45% PVC Mg-rich primer was prepared according to Section 4.2.3.2 using an epoxy polyamide binder and air sprayed onto AA 2024-T3. The target thickness for the panels varied from 80 to 250 µm.

Following one week ambient cure, the primer thicknesses were measured using a coating thickness gauge from Elcometer (Rochester Hills, MI). A sample set of varying film thicknesses was chosen for the experiment. The mean primer thickness is given in

Table 4.2 for each sample along with the absolute and relative (%) standard deviations. Five data points were taken from each sample to calculate the statistics. The thickness varied from 87 to 246 μm. All of the samples had a relative standard deviation of 7% or less.

Table 4.2. Thickness data for the samples used in primer thickness experiment.

Statistical Method		Primer Thickness by Sample								
Mean (μm)		87	109	121	160	168	188	206	231	246
Standard deviation	Absolute	6.3	6.3	7.7	5.9	7.2	6.4	6.2	8.7	14.2
	Relative	7	6	6	4	4	3	3	4	6

Each sample is secured with a ERE and then air sprayed with polyurethane topcoat at a target film thickness of 50 μm. Following one week ambient cure, the topcoat thickness was measured and showed good uniformity across the sample set. The mean was 48 μm with a standard deviation of 12 μm and range 30 to 68 μm. The samples were exposed to accelerated weathering in an ASTM B117 salt spray cabinet and removed regularly to make corrosion potential measurements. A Gamry PCI4/300 potentiostat/galvanostat with dedicated EIS 300 software was used to gather the data. The ERE was connected to the RE lead and the substrate to the WE lead, according to Figure 4.5.

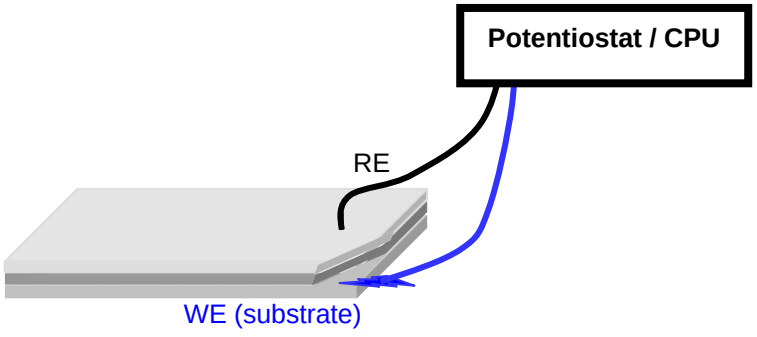

Figure 4.5 Instrumental set-up for corrosion potential measurement of Zn / Mg primer coating systems.

4.2.3.2. Examination of ERE for Zn / Mg primer on AA 2024-T3

Zn / Mg primer formulations were prepared to examine the corrosion potential behaviors of the experimental ERE in the presence of Zn. Table 4.3 shows the formulations studied. All were formulated at 53% PVC using Zinc Clad® IV and Mg 3820 pigments. The Mg and Zn pigments were ground with mortar and pestle before adding to an epoxy polyamide resin, prepared with Epon 828 binder. Epikure 3164 was the curing agent. The primer coatings were air spray applied to the substrate. Each panel is equipped with one Ag wire ERE and then sprayed with a pigmented polyurethane topcoat. The target dry film thickness was 50 μm for both coating layers.

Table 4.3. Experimental design for Zn / Mg primer formulations.

Experiment	Name	Electrode	Substrate	Zn / Mg (wt. %)	Replicates
AA 2024-T3 Standard	Mg control	Ag ERE	AA 2024	0 / 100	3
Formulation 1	10% Zn	Ag ERE	AA 2024	10 / 90	3
Formulation 2	20% Zn	Ag ERE	AA 2024	20 / 80	3
Formulation 3	40% Zn	Ag ERE	AA 2024	40 / 60	3

The coating systems were exposed to ASTM B117 accelerated weathering in a salt spray cabinet. The panels were removed regularly to make corrosion potential measurements. A Gamry PCI4/300 potentiostat/galvanostat with dedicated EIS 300 software was utilized for the measurements. The ERE was connected to the RE lead and the substrate to the WE lead, according to Section 4.2.3.2 (Figure 4.5).

4.3. Results and discussion

4.3.1. *In-situ* corrosion potential monitoring

An experiment was developed to monitor corrosion potential for two standard coating systems from within an ASTM B117 salt spray cabinet using an experimental ERE.

This *in-situ* experiment examines the reliability of ERE measurements during the environmental conditions experienced within the cabinet. Electrochemical measurements were obtained through the use of electrical grade wire, which connected the instrumentation to the ERE / coating system and substrate / coating system. No interruption was made to the constant 5% NaCl salt fog during the corrosion potential measurement and the thermostat was 35 °C.

The electrical wire connecting the ERE / coating system to the electrochemical equipment presented an unexpected challenge for this experiment. This wire quickly separated from the ERE / coating system for many samples. The failure of the epoxy glue was the main cause for this separation. The purpose of the glue was to secure the wire to the ERE for the duration of the experiment, but the high temperature and humidity of the cabinet seems to have promoted this failure.

4.3.1.1. Mg primer / AA 2024-T3

Good results were obtained for the *in-situ* monitoring of Mg primer / AA 2024-T3 coating system with pigmented polyurethane topcoat. Corrosion potential monitoring data is presented in Figure 4.6 for the two replicates representing the best experimental results. No standard reference electrode was available for comparison under these test conditions. The standard deviations are low for most of the mean corrosion potentials. This suggests that the corrosion potential was stable over the course of the measurement. Additionally, the data lies within -0.2 to -0.6 V vs ERE for both figures and varies significantly across exposure times. The cause of this inconsistency is not easily understood. However, the small standard deviations indicate they are an accurate representation of the electrochemical environment within the coating.

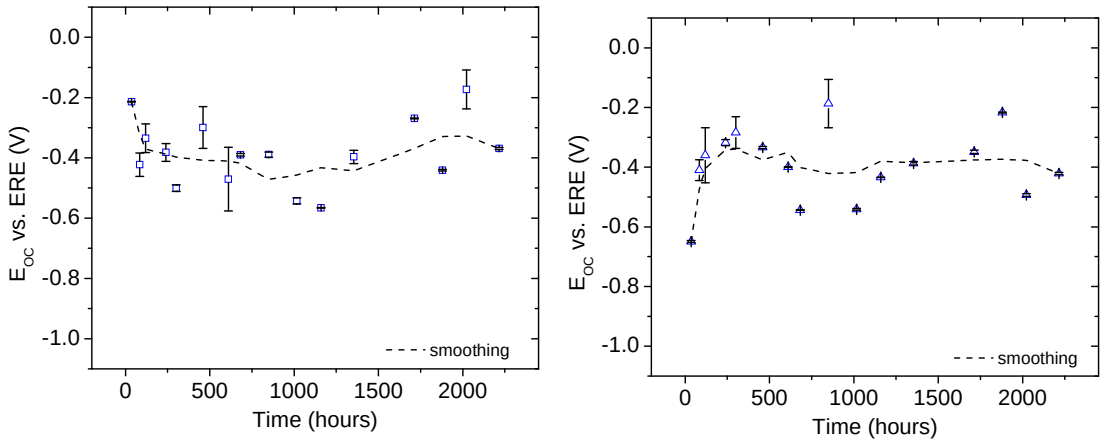

Figure 4.6. Mg primer / AA 2024-T3 *in-situ* corrosion potential monitoring results for two replicates with good results plus smoothing trend line.

A smoothing trend line was applied to the mean corrosion potential data. Good agreement is shown between the replicates, and the trend line is approximately -0.4 V vs ERE. This is 0.1 to 0.2 V more positive than those observed in constant immersion experiments measured at 25 °C (Section 3.4.2.2.1). A 5% NaCl constant salt fog is applied at 100% relative humidity and 35 °C in the salt spray cabinet. According to the Nernst equation for Ag/AgCl at 35 °C,

$$E = -0.046 - 0.061[Cl^-] \quad (4.1)$$

corrosion potential measurements should yield an estimated +0.002 V. This is insignificant for the present experiment. However, the corrosion potential is 0.061 V more positive for each order of magnitude decrease in coating $[Cl^-]$ which is the likely cause of the change in potential. However, a suitable configuration for a standard reference electrode measurement was not found so the coating $[Cl^-]$ could not be measured.

A 3rd order polynomial fitting was also applied to the mean corrosion potential data (not shown). Although an adequate fit was eventually obtained, improved consistency

within the data is needed for this sensor to be useful. The use of a continuous data acquisition method would satisfy this constraint.

4.3.1.2. Zn primer / steel

Poor results were observed for the ERE *in-situ* corrosion potential measurements in the Zn primer / steel coating system. The replicate representing the best experimental results is given in Figure 4.7. The figure shows numerous data points above 0.2 V vs ERE, often at 0.0 V vs ERE. As discussed in 3.4.2.2.2, the value 0.0 V vs ERE is not representative of the Zn primer / steel coating system and is assumed to be a short circuit [4]. A line is given on the figure to indicate this value. Mean corrosion potentials more positive than 0.2 V vs ERE cannot be used with great confidence because they are both more positive than expected for the coating system and very close to the short circuit value.

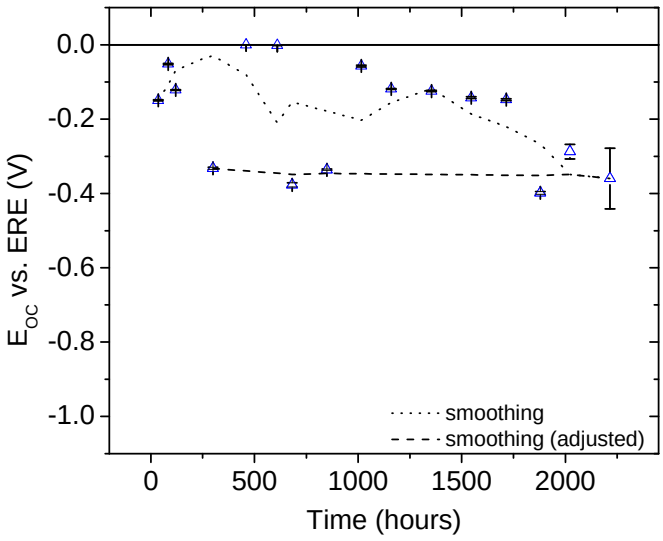

Figure 4.7. Zn primer / steel in-situ mean corrosion potential for replicate with best results.

Smoothing trend lines were applied for all data (dotted) and an adjusted data set which excluded data more positive than -0.2 V vs ERE (dashed). A significant difference is observed between the two trends. It is recommended that a filter is used for the implementation of an experimental ERE to discard data which is not an accurate representation of the electrochemical environment within the coating. In this example, the filter was placed at -0.2 V vs ERE. A linear fit with 95% confidence intervals gave very similar results to the smoothing (adjusted) and is not shown here.

The limited number of mean corrosion potential data points included in the adjusted fit creates a challenge. In order to implement the experimental ERE as a corrosion potential monitoring device for Zn primer / steel coating systems, a higher percentage of useful data must be obtained. The causes of frequent poor data are addressed in Section 4.3.4. and remedies are discussed.

4.3.1.3. SEM analysis

The samples were removed from the chamber following more than 2000 hours of exposure. Visual inspection showed that separation or detachment was occurring for many of the replicates for each coating system. A cross-section was prepared from the Mg primer / AA 2024-T3 sample set for SEM analysis (Figure 4.8). The substrate, primer, ERE, layer of epoxy surrounding the ERE, and topcoat are easily distinguished.

The ERE is spaced between the topcoat and primer. The rapid cure epoxy provides a stable coating around the Ag wire ERE in this case. Additionally, SEM can be used to analyze the condition of the sacrificial primer. The Mg pigments are elliptical or granular in nature. A few pigments have a noticeable bright edge around the pigment. This indicates the presence of Mg oxidation products and is a result of the active cathodic protection. The

SEM micrograph in Figure 4.8 suggests that the incorporation of the Ag wire ERE does not negatively affect the sacrificial coating system.

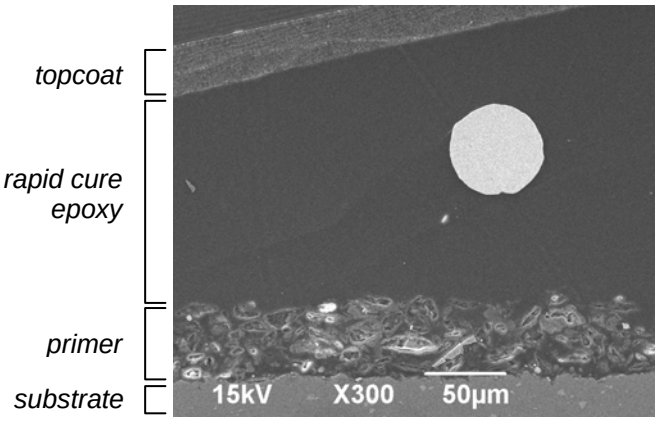

Figure 4.8. SEM results for a 2 mil Ag wire ERE / coating system cross-section.

4.3.2. ERE replicates experiment

An experiment was designed to replicate the experimental ERE measurements for a Mg primer / AA 2024-T3 coating system. Three EREs were placed within each coating, spaced 1 cm apart. The samples were placed in ASTM B117 salt spray cabinet for accelerated weathering and removed regularly to make corrosion potential measurements. Each measurement represents the average mixed electrochemical potential for the Mg primer / AA 2024-T3 coating system with respect to the average electrochemical potential at the surface of the reference electrode.

Good corrosion potential results were obtained for the ERE replicates in this experiment. Figure 4.9 shows mean corrosion potential data for the sample representing the best results. A smoothed trend line is applied to all of the data. The mean corrosion potential values more positive than -0.2 V vs ERE were excluded. Most standard deviations were small and no additional filter was applied. The experimental ERE data is

approximately 0.1 to 0.2 V more positive than the SCE standard data. This is consistent with Ag wire ERE corrosion potentials recorded in Chapter 3 for Mg primer / AA 2024-T3.

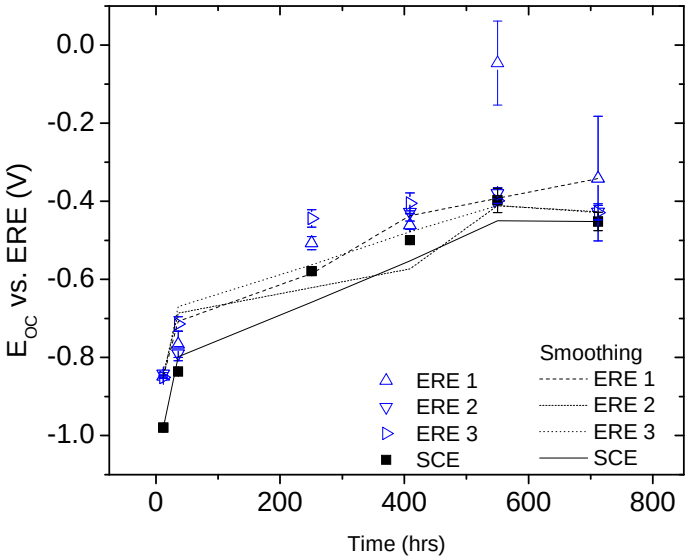

Figure 4.9. Mean corrosion potential versus exposure time for EREs and laboratory SCE.

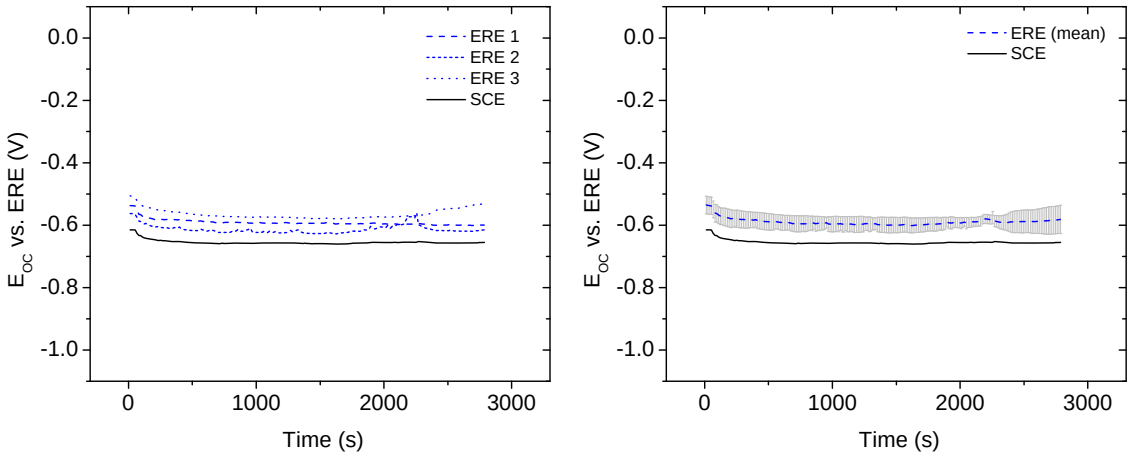

Figure 4.10. Corrosion potential data versus time for (a) raw data and (b) ERE mean and standard deviation.

Raw corrosion potential data is given in Figure 4.10 (a) for one of the samples following 251 hours of exposure. The corrosion potential is very stable during this period

of exposure and excellent agreement is again observed between the SCE standard and the three experimental EREs.

The mean and standard deviation for the experimental ERE data is given in Figure 4.10 (b) along with the SCE standard. The mean corrosion potential is approximately 0.1 V more positive than the SCE.

The small difference between experimental EREs is a combination of varying [Cl^-] at the Ag wire ERE surface as well as local mixed corrosion potential fluctuations within the sacrificial coating system. Local fluctuations are more variable than the global average and these are recorded by the experimental ERE. The local corrosion potential of sacrificial coatings systems measured by thin wire EREs is not previously reported outside of this work.

The main cause for the ERE electrochemical potential differences is the local variations in [Cl^-]. Recall that, at 25 °C, a one order of magnitude decrease in [Cl^-] increases the electrochemical potential by 0.059 V. Therefore, it is suggested that concentration gradients may be as high as one or two orders of magnitude within active sacrificial coating systems.

The mobility and concentration of Cl^- within the coating increases as coating degradation proceeds and pathways develop from the diffusion of water and ions. One of the driving forces for Cl^- concentration gradients is the presence of OH^- formed by the cathodic reduction reactions. These reaction sites have locally high [OH^-] which acts to repel the Cl^-. Likewise, [Cl^-] may be higher near oxidation reaction sites due to the presence of Mg cations. The effect of Mg cations may be greater due to the close proximity

of Mg pigments to the Ag wire ERE whereas OH^- is generated at the substrate / coating interface.

The figures given in this section show that raw corrosion potential data can be more useful than mean corrosion potential results. This is in part due to the large amount of data obtained and supports the suggestion that the Ag wire ERE is more useful for continuous monitoring applications. Additionally, the use of multiple reference electrodes improves confidence in corrosion potential measurements and allows for the examination of local corrosion potential fluctuations.

4.3.3. Examination of the effects of primer thickness

An experiment was designed to determine whether the primer thickness, i.e. distance between the substrate and ERE, has a significant effect on corrosion potential measurements. Samples were prepared of varying thicknesses, from 87 to 246 μm. This represents an average to thick set of samples, relative to sacrificial coating systems. Figure 4.11 illustrates the mean values and their standard deviation based on five measurements.

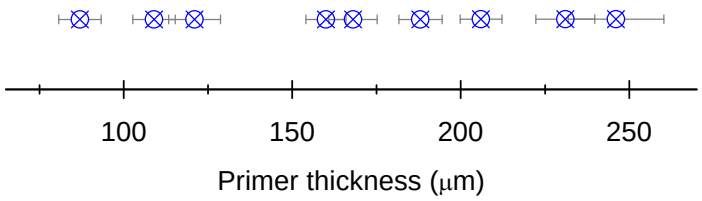

Figure 4.11. Mean primer thickness and standard deviation for each sample.

The primers were equipped an experimental ERE and then air sprayed with a pigmented polyurethane topcoat. The samples were exposed to ASTM B117 accelerated weathering and removed periodically for corrosion potential testing.

4.3.3.1. Effects of primer thickness on experimental ERE corrosion potential

Sacrificial coatings are applied at a broad range of primer thicknesses throughout the coatings industry. Therefore, it is necessary to distinguish effects of the coating thickness to Ag wire ERE corrosion potential measurements prior to implementation of the device. The primer thickness is plotted versus mean corrosion potential and exposure time in Figure 4.12 for the thicknesses examined. Data for 0 hours was not included because it took a few hours for the system to reach steady-state. Additionally, mean corrosion potential data more positive than -0.2 V vs ERE or with standard deviation greater than 0.05 V were removed because they are not experimentally realistic. In total, 82% of the mean corrosion potential data was included in the following analysis.

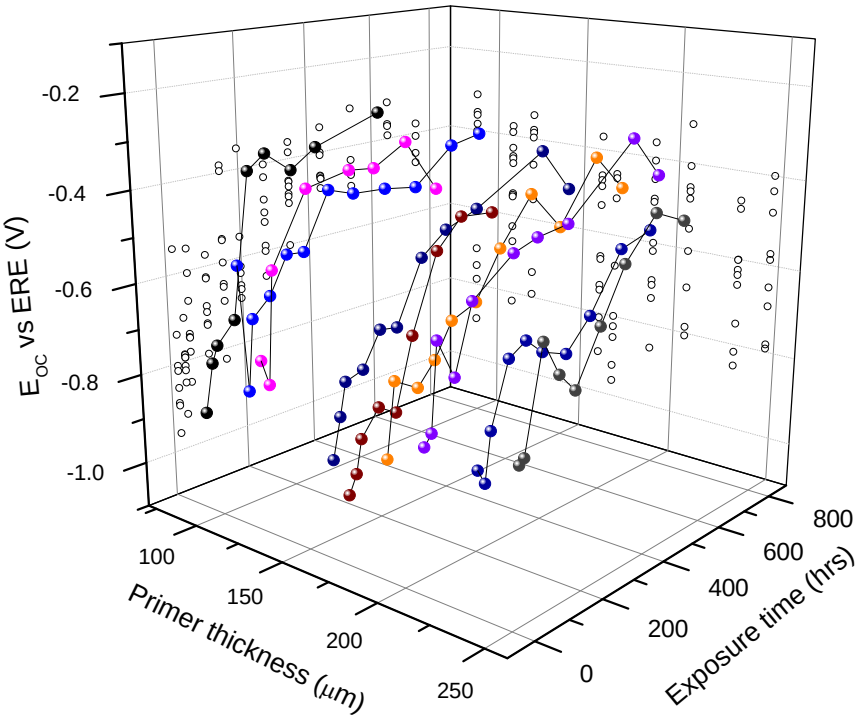

Figure 4.12. Primer thickness versus mean corrosion potential and exposure time.

The results are examined more closely in Figure 4.13 for corrosion potential versus primer thickness. The first 100 hours is given in Figure 4.13 (a) and the later measurements are in Figure 4.13 (b). Each series is presented with a smoothed trend line. A grid line is place at -0.5 V vs ERE to serve as a point of reference in the analysis. The mean corrosion potential becomes more positive with each subsequent exposure time measured. This is indicated with an arrow on the graphs and is expected during activation of the Mg primer / AA 2024-T3 sacrificial cathodic protection. However, a relationship between primer thickness and corrosion potential is not apparent in Figure 4.13 (a).

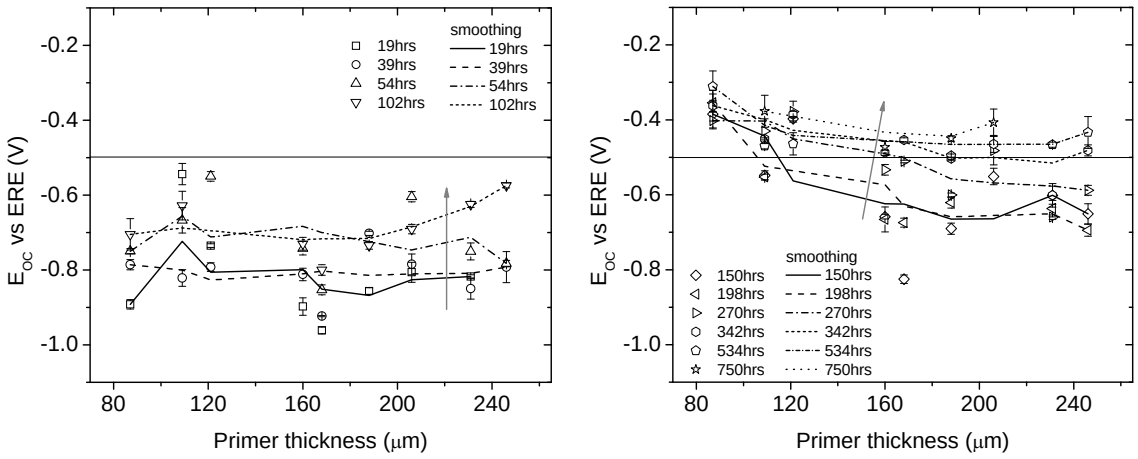

(a) (b)

Figure 4.13. Mean corrosion potential versus primer thickness for exposure times (a) up to 100 hours and (b) after 100 hours.

Figure 4.13 (b) shows a similar trend to Figure 4.13 (a); however, a significant relationship appears between mean corrosion potential and primer thickness. More negative corrosion potentials are measured for thicker primers after long exposure times. This is consistent with a greater amount of available Mg to give a lower mixed corrosion potential and suggests that the observed effects are a result of the activation of the Mg primer / AA

2024-T3 sacrificial coating system rather than the Ag wire ERE. This is examined further in Section 4.3.3.2. A linear fit produced the same results and is not shown here.

4.3.3.2. Effect of primer thickness on Mg primer / AA 2024-T3 corrosion potential

The mean corrosion potential results are shown versus exposure time in Figure 4.14. Results for the primers less than 130 μm are given in Figure 4.14 (a) while those greater than 180 μm are in Figure 4.14 (b). All series are fitted with a smoothing trend line. A grid line is place at -0.5 V vs ERE to serve as a point of reference in the analysis.

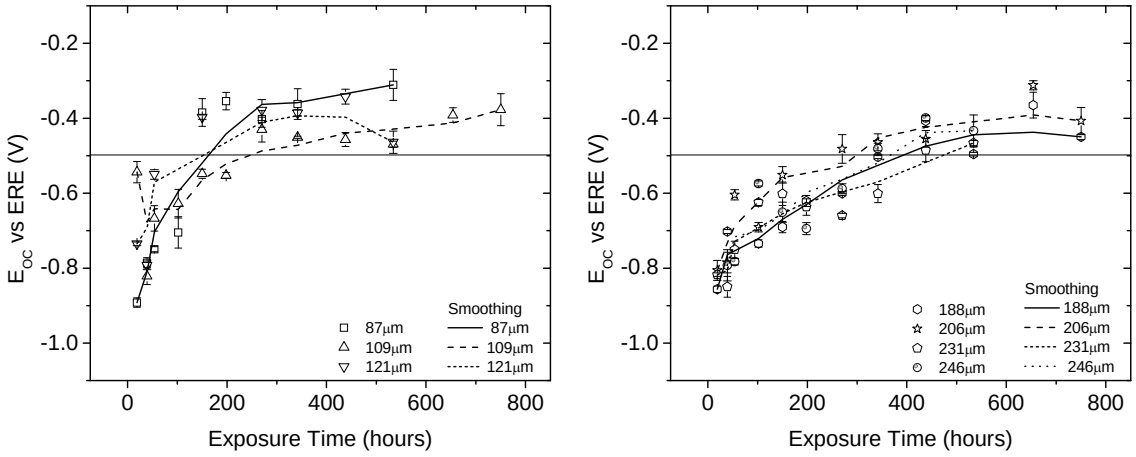

Figure 4.14. Mean corrosion potential versus exposure time for samples with primer thickness (a) below 130 μm and (b) above 180 μm.

Based on the trend lines, a slight difference appears between Figures 4.14 (a) and (b). The trend lines approach more positive values very quickly for the former. This is the activation period for cathodic protection and occurs over a time period of 50 to 250 hours in Figure 4.14 (a), followed by a stable corrosion potential. Figure 4.14 (b) shows a much a longer activation period, lasting between 300 and 500 hours. This is again consistent with the greater amount of Mg pigment available to polarize the mixed corrosion potential to more negative potentials.

The relationship between corrosion potential and activation period is examined further in Figure 4.15. Here the exposure time to reach -0.5 vs ERE is plotted versus primer thickness. This value is chosen because the trend lines in Figure 4.14 establish a stable corrosion potential shortly after reaching this mark. A smoothing trend line and a linear fit are also applied to the figure. The linear fit is experimentally significant with a P-value less than 0.01 demonstrating that the activation period is longer for thicker Mg primers.

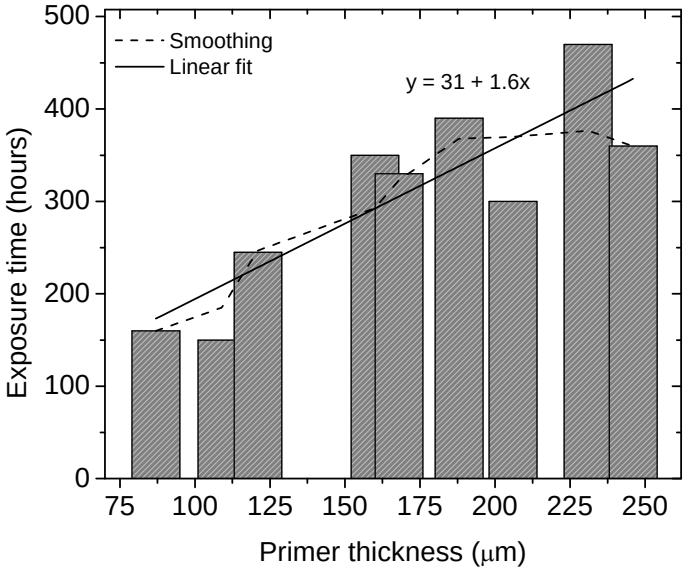

Figure 4.15. Time to reach -0.5 V vs ERE versus primer thickness for all samples.

The present results show that thicker primers have more negative corrosion potentials for longer time periods as an effect of the greater amount of Mg pigment. However, no discernable effect of primer thickness on the corrosion potential measurements recorded by Ag wire EREs can be observed in this experiment.

4.3.4. Examination of ERE for Zn / Mg primer on AA 2024-T3

A series of experiments were conducted on AA 2024 substrates in which Zn pigment was introduced into the standard Mg-rich primer / AA 2024-T3 system. The

purpose of the experiment was to positively identify Zn pigments as a contributor to the poor corrosion potential monitoring results obtained in 3.4.2.2.2**.** for the Zn primer / steel coating system. Incremental amounts of Zn pigment were added to the Mg primer / AA 2024-T3 system to evaluate this effect.

The primer thickness was recorded using five measurements for each sample (Table 4.4) The PVC was 53% for all formulations. All formulations were secured with an experimental ERE. A pigmented polyurethane topcoat was air sprayed at 50 μm. The measured mean topcoat thickness was 48 μm with a standard deviation of 6 μm. Due to the uniform coatings, thickness was not a variable for this experiment. The samples were placed in a salt spray cabinet and removed regularly for corrosion potential measurements.

Table 4.4. Primer thickness is given for all samples in Zn / Mg primer experiment.

Statistical Method		**Primer Thickness by Sample Set**											
		Mg Control			**10 % Zn**			**20 % Zn**			**40 % Zn**		
Mean (μm)		80	80	75	54	50	54	39	43	44	41	41	39
Standard deviation	Absolute	11	11	9	11	14	2	3	4	9	9	3	4
	Relative	14	14	12	20	28	4	8	9	20	22	8	11

The purpose of this experiment is to discern whether Zn pigment induced changes to the corrosion potential are a result of the primer, the experimental ERE, or both. Examples from previous experiments (3.3.2.3) are given for the Zn primer / steel coating system to aid in this (Figure 4.16). The most significant observation is the mean corrosion potentials at 0.0 V vs ERE. Although this is a legitimate corrosion potential, the data at 0.0 V in Figure 4.16 (b) does not appear to reflect the electrochemical environment of the coating system and is, therefore, suggested to be representing a system with insufficient electrical resistance.

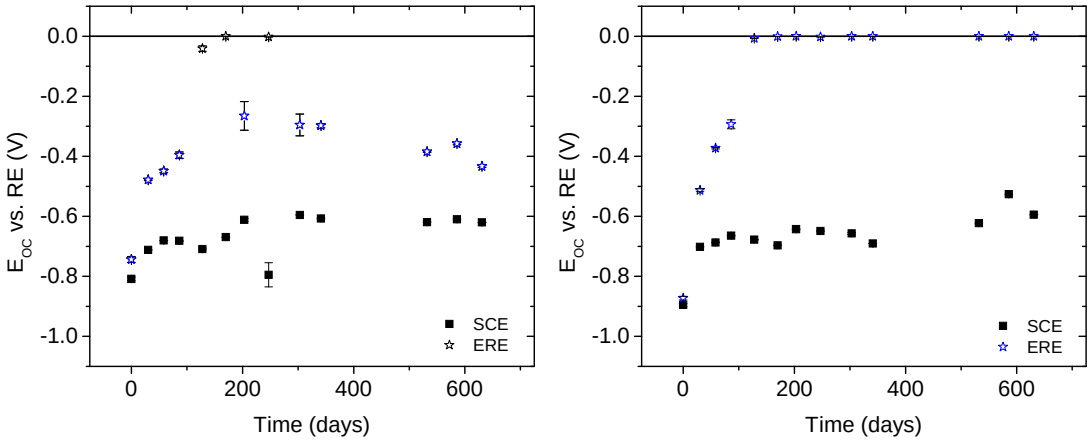

Figure 4.16. Examples are given for Zn primer / steel experimental ERE corrosion potential measurements for (a) good data and (b) poor data.

Results for the four Zn / Mg primer sample sets are given in Figure 4.17. No filter was applied because all data is of great interest for the initial evaluation. The y-axis is -1.2 to 1.6 V vs ERE. Grid lines are placed at y = 0 (solid) and -0.5 V vs ERE (dotted) to identify short circuits and to serve as a point of reference in the analysis, respectively. An obvious feature in Figure 4.17 is the mean corrosion potential measurements greater than 0.0 V vs ERE. At this value, the system is not at steady state. Most samples achieve steady state within a few hours of exposure; however, one of the samples in Figure 4.18 (d) is greater than 0.0 V vs ERE until 100 hours. A second sample from Figure 4.18 (d) is equal to 0.0 V vs ERE until 100 hours. All other measurements are more negative than 0.0 V vs ERE as expected.

The Mg control (Figure 4.17 (a)) shows a characteristic dip in mean corrosion potential for the first 40 hours. This is consistent with the activation of sacrificial protection for a Mg primer / AA 2024-T3 coating system. There is a quick transition to a smooth, stable region of cathodic protection which is in good agreement with the behavior reported

for Mg primer on AA 2024-T3 [5; 6]. The experimental Zn / Mg coatings show a broadened activation period, i.e. lower corrosion potentials for longer time periods, making it apparent that the mean corrosion potential is affected by the addition of Zn pigment. The effect of Zn on Mg primer / AA 2024-T3 cathodic protection is examined in Section 4.3.4.2.

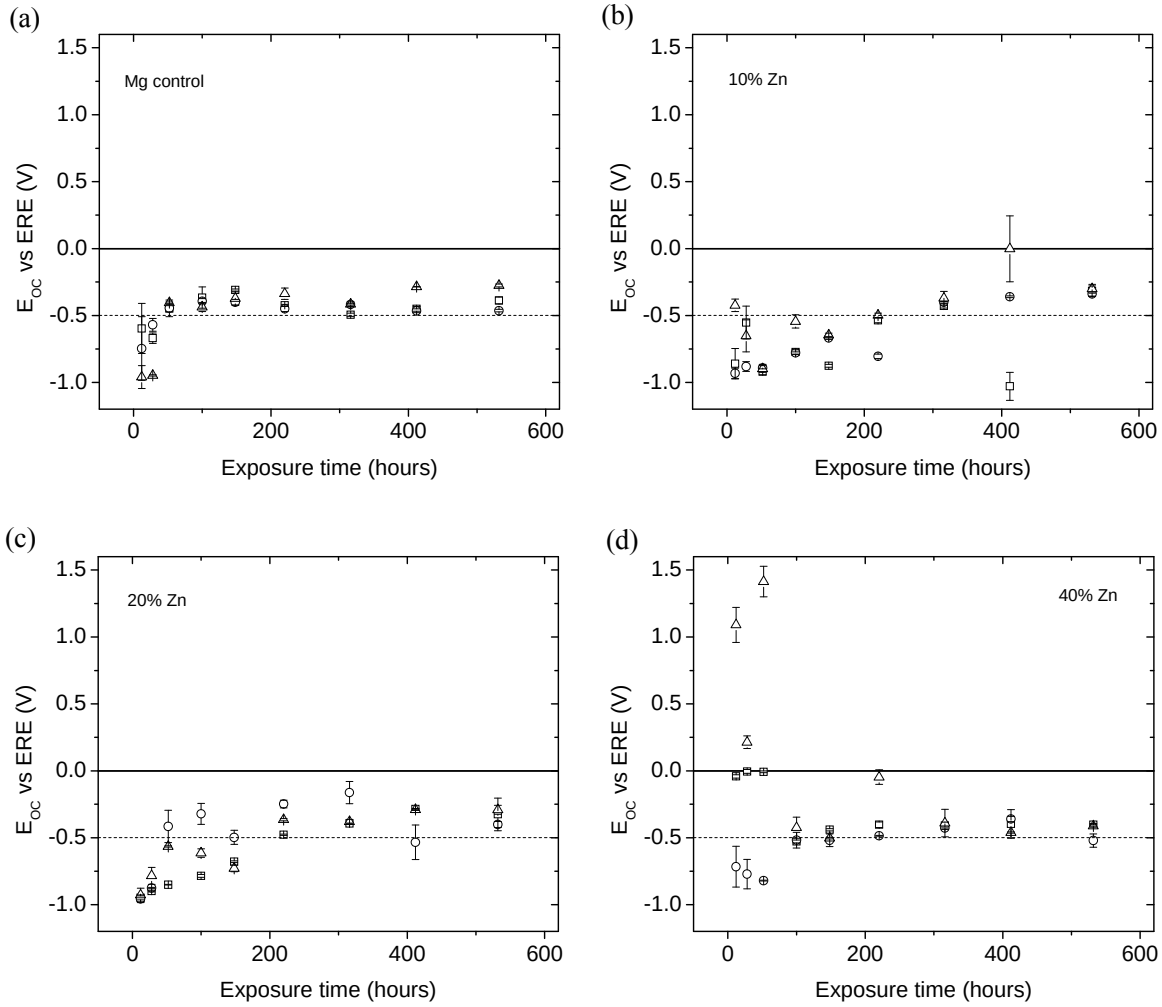

Figure 4.17. Mean corrosion potential versus exposure time for (a) Mg control, (b) 10 % Zn, (c) 20 % Zn, and (d) 40 % Zn.

4.3.4.1. Effect of Zn pigment on experimental ERE measurements

Preliminary examination of the experimental Ag wire ERE in a Zn primer / steel coating system using constant immersion exposure conditions gave poor results (Section 3.3.2.3). Two suggestions have been made for the cause of these poor results. The first is that Zn or Fe cations replace Ag atoms on the surface of the reference electrode. The addition of these atoms disrupts the stable Ag/AgCl corrosion potential and is known as electrode poisoning. Bro [7] has found that the AgCl layer dissolves quickly in the presence of ZnCl and Maminska [8] identified S^{2-}, I^-, and Br^- as interfering species for this electrode. These are possible due to the absence of an impermeable casing for the reference electrode. Instead, the wire ERE is protected by a semi-permeable epoxy coating.

The second possibility for poor Zn primer / steel results is caused by the Zn oxidation products and by-products resulting from active cathodic protection. Zn oxidation products are less dense than Zn. The opposite is true for Mg oxidation. Therefore, the oxidation of Zn transfers internal stress to the nearby polymer while the Mg creates voids or pores. These conditions are illustrated in Figure 4.18 for the two primer systems. Furthermore, Zn oxides such as $Zn(OH)_n(Cl)\cdot(H_2O)_n$ are conductive while Mg oxides are not. The swelling Zn oxide particles come into electrical contact with one another, the substrate, and the ERE. This results in a short circuit condition for the ERE due to the insufficient resistance between the two elements. A white line is given in the figure to demonstrate a pathway for the short circuit of the Zn primer.

A few 0.0V vs ERE mean corrosion potential measurements were measured by experimental ERE's in present experiments. The most notable occurrence is for one of the 40 % Zn replicates (Figure 4.17 (d)) which occurred during in first 75 hours of the cathodic

protection activation period. The observed value is consistent with the measurements in Figure 17 (b) and suggests that the effect is caused by the presence of Zn short circuits with the swelling oxide.

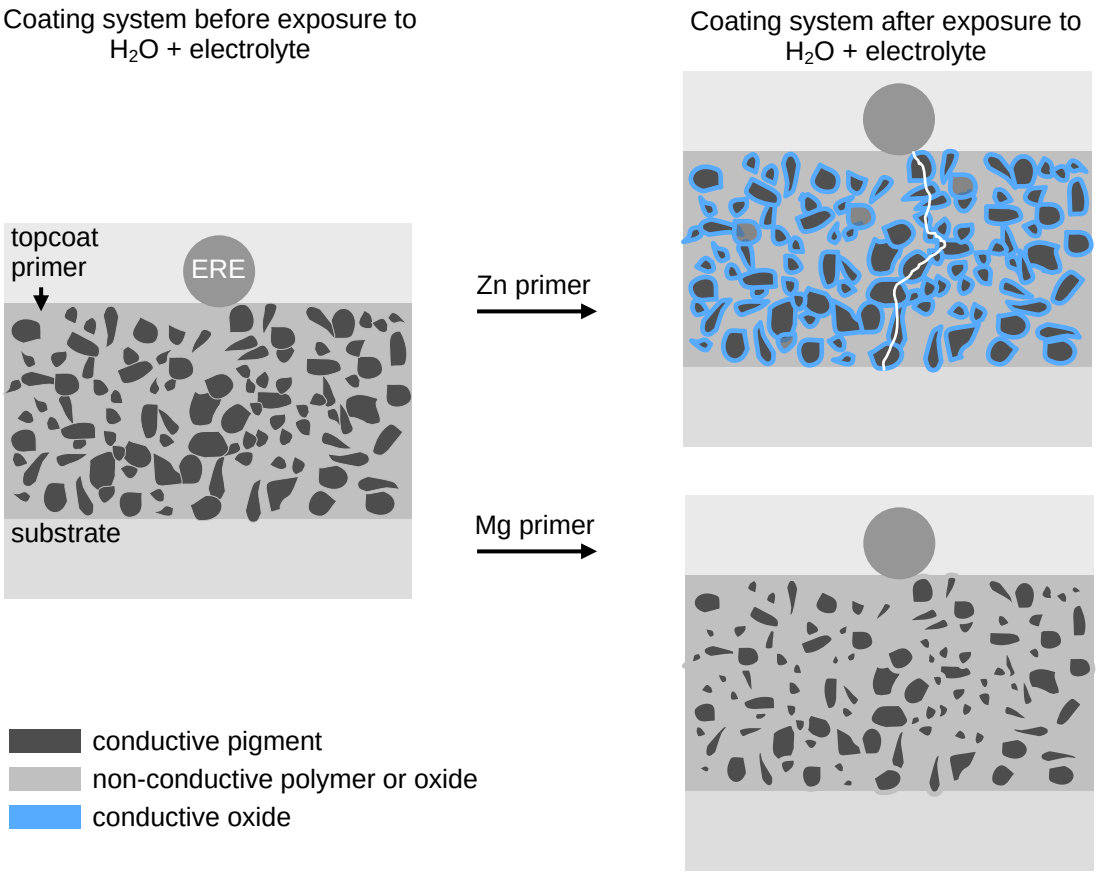

Figure 4.18. An example is given for the dissolution and oxide formation of active Zn and Mg pigments upon exposure to H_2O and electrolyte.

The present study suggests that the experimental ERE measurement at 0.0 V vs ERE are an effect of low resistance within the primer coating system, supporting the suggestion that the Zn oxidation products and by-products penetrate the highly resistive polymer matrix surrounding the experimental ERE. Additionally, Figure 4.16, Figure 4.17, and Section 3.3.2.3 show that a shorted circuit can be recovered through a rebuilding of the

resistive elements within the active coating system. The condition is not necessarily permanent and accurate ERE corrosion potential measurements can be regained.

Electrode poisoning decreases stability and causes a shift in the Ag/AgCl electrochemical potential. However, it has been shown here that the value of 0.0 V vs ERE reflects a shorted measurement, not a shift of electrochemical potential. Therefore, the possibility of electrode poisoning is neither supported nor eliminated by the present results.

In order to strengthen the present conclusions, Zn / Mg primer should be prepared at higher Zn loading and applied to the AA 2024-T3 substrate. Additionally, a 100 % Zn / 0% Mg formulation on AA 2024-T3 is also desired.

4.3.4.2. Effect of Zn pigment on cathodic protection for AA 2024-T3

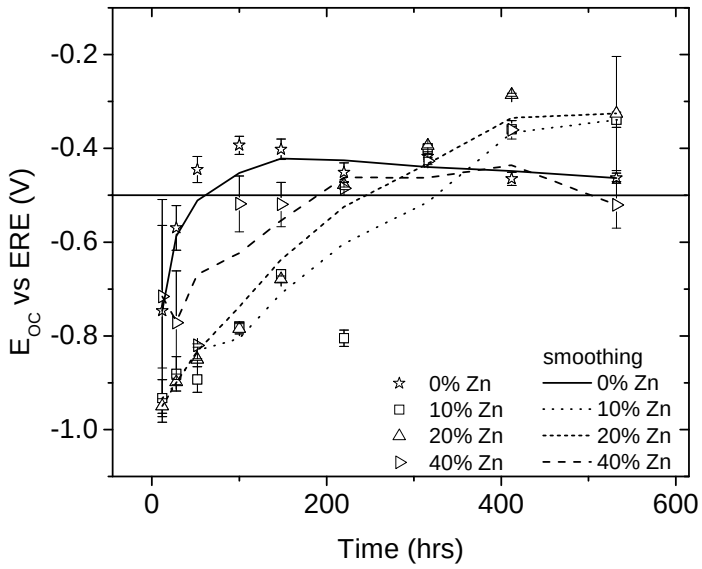

Figure 4.19. Representatives for each Zn / Mg primer sample set plus smoothing trend line.

The effect of Zn pigment on the cathodic protection provided to the AA 2024-T3 substrate by Mg pigment is examined more closely in Figure 4.19. The figure gives the mean corrosion potential versus exposure time using one replicate from each sample set as

the most representative for that set. Good reproducibility was observed for all sets except for the 40% Zn primer (Figure 4.17). A smoothing trend line is added for each using an adjacent-averaging method. A solid grid line is place at -0.5 V vs ERE to serve as a point of reference in the analysis.

The addition of Zn causes a significant broadening of the cathodic protection activation period, compared to the Mg control. The effect is most significant for the 10% Zn pigment coating. The data was further analyzed using a filter for values more positive than -0.2 V vs ERE or with standard deviations greater than 0.05 V. Smoothing trend lines were applied using the filtered data set. The time to reach -0.5 V vs ERE is approximated based on this trend line. Table 4.5 gives these results.

Table 4.5. The time to reach -0.5 V vs ERE is for all Zn / Mg primer samples.

Sample #	Time to reach -0.5 V vs ERE (hours)			
	Mg Control	10 % Zn	20 % Zn	40 % Zn
1	50	323	187	-
2	45	205	236	250
3	100	270	133	-
Mean (stan dev)	65 (30)	266 (59)	185 (50)	250 (-)

It is suggested that galvanic interactions between the Zn and Mg pigments within the primer cause the broadened activation period. The Zn pigments and their oxides increase the overall conductivity of the primer. Additionally, the Zn pigments are approximately one order of magnitude smaller than the Mg pigments allowing them to occupy the interstitial spaces. The small radius of the Zn pigments ensures large surface areas for cathodic reactions to place. This increases the rate of Mg oxidation and generates a more negative corrosion potential. The effect is most noticeable in for the 10% Zn primer.

The phenomenon shifts as the amount of Zn pigment increases. At 20% Zn the pigment contributes more significantly to the mixed potential of the system. Figure 4.20 shows the 20% Zn to be approximately 0.1 V more positive than 10% Zn. This behavior is expected because the electrochemical potential for Zn is approximately 0.6 V more positive than Mg. A further increase in mixed corrosion potential is observed at 40% Zn at which point the volume ratio for the two pigments is roughly 50:50. At this ratio short circuit effects are observed.

It is suggested that the small amount of Zn pigment accelerates the Mg reactions related to cathodic protection. Figure 4.19 shows mean corrosion potentials near -0.3 V vs ERE at 400 hours of exposure. It is likely that the available Mg pigment has been exhausted and that cathodic protection is no longer active. Further experimentation with Zn / Mg primer coating systems is necessary to confirm their effectiveness as sacrificial coatings for AA 2024-T3. The present sample sets were examined at short time periods. Additionally, a standard laboratory reference electrode is preferred to increase confidence in the results.

4.4. Conclusions

In-situ corrosion potential monitoring of sacrificial coating systems was presented in this chapter. The experimental ERE gave good results for the Mg primer / AA 2024-T3. However the results were poor for the Zn primer / steel. This is consistent with Chapter 3 results for these coating systems and suggests that the experimental ERE can be used effectively *in-situ* for a salt spray cabinet. This may be a very useful for research and development applications. The electrical wiring disconnected from the sample in many cases. This challenge can be alleviated through additional engineering efforts.

Experimental ERE replicates were measured in this chapter. Slight changes in corrosion potential were observed throughout the experiment. It is hypothesized that this is a combination of local changes in electrochemical potential as well as the [Cl^-]. The latter is influenced by the anionic and cationic products of the sacrificial protection reactions and is suggested to be the main source of the variation. The results suggest that [Cl^-] changes as much as one or two orders of magnitude.

The ERE replicate experiment showed that raw corrosion data reveals information which may be masked by a mean corrosion potential. Therefore, the Ag wire ERE may be more useful for continuous monitoring applications where large amounts of data are obtained. Additionally, the use of multiple reference electrodes improves confidence in corrosion potential measurements.

The primer thickness results suggest that no effect is expected for sacrificial primers of medium to thick relative thicknesses. Further work on thin coatings is desired to confirm the absence of an effect. The experimental ERE was also used to gauge the effect of primer thickness on the Mg primer / AA 2024-T3. There is some indication that thicker primers undergo a longer cathodic protection activation period. This is expected for greater amounts of Mg pigment for longer periods. Further experimentation with improved primer thickness control is needed to confirm this correlation.

Experiments within this chapter indicate that Zn is partially responsible for disrupted accuracy of experimental ERE measurements by means of a short circuit. It is suggested that this is promoted by the Zn oxidation products and by-products, which are less dense than the Zn metal. Further experimentation at higher Zn loading and a 100 % Zn / 0% Mg formulation on AA 2024-T3 is desired. Overall, good results were obtained by the

experimental ERE at low Zn content. Formulations with 10% and 20% Zn were ineffective at providing long-term sacrificial protection to AA 2024-T3. However, the 40% Zn formulation provided stable cathodic protection. The length of this protection can be determined by testing at longer exposure times.

A method of statistical analysis was developed to improve the usefulness of the corrosion potential data measured by ERE. Data more positive than -0.2 V vs ERE was discarded from analyses because it is unrealistic for the system being measured. The filter greatly aided in the interpretation of the data in this chapter.

4.5. References

[1]D.A. Jones, Principles and Prevention of Corrosion 2nd ed., Prentice Hall, Upper Saddle River, NJ, 1996.

[2]K.B. Oldham, J.C. Myland, Fundamentals of Electrochemical Science, Academic Principles, Inc., San Diego, CA, 1994.

[3]B.E. Merten, D. Battocchi, D.E. Tallman, G.P. Bierwagen, Embedded reference electrode for potential-monitoring of cathodic protective systems. Journal of the Electrochemical Society 157 (2010) C244-C247.

[4]J.N. Murray, Electrochemical test methods for evaluating organic coatings on metals: an update. Part II: single test parameter measurements. Progress in Organic Coatings 31 (1997) 255–264.

[5]D. Battocchi, A.M. Simoes, D.E. Tallman, G.P. Bierwagen, Electrochemical behaviour of a Mg-rich primer in the protection of Al alloys. Corrosion Science 48 (2006) 1292–1306.

[6]D. Battocchi, A.M. Simoes, D.E. Tallman, G.P. Bierwagen, Comparison of testing solutions on the protection of Al-alloys using a Mg-rich primer. Corrosion Science 48 (2006) 2226–2240.

[7]P. Bro, N. Marincic, The high rate oxidation of silver electrodes in chloride solutions. Journal of the Electrochemical Society 116 (1969) 1338-1341.

[8]R. Maminska, A. Dybko, W. Wroblewski, All-solid-state miniaturised planar reference electrodes based on ionic liquids. Sensors and Actuators B 115 (2006) 552–557.

CHAPTER 5. EXPLORING NOVEL Mg-RICH PRIMER FORMULATIONS AND CHARACTERIZATION BY ERE

5.1. Introduction

Mg-rich coatings have been explored extensively in recent years as a totally chromate-free alternative to chromium-based coatings for aluminum alloy (AA) 2024-T3 [1-5]. It has been suggested that the success of Mg-rich coatings is directly related to Mg oxidation products and their solution by-products formed during the oxidation of active Mg pigments (Equation 5.1) [6-7]. The complementary reduction of water (or oxygen) occurs at a high rate, leading to local, high concentrations of hydroxyl ions (Equation 5.2).

$$Mg \rightarrow Mg^{2+} + 2e^{-} \quad (5.1)$$

$$2H_2O + 2e^{-} \rightarrow H_2 + 2OH^{-} \text{ (or } 2H_2O + O_2 + 4e^{-} \rightarrow 4OH^{-}) \quad (5.2)$$

Aluminum and its alloys dissolve at both high and low pH. However, $Mg(OH)_2$ and $MgCO_3$ compounds act as a buffer and form an oxide film at high pH, thus protecting the substrate [6]. Secondary corrosion protection has also been observed in the analogous Zn-rich coating system for steel substrates by Zn oxidation products [8].

5.1.1. Electrochemical analysis by embedded electrodes

Embedded sensors and electrodes have gained much interest in the field of structural health monitoring (SHM) [9-12]. The most active areas of SHM research include reinforced concrete [13-20] and aircraft [21-25] structures. The embedded material is utilized to obtain pertinent physical, chemical, or electrochemical information *in-situ*. The information is to determine the condition, or health, of the infrastructure. Often, its

remaining useable lifetime may also be estimated. Industrial standards have been established for determining the health of various infrastructures.

Sophisticated electrochemical methods have been applied to structural health monitoring efforts. Kittel et al. [26-27] deposited a gold and nickel electrodes between coating layers to identify the coating properties of the inner and outer coating layer by EIS. The results highlight the significant contributions to corrosion protection by the adhesion interlayer connecting the substrate and primer [27]. Misczyck [28] measured EIS using electroconductive ink sensors between coating layers in an attempt to measure the effect of humidity on interlayer adhesion. However, electric field experiments by Nogueira et al. [29] have suggested that the current applied between two embedded platinum wire electrodes passes through the substrate beneath each electrode. Allahar et al [30] has used EIS measured by embedded electrodes to show that current travels through coating systems as degradation progresses. Therefore, it is shown to maintain the path of least resistance which is a complex function of factors including electrolyte concentration, humidity, temperature, and coating degradation processes.

EIS is a well-accepted method for measuring the dielectric and resistive properties of protective coatings [31-36]. The low frequency impedance, $Z_{0.01Hz}$, of coating systems is frequently reported in literature. The measurement is taken at regular intervals to qualitatively analyze the degradation process. The onset of substrate corrosion results as the coating degrades. Davis and coworkers [37-42] developed numerous prototypes for surface mounted sensors for *in-situ* EIS measurements. Hong and Harichandran [15] applied copper tape to the surface of carbon fiber reinforce plastic as an embedded electrode for *in-situ* EIS monitoring of reinforcement bars within concrete.

Wang et al. [43-44] used electrochemical noise measurement (ENM) for in-situ corrosion monitoring. ENM is completely non-destructive, does not require potentiostatic instrumentation, and can be applied at shorter time periods than EIS. The noise resistance, R_n, is most often reported and is roughly analogous to $Z_{0.01Hz}$ [45-47]. The method can be further evaluated to characterize the corrosion processes, ranging from uniform corrosion to localized corrosion. Uniform corrosion is preferable. However, localized corrosion can be severe and unpredictable. Catastrophic infrastructural damage may result if not carefully monitored.

Su [48] applied embedded platinum foil leaves for in-situ examination of aerospace and vehicular protective coatings by EIS and ENM. Allahar et al. [49-52] used embedded platinum foil leaves extensively for electrochemical analysis. Additionally, platinum foil embedded electrodes have been utilized for non-substrate EIS [30] and to model water transport in multilayer coatings [53]. Bierwagen et al. [54] used the electrode to characterize the corrosion mechanisms caused by AC-DC-AC accelerated testing method. Wang et al. [55] utilized the electrode to monitor the electrochemical properties of a Mg-rich primer by EIS and ENM.

In this chapter, the Ag wire embedded reference electrode (ERE) is examined for electrochemical measurement of a sacrificial coating system by EIS and ENM. This is the first use of an ERE for the application of these measurements. The feasibility of Ag wire ERE for corrosion potential monitoring of Mg primer / AA 2024-T3 was reported in Chapter 3. Corrosion potential data is also provided here. Visual observations as well as standard electrochemical measurements are used as supporting characterization methods.

5.1.2. Next generation Mg primers for AA 2024-T3 corrosion protection

Aluminum alloy (AA) 2024-T3 has been used extensively as an aircraft alloy due to its low density and high strength. A major disadvantage to the alloy is its susceptibility to localized corrosion. This is due in part to the copper content (up to 4%) which can establish galvanic cells with the aluminum matrix and lead to localized corrosion. Strontium chromate ($SrCrO_4$) treatments have served as a dependable corrosion inhibitor for this substrate and effectively inhibit both the growth and development of localized corrosion in AA 2024-T3.

Chromate pigments contain hexavalent chromium (VI), a known carcinogen. This poses significant health risks to applicators and maintenance personnel. It also raises concerns for the safe disposal of coatings once removed from service. The Department of Defense (DoD) recently prohibited the delivery of items containing greater than 0.1 wt% hexavalent chromium [56]. Other organizations have passed similar regulations to ensure that chromate-related risks to human and environmental health are minimized. The complexity of the protection provided by chromium inhibitors, and the challenges associated with finding a suitable replacement is well-documented [57-58].

Tremendous research expenditures have been applied to the development of an environmentally safe, totally chromate-free alternative to strontium chromate corrosion inhibitors. Bierwagen and co-workers [1, 3, 6, 59-60] have accomplished this by the use of Mg-rich primers as a sacrificial coating system for AA 2024-T3. Studies have now shown this primer to provide corrosion protection for more than 10,000 hours of cyclic Prohesion® exposure [3].

The present chapter examines the Mg-rich primer system combined with magnesium nitrate and lithium carbonate, which have recently been reported to inhibit corrosion for AA 2024-T3. Varma et al. [61] found that magnesium nitrate provided optimal corrosion inhibition for the aluminum substrate near 0.7 wt%. Lithium salt solutions have been used previously as a pretreatment for AA 2024-T3 [62]. Visser and Hayes [63] formulated lithium salts directly formulated into the coating system to provide protection. Optimal results were achieved with the use of lithium carbonate at a pigment loading of 3-9 vol%.

A three component mixture analysis is used in this paper to explore mixtures of magnesium metal particulates, magnesium nitrate, and lithium carbonate. The analysis method is designed to identify possible synergistic effects between the mixture components without testing an exorbitant amount of combinations. This preliminary examination is designed to determine if a subsequent full-scale combinatorial study is worthwhile. The results also include the first known experimentation with magnesium nitrate/lithium carbonate and magnesium nitrate/magnesium metal particulate based corrosion resistant primers.

The magnesium metal particulate loading is greatly reduced to examine the ingredient effects at low pigment loadings. Additionally, is it desirable to determine if Mg-rich primers plus corrosion inhibitors provides cathodic protection at lower-than-expected concentrations of Mg pigment. The goal is to effectively reduce material costs as well as safety concerns for the manufacture of Mg-containing primers.

5.2. Experimental methods

5.2.1. Design of experiment

The present experiment was designed to obtain preliminary results for an epoxy-based corrosion protective coating containing lithium carbonate (Li_2CO_3) and magnesium nitrate ($Mg(NO_3)_2$) metal salts as well magnesium (Mg) metal particulates. The formulations were developed with the interest of obtaining desirable corrosion protection at reduced total pigment loading, as calculated by pigment volume concentration (PVC). Equation 5.3 is used to determine PVC.

PVC = (volume pigments + binder) / (volume pigments + binder + solvents) (5.3)

Mg metal particulate levels were tested between 0 and 16% by volume. Common literature values for successful Mg-rich pigments are 40% or higher. Therefore, the effects of metal salts at reduced Mg metal loadings were examined. The upper and lower boundary limits are given for each ingredient in Table 5.1. The Li_2CO_3 and $Mg(NO_3)_2$ limits were chosen based on literature results for those salts.

Table 5.1. Boundary limits for the metal salts and pigment to be tested.

Boundary Limit	Mixture composition		
	Li_2CO_3 (vol%)	$Mg(NO_3)_2$ (wt%)	Mg (vol%)
Upper	10	1.0	20
Lower	0	0	0

Based on the designated boundaries, seven experimental formulations were chosen. As shown in Figure 5.1, these include four formulations combining all three ingredients: the mid-point and three central points. Three two-ingredient mixtures are positioned on axis lines. Dashed lines are included on the figure. The experiments sharing each line are formulated at a fixed ratio between two ingredients. To the knowledge of these authors, this

is the first experiment to measure the corrosion protective nature of these three ingredients as well as a Mg-rich primer with $Mg(NO_3)_2$ corrosion inhibitor and Li_2CO_3 with $Mg(NO_3)_2$ corrosion inhibitors.

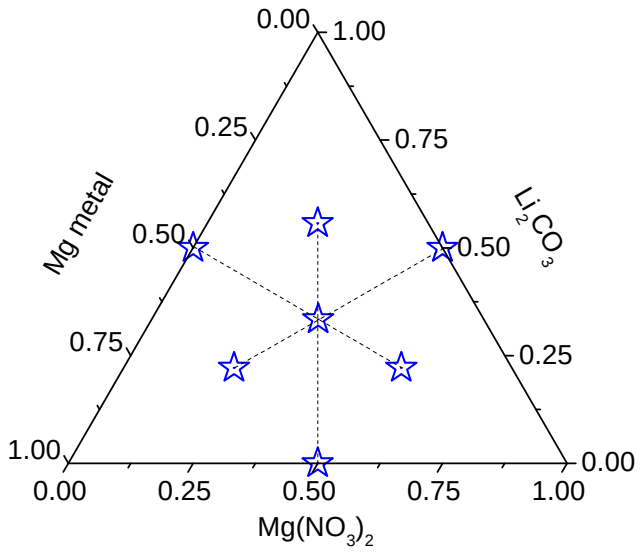

Figure 5.1. Design space for experimental formulations. The axes represent % composition for each, normalized to the boundaries in Table 5.1.

5.2.2. Coating system

5.2.2.1. Materials

AA 2024-T3 panels (12 cm x 5 cm x 0.3 cm) from Q Panel Lab products (Cleveland, OH) were used in this study. The pigments used were Mg metal particulates from Ecka-Granules of America (Louisville, KY) as well as $Mg(NO_3)_2 \cdot 6H_2O$ and Li_2CO_3 from Sigma-Aldrich (St. Louis, MO). An epoxy-polyamide was used as the binder for this system and high gloss polyurethane from Akzo Nobel Aerospace Coatings (Waukegan, IL) served as the topcoat.

5.2.2.2. Formulations and nomenclature

The primer formulation and PVC varied for each experiment and is described in Table 5.2. The nomenclature follows the rule of "vol. % Li_2CO_3, wt. % $Mg(NO_3)_2 \cdot 6H_2O$, and vol. % Mg metal" to be referred to as "*x*Li *x*Mg *x*" within the results and discussion of this chapter. The balance for each formulation is an epoxy polyamide binder. A pigmented polyurethane topcoat is added to the novel primer for exposure analysis. Eight replicates were prepared for each control formulation; four replicates were prepared for each experimental formulation.

Table 5.2. Formulations for two control experiments and seven experimental coatings.

Exp.	Name	Li_2CO_3 (vol%)	$Mg(NO_3)_2$ (wt%)	Mg (vol%)	PVC
A	n-Mg Control	0	0	0	0
B	Mg Control	0	0	40.0	40
1	0Li .5Mg 10	0	0.50	10.0	11
2	5Li 0Mg 10	5.0	0	10.0	15
3	5Li .5Mg 0	5.0	0.50	0	6
4	6Li .6Mg 13	6.7	0.67	13.3	20
5	3Li .3Mg 16	3.3	0.33	16.6	20
6	3Li .8Mg 6	3.3	0.83	6.6	11
7	8Li .3Mg 6	8.3	0.33	6.6	15

5.2.2.3. Procedure

The dry ingredients were carefully measured and then ground to a fine powder using a mortar and pestle. The pigment powder was then added to the epoxy resin plus solvents and stirred well before addition of Epikure 3164 curing agent. AA 2024-T3 panels were sandblasted, wiped with hexane, and rinsed with 18 MΩ·cm water. The coatings were applied to the substrate by air spray gun at a dry film thickness of ~20 μm. The pigmented polyurethane topcoat was applied air spray gun at a dry film thickness of ~50 μm.

The coating system is cured at ambient conditions for a period of one week prior to the initiation of testing. Additionally, each coating system was scribed through both coating layers, exposing the metal substrate. The advancement or inhibition of corrosion at the coating defect was observed to gain insight to the protective properties of each formulation.

5.2.3. Ag/AgCl wire reference electrode preparation

Reference electrodes were prepared using 50 μm silver wire, supplied by Goodfellow Corporation (Huntingdon, England). A chemical oxidation method was performed to create the reference electrode using a 0.03 M $FeCl_3$ solution and a 60 second immersion period. This method is described in detail in Section 3.2.1.

5.2.4. Placement of reference electrode within coating system

The corrosion potential of each Ag wire reference electrode is measured versus a standard reference electrode to ensure that stable electrochemical potential has developed. It is then secured to the primer surface using a small amount of commercial rapid cure epoxy. A piece of conductive tape tab is also applied to use as a lead for electrochemical measurement via the ERE. This tab is covered with masking tape, and the topcoat is applied. The coating system is scribed prior to exposure. See Figure 5.2 and Section 3.2.3 for more details.

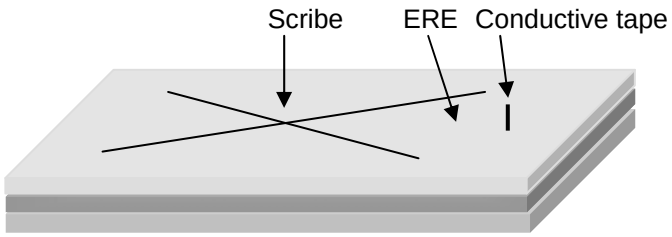

Figure 5.2. The coating system is illustrated to show the coating scribe, embedded reference electrode, and conductive tape lead.

5.2.5. Experimental analysis

Panels were exposed to accelerated weathering according to ASTM B117. They were placed in a 5% NaCl constant salt spray chamber, maintained at 35°C, and removed at regular intervals for physical and electrochemical examination. The panels were inspected for blistering, corrosion products, and defects each time they were removed from the salt spray cabinet. Photographic scans were taken for further analysis of the effects of weathering at various exposure times. Subsequently, the samples were fixed with an *o*-ring, glass cylinder, and clamp to create an electrolytic cell for the electrochemical measurements. The cell was filled with dilute Harrison's solution (DHS), composed of 0.05 wt% NaCl and 0.35 wt% $(NH_4)_2SO_4$. The area exposed to the solution is 7.06 cm^2.

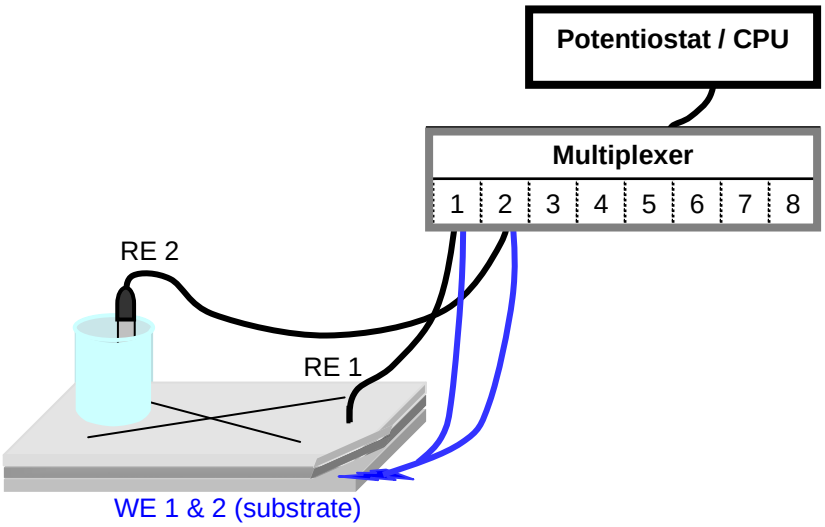

Figure 5.3. Illustration depicts the ERE and control experimental arrangements for corrosion potential.

A Gamry PCI4/300 potentiostat/galvanostat with dedicated EIS 300 and ESA 410 software, supplied by Gamry Instruments, Inc. (Warminster, PA), was utilized for the

electrochemical measurements, including corrosion potential. Visual analysis is produced by photo-scanning at each test period to accompany the data.

5.2.5.1. Corrosion potential

Corrosion potential measurements were made according to the instrumental set-up in Figure 5.3. A control measurement was made using the SCE standard as the RE and the substrate as the working electrode WE. Additionally, the measurement was performed using the experimental ERE is the RE and the substrate as the WE. Experiments were performed using a multiplexer for a period of twenty minutes at 0.5 measurements per minute.

5.2.5.2. Electrochemical noise measurement (ENM)

ENM measurements are made at a 5 Hz acquisition frequency in zero resistance ammeter (ZRA) mode. The experimental duration was 15 minutes and 128 points were taken per block for a total of seven blocks per test. The noise resistance (R_n) is calculated from this data by dividing the standard deviation of the voltage noise (σ_V) by the standard deviation of current noise (σ_I) [47].

$$R_n = \sigma_V (t) / \sigma_I (t) \quad (5.4)$$

The measurement is made using the "reverse electrode" set-up in which the substrates of two nominally identical coating systems are electrically connected via electrical grade wire and subsequently to the instrumentation [64]. This is the RE for the measurement. Allahar [50] has successfully applied this method to embedded sensors. Platinum mesh electrodes are placed in each electrolytic cell to serve as WE 1 and WE 2, as shown in Figure 5.4.

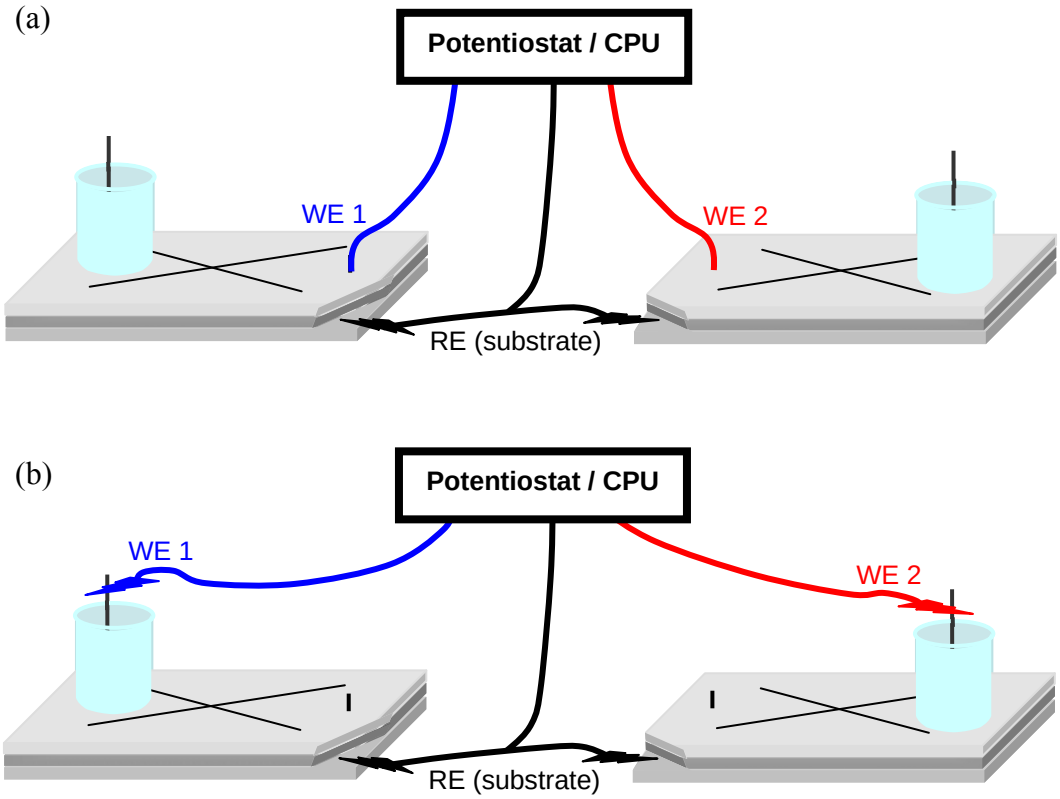

Figure 5.4. Illustration is given for the ENM instrumental set-up for the (a) experimental ERE and (b) SCE standard control experiment.

5.2.5.3. Electrochemical impedance spectroscopy (EIS)

EIS is conducted in the frequency range of 10^{5} to 10^{-2} Hz at 10 points per decade and 10 mV voltage perturbation. The experimental measurement is made using the substrate as the WE, a SCE as the RE, and platinum mesh as the counter electrode (CE). Figure 5.5 illustrates this set-up.

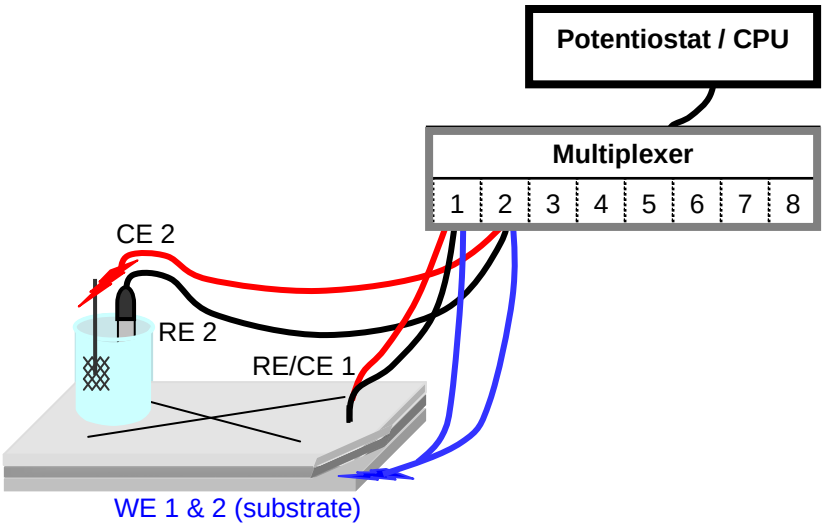

Figure 5.5. Illustration depicts the ERE and control experimental arrangements for EIS.

5.3. Results

5.3.1. Visual analysis

The coating systems were rinsed with distilled water and examined following removal from the salt spray chamber. This inspection included a detailed analysis of the area within and adjacent to the scribe. The purpose of the scribe is to detect the response of the coating to a scratch or other defect. The present coatings have been formulated with both sacrificial pigments and corrosion inhibitors to maximize the coating's ability to resist corrosion. Should a defect occur to a coating system while in service, one or more mechanisms could provide continued substrate protection. First, the Mg-rich pigments within the coating will corrode preferentially when in electrical contact with each other and the substrate. The reduction of water or oxygen proceeds on the exposed substrate surface, thus preserving its integrity. Second, the metal salts could provide a passivating effect on the exposed metal surface. The by-products of Mg-rich primer sacrificial protection are known to precipitate, providing a potentially passivating magnesium oxide barrier layer [6].

The main requirement is that mass transport, and thus corrosion reaction rates, are reduced at the metal surface. Precipitates may also block coating pores, achieving a similar effect.

Visual analysis results are given in Table 5.3 at three early exposure times to highlight the development of coating defects. All experimental formulations were blister-free at 15 hours of salt spray exposure. Following 80 hours a clear distinction is seen, demarcated by a dotted line in Table 5.3. Above this mark, each experiment has extensive blistering within 200 hours of exposure, while below, excellent performance was observed.

Table 5.3. Results for the average number of blisters per panel (#) and average size of blisters (d) in millimeters as well as the appearance of the scribe and the percentage corrosion-free (scribe) are given at three early exposure times.

Formulation	15 hrs			80 hrs			200 hrs		
	#	d	Scribe	#	d	Scribe	#	d	Scribe
n-Mg Control	n/a	n/a	n/a	20	2	dark (<5)	25	8	dark (<5)
Mg Control	8	1	dull (60)	10	3	dull (40)	20	3	dull (25)
0Li .5Mg 10	-	-	shiny	3	1	dark (10)	5	3	dark (<5)
5Li 0Mg 10	-	-	shiny	15	3	shiny (>50)	15	8	shiny (>50)
5Li .5Mg 0	-	-	shiny	5	1	shiny (50)	15	2	shiny (25)
6Li .6Mg 13	-	-	shiny	-	-	shiny (70)	3	1	shiny (75)
3Li .3Mg 16	-	-	shiny	-	-	shiny (75)	-	-	shiny (>50)
3Li .8Mg 6	-	-	shiny	1	1	shiny (75)	1	1	shiny (50)
8Li .3Mg 6	-	-	shiny	-	-	shiny (75)	-	-	shiny (50)

The positive control for this experiment, Mg Control, which contains 40% Mg by volume, developed numerous small blisters during the time period. Larger blisters had formed on a few replicates. The blisters are a result of the rapid oxidation of Mg particles in the humid environment and subsequent reduction of water to evolve hydrogen gas.

$$Mg + 2H_2O \rightarrow Mg(OH)_2 + H_2\uparrow \quad (5.5)$$

The n-Mg Control panel is the negative control for this experiment. It has many blisters and a dark scribe after and a very small percentage of the scribe remains shiny

following 80 hours of exposure. It is likely that anodic and cathodic reduction reactions occur at the bare metal surfaces. The blister size increases fourfold between 80 and 200 hours, reaching nearly 1 cm in a few cases as shown in Figure 5.6. Scale is approximate.

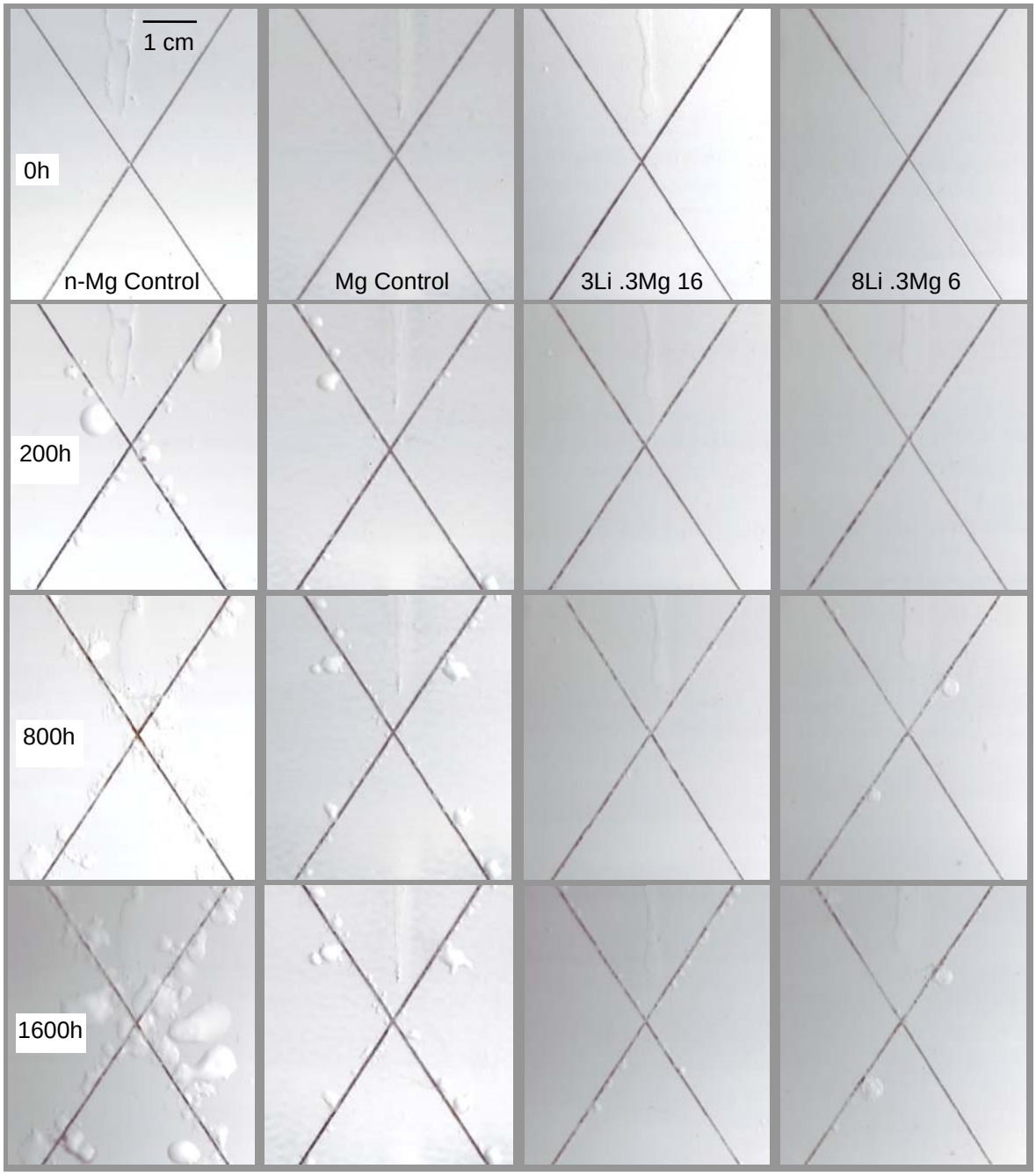

Figure 5.6. Photoscans at various hours of exposure. The experimental ERE_{Ag} utilized for corrosion potential measurements is faintly visible within the top of each "X" or scribe.

Although formulations containing a mixture of two ingredients gave poor results, careful examination showed different responses to the exposure conditions. The coatings formulated with $Mg(NO_3)_2$ and Mg metal particulates had some large and small blistering, but the scribe was heavily corroded after 200 hours. The appearance is very similar to the n-Mg Control experiment but with 80% blister reduction. This may indicate a positive anti-blistering effect by $Mg(NO_3)_2$. Coatings formulated with Li_2CO_3 and Mg metal particulates showed the opposite effect: many large blisters with a 50% shiny scribe following 200 hours of exposure. The work by Visser and Hayes [63] reported similar anti-corrosion effects to the scribe with the use of lithium carbonate and magnesium metal particulates. The blister size is comparable to the n-Mg Control panels. The coatings formulated with Li_2CO_3 and $Mg(NO_3)_2$ have intermediate performance compared to the two previous. There are many blisters, but their growth is much slower. Additionally, the scribe remains 25% shiny after 200 hours of exposure. It is clear that the Li_2CO_3 is responsible for improved scribe conditions.

Following 1600 hours of ASTM B117 exposure, the coating with $Mg(NO_3)_2$ and Mg metal particulates had the best visual appearance of the coatings formulated with two ingredients. The average number of blisters is ten and the size is up to 15 mm. The coating with Li_2CO_3 and Mg metal particulates had the most severe blistering while Li_2CO_3 plus $Mg(NO_3)_2$ is slightly less severe. It is noted that, compared to the negative control for the experiment, blisters were contained to the scribe area.

The four experimental formulations containing all three constituents maintained very good anti-corrosion results following 200 hours of exposure. The scribe was 50% shiny or greater. Formulations 3Li .3Mg 16 and 8Li .3Mg 6 remained blister-free while 3Li

.8Mg 6 had approximately one blister per panel. The center-point of the experiment, 6Li .6Mg 13, showed a few blisters; however the scribe was 75% shiny, higher than any other formulation tested. It is clear that the incorporation of all three ingredients to the epoxy primer improved anti-corrosion performance significantly at early exposure times, compared to experimental controls and primers with only two ingredients.

Formulations 3Li .3Mg 16 and 8Li .3Mg 6 maintained the best visual appearance following 1600 hours of ASTM B117 exposure. Photo scans are provided in Figure 5.6, above, for these. They were free of visible coating defects until 600 and 450 hours, respectively. The former has many small blisters (< 1 mm) at the scribe following 1600 hours. A few replicates have slightly larger blisters as well. The blister shape of the small blisters is consistent with the positive control for the experiment but to but it is less extensive. This behaviour is a result of the Mg pigments in the formulation: it has the highest volume concentration of Mg = 16.6. This type of blistering was not observed on the coatings formulated with 3Li .8Mg 13 which had the next highest volume of Mg = 13.3.

Formulation 8Li .3Mg 6 averaged 5 blisters. The size ranged from < 1 to 3 mm in diameter. Formulation 6Li .6Mg 13 averaged 15 blisters per replicate, ranging from < 1 to 6 mm. Similarly, 3Li .8Mg 6 averaged 20 blisters at < 1 to 6 mm.

When appropriate in the following analysis, formulation 8Li .3Mg 6 to represent a sample with good experimental results. Formulation 3Li .3Mg 16 is also used. The PVC for these are 15 and 20, respectively.

5.3.2. Corrosion potential

Corrosion potential measurements are a known and effective method of determining the presence of sacrificial protection in a metal-rich coating system [8]. The corrosion

potential of Mg metal is reported as -1.8 V vs SCE in DHS while that of AA 2024-T3 is near -0.5 V vs SCE for the same solution [59]. In order for cathodic protection to occur the corrosion potential must lie at an intermediate value, known as the mixed potential. This value should be lower than -0.7 or -0.8 V vs SCE to conclude that cathodic protection is occurring.

Corrosion potential results versus time of exposure to ASTM B117 salt spray is presented in the Figures 5.7 and 5.8 for all coating samples. There are eight replicates for each experimental control and four for each experimental formulation. The average corrosion potential and standard deviation is plotted for each. The data was smoothed by an adjacent-averaging method using Origin Lab (Northampton, MA) software, version 8.1.

Figure 5.7 gives the corrosion potential results for the positive and negative control panels as well as the two-ingredient formulations. A shaded region is provided at -0.40 to -0.55 V vs SCE for reference; it is a reasonable estimate for the corrosion potential of a bare AA 2024 substrate. The actual corrosion potential is dependent on the surrounding electrolytic environment which is unknown at the coating/metal interface [59]. Some measured corrosion potentials were as high as 3.0 V vs SCE, especially for the non-pigmented primer. Potential measurements more positive than 0.0 V vs SCE are not a realistic measurement of the substrate's corrosion potential and generally indicate that a coating resistance too high for the instrument to make an accurate measurement. This is in part because the non-pigmented primer does not contain semi-conductive or conductive materials such as metal particulates or metal salts. Additionally, the polyurethane pigmented topcoat which creates an added resistance. Data more positive than 0.0 V was removed from the analyses below because it is not realistic.

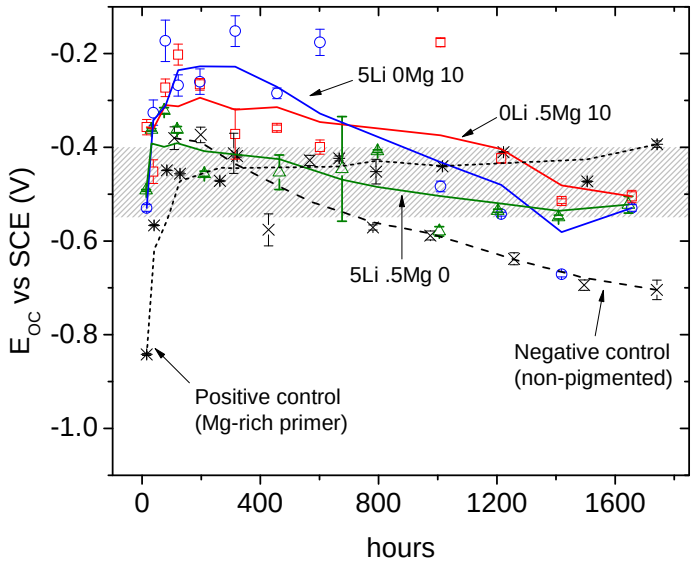

Figure 5.7. Averaged corrosion potential results for controls and two ingredient mixtures, smoothed by adjacent-averaging.

The Mg Control primer contains 40% PVC Mg metal particulates. The first average corrosion data point is -0.85 V vs SCE and suggests that the Mg metal particulates have been activated by the progression of water and electrolyte into the coating, as previously reported by Battocchi [1, 6]. However, the cathodic protection quickly ceases as the corrosion potential rises to a steady -0.45 V vs SCE. This coating was prepared at the low end of the formulating window for Mg-rich primers. However, the influence of Li_2CO_3 and $Mg(NO_3)_2$ may still be estimated with the results of this control experiment.

The 0Li .5Mg 10 primer contains only $Mg(NO_3)_2$ and Mg metal particulates. They are formulated at 50% of the upper boundary presented in Table 5.1. A few replicates give initial corrosion potentials near -0.7 vs SCE. This value may suggest momentary polarization, or cathodic protection, by the Mg metal particulates. As presented in Table

5.2, the total PVC for this coating is 11%. The corrosion potential quickly shifts to more positive values. Significant variability was observed between replicates.

Good reproducibility was observed between the replicates of 5Li .5Mg 0, containing only the metal salts $Mg(NO_3)_2$ and Li_2CO_3, especially at exposure times less than 200 hours. This differs greatly from formulations containing Mg metal. The corrosion potential at the beginning of the experiment is consistent with AA 2024-T3 and indicates that cathodic protection is not available. A slight rise in potential is realized in the first 80 hours followed by a slow decline and is not fully understood at this point in time.

Results for 5Li 0Mg 10 closely resemble 0Li .5Mg 10 for the first half of the experiment with more pronounced variance between replicates. Both formulations contained 10 vol% Mg metal and one metal salt.

The above results seem to suggest that Mg metal particulates in 0Li .5Mg 10 provide momentary cathodic protection at 10% PVC loading. However, they failed to polarize the corrosion potential beyond 80 hours of exposure. It is also suggested that the $Mg(NO_3)_2$ provides a stabilizing effect on the corrosion potential at very short exposure times, this is most pronounced between 5Li .5Mg 0 replicates.

The corrosion potential results for mixtures of Li_2CO_3, $Mg(NO_3)_2$, and Mg metal are given in Figure 5.8. The total PVC for each is provided in the caption. All formulations suggest that cathodic protection is active at the initial hours of exposure. The effect is least pronounced for experimental formulation 3Li .8Mg 6 which has a total PVC = 11. This can be expected because of the extremely low PVC, making it difficult for the conductive pigments to be in electrical contact with each other and the substrate.

The standard deviation is small throughout the course of the experiment for all formulations, indicating good reproducibility. Beyond 1000 hours the corrosion potentials are intermediate to the positive and negative controls. The slope of the smoothing average for 8Li .3Mg 6 is most similar to the negative control. This formulation had the poorest ranking by visual analysis. Further interpretation of the corrosion potential data lies outside the scope of this analysis.

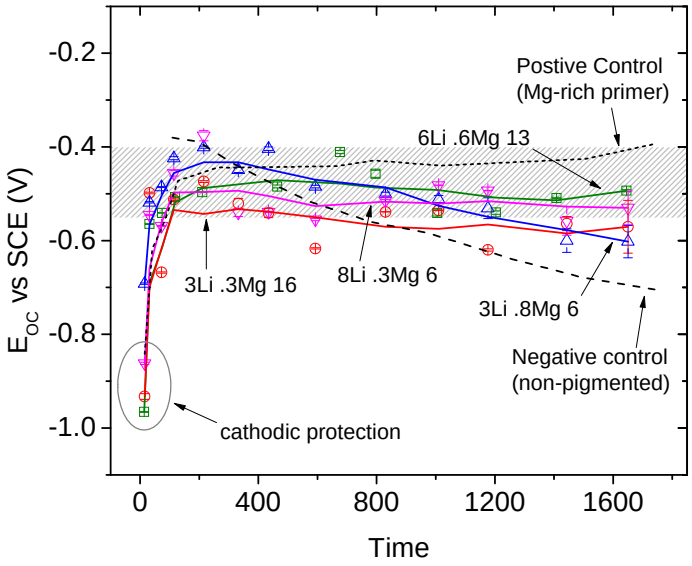

Figure 5.8. Averaged corrosion potential results for mixtures of Li_2CO_3, $Mg(NO_3)_2$, and Mg, smoothed by adjacent-averaging.

Formulations 3Li .3Mg 16 and 8Li .3Mg 6 have the most negative corrosion potential which is stable at all times. It may be suggested that the $Mg(NO_3)_2$ and Mg metal particulates are present at a synergistic ratio. However, by comparison to Figure 5.7, above, it can be seen that the Li_2CO_3 is necessary to obtain the positive anti-corrosion effect and, therefore, reduced corrosion reaction rates.

Figure 5.9 presents the three ingredient mixtures corrosion potential for the first 150 hours of the experiment. The lines are connected and the smoothing average is not included to show detail. Formulation 6Li .6Mg 13 and 3Li .8Mg 6 have a similar shape, with a small, positive slope beyond 40 hours. The corrosion potential has a slight decrease at 70 hours for formulation 8Li .3Mg 6. The same is observed for 3Li .3Mg 16 however it is more pronounced. The dip is cause by the Mg metal. This plot may suggest that $Mg(NO_3)_2$ provides a stabilizing effect on the active Mg particles. More data is needed to confirm this; however, the standard deviations are on the order of 0.001 V vs SCE.

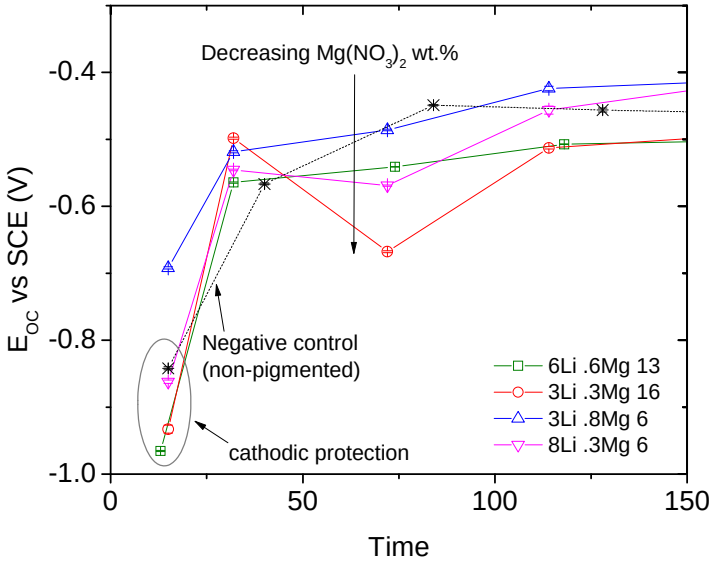

Figure 5.9. Averaged corrosion potential results to 150 hours for mixtures of Li_2CO_3, $Mg(NO_3)_2$, and Mg, plus connecting lines.

5.3.2.1. Corrosion potential measured by ERE

The corrosion potential for the primer containing Li_2CO_3, $Mg(NO_3)_2$, and Mg pigment was also measured by the Ag wire ERE described in Chapter 3. The experimental ERE_{Ag} is located between the primer and topcoat. Corrosion potential measurements were

made concurrently to the SCE measurements presented in Section 5.3.2 which allows the data to be compared directly.

Figure 5.10 the average plus standard deviation of four replicates along with the positive and negative control vs SCE. Smoothing by adjacent-averaging was applied to this for ease of interpretation. Again all data more positive than 0.0 V was omitted because it is not realistic. The shaded area in the graph is identical to Figures 5.7 and 5.8; however, it is shifted 0.2 V in the positive direction to correct to the ERE_{Ag} scale. A potential difference of 0.1 to 0.2 V versus an SCE standard was established for Mg-rich primers plus a polyurethane topcoat in Chapter 3 and Reference [65].

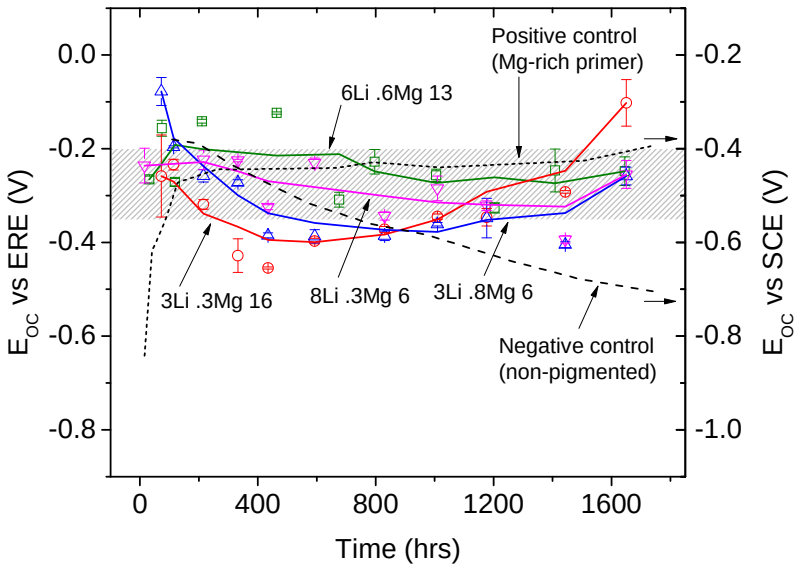

Figure 5.10. Averaged corrosion potential results for Li_2CO_3, $Mg(NO_3)_2$, and Mg as measured by ERE_{Ag} and controls vs SCE, smoothed by adjacent-averaging.

The corrosion potentials obtained at early exposure times show somewhat different behaviour than Figure 5.8 and cathodic protection was not detected. Beyond 1000 hours, there is good agreement. There is some indication that this improves with coating

performance, for example see 8Li .3Mg 6. When using the ERE_{Ag} for corrosion potential measurements, it is important to remember that shifts could indicate a change in $[Cl^-]$.

As stated previously, corrosion potential measurements are a standard method for assessing the corrosion protection afforded by cathodic protection systems. This section provides the first results of its kind for use of an embedded reference electrode (ERE) to research and develop novel cathodic protection coating systems. The accompaniment of standard electrochemical measurements such as EIS and ENM is desired to explore the dielectric properties of the coating system.

5.3.3. Electrochemical impedance spectroscopy (EIS)

5.3.3.1. Total impedance as a function of exposure time

The impedance modulus, $|Z|$, measured at 0.01 Hz has been used to represent the results. At very low frequencies the measurement is assumed to include resistances occurring at the substrate/coating interface as well as those within the coating. All experiments were conducted using the same cylindrical glass solution cells. Therefore, the measured surface area is assumed identical and impedance results were not calculated to impedance per unit area.

Figures 5.11 (a) and (b) give the results for the two-ingredient and three-ingredient formulations, respectively. The positive and negative controls are included for each. The average corrosion potential and standard deviation is plotted for each. The data was smoothed by an adjacent-averaging method. Measured values greater than 10^{10} Ω and less than 10^4 Ω were excluded from this data set. These values are not realistic for the coating systems being measured and generally indicate an instrumental error or potential drift during measurement.

At early exposure times, n-Mg Control impedance is on the order of 10^8 to 10^{10} Ω as which is expected for barrier coatings. At long exposure times, the value is below 10^5 Ω, indicating total coating failure. This is consistent with the values reported for AA 2024-T3 bare substrate in DHS. Here, water and electrolytes permeate the coating system and participate in cathodic reactions on the substrate. Low frequency impedance values in the range of 10^6 to 10^8 Ω are observed for sacrificial coating systems [6]. Results for the Mg Control, comprised of Mg-rich primer plus pigmented polyurethane topcoat, are in this range. Low-resistance pigments within the primer lower the total impedance compared to the non-pigmented primer.

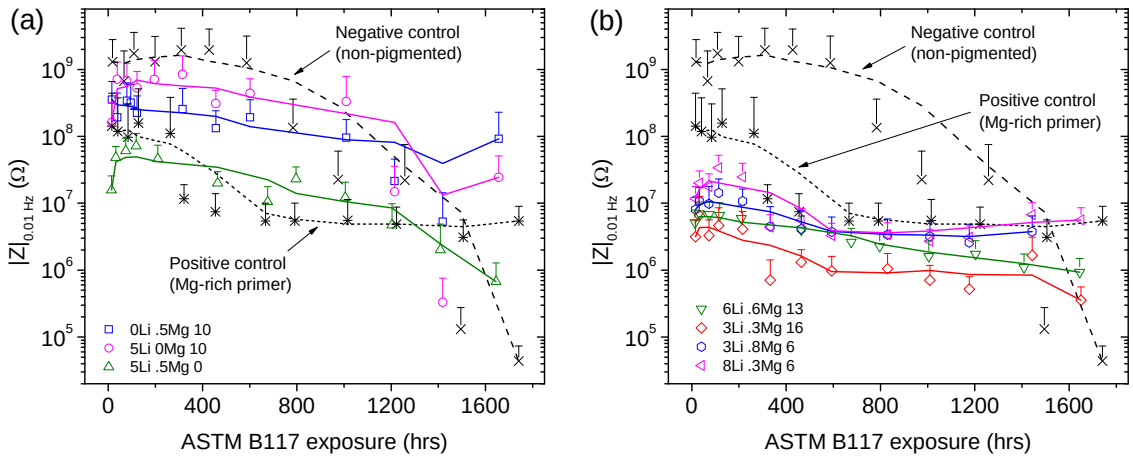

Figure 5.11. Total impedance ($|Z|_{0.01\ Hz}$) versus time for (a) two-ingredient and (b) three-ingredient mixtures. The positive and negative controls are included in each. Data was smoothed by adjacent-averaging method.

The results for formulations containing two ingredients, Figure 5.11 (a), are characterized by two distinct trends. First, the coatings containing Li_2CO_3 experienced a 0.5 to 1.5 orders of magnitude increase in impedance during the first 100 hours of exposure. This seems to indicate a passivating effect, possibly by the deposition of carbonate containing compounds within coating pores. Second, the coatings containing Mg

pigment had significant variability between replicates and very high impedance for more than 1000 hours of exposure. The values are more than an order of magnitude higher than the 5Li .5Mg 0 and Mg Control.

Based on the visual analysis, corrosion potential, and total impedance results it is clear that neither cathodic nor sufficient barrier protection is provided to the substrate for the two ingredient mixtures examined beyond 200 hours of exposure.

Low frequency impedance plots are provided in Figure 5.11 (b) for the three ingredient primer formulations. All show impedance values above 10^5 Ω for all hours. Reproducibility was very good compared to the positive control for this experiment. Formulation 8Li .3Mg 6 had the least variation between replicates. The impedance values are approximately 10^7 Ω at all exposure times. Formulations 3Li .8Mg 6 and 3Li .3Mg 16 had the most variation between replicates.

Figures 5.11 (b) compare very well to the analysis of the two ingredient mixtures. The increase in impedance during the first 100 hours was most significant for coating formulated at Li_2CO_3 volume content. Also by this figure, the magnitude of impedance, as well as variability between replicates, decreases within increasing Mg metal PVC. However, there is indication that $Mg(NO_3)_2$, at the proper concentration, stabilizes the Mg reactions. It seems that the mechanism is by forming insoluble magnesium precipitates to block coating pores and act as a barrier [61]. More than likely, cathodic protection is not the main mechanism of corrosion protection in these formulations.

5.3.3.1.1. Total impedance measured by ERE_{Ag}

Low frequency impedance results are also provided for measurements performed using the ERE_{Ag} as the RE and CE (Figure 5.5). The main difficulty in applying the ERE_{Ag}

to EIS measurements is that small polarizations may significantly affect the results. The [Cl^-] at the ERE is not controlled or calibrated other than by the epoxy coating it is embedded within. This is the first known EIS measurement of a coating system by an Ag wire embedded reference electrode.

Figure 5.12 gives the ERE_{Ag} results for (a) two-ingredient and (b) three-ingredient mixtures. The same statistical procedures were applied to this data set as those presented in Figure 5.11. Somewhat surprisingly, the negative control correlates well with the standard results in Figure 5.11. Additionally, an accurate impedance ranking is given in Figure 5.12 (b) following 1000 hours of exposure.

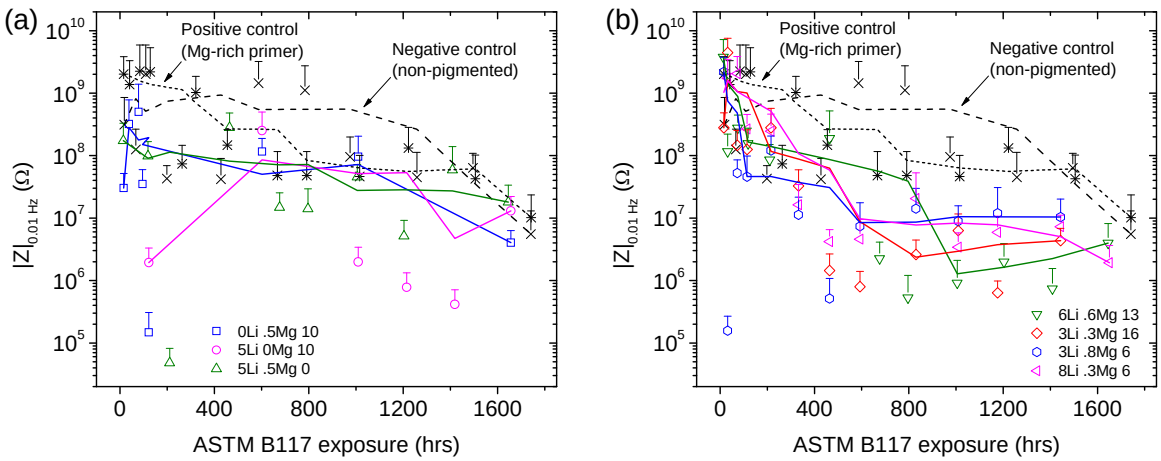

Figure 5.12. Total impedance ($|Z|_{0.01\ Hz}$) measured by ERE_{Ag} versus time for (a) two-ingredient and (b) three-ingredient mixtures. The positive and negative controls are included in each. Data was smoothed by adjacent-averaging method.

The other significant observation is that the $|Z|_{0.01\ Hz}$ is very high for the three ingredient mixtures, which provided excellent corrosion resistance, as well as the positive at initial exposure times. The two ingredient mixtures in Figure 5.12 (b) are an order of magnitude lower and failed to protect the substrate. It is important to note that the ERE_{Ag}

measures dielectric response between itself and the AA 2024-T3 substrate while the standards in Figure 5.11 are external to the coating and include the topcoat. Therefore, direct comparison would not be entirely accurate. Additionally, the ERE_{Ag} does not have well-defined solution cell, and the impedance measurement is dependent on a number of indeterminate factors including the path length of current flow. The accuracy of EIS instrumentation lessens at very high impedances; thus, further experimentation is required to determine if the ERE measurement is valid or, more importantly, whether or not this information is useful for the ranking of experimental coating systems.

5.3.3.2. Impedance versus frequency

Figure 5.13 presents impedance data for the Mg Control coating system to highlight characteristics as a function of the frequency. The replicate presented was chosen to be most representative of the sample set. Small inconsistencies at 10^3 or 10^4 Hz reveal an instrumental error and are, therefore, omitted from the following analysis.

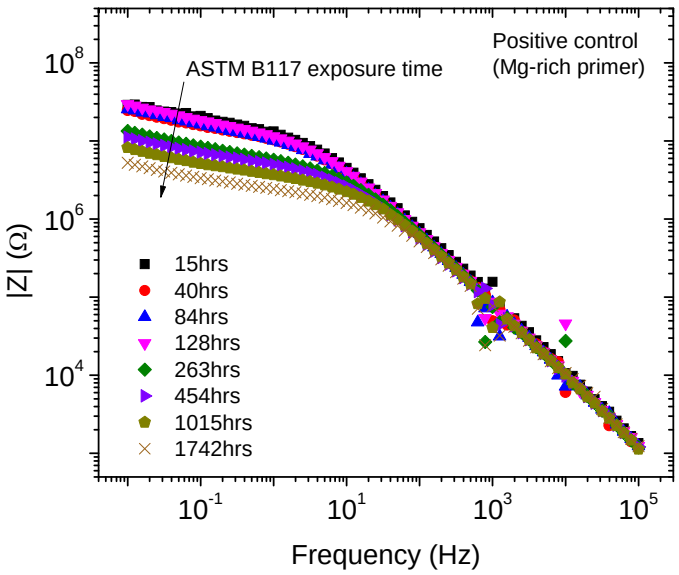

Figure 5.13. Impedance versus frequency for Mg Control.

Below 10^1 Hz a slight negative slope is observed at all exposure times. This is associated with the resistive properties of the coating. It is not purely resistive, however, due to the fact that the slope is not parallel to the x-axis. There is a steady decrease in resistance with increased exposure time, indicated by an arrow. This is consistent with the low frequency impedance data above.

A consistent slope of -1 is observed at frequencies greater than 10^2 Hz. Here the coating is functioning as a pure capacitor. The impedance value at 10^3 or 10^4 Hz can be utilized to calculate the diffusion rate for the coating system as well as water uptake. This lies outside the scope of the present preliminary examination.

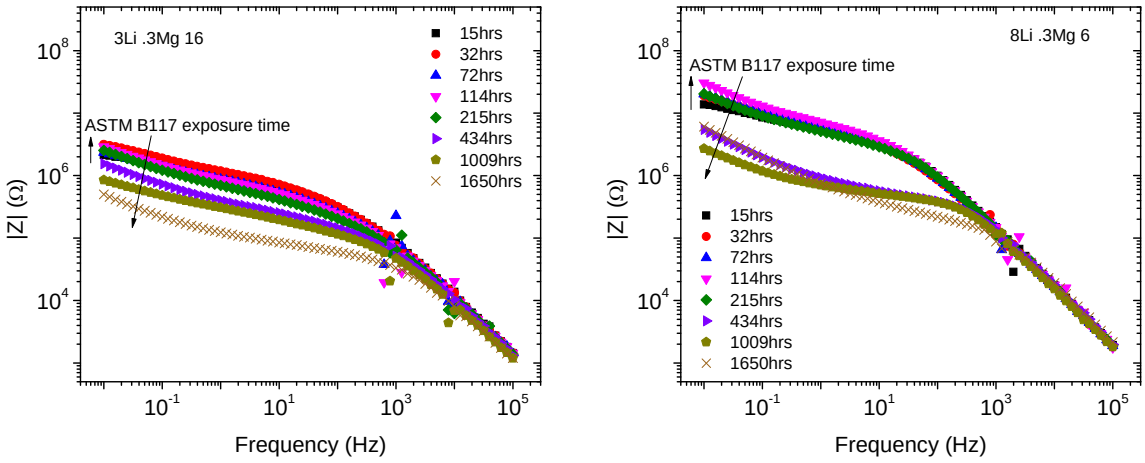

Figure 5.14. Impedance versus frequency for (a) 3Li .3M 16 and (b) 8Li .3Mg 6.

Figure 5.14 gives results for formulations 3Li .3M 16 and 8Li .3Mg 6, using a replicate which well-represented the sample set. These two formulations have the best anti-corrosion performance according to previous analyses. Compared to the Mg Control, resistive properties are observed at higher frequencies, indicating lower coating resistance. Also, these plots indicate that there are more corrosion processes occurring for these formulations than apparent in Figure 5.13. Specifically, the increasingly negative slope

below 10^{-1} Hz in Figure 5.14 (b) suggests there may be additional processes at the coating/metal interface. Once the phase angle reaches 45°, or a slope equal to -1, Warburg diffusion is occurring [66]. The phase angle is 45° following 1600 hours for 8Li .3Mg 6 (not shown). The effect is less pronounced in the 6Li .6Mg 13 and 3Li .8Mg 6.

5.3.3.3. Nyquist plots

Figure 5.15 presents data for the Mg Control in the form of a Nyquist plot. The purpose of these plots is to distinguish frequency-dependent behaviors associated with each primer system. An arrow is placed on the figure to indicate the high and low frequency regions of the plot. The plot shows semi-circular behavior at high frequencies which is characteristic of charge transfer reactions. Additionally, the presence of linear trend at low frequencies indicates diffusion control. Foyet [67] achieved similar results for a chromate free primer on AA 2024-T3 and has attributed this to percolation pathways developed by water and oxygen.

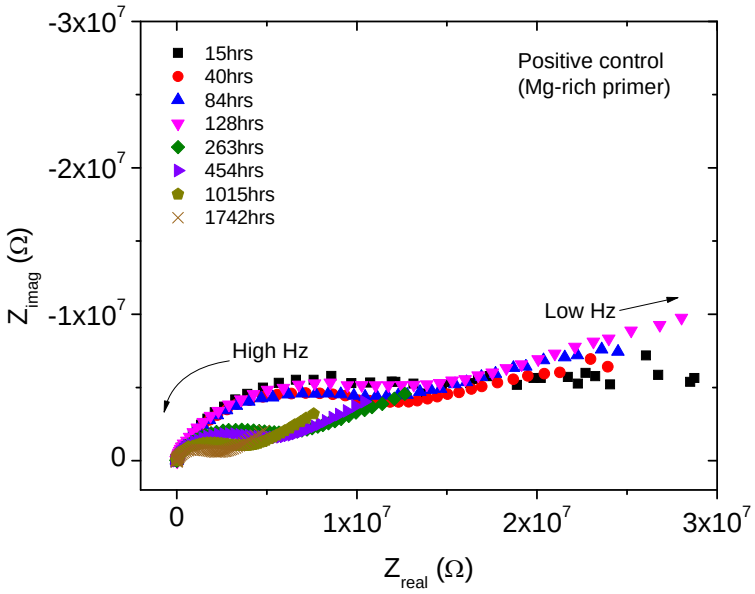

Figure 5.15. Nyquist plot for Mg Control.

Nyquist plots for the two formulations with superior anti-corrosion performance, 3Li .3Mg 16 and 8Li .3Mg 6, are given in Figure 5.16. Both are similar to the Mg Control results, with diffusion contributing to low frequency impedance values. The corresponding line is greatest for formulation 8Li .3Mg 6 at 200 hours of exposure. Formulation 3Li .3Mg 16 is exhibits Warburg diffusion following 1600 hours of exposure (Figure 5.16 (a)). The increase in diffusion control seems to follow a decrease in total PVC as well as Mg metal PVC in these figures. Despite the processes, the coatings have minimal visual defects following 1600 hours.

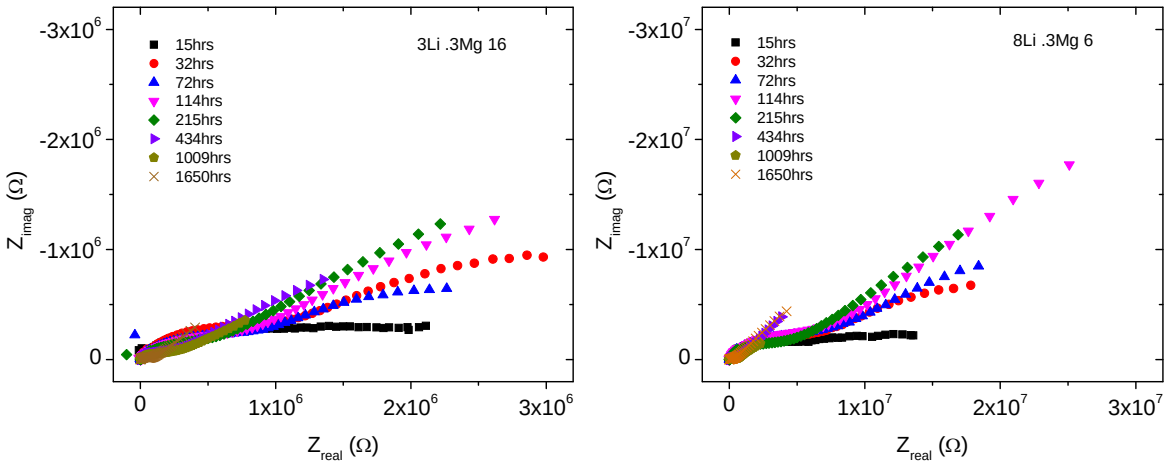

Figure 5.16. Nyquist plots for (a) 3Li .3M 16 and (b) 8Li .3Mg 6.

5.3.4. Electrochemical noise method (ENM)

Electrochemical noise measurements were performed to determine noise resistance (R_n). The method is generally used to characterize the type and rate of corrosion reactions occurring at the substrate's surface [47, 68-69]. Here, noise resistance values have been plotted as a function of exposure time. These measurements are theoretically comparable to impedance values obtained by EIS at low frequencies [45-46].

Results are given in Figure 5.17 for all formulations along with the positive and negative experimental controls. Seven measurement blocks are calculated for each ENM exposure time. Since replicates are paired for ENM measurements the data presented below is an average of four n-Mg Control, three Mg-Control, and two data sets for experimental formulations (Figure 5.4). There was adequate reproducibility between the block as well as sample replicates.

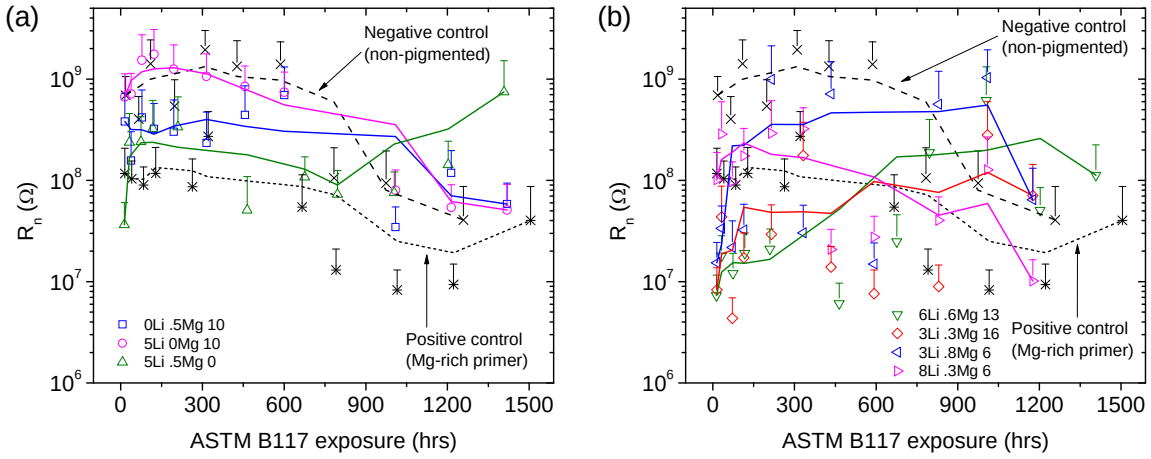

Figure 5.17. Noise resistance (R_n) versus time for (a) two-ingredient and (b) three-ingredient mixtures. The positive and negative controls are included in each. Data was smoothed by adjacent-averaging method.

Figure 5.17 (a) is in good agreement the $|Z|_{0.01\ Hz}$ results in Figure 5.11 (a). The coating formulated with Li_2CO_3 and Mg metal alone had $R_n = 10^9\ \Omega$ at early exposure times. Therefore, it must be emphasized that $Mg(NO_3)_2$ is necessary to provide corrosion protection. The three ingredient mixture results are similar to Figure 5.11 (b) during the first 200 hours of exposure. Afterward, the variability in the measurements becomes quite large. An increased number of replicates would improve the usefulness of these results.

The R_n values obtained by ENM are about one order of magnitude greater than the $|Z|_{0.01\ Hz}$ values reported by EIS in Figures 5.10 and 5.11, with the exception of the negative

control. These high values may be, in part, attributed to the use of the substrate as the reference electrode, compared to a SCE used for EIS measurements. An increase in σ_V, or the variation in corrosion potential measurement, increases R_n according to Equation 5.4 (Section 5.4.3.2). The present results are valid, however, since the ranking of coating performance achieved by ENM is consistent with previous electrochemical and visual analyses.

5.3.4.1. Electrochemical noise method (ENM) measured by ERE

ENM results were also obtained by ERE_{Ag} to calculate R_n for the coating formulations. Measurement of the ENM by a thin wire reference electrode, embedded in a coating system is not previously reported. Similar work by Bierwagen and co-workers has demonstrated the use of Pt wires or foils as an embedded, chemically inert electrode [43-44, 48, 52].

Figures 5.18 (a) and (b) give these results for the two-ingredient and three-ingredient mixtures, respectively. The negative control results are in agreement with Figure 5.16 (a). The two-ingredient formulations become more consistent with the standard measurement at long exposure times. However, an interesting anomaly is observed at early exposure times. The R_n is below 10^7 Ω and the rank of the coating performance is reversed, compared to the above results. For instance, 5Li 0Mg 10 has consistently shown poorer results than the other two. Formulation 0Li .5Mg 10 gave intermediate results, but was nearer to 5Li 0Mg 10, while 5Li .5Mg 0 was quite stable with the lowest impedance. The stabilizing effect has been attributed to $Mg(NO_3)_2$ in the presence of Li_2CO_3.

Figure 5.18 (b) is quite noisy, but the smoothing trend lines for the three ingredient mixtures are very similar. This is in agreement with previous results. Formulation 3Li .3Mg

16 has noticeably smaller R_n values, based on this trend line which seems to correlate well to Figure 5.11 (b). Additionally 8Li .3Mg 6 has the highest R_n overall which was often the case in the previous analyses. Again, additional replicates would improve the accuracy on these interpretations and allow one to determine if there is in fact a unique correlation.

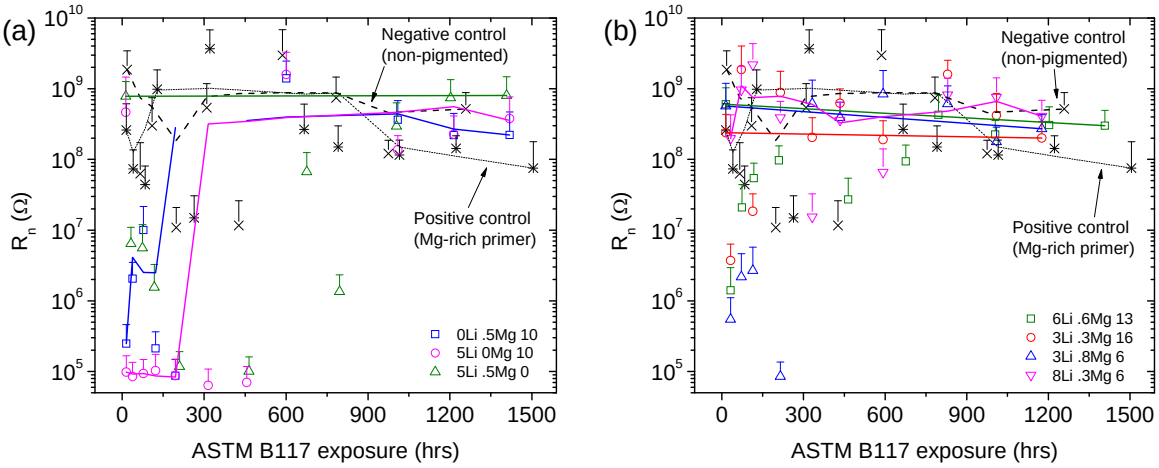

Figure 5.18. Noise resistance (R_n) measured by ERE_{Ag} versus time for (a) two-ingredient and (b) three-ingredient mixtures. The positive and negative controls are included in each. Data was smoothed by adjacent-averaging method.

Much like the EIS data obtained by the ERE_{Ag}, there is much to understand about the R_n data presented here. Further interpretation is beyond the scope of the present analysis.

5.4. Discussion

5.4.1. Effect of metal salts and reduced Mg metal PVC on cathodic protection

The coatings examined in this study were formulated well below the normal PVC of metal-rich coatings in order to observe the effects of the metal salts as well as to test for cathodic protection at these values. The rule-of-thumb for metal rich coatings is to formulate at or near the system's CPVC in order for the metal particulates to be electrically connected to each other and the substrate. The lower limit for cathodic protection is

estimated as the PVC at the percolation threshold for the metal particulates. This is approximately 30% for spherical particles [70] and may be lower for pigments of other shapes [71]. The Mg pigments used here are granular shaped. Therefore it is likely that the percolation threshold is less than 30%.

Formulation 5Li .5Mg 0 did not contain Mg metal particulates and the corresponding corrosion potential measurements provide no indication of cathodic protection, as expected. Formulation 5Li 0Mg 10 also showed no cathodic protection. The few data points near -0.7 V vs SCE for formulation 0Li .5Mg 10 may be a result of cathodic protection, but it is ultimately inconclusive.

Formulation 3Li .8Mg 6 also had a few points near -0.7 vs SCE. All other three ingredient formulations provided cathodic protection at the initial exposure time. The duration was less than 40 hours. The pigments in formulation 8Li .3Mg 6 were predominantly Li_2CO_3, suggesting that cathodic protection can be achieved as low as Mg metal PVC = 6. In order for this to occur, both lithium and magnesium salts are required.

Cathodic protection is exhausted very quickly in these coatings. This may be an effect of the oxidation of all free Mg. However, it is more likely that the resistance between Mg particles and the substrate reaches a critical limit due to these coatings being very low PVC. The high resistances may be assisted by barrier layers formed as a result of magnesium oxidation products and by-products. Despite the loss of cathodic protection, the resulting coatings remain resistant to corrosion following 1600 hours of exposure. The visual and electrochemical analyses indicate comparable or better corrosion resistance the Mg Control which was used as a positive control for this experiment. Additionally, there is indication of some degree of dissimilarity in the protection mechanism or mechanisms.

5.4.2. Magnesium nitrate behavior in Mg-rich primers

There are indications that the addition of $Mg(NO_3)_2$ to coatings prepared by Li_2CO_3 and Mg metal particulates improves the corrosion protection throughout coating exposure. Varma proposed that in the presence of cathodic reactions, in which water is reduced to hydroxyl ions (Eq. 5.6), the insoluble magnesium hydroxide is formed (Eq. 5.7) [61].

$$2H_2O + O_2 + 4e^- \rightarrow 4OH^- \quad (5.6)$$

$$Mg^{2+} + 2OH^- \rightarrow Mg(OH)_2 \quad (5.7)$$

The insoluble material is suggested to inhibit corrosion by blocking pores. The result is low frequency impedance values which remain constant with exposure time. Lu [72] noted similar results for a Mg-rich coating applied to AZ91D magnesium alloy. The present results are consistent with this finding. Furthermore, the incorporation of at least 5 vol. % Li_2CO_3 to coatings resulted in an increase in low frequency impedance values, at low exposure times. The increase is greater than one order of magnitude in some cases.

As shown in Equation 5.5, the dissolution of Mg metal particulates in water at neutral pH creates unwanted hydrogen evolution. However, the activation of cathodic protection creates very high pH which promotes the formation of $Mg(OH)_2$ without hydrogen evolution. Magnesium nitrate provides an additional and immediate Mg^{2+} source for this reaction. The result is immediate corrosion protection and controlled charge transfer reactions. The effect is most pronounced during the first 200 hours of exposure. Afterward, it is suggested that a compact barrier layer provides corrosion protection for greater than 1600 hours.

Battocchi et al. [6] first reported the formation of a magnesium oxide barrier layer which precipitates in a second stage of Mg-rich primer protection. The composition of this

oxide material has been of much interest. Mg-rich primers have provided excellent results in field and Prohesion testing but have failed rapidly for ASTM B117 in some reports, especially in cabinets excluding CO_2. Pathak and coworkers [5, 7] have carefully examined the testing conditions and shown that CO_2 is necessary for the second stage of Mg-rich primer protection to occur. $Mg(OH)_2$ is not stable in atmospheric levels of CO_2 and is converted to $MgCO_3$.

$$Mg(OH)_2 + CO_2 \leftrightarrow MgCO_3 + H_2O \quad (5.8)$$

Furthermore, Lindström et al. [73] and Jonssön et al. [74] have shown that complex, slightly-soluble carbonates form in humid environments which greatly affect the Mg metal corrosion rate. These magnesium carbonates provide a uniform and compact barrier layer which inhibits diffusion of water and ions [5]. Incorporation of $Mg(NO_3)_2$ into the coating formulation provides an immediate source for production of $Mg(OH)_2$ to initiate the production of magnesium carbonates in the coating system.

Encapsulation of the metal particulates in organic coatings has been shown to reduce the kinetics of magnesium oxidation, allowing Mg-rich primers to provide prolonged cathodic protection [6]. It may be possible for magnesium nitrate to further expand this protection. Additional experimentation is necessary to determine the effect that $Mg(NO_3)_2$ has on the service lifetime of Mg-rich primer systems.

5.4.3. Electrochemical analysis of novel sacrificial coatings by ERE

The results of ERE measurement for corrosion potential, low frequency EIS, and ENM were presented within this chapter. The ERE had previously been utilized as a corrosion potential monitoring device for Mg-rich coatings on AA 2024-T3 [65]. Here, they have been applied for research and development of a novel sacrificial coating system.

Corrosion potential results showed very good correlation with the SCE standard data following a short activation period in which realistic values could not be obtained. By the time the ERE had equilibrated, the cathodic protection had been lost. Despite the short period of inactivity, the results seem to suggest that the ERE is a versatile tool for measuring corrosion potential. Good measurement performance is observed following 1600 hours of ASTM B117 exposure in the present experiment. It is essential for the ERE outlast the system it is monitoring.

EIS measurements were performed using the ERE as the working and counter electrodes. No solution cell was used which offers a crude, yet practical technique for in-situ impedance monitoring. If the ERE were employed as a corrosion potential monitoring device for SHM, it would be ideal for the device to be used to collect additional electrochemical information. Low frequency impedance results were provided in the present chapter. There is some indication that useful information can be obtained from this measurement. The limited understanding of the ERE as an impedance monitoring device prevented further interpretation of the data in regards to the novel sacrificial coating system. The present objective was to utilize the ERE as an impedance monitoring device for a broad range of coating systems to determine feasibility for such an application. Here, it has been shown that a thin wire reference electrode, embedded between the primer and topcoat, can be used to perform EIS measurements and obtain low frequency impedance data.

The ENM results presented here are also the first of its kind in regards to a performing the measurement by a reference electrode embedded within the coating. The

sample size presented here is not large enough to statistically analyze the performance of this measurement. This is outside the scope of the present analysis.

The material cost for the ERE is low and the preparation can be simple as 30 seconds of immersion in dilute (0.1 M) $FeCl_3$ solution. The placement of the ERE between the topcoat and primer has been shown to protect the integrity of the electrode without introducing significantly detrimental effects to the coating. The present results suggest that the ERE is applicable to use with research and development of novel coating systems.

5.5. Conclusions

A mixture analysis of lithium carbonate, magnesium nitrate, and Mg metal particulates was performed to examine corrosion inhibition and cathodic protection for AA 2024-T3. To the knowledge of the authors, this is the first experimentation with this combination of materials for corrosion protective coatings. The samples were subjected to accelerated weathering by ATSM B117 salt spray chamber and removed periodically for analysis by electrochemical impedance spectroscopy (EIS) and electrochemical noise measurements (ENM). Conventional, macroscopic examination was also used to rank coating performance.

Coatings formulated with only two ingredients gave poor results. On the contrary, the formulations tested with three ingredients maintained anti-corrosion and anti-blistering effects to a greater extent than a Mg-rich primer control following 1600 hours. Continued optimization of the proposed primer formulations offers the opportunity to design and implement unique cathodic protection plus corrosion inhibitor coating systems for use on aluminum.

ERE results in this chapter suggest that it is applicable for use in the research and development of novel coating systems. Feasibility is shown here for corrosion potential monitoring of various coating systems with wide-range corrosion protection performance as well as protection mechanisms. Additionally, low frequency impedance and noise resistance measurements were obtained by the ERE. This confirms the feasibility of these measurements and provides insight for possible applications. Some agreement was observed between the ERE and the SCE standard for both techniques although the experimental configurations are fundamentally not equivalent.

5.6. References

[1] M.E. Nanna and G.P. Bierwagen, Mg-rich coatings: a new paradigm for Cr-free corrosion protection of Al aerospace alloys, Journal of Coatings Technology Research, 1 (2004) 69-80.
[2] A.M. Simoes, D. Battocchi, D.E. Tallman and G.P. Bierwagen, SVET and SECM imaging of cathodic protection of aluminium by a Mg-rich coating, Corrosion Science, 49 (2007) 3838–3849.
[3] G. Bierwagen, R. Brown, D. Battocchi and S. Hayes, Active metal-based corrosion protective coating systems for aircraft requiring no-chromate pretreatment, Progress in Organic Coatings, 68 (2010) 48–61.
[4] L. Liu, R. Xu and G. Song, Corrosion behaviour of Mg-rich Al coatings in the protection of Al alloys, Surface & Coatings Technology, 205 (2010) 332–337.
[5] S.S. Pathak, M.D. Blanton, S.K. Mendon and J.W. Rawlins, Investigation on dual corrosion performance of magnesium-rich primer for aluminum alloys under salt spray test (ASTM B117) and natural exposure, Corrosion Science, 52 (2010) 1453–1463.
[6] D. Battocchi, A.M. Simoes, D.E. Tallman and G.P. Bierwagen, Electrochemical behaviour of a Mg-rich primer in the protection of Al alloys, Corrosion Science, 48 (2006) 1292–1306.
[7] S.S. Pathak, M.D. Blanton, S.K. Mendon and J.W. Rawlins, Carbonation of Mg powder to enhance the corrosion resistance of Mg-rich primers, Corrosion Science, 52 (2010) 3782–3792.
[8] S. Felix, R. Barajas, J.M. Bastidas, M. Morcillo and S. Feliu, Study of protections mechanism of zinc-rich paints by electrochemical impedance spectroscopy, in: J.R. Scully, D.C. Silverman and M. Kendig (Eds.) Electrochemical Impedance Spectroscopy, ASTM STP 1188, American Society of Testing and Materials (ASTM), Philadelphia, PA, 1993, pp. 438–449.
[9] S. Egusay and N. Iwasawaz, Piezoelectric paints as one approach to smart structural materials with health-monitoring capabilities, Smart Materials and Structures, 7 (1998) 438-445.

[10] J.B. Ong, Z. You, J. Mills-Beale, E.L. Tan, B.D. Pereles and K.G. Ong, A wireless, passive embedded sensor for real-time monitoring of water content in civil engineering materials, IEEE Sensors Journal, 8 (2008) 2053-2058.
[11] X.P. Qing, S.J. Beard, A. Kumar, T.K. Ooi and F.-K. Chang, Built-in sensor network for structural health monitoring of composite structure, Journal of Intelligent Materials and Structures, 18 (2007) 39-49.
[12] V. Giurgiutiu, Structural Health Monitoring with Piezoelectric Wafer Active Sensors, Academic Press, Burlington, MA, 2008.
[13] P.A. Cella and S.R. Taylor, Electrical resistance changes as an alternate method for monitoring the corrosion of steel in concrete and mortar, Corrosion, 56 (2000) 951-959.
[14] E.V. Pereira, R.B. Figueira, M.M.L. Salta and I.T.E. da Fonseca, A galvanic sensor for monitoring the corrosion condition of the concrete reinforcing steel: Relationship between the galvanic and the corrosion currents, Sensors, 9 (2009) 8391-8398.
[15] S. Hong and R.S. Harichandran, Sensors to monitor CFRP/concrete bond in beams using electrochemical impedance spectroscopy, Journal of Composites for Construction, 9 (2005) 515-523.
[16] H.-W. Song and V. Saraswathy, Corrosion monitoring of reinforced concrete structures - A review, International Journal of Electrochemical Science, 2 (2007) 1-28.
[17] K. Kumar, C.S.U. Nair, H.T. Jegadish, S. Muralidharan, A.K. Parande, M.S. Karthikeyan and N. Palaniswamy, Online corrosion and force monitoring for inner containment concrete structures, Sensors & Transducers Journal, 92 (2008) 108-121.
[18] Y. Yu, G. Qiao and J. Ou, Self-powered wireless corrosion monitoring sensors and networks, IEEE Sensors Journal, 10 (2010) 1901-1902.
[19] S. Lu and H.-J. Ba, Corrosion sensor for monitoring the service condition of chloride-contaminated cement mortar, Sensors, 10 (2010) 4145-4158.
[20] F. Rajabipour and J. Weiss, Parameters affecting the measurements of embedded electrical sensors for concrete health monitoring applications, in: J.S. Popovics (Ed.) Health monitoring systems and sensors for assessing concrete, Curran Associates, Inc., Los Angeles, CA, 2008, pp. 7-22.
[21] I.S. Cole, P.A. Corrigan, G.C. Edwards, D. Followell, S. Galea, W. Ganther, B.R. Hinton, T. Ho, C.J. Lewis, T.H. Muster, D. Paterson, D.C. Price, D.A. Scott and P. Trathen, A sensor-based learning approach to prognostics in intelligent vehicle health monitoring, Materials Forum, 33 (2009) 27-35.
[22] D.A. Scott, D.C. Price, G.C. Edwards, A.B. Batten, J. Kolmeder, T.H. Muster, P. Corrigan and I.S. Cole, Development of a corrosion sensor for an aircraft vehicle health monitoring system, in: D.O. Thompson and D.E. Chimenti (Eds.) American Institute of Physics, American Institute of Physics, 2010, pp. 1005-1012.
[23] M. Lin and F.-K. Chang, The manufacture of composite structures with a built-in network of piezoceramics, Composites Science and Technology, 62 (2002) 919–939.
[24] J.-B. Ihn and F.-K. Chang, Detection and monitoring of hidden fatigue crack growth using a built-in piezoelectric sensor/actuator network: II. Validation using riveted joints and repair patches, Smart Materials and Structures, 13 (2004) 621–630.
[25] P.G. Venâncio, R.A. Cottis, R. Narayanaswamy and J.C.S. Fernandes, Corrosion sensors for aircraft aging, Corrosion Protective Materials, 28 (2009) 78-86.

[26] J. Kittel, N. Celati, M. Keddam and H. Takenouti, New methods for the study of organic coatings by EIS - New insights into attached and free films, Progress in Organic Coatings, 41 (2001) 93–98.
[27] J. Kittel, N. Celati, M. Keddam and H. Takenouti, Influence of the coating–substrate interactions on the corrosion protection: characterisation by impedance spectroscopy of the inner and outer parts of a coating, Progress in Organic Coatings, 46 (2003) 135–147.
[28] A. Miszczyk and T. Schauer, Electrochemical approach to evaluate the interlayer adhesion of organic coatings, Progress in Organic Coatings, 52 (2005) 298–305.
[29] A. Nogueira, X.R. Novoa and C. Perez, On the possibility of using embedded electrodes for the measurement of dielectric properties in organic coatings, Progress in Organic Coatings, 59 (2007) 186–191.
[30] K. Allahar, Q. Su and G. Bierwagen, Non-substrate EIS monitoring of organic coatings with embedded electrodes, Progress in Organic Coatings, 67 (2010) 180–187.
[31] G.W. Walter, The review of impedance plot methods used for corrosion performance analysis of painted metals, Corrosion Science, 26 (1986) 681-703.
[32] J.G.N. Thomas, The use of AC impedance spectroscopy for the study of coated metals: A review, in, Paint Research Association, Princeton, NJ, 1990.
[33] A. Amirudin and D. Thierry, Application of electrochemical impedance spectroscopy to study the degradation of polymer-coated metals, Progress in Organic Coatings, 26 (1995) 1-28.
[34] G.P. Bierwagen and D.E. Tallman, Choice and measurement of crucial aircraft coatings system properties, Progress in Organic Coatings, 41 (2001) 201–216.
[35] D. Loveday, P. Peterson and B. Rodgers, Evaluation of organic coatings with electrochemical Impedance Spectroscopy Part 1: Fundamentals of electrochemical impedance spectroscopy, in: JCT Coatings Tech, www.coatingstech.org, 2004, pp. 46-52.
[36] D. Loveday, P. Peterson and B. Rodgers, Evaluation of organic coatings with electrochemical impedance spectroscopy Part 2: Application of EIS to coatings, in: JCT Coatings Tech, www.coatingstech.org, 2004, pp. 88-93.
[37] G.D. Davis and C.M. Dacres, Electrochemical sensors for evaluating corrosion and adhesion on painted metal structures, in: U.S. Patent 5,859,537, 1999, pp. 1-19.
[38] T.C. Simpson, P.J. Moran, W.C. Moshier, G.D. Davis, B.A. Shaw, C.O. Arah and K.L. Zankel, An electrochemical monitor for the detection of coating degradation in atmosphere, Journal of the Electrochemical Society, 136 (1989) 2761-2762.
[39] G.D. Davis, K. Thayer, M.J. Rich and L.T. Drzal, Inspection of composite and metal adhesive bonds with an electrochemical sensor, Journal of Adhesion Science and Technology, 16 (2002) 1307–1326.
[40] G.D. Davis, L.A. Krebs and C.M. Dacres, Coating evaluation and validation of accelerated test conditions using an in-situ corrosion sensor, Journal of Coatings Technology, 74 (2002) 69-74.
[41] G.D. Davis, T.G. Vargo, A.W. Dalgleish and D. Deason, Corrosion protection and condition monitoring using 'Smart' appliqués, in: Materials Performance, Materials Performance, 2004, pp. 32-36.
[42] G.D. Davis, Electrochemical impedance evaluation of aluminum/boron–epoxy composite bonds, Journal of Adhesion Science and Technology, 19 (2005) 1397–1408.

[43] X. Wang, R. Bennett, K. Spenningsby and G. Bierwagen, Use of electrochemical noise methods for in situ corrosion monitoring, in: D.R.A. Mantz and D.P.C. Trulove (Eds.) Tri-Service Corrosion Conference, San Antonio, TX, 2002, pp. 18.
[44] G.P. Bierwagen, X. Wang and D.E. Tallman, In situ study of coatings using embedded electrodes for ENM measurements, Progress in Organic Coatings, 46 (2003) 163–175.
[45] U. Bertocci, C. Gabrielli, F. Huet and M. Keddam, Noise resistance applied to corrosion measurements I. Theoretical analysis, Journal of the Electrochemical Society, 144 (1997) 31-37.
[46] U. Bertocci, C. Gabrielli, F. Huet, M. Keddam and P. Rousseau, Noise resistance applied to corrosion measurements II. Experimental tests, Journal of the Electrochemical Society, 144 (1997) 37-43.
[47] G.P. Bierwagen, Calculation of noise resistance from simultaneous electrochemical voltage and current noise data, Journal of the Electrochemical Society, 141 (1994) L155-L157.
[48] Q. Su, The application of embedded sensors for in-situ monitoring of protective coatings on metal substrates, in: Coatings and Polymeric Materials, North Dakota State University, Fargo, ND, 2008, pp. 259.
[49] K.N. Allahar, Q. Su, G.P. Bierwagen, D. Battocchi, V.J. Gelling and D. Tallman, Examination of the feasibility of the use of in-situ corrosion sensors in army vehicles, in: Tri-Service Corrosion Conference, 2005, pp. 1-11.
[50] K.N. Allahar, Q. Su, G.P. Bierwagen and D.-H. Lee, Monitoring of the AC-DC-AC degradation of organic coatings using embedded electrodes, Corrosion, 64 (2008) 773-787.
[51] K.N. Allahar, V. Upadhyay, G.P. Bierwagen and V.J. Gelling, Monitoring of a military vehicle coating under Prohesion exposure by embedded sensors, Progress in Organic Coatings, 65 (2009) 142–151.
[52] K.N. Allahar, Q. Su and G.P. Bierwagen, Electrochemical noise monitoring of the cathodic protection of Mg-rich primers, Corrosion, 66 (2010) 1-12.
[53] K.N. Allahar, B.R. Hinderliter, D.E. Tallman and G.P. Bierwagen, Water transport in multilayer organic coatings, Journal of the Electrochemical Society, 155 (2008) F201-F208.
[54] G.P. Bierwagen, K.N. Allahar, Q. Su and V.J. Gelling, Electrochemically characterizing the ac–dc–ac accelerated test method using embedded electrodes, Corrosion Science, 51 (2008) 95–101.
[55] D. Wang, D. Battocchi, K.N. Allahar, S. Balbyshev and G.P. Bierwagen, In situ monitoring of a Mg-rich primer beneath a topcoat exposed to Prohesion conditions, Corrosion Science, 52 (2010) 441–448.
[56] Defense federal acquisition regulation supplement; minimizing the use of materials containing hexavalent chromium (DFARS Case 2009-D004), Federal Register, 76 (2011) 25569-25576.
[57] J. Sinko, Challenges of chromate inhibitor pigments replacement in organic coatings, Progress in Organic Coatings, 42 (2001) 267–282.
[58] M.W. Kendig and R.G. Buchheit, Corrosion inhibition of aluminum and aluminum alloys by soluble chromates, chromate coatings, and chromate-free coatings, Corrosion, 59 (2003) 379-400.

[59] D. Battocchi, A.M. Simoes, D.E. Tallman and G.P. Bierwagen, Comparison of testing solutions on the protection of Al-alloys using a Mg-rich primer, Corrosion Science, 48 (2006) 2226–2240.
[60] G. Bierwagen, D. Battocchi, A. Simoes, A. Stamness and D. Tallman, The use of multiple electrochemical techniques to characterize Mg-rich primers for Al alloys, Progress in Organic Coatings, 59 (2007) 172–178.
[61] P.C.R. Varma, B. Duffy and J. Cassidy, Influence of magnesium nitrate on the corrosion performance of sol-gel coated AA2024-T3 aluminium alloy, Surface & Coatings Technology, 204 (2009) 277-284.
[62] R.G. Buchheit, M.D. Bode and G.E. Stoner, Corrosion-resistant, Chromate-free talc coatings for aluminum, Corrosion, 50 (1994) 205-214.
[63] P. Visser and S.A. Hayes, Anti-corrosive coating composition, in: W.I.P. Organization (Ed.) WO 2010/112605 A1, 2010.
[64] S.J. Mabutt and D.J. Mills, Novel configurations for electrochemical noise measurements, British Corrosion Journal, 33 (1998) 158-160.
[65] B.E. Merten, D. Battocchi, D.E. Tallman and G.P. Bierwagen, Embedded reference electrode for potential-monitoring of cathodic protective systems, Journal of the Electrochemical Society, 157 (2010) C244-C247.
[66] K.B. Oldham and J.C. Myland, Fundamentals of Electrochemical Science, Academic Principles, Inc., San Diego, CA, 1994.
[67] A. Foyet, T.H. Wu, A. Kodentsov, L. Van der Ven, G. De With and R. Van Benthem, Impedance evaluation of permeability and corrosion of Al-2024 aluminum alloy coated with a chromate free primer, Progress in Organic Coatings, 65 (2009) 257–262.
[68] A. Aballe, A. Bautista, U. Bertocci and F. Huet, Measurement of the noise resistance for corrosion applications, Corrosion, 57 (2001) 35-42.
[69] R.A. Cottis and S. Turgoose, Electrochemical noise measurements - a theoretical basis, Materials Science Forum, 192-194 (1995) 663-672.
[70] S. Bohm, R.J. Holness, H.N. McMurray and D.A. Worsley, Charge percolation and sacrificial protection in zinc-rich organic coatings, in: Eurocorr 2000, Queen Mary and Westfield College, London, 2000.
[71] A. Kalendová, Effects of particle sizes and shapes of zinc metal on the properties of anticorrosive coatings, Progress in Organic Coatings, 46 (2003) 324–332.
[72] X. Lu, Y. Zuo, X. Zhao, Y. Tang and X. Feng, The study of a Mg-rich epoxy primer for protection of AZ91D magnesium alloy, Corrosion Science, 53 (2011) 153–160.
[73] R. Lindström, J.-E. Svensson and L.-G. Johansson, The Influence of Carbon Dioxide on the Atmospheric Corrosion of Some Magnesium Alloys in the Presence of NaCl, Journal of the Electrochemical Society, 149 (2002) B103-B107.
[74] M. Jönsson, D. Persson and D. Thierry, Corrosion product formation during NaCl induced atmospheric corrosion of magnesium alloy AZ91D, Corrosion Science, 49 (2007) 1540–1558.

CHAPTER 6. PROCESS FOR CONTROLLED-POTENTIAL CATHODIC PROTECTION OF COATED METALS BY EMBEDDED SENSORS

6.1. Introduction

A systematic method of quality control is desired for in service evaluation of civil and industrial infrastructure. This is especially true for structures which are very large, expensive, uniquely susceptible to stress- or corrosion-based catastrophic failures, or inaccessible to more traditional methods such as visual inspection. Structural health monitoring (SHM) refers to the developmental field of sensor-based and remote measurement techniques. The most common methods measure corrosion rate, changes in mechanical properties, or other important material characteristics [1-12]. A major focus for SHM research is on new construction; however, the need for incorporation into existing infrastructure remains.

Researchers at NDSU are exploring ways to improve corrosion mitigation and provide SHM through the application of embedded electrodes for controlled-potential cathodic protection (CPCP). Here, the electrochemical potential of a substrate is polarized directly by means of the electrodes using an external imposed potential. CPCP is analogous to imposed-current cathodic protection (ICCP), which is used extensively in pipeline applications. However, it has the potential to eliminate the IR drop [13] and high voltage concerns associated with ICCP [14].

Cathodic protection suppresses the rate of corrosion for infrastructural substrates by polarizing the metal or alloy at a sufficiently negative corrosion potential to force reduction

reactions at the substrate surface. This corrosion potential lies in a passive region of the corresponding potentiodynamic curves. An example of an Evans Diagram [15] is given below for steel substrate with and without ICCP (Figure 6.1).

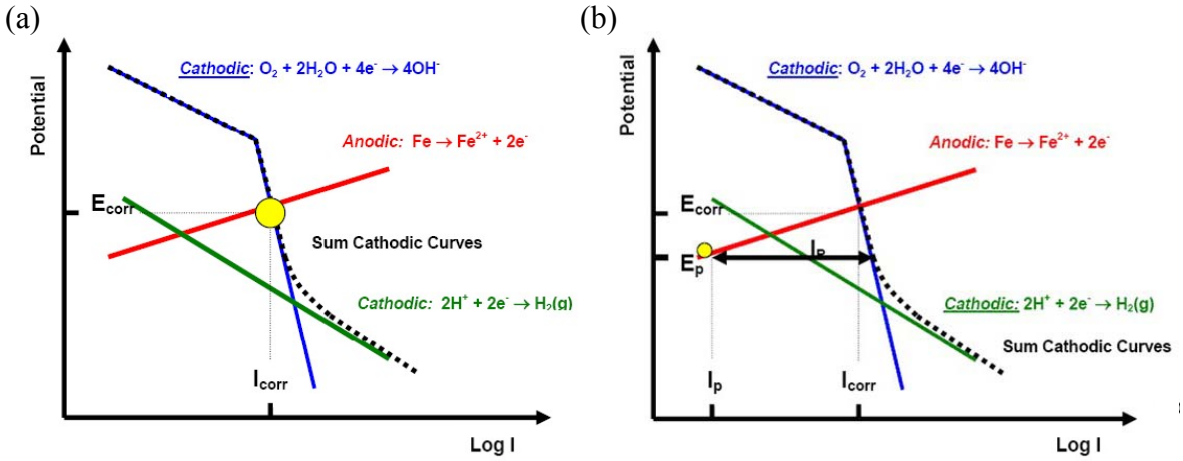

Figure 6.1. Potentiodynamic polarization plots (Evans diagrams) are given for a steel ICCP system: (a) passive, (b) active. Reproduced from Reference [16].

The anodic reaction rate of corrosion in Figure 6.1 (b) is decreased at the expense of increased cathodic reaction rates. Oxygen reduction and hydrogen evolution are the cathodic reactions given for this example. The major reaction product is OH^- which increases alkalinity [17]. However, as the polarization potential, E_p, becomes more negative, hydrogen evolution predominates at very negative potentials. This leads to the unwanted production of H_2 gas at the metal/coating interface for coated systems and cathodic disbondment once the hydrogen gas pressure exceeds the coating's adhesive strength. Disbondment also prevents cathodic protection currents from reaching the substrate due to very high resistance in the new-formed interfacial region [18]. The operating window for effective cathodic protection is generally small as a result of the unwanted H_2 generation occurring at large polarizations.

Traditional ICCP achieves the desired E_p by applying the current which corresponds to that value, indicated by in Figure 6.1 (b). This is an indirect method of E_p control. An IR drop occurs between the inert anode and the substrate in this process which must be accounted for by I_P. This presents a significant engineering challenge and often results in reduced accuracy for E_p. Soil is the most common medium for current flow, often at long distances. Figure 6.2 illustrates the ICCP system for an underground tank structure. The magnitude of the IR drop is affected by daily and seasonal soil resistivity changes as a result of variations in atmospheric humidity or soil water content. High-pH stress corrosion cracking is a significant concern for buried pipelines during these transitions [19].

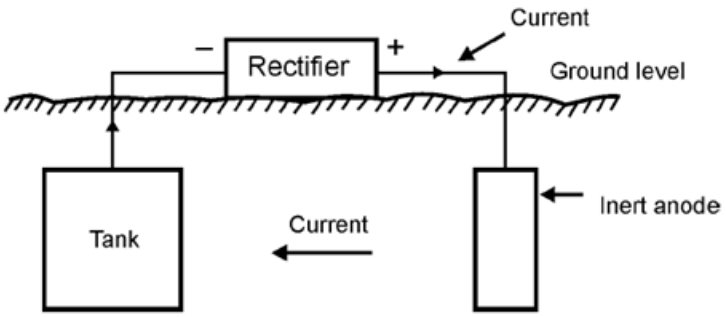

Figure 6.2. Illustration for ICCP applied to underground tank structure. Reproduced from Reference [20].

CPCP is a direct method of E_p control. A potentiostatic device is required which increases the instrumentation for this method. Most notably, CPCP has been used in marine applications for the protection of ship hulls. The system operates by means of a reference electrode, immersed ship-side in the sea water. The reference electrode provides the necessary feedback to control the potential. The body of water serves as an electrolyte for the flow of current, and the IR drop is negligible. Subsequently, the E_p of the cathode, a ship hull in this case, is controlled by the reference electrode.

A major design challenge for ship hull CPCP is the reference electrode reliability. The reference electrode must remain stable for long service periods. Potential drifts reduce the accuracy of E_p. A robust reference electrode is required for successful implementation.

The present study applies marine-based CPCP to a coated metal system. Embedded sensors are utilized to achieve the E_p control. The Ag wire ERE is placed between the primer and topcoat layers of a polymeric system. The close proximity of this arrangement minimizes IR drop, as desired. Additionally it creates a slow, diffusion-controlled environment for electrochemical potential stability. The Ag wire ERE has been evaluated previously as a device for monitoring the corrosion protection of Mg primer / AA 2024-T3 as shown in Chapter 3 [21]. The feasibility of the Ag wire ERE in the development of a novel CPCP system for improved corrosion control is explored in this chapter.

Au and Pt wire embedded electrodes (EE) were also examined for their electrochemical stability and suitability to this application. A non-substrate electrochemical analysis was performed as well as introductory controlled-potential tests to provide a foundation for this method. The experimental CPCP was then applied to a sample coating system. More sophisticated prototypes for CPCP are proposed in the discussion of these results.

6.2. Experimental methods

6.2.1. Coating system

AA 2024-T3 panels (12 cm x 5 cm x 0.3 cm) from Q Panel Lab Products (Cleveland, OH) were sandblasted, wiped with hexane, and rinsed with 18 MΩ·cm water. Mg 3820 metal particulates, from Ecka-Granules of America (Louisville, KY), were used as a pigment. An epoxy-polyamide was used as the binder for this system by means of

Epon 828 resin and Epikure 3164 curing agent, both from Hexion Specialty Products (Stafford, TX). High solids polyurethane gloss enamel from Akzo Nobel Aerospace Coatings (Waukegan, IL) served as the topcoat. Replicates were prepared at primer PVC = 10, 30, and 45. A commercial rapid cure epoxy was also utilized to form a PVC = 0 coating system. Tables 6.1 shows the coating systems prepared for this chapter.

Table 6.1. Coating / electrode systems prepared for experimentation.

Sample name	Primer	PVC (%)	Embedded electrode (#)	Replicates
Mg 10 ERE_{Ag}	Mg epoxy	10	Ag/AgCl	5
Mg 30 ERE_{Ag}	Mg epoxy	30	Ag/AgCl	5
Mg 45 EE_{Au}	Mg epoxy	45	Au (4)	1
Mg 45 EE_{Pt}	Mg epoxy	45	Pt (4)	1
Mg 45 $EE_{Au, Pt}$	Mg epoxy	45	Au, Pt (2 each)	1
Epoxy ERE_{Ag} / EE_{Pt}	Epoxy	0	Ag/AgCl, Pt (2 each)	1

The application method was air spray gun with the exception of the Epoxy ERE_{Ag} / EE_{Pt} sample. This film was drawn down onto four 5 cm x 2 cm sections on the panel. The target thickness for each coating layer was 50 μm.

6.2.2. Electrode preparation

Ag wire reference electrodes were prepared using 50 μm silver wire, obtained from Goodfellow Corporation (Huntingdon, England). A chemical oxidation method was performed to create the reference electrode using a 0.03 M $FeCl_3$ solution and a 60 second immersion period. This method is described in detail in Section 3.2.1 and will not be explained further here.

Au (25 μm) and Pt (50 μm) wire electrodes were used as received from Goodfellow Corporation (Huntingdon, England). Electrodes were cut to a length of approximately 5 cm, cleaned using hexane and distilled water, and then embedded within a coating system.

6.2.3. Placement of electrode within coating system

The corrosion potential of each Ag wire reference electrode is measured versus a standard reference electrode to ensure that the stable electrochemical potential has developed. The measurement is also made for Au and Pt wire electrodes. Each electrode is secured to the primer surface using a small amount of commercial rapid cure epoxy. A tab is also applied using a piece of conductive tape to use as a lead for electrochemical measurement via the ERE. This tab is covered with masking tape, and the topcoat is applied. See Figure 6.3 and Section 3.2.3 for more details.

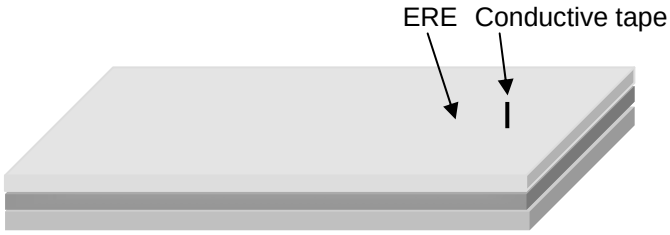

Figure 6.3. The coating system is illustrated to show the ERE and conductive tape lead.

For several panels, four electrodes were embedded within the coating system by the same method. Two parallel wires were placed at each side of the panel (Figure 6.4). These samples contained Au and Pt wire electrodes as well as Ag/AgCl wire reference electrodes.

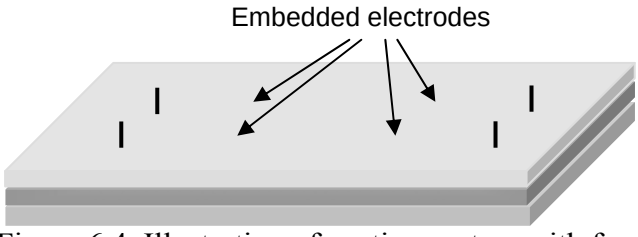

Figure 6.4. Illustration of coating system with four embedded electrodes.

6.2.4. Experimental studies

Experiments were prepared to explore the feasibility of embedded electrodes and reference electrodes for the implementation of CPCP to coated metal systems. Preliminary experiments are given to demonstrate the versatility of the embedded wire sensors for controlled-potential applications. Au and Pt wire electrodes are introduced as pseudo reference electrodes as well as working electrodes for non-substrate electrochemical analysis by EIS.

6.2.4.1. Noble metal wire embedded electrodes

An experiment was prepared to examine the accuracy and reliability of thin Au and Pt wires as embedded pseudo reference electrodes. Samples Mg 45 EE_{Au}, Mg 45 EE_{Pt}, and Mg 45 $EE_{Au,\ Pt}$ from Table 6.1 were used for this experiment. A total of six Au embedded electrodes (EE_{Au}) and six Pt embedded electrodes (EE_{Pt}) replicates were examined. The arrangement of these twelve embedded electrodes is given in Figure 6.6.

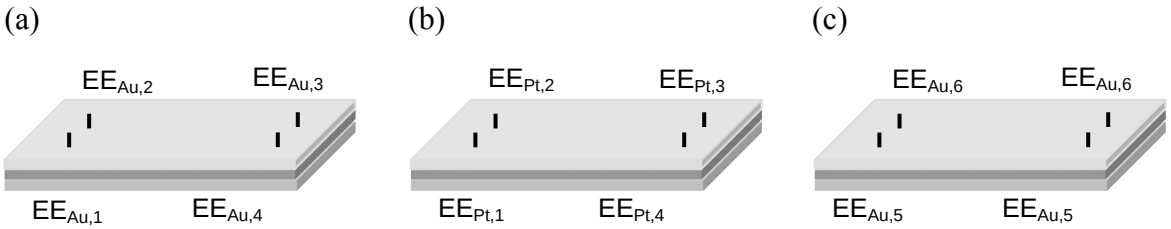

Figure 6.5. The embedded electrode arrangement is illustrated for samples (a) Mg 45 EE_{Au}, (b) Mg 45 EE_{Pt}, and (c) Mg 45 $EE_{Au,\ Pt}$.

A Gamry PCI4/300 potentiostat/galvanostat with dedicated EIS 300 software, supplied by Gamry Instruments, Inc. (Warminster, PA), was utilized for the measurements. Four multiplexor channels are used for each sample. No solution cell is attached. The EEs are connected to the RE lead while the substrate serves as the WE (Figure 6.6).

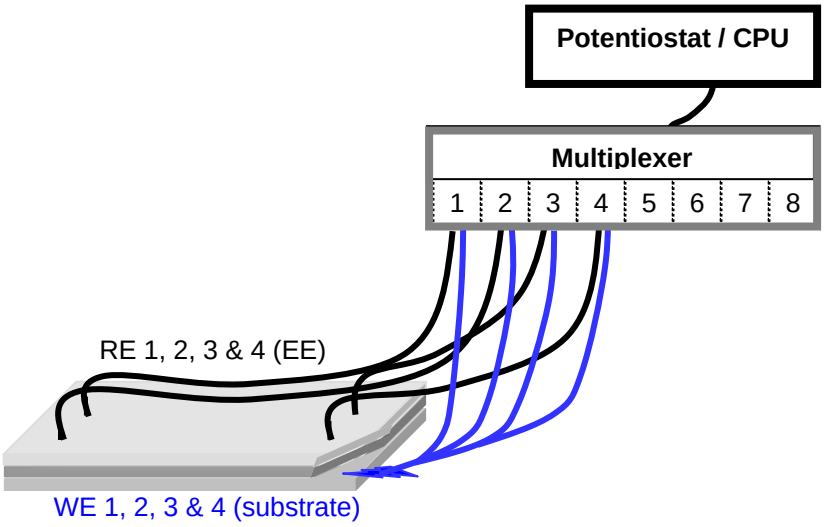

Figure 6.6. Instrumental set-up for corrosion potential measurement of EE_{Au} and EE_{Pt}.

The samples were exposed to ASTM B117 accelerated weathering in a salt spray cabinet and removed regularly for corrosion potential measurement. The test was performed for twenty minutes at a sample period of 0.5 minutes.

6.2.4.2. Non-substrate EIS analysis

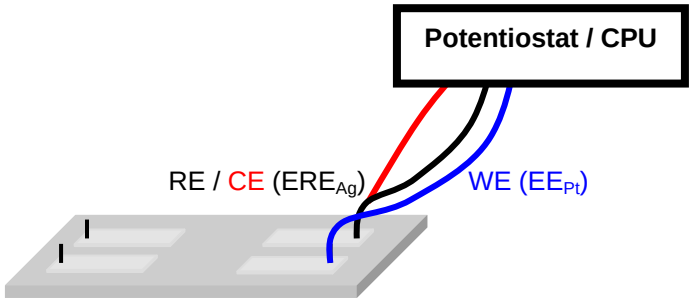

Figure 6.7. Coating system for Epoxy ERE_{Ag} / EE_{Pt} and instrumental set-up for non-substrate EIS.

An experiment was prepared to examine the feasibility of a combined ERE and EE system for a non-substrate electrochemical analysis. Epoxy ERE_{Ag} / EE_{Pt} from Table 6.1 was utilized for this experiment. The system contains two Ag wire ERE and EE_{Pt} sensors

on a single substrate. Each sensor is embedded within a solitary coating/polymer matrix (Figure 6.7). The absence of a shared polymer matrix assures that the electrical current must flow through the substrate during experimentation.

A damp paper towel is momentarily placed on each coating / sensor system prior to electrochemical analysis. The small amount of moisture improved conductivity and enabled the measurement to be performed. A Gamry PCI4/300 potentiostat/galvanostat with dedicated EIS 300 software was utilized for the measurements. No solution cell is attached. The ERE_{Ag} is connected to the RE and CE lead and the EE_{Pt} serves as the WE. EIS measurements were performed for the range of 10^{5} to 10^{-2} Hz at ten points per decade and 10 mV perturbations versus the open circuit potential (OCP).

A second measurement is performed using the standard three electrode set-up as a control for the experiment. A solution cell is attached with DHS. A SCE serves as the RE, a Pt mesh as the CE, and the substrate as the WE.

6.2.4.3. CPCP of Mg primer / AA 2024-T3 with reduced PVC

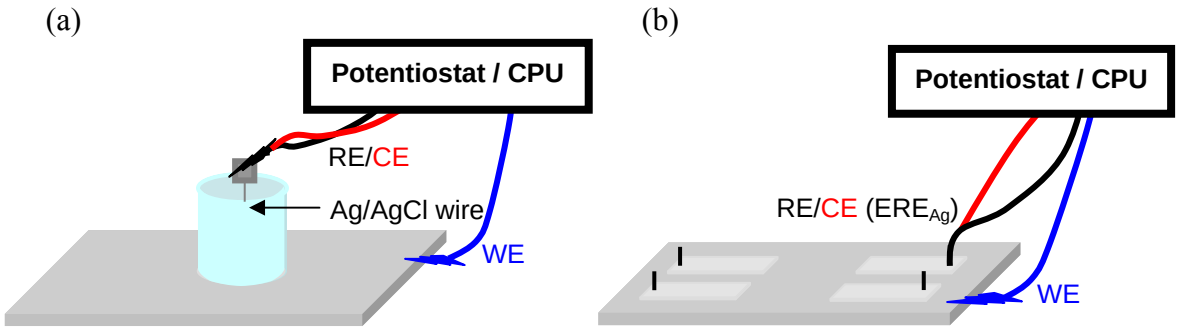

Figure 6.8. Instrumental set-up for CPCP test controls (a) bare AA 2024-T3 and (b) coated AA 2024-T3.

Controlled-potential tests were performed on various coating system / embedded sensor arrangements. The first test uses the Ag wire reference electrode suspended in

solution over a bare AA 2024-T3 substrate. The Ag wire was the RE/CE and the substrate the WE, as shown in Figure 6.8 (a). A second control test examines the controlled-potential test using coated AA 2024-T3. Sample epoxy ERE_{Ag} / EE_{Pt} was utilized for the experiment. The ERE_{Ag} is used as the RE/CE and the substrate as the WE. Figure 6.9 (b) illustrates the instrumental set-up for this test.

A potential of -0.5 V vs OCP was applied for the potentiostatic test. This experiment is analogous to marine-based CPCP and serves as a control. A Gamry PCI4/300 potentiostat/galvanostat with dedicated EIS 300 software was utilized for the measurements.

An experiment was prepared to apply CPCP to a reduced PVC Mg primer / AA 2024-T3 coating system by means of the ERE_{Ag}. It is proposed that the Mg pigments improve the conductivity of the primer, facilitating the application of uniform CPCP at low current requirements. Additionally, some sacrificial cathodic protection is possible which would provide a secondary protection mechanism at times when the CPCP is not applied.

The standard formulating window for Mg primers is 40% to 60% PVC [22-23]. The present experiments were formulated at 10% and 30% PVC, samples Mg 10 ERE_{Ag} and Mg 30 ERE_{Ag} in Table 6.1. Each sample was equipped with one Ag wire ERE.

The samples were exposed ASTM B117 accelerated weathering in a salt spray cabinet and removed regularly. The corrosion potential was measured for each sample using the ERE_{Ag} as the RE and the substrate as the WE. For corrosion potential measurements less than 0.0 V vs ERE_{Ag}, a potentiostatic experiment was applied using ERE_{Ag} as RE, Pt mesh as CE, and the substrate as WE. Figure 6.9 gives the instrumental set-up for this experiment.

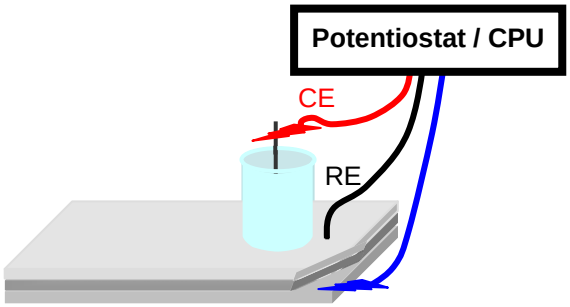

Figure 6.9. Instrumental set-up of CPCP for 10% and 30% PVC Mg primer / AA 2024-T3 experiment.

The applied potential was -0.95 V vs ERE_{Ag}. A Gamry PCI4/300 potentiostat/galvanostat with dedicated EIS 300 software was utilized for the measurements. Samples were examined for blistering or other defects before and after the potentiostatic test. The length of CPCP varied from eight to sixteen hours. Shorter times were applied for early experiments. The CPCP was applied at longer times to observe the effects of extended application periods.

6.3. Results and discussion

6.3.1. Noble metal wire embedded electrodes

The Au and Pt wire electrodes were suspended in DHS as a control experiment. Additionally, sample Epoxy ERE_{Ag} / EE_{Pt} was used to obtain AA 2024-T3 corrosion potential versus a Pt wire EE in a non-pigmented coating system. The experimental set-up for these is analogous to Figure 6.8 (a) and (b), respectively. Connection by the CE is not necessary, however, for the corrosion potential measurement. These control results are presented in Figure 6.10.

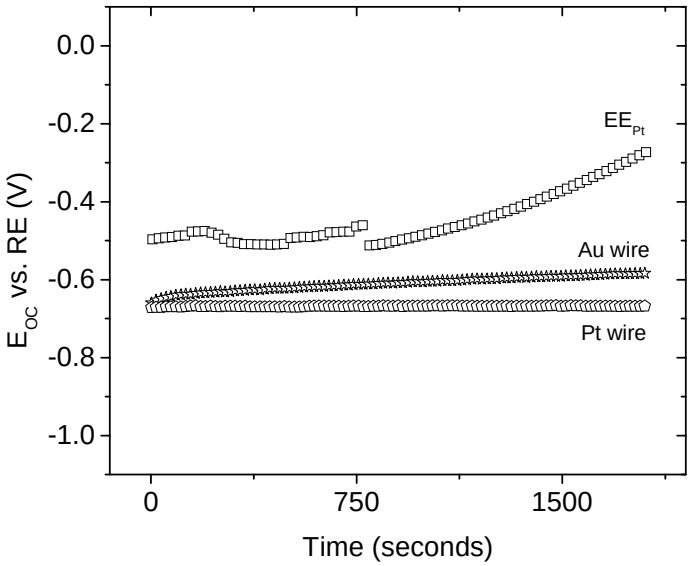

Figure 6.10. Corrosion potential data for AA 2024-T3 vs electrode controls. Au and Pt wire are in DHS solution, while EE_{Pt} is embedded in non-pigmented epoxy primer.

Greater stability is observed for the Pt wire electrode in DHS than the Au wire electrode. It is assumed that the AA 2024-T3 is at steady-state. Therefore, the shift in data for AA 2024-T3 vs Au is a result of the Au wire and not the AA 2024-T3 substrate. Figure 6.10 also shows the corrosion potential to be 0.2 to 0.3 V more positive versus EE_{Pt}. The corrosion potential for EE_{Au} was not tested, but it is estimated to be 0.0 to 0.1 V more positive than EE_{Pt}. Table 6.2 provides a statistical analysis of Figure 6.10 data.

Table 6.2. Coated (EE_{Pt}) and uncoated (Au, Pt wire) AA 2024-T3 corrosion potential as measured by wire reference electrodes.

Reference Electrode	Statistics (V vs RE)					
	Mean	Stan.dev.	Median	High	Low	Range
Au wire	-0.610	0.018	-0.608	-0.584	-0.660	0.076
Pt wire	-0.669	0.001	-0.668	-0.667	-0.672	0.005
EE_{Pt}	-0.447	0.067	-0.477	-0.512	-0.273	0.239

The corrosion potential measured by the Pt wire in solution is very stable. The range and standard deviation are 0.005 and 0.001 V, respectively. The Au wire has values of 0.076 V and 0.018 V, respectively. The bottom row in Table 6.2 gives statistics for the Pt wire embedded in a non-pigmented epoxy coating. It is approximately 0.2 V more positive than the wire in solution, and the scatter is much more significant. The range and standard deviation are 0.239 and 0.067 V, respectively. This gives the best estimation of expected corrosion potentials for Pt or Au wire embedded in a coating system.

Based on the mean, standard deviation, and median the expected corrosion potential of AA 2024-T3 versus a Pt embedded wire electrode is estimated to be -0.5 to -0.3 V vs EE_{Pt}. This same broad range is assumed for EE_{Au} and is used in the following analysis.

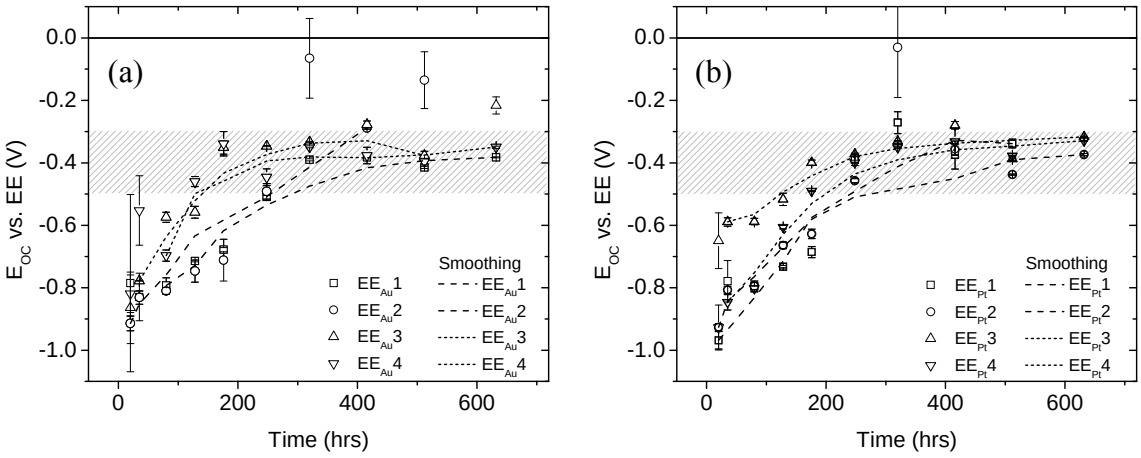

Figure 6.11. Mean corrosion potential for noble metal embedded electrodes (a) Mg 45 EE_{Ag} and (b) Mg 45 EE_{Pt}. Standard deviations are included in the plot.

Mean corrosion potential results for samples Mg 45 EE_{Au} and Mg 45 EE_{Pt} are given in Figure 6.11. Good results were observed for corrosion potential monitoring by means of the Au and Pt wire embedded pseudo reference electrodes. The data was filtered for mean corrosion potentials more positive than -0.2 V vs EE and standard deviations greater than

0.05 V. Data with either property was not included in the smoothing applied to Figure 6.11 data. An adjacent-averaging method was utilized.

Two important reference potentials are included on these plots. The first is the corrosion potential of the bare AA 2024-T3 substrate measured versus EE_{Au} and EE_{Pt}. This is designated by a shaded region from -0.5 to -0.3 V vs EE. The second is the solid line at y = 0.0 V vs EE. This value is given to detect short circuit measurements which do not provide an accurate representation of the electrochemical potential and should not be used for analysis. See Chapters 3 and 4 for more information on determining the usefulness of a mean corrosion potential data for analysis.

According to the smoothed trend line, the range of the mean corrosion potential values in Figure 6.11 as well as the shape of the curves is very similar to those obtained by the ERE_{Ag} in Chapters 3 and 4. The mean corrosion potentials are near -1.0 V vs EE after the initial exposure and drift to a more positive corrosion potential as the Mg oxidation reactions deplete the Mg available. This behavior is similar to that expected for a Mg primer / AA 2024-T3 coating system [23-24]. It is likely that the sacrificial protection is no longer active following 300 hours.

The results for sample Mg 45 $EE_{Au/Pt}$ show equivalent behavior to Figure 6.11 for both the Au and Pt embedded electrodes. These results are included in the following statistical analysis.

The EE_{Pt} corrosion potential measurements in Figure 6.11 and for sample Mg $EE_{Au/Pt}$ (not shown) have slightly less scatter than EE_{Ag}. The magnitude of the standard deviations is the main factor for this observation. The standard deviations are statistically

examined in Table 6.3 to confirm this. The mean and median are calculated for all of the mean corrosion potential standard deviations, ten total per each of the six electrodes.

Table 6.3. Standard deviations of the Au and Pt wire mean corrosion potential data.

Statistical method	Wire	Standard deviation (V vs EE) Embedded electrode (#)						$Mean_{all}$
		1	2	3	4	5	6	
Mean	Au	0.076	0.048	0.049	0.058	0.081	0.050	0.060
	Pt	0.066	0.031	0.029	0.034	0.018	0.047	0.038
Median	Au	0.006	0.035	0.016	0.026	0.014	0.015	0.019
	Pt	0.018	0.012	0.010	0.005	0.008	0.009	0.010
Adjusted mean	Au	0.007	0.020	0.013	0.018	0.013	0.010	0.014
	Pt	0.022	0.010	0.008	0.010	0.008	0.009	0.011

At the far right column ($mean_{all}$)—the mean of all electrodes—is given. The $mean_{all}$ of the mean is 0.060 and 0.038 V for Au and Pt, respectively, while it is 0.019 and 0.010 V for the median. Therefore, the data for Au does have significantly higher scatter than the Pt electrode since it is assumed that the corrosion potential of the AA 2024-T3 is at steady-state for all measurements. The $mean_{all}$ of the mean is more than three times larger than the median for both Au and Pt. This suggests that, on average, most standard deviations are small but that a few are large and shift the mean to a higher value.

The *adjusted mean* calculates the statistic for only the data with standard deviation less than 0.05 V. Recall that all other data was omitted from the smoothing applied in Figures 6.11 and for sample Mg $EE_{Au/Pt}$ (not shown). The $mean_{all}$ is now similar to the median. The use of a filter is necessary to accurately interpret the corrosion potential results. Additionally, a standard deviation on the order of 0.01 V is sought for implementation of these electrodes [25].

Noble metals have relatively stable electrochemical potentials at the metal surface and very low reactivity toward other metals which makes them an ideal material to use as a counter electrode or pseudo reference electrodes. Electrochemical processes occur very rapidly on Pt and they can be used in acidic solution; therefore, they are often preferred to Au [14]. This stability indicates that Au and Pt wire EEs can be used as embedded counter electrodes for electrochemical analysis of organic coatings. Both electrodes provided useful corrosion potential results in the present experiment. The Pt wire electrode had greater accuracy compared to the Au wire and is utilized in subsequent experiments.

6.3.2. Non-substrate electrochemical analysis

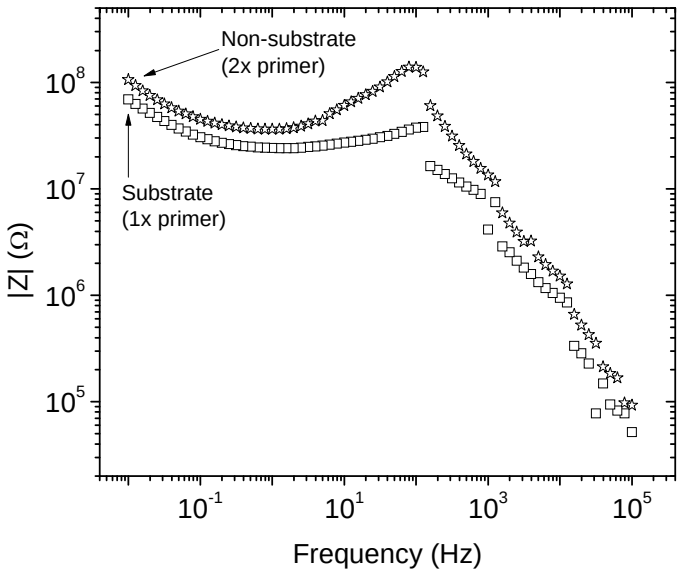

Figure 6.12. Substrate and non-substrate EIS Bode plot results for Epoxy ERE_{Ag} / EE_{Pt}.

The non-substrate electrochemical analysis explores the versatility of the Ag wire reference electrode as well as the Pt wire electrode. Sample Epoxy ERE_{Ag} / EE_{Pt} from Table 6.1 was utilized for the experiment. The experimental set-up is provided in Figure 6.7, above. Good results were obtained for the two samples examined. One example is

given in Figure 6.12. An irregularity was observed across the frequency spectrum, which should be smooth, monotonically decreasing curve. This discontinuity is most apparent at 10^2, 10^3, and 10^4 Hz and appears to equally affect both samples and the pattern suggests an instrumental error. The non-substrate impedance measurement is larger than the substrate measurement at all frequencies, as expected; therefore, no correction is made to the data.

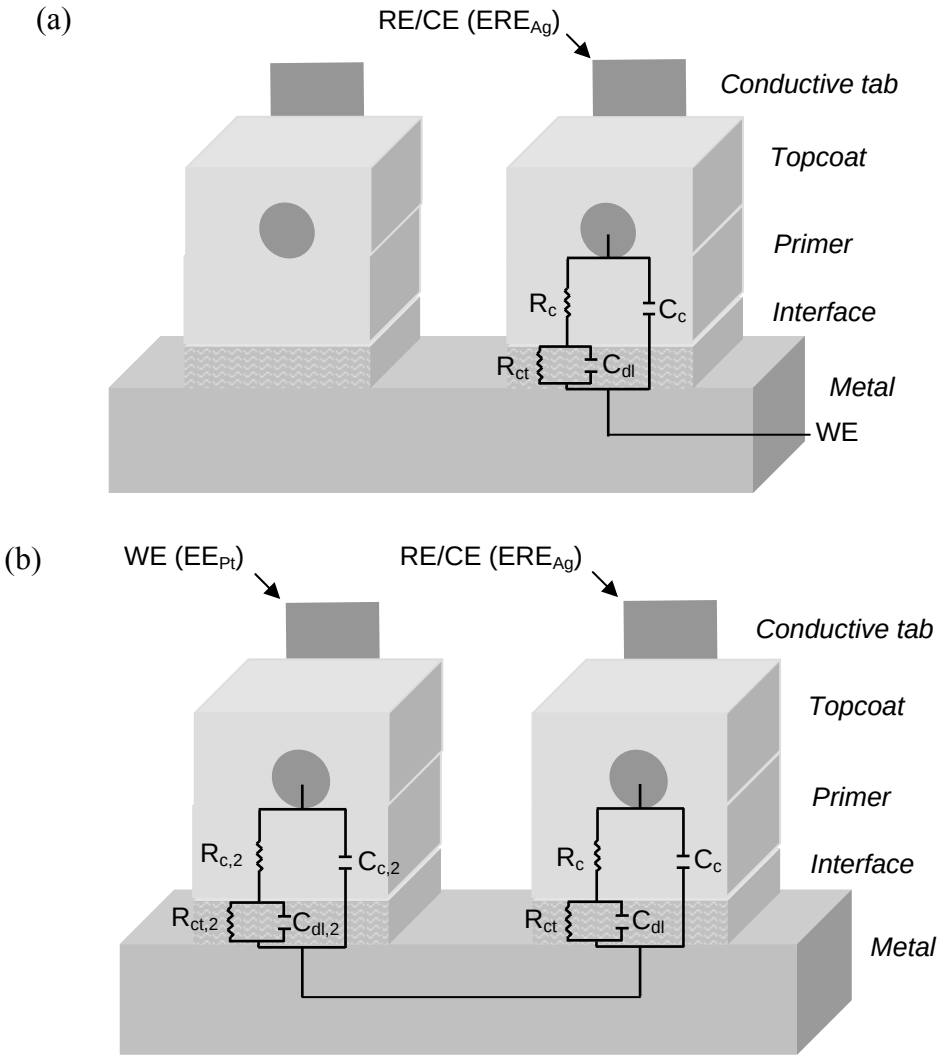

Figure 6.13. Circuit models for (a) substrate and (b) non-substrate EIS experiments. The coating layers are not drawn to scale.

Equivalent circuit modeling can be used to interpret the EIS results using physical elements. The resistive and capacitive properties are simulated by mathematical simulation of capacitors and resistors. The coating's polymer matrix is the main capacitive element for an intact coating. Small pores and imperfections act as resistors in the presence of electrolyte. These two elements are represented in series in an equivalent circuit model.

Once electrolyte reaches the coating/metal interface an electrical double layer develops [26]. This is also represented by a resistor and capacitor in series. Equivalent circuit models are presented for the substrate and non-substrate experimental set-ups in Figure 6.13. Any solution or uncompensated resistance is assumed negligible and not included in these circuit models. The impedance, $|Z|$, at low frequencies (< 1 Hz) measures the total coating impedance. Since coating resistance, R_c, in the figure below is much smaller than charge transfer resistance, R_{ct}, at the interface, $|Z|_{0.01\ Hz}$ gives a good estimate for R_{ct} [25, 27-28].

Theoretically, $|Z|_{0.01\ Hz}$ for the non-substrate experiment is equal to twice the value for the substrate experiment, assuming uniformity of the metal/coating interface. Factors which affect this measurement include surface condition prior to coating, heterogeneous substrate electrochemistry, and interfacial coating degradation [25]. Therefore, the two primer layers in this experiment are considered nominally identical. Coating uniformity is assumed for the following interpretation of Figure 6.13.

Capacitive properties are negligible at low frequencies (< 1 Hz) and all current can be expected to flow through the circuit resistors. Therefore, for charge transfer resistance, R_{ct}, and coating/metal interface double layer resistance, R_{dl}, if

$$R_c = R_{c,2} \qquad \text{(Eq. 6.1)}$$

and

$$R_{ct} = R_{ct,2} \quad \text{(Eq. 6.2)}$$

then the measured impedance for the substrate, $|Z|_{substrate}$, and non-substrate, $|Z|_{non\text{-}substrate}$, configurations can be calculated by Equations 6.3 and 6.4. This is assuming negligible contribution from the capacitive elements in the equivalent circuit model.

$$|Z|_{substrate} = R_c + R_{ct} \quad \text{(Eq. 6.3)}$$

and

$$|Z|_{non\text{-}substrate} = R_c + R_{ct} + R_{c,2} + R_{ct,2} \quad \text{(Eq. 6.4)}$$

Equations 6.1, 6.2, and 6.3 can be substituted into Equation 6.4 to provide the relationship for the total impedance between the two configurations.

$$|Z|_{non\text{-}substrate} = 2 \cdot |Z|_{substrate} \quad \text{(Eq. 6.5)}$$

Equation 6.5 is utilized to analyze the low frequency impedance results for the coating samples and is provided in Table 6.4. The multiplicative factor used in the table is defined by Equation 6.6. R_{ct} is the primary resistive element at 0.01 Hz. The factor is nearly two for both samples.

$$|Z|_{non\text{-}substrate} = x \cdot |Z|_{substrate} \quad \text{(Eq. 6.6)}$$

Table 6.4. Low frequency impedance for substrate and non-substrate EIS configurations.

Experiment		$\|Z\|_{0.01Hz}$ (10^7 Ω)	
Configuration	**Elements**	**Sample A**	**Sample B**
Non-substrate	R_{ct}, $R_{ct,2}$	7.1	10.6
Substrate	R_{ct}	2.8	6.9
Factor (x)		2.5	1.5

The departure from the theoretical value may be attributed to small non-uniformities in the film and interface. A second $|Z|_{substrate}$ measurement for $R_{ct,2}$ could be

determine the validity of the assumptions in Equation 6.2. Resistivity is a function of distance; therefore, additional resistances may need to be added to Equation 6.3 and 6.4.

Kittel et al. [26, 29] measured coating inner and outer impedance via an embedded sensor. Brossia [30] also used embedded electrodes to monitor corrosion protection. The present results suggest that the ERE_{Ag} can be used for electrochemical analysis, such as EIS.

The non-substrate test forces the current to flow through the substrate of epoxy Epoxy ERE_{Ag} / EE_{Pt} because there is no shared coating layer. Nogueira [31] studied electric field distribution between sensors for a continuous alkyd coating layer and found a majority of the current to flow through the substrate. Misczyck and Schauer [32] measured interlayer adhesion for an automotive basecoat / clearcoat systems assuming current flow along the interlayer. Allahar [33] later showed that an epoxy primer may be applicable to long term primer / metal interface monitoring whereas the alkyd system experiences current flow between the sensors once a critical level of coating saturation or degradation is reached. This suggests that embedded electrodes may be used to monitor total coating impedance in a two electrode, non-substrate set-up for epoxy coatings.

6.3.3. CPCP of Mg primer / AA 2024-T3 by means of ERE_{Ag}

6.3.3.1. Bare and 0% PVC coated experimental controls

EIS measurements demonstrate a controlled-potential technique in which the applied voltage perturbation is guided by the feedback of the ERE_{Ag}. This is analogous to the CPCP technique utilized for marine applications.

A control experiment is provided using a Ag/AgCl wire reference electrode suspended in solution. The resistance between the substrate and the wire Ag RE suspended

in solution is assumed negligible. A stable corrosion potential of -0.60 V vs ERE_{As} was recorded prior to the potentiostatic test. A polarization of -0.5 V vs OCP was applied for this examination for an applied surface potential of -1.1 V vs ERE_{Ag}. The experimental set-up is provided in Figure 6.8 (a) and (b) for the bare and coated AA 2024-T3 configurations, respectively

Figure 6.14 gives the current demand required for potentiostatic control of the bare AA 2024-T3. It is approximately 5 x 10^{-4} A. The initial values are slightly higher and the data is fit to an exponential curve. A subsequent test was performed for 18 hours and gave the same results with a current demand of 2 X 10^{-4} A at the end of the experiment.

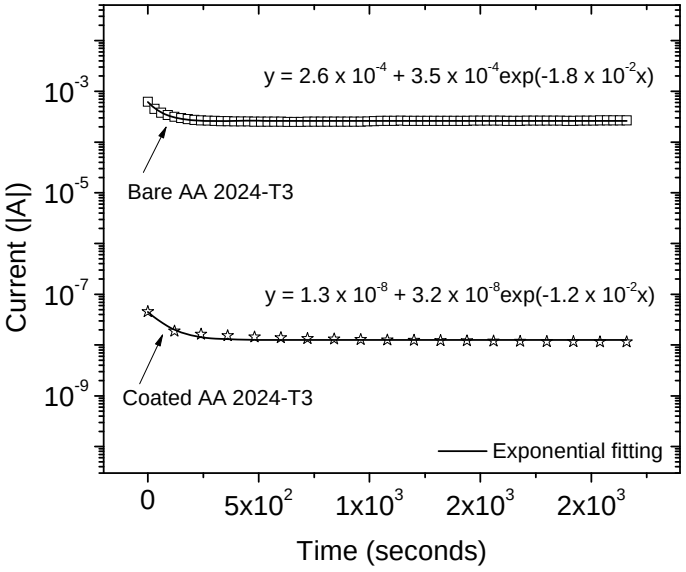

Figure 6.14. Potentiostatic polarization of coated and bare AA 2024-T3. The applied potential is -0.5 V vs OCP.

The second control experiment measured the current demand required for potentiostatic control of coated AA 2024 substrate. Sample epoxy ERE_{Ag} / EE_{Pt} was utilized and the results provided in Figure 6.14. The corrosion potential is -0.21 V vs EE_{Pt}

and -0.5 V vs OCP, -0.71 V vs EE_{Pt}, was applied for the forty minute test period. The current input was approximately 1 x 10^{-8} A. As with the bare AA 2024-T3, the initial values are slightly higher and an exponential curve is applied to the data. A subsequent test was performed for 18 hours and gave the same results with a current output of 0.5 x 10^{-8} A at the end of the test.

It is important to note that diffusion is not a significant factor in bare AA 2024-T3 experimental set-up. For a coated panel, however, diffusion of reduction reactants may be significant. The coated AA 2024-T3 experiment serves as a suitable control for the coated systems in the following analysis. It is assumed that the total area of available metal substrate reaction sites is similar for the coated AA 2024-T3 sample and the Mg primer / AA 2024-T3 samples explored in the following section.

6.3.3.2. Mg primer / AA 2024-T3

Previous potentiodynamic experimentation has shown the ERE_{Ag} to be robust under externally applied polarization as shown in Section 3.3.3 for -1.5 to 1.5 V vs OCP. Additionally, long-term corrosion potential monitoring results were favorable for the ERE_{Ag} in a Mg-rich / AA 2024-T3 coating system. Section 6.3.2 also represents the application of a controlled-potential method via ERE_{Ag}. The present analysis goes one step further to examine the ERE for controlled-potential of the AA 2024-T3 substrate in which the ERE_{Ag} provides feedback of the corrosion potential. The experimental set-up is provided in Figure 6.9, above.

The samples used in this experiment were 10% and 30% PVC. Mg-rich primers require PVCs in the range of 40-50% or higher to effectively provide cathodic protection for long service times. The Mg pigment loadings increase the overall conductivity of the

primer in the present experiment. Some cathodic protection is also expected, particularly for the 30% PVC coating system. A value of -0.95 V vs ERE_{Ag} was selected for the applied potential which is in agreement with marine aluminum alloy protection potentials [34].

Samples were exposed to ASTM B117 and removed regularly to apply the controlled-potential experiment. The surface area of substrate and ERE_{Ag} as well as the cylindrical glass cell attached were assumed to be equal for all coating samples. Therefore, the results have not been adjusted to show current density. The current required to polarize the substrate corrosion potential to -0.95 V vs ERE_{Ag} is the key variable of this experiment. Visual analysis of the coating surface aided in the interpretation of this data.

The current ranged from 10^{-9} to 10^{-3} A for the experimental results. At initial ASTM B117 exposure times, this current demand was low. However, this increased to 10^{-6} A or higher for many samples. The shift signifies a change to the coating system that draws this increased current, such as an increase in exposed substrate surface area. Closer examination of the corrosion potential indicates a possible correlation between corrosion potential and current input. These observations are examined in the subsequent sections.

6.3.3.2.1. Current versus test time

A potential of -0.95 V vs ERE_{Ag} was applied to coating systems presented here. Mixed results were obtained for the controlled-potential experiment. Figure 6.20 presents current versus test time for the coating sample with the most desired results. An exponential decay in current is observed for each experiment. The greatest change occurs over the first 3 hours of the controlled-potential test (left of dotted line). The current input is approximately 10^{-8} A at this point for the three curves and decreases to 0.5×10^{-8} A. This same result was obtained by the EE_{Pt} for the coated AA 2024-T3 control test in Section

6.3.3.1. This coating sample had no visual defects following the 537 hours of exposure to ASTM B117 and three controlled-potential tests. The PVC of the coating is 10%.

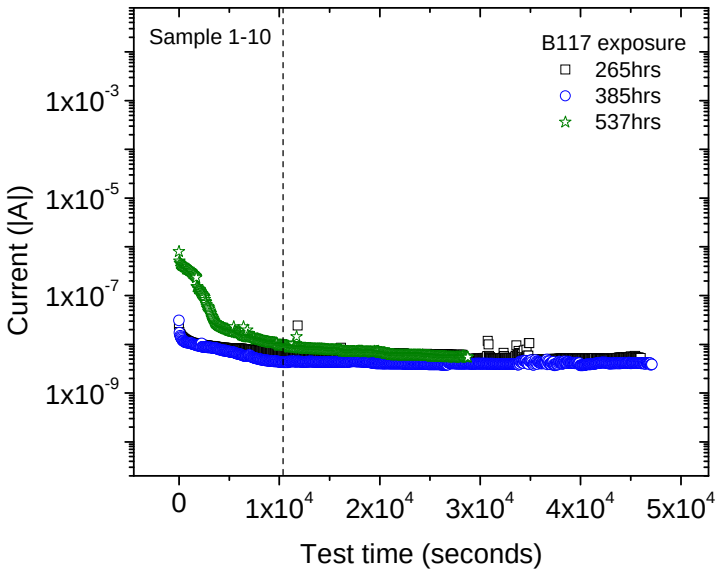

Figure 6.15. Current demand versus time at -0.95 V vs ERE_{Ag} for three B117 exposure times. Results shown for a sample with visual coating defects.

Figure 6.15 gives the current versus test time for all 10% and 30% PVC coating samples at total ASTM B117 exposure time equal to 537 and 324 hours, respectively. A broad range of current inputs are recorded for both sets. For the 10% PVC coating, results between 10^{-7} and 10^{-8} A result. This is in good agreement with the AA 2024-T3 coated control in Figure 6.14, above. The range for the 30% PVC samples is about one order of magnitude larger. This can be seen in the figure and is consistent with all other test results. A shaded region is placed on the figure to indicate the approximate regions which did not result in blistering.

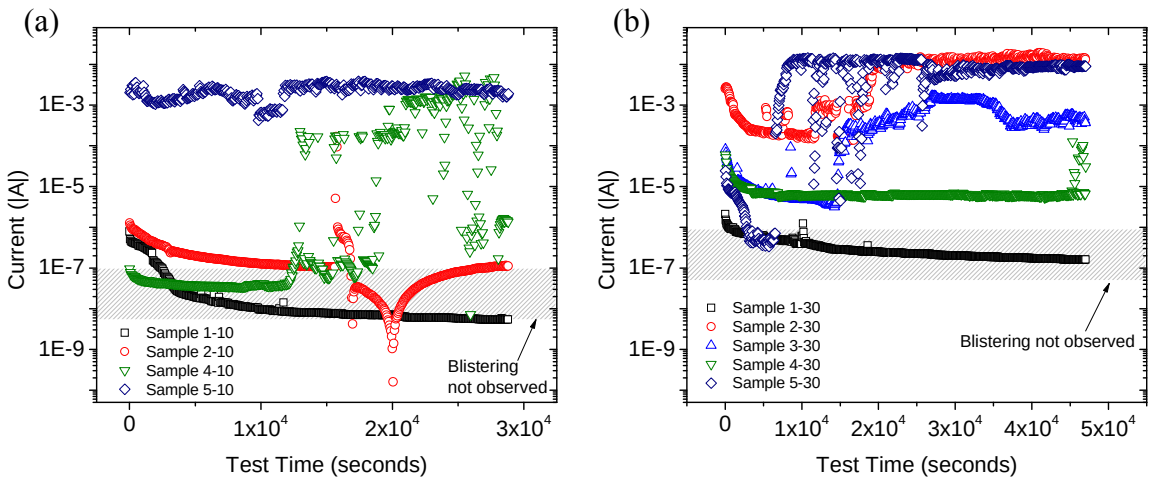

Figure 6.16. Current demand versus time at -0.95 V vs ERE_{Ag} for (a) 10% and (b) 30% PVC samples. The test length is 8 and 12 hours and B117 exposure is 537 and 324 hours, respectively.

The poor results are as large as 10^{-3} and 10^{-2} A for 10% and 30% PVC coatings, respectively. A characteristic difference between good and poor data is the precision of the data points. The poor data values are often scattered over a few orders of magnitude. In some cases, such as sample 4-10 in Figure 6.16 (a), the data is good, i.e., the current demand is small at the beginning of the experiment and deteriorates to large, wide-ranging currents as the test progresses.

The visual analysis for the 10% and 30% PVC coating samples support the previous discussion. Samples 5-10, 2-30, 3-30, 4-30, and 5-30 blistered as a result of the test applied in Figure 6.16. The blister area is directly related to the magnitude of the current. As the exposed metal surface area increases, the number of cathodic reaction sites, and therefore, the total current demand is increased [35]. For sample 2-30, much of surface area of the cylindrical cell was disbonded prior to the experiment. Additional disbondment occurred during the experiment. Photo-scans are shown in Figure 6.17 to give an example of blistering for both sample sets. The red circles represent the location of the cylindrical cell.

Blistering did not occur outside of the cell boundary. This experimental set-up for this is shown in Figure 6.9, above.

(a) (b)

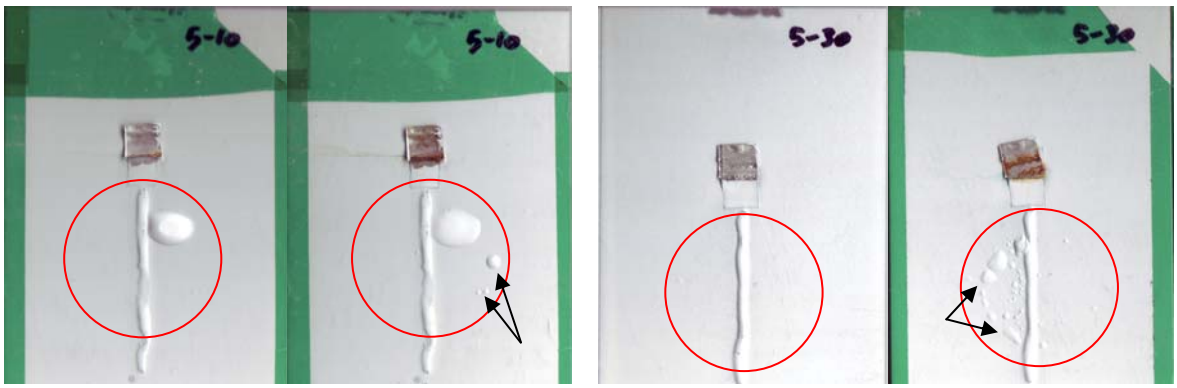

Figure 6.17. Photo-scans of the samples before and after polarization to -0.95 V vs ERE_{Ag} for (a) sample 5-10 and (b) sample 5-30.

The controlled-potential caused less blistering for the 10% than the 30% PVC coating samples. The 30% PVC experiments caused extensive blistering such as the numerous, large blisters to sample 5-30 following the initial 12 hour test. The visual analysis suggests that the large current input caused coating disbondment by high cathodic reaction rates. Disbondment may be caused by trapped H_2 gases, hydrolysis of interfacial bonds, or depolymerization [35-38]. The radial growth of the blisters suggest that H_2 evolution is the likely cause [39].

It is suggested that the Mg pigment is activated during the controlled-potential test because the substrate is polarized to a region of active metal oxidation for Mg. The result is over-polarization of the substrate. Rapid oxidation of the Mg pigments is coupled with an increase in cathodic reactions at the substrate. Hydrogen gas is produced at a rate greater than it is able to diffuse out of the coating. The pressure breaks the organic coating / metal adhesive bonds and forms a blister. Once blisters have developed within the coating, the total current required to polarize the exposed surface to -0.95 V vs ERE_{Ag} is significantly

larger as a result of increased resistance. This is consistent with the observations in Figure 6.16 and 6.17.

6.3.3.2.2. Correlation between current input and corrosion potential

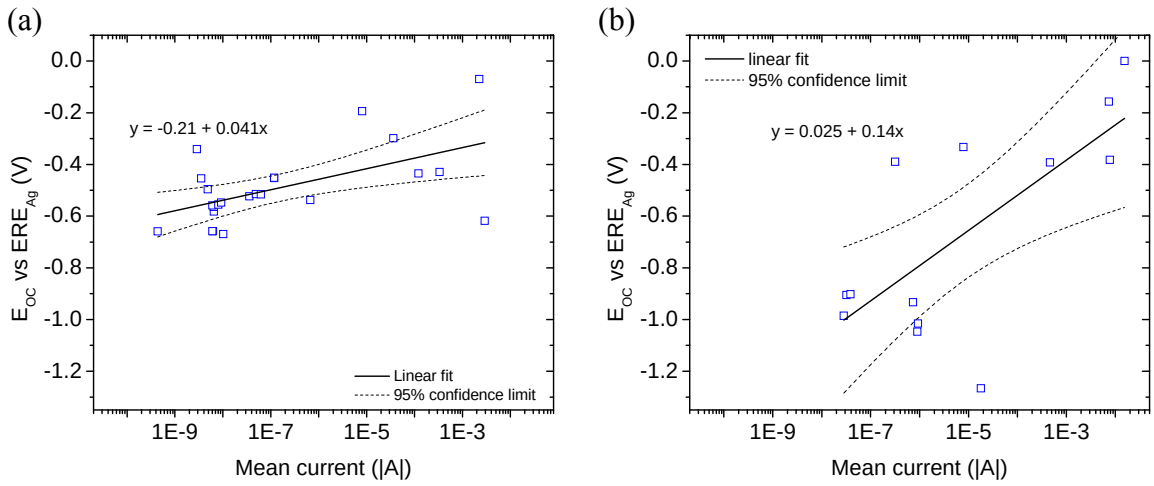

Figure 6.18. Corrosion potential versus mean current demand for all samples tested at all hours for (a) 10% and (b) 30% PVC.

Figure 6.18 gives the corrosion potential versus the mean current for all controlled-potential tests. This is an unperturbed measurement. The x-axis provides the mean current demand for the subsequent polarization of -0.95 V vs ERE_{Ag}. The 10% and 30% PVC coating systems are shown. Both coating systems experience an increase in mean current for more positive corrosion potentials. A linear fit is provided for the data to show this. It is also likely that the data can be qualified by one of two conditions: before blistering or after blistering. The data with low mean current (low, left-section of the graph) represents a coating which has not blistered, while higher mean currents and greater variability is observed after the coating has blistered (upper, right-hand section of the graph).

The corrosion potential for the 30% PVC coating system indicates cathodic protection at early exposure times. These are more negative than -0.9 V vs ERE_{Ag}. Exposure time is not provided by Figure 6.18.

Figure 6.18 suggests that cathodic overprotection caused blistering for the 30% PVC coating samples. The introduction for this chapter and Figure 6.1 illustrate the high hydrogen reduction rates that occur when a coated substrate is polarized outside of the narrow window for cathodic protection. Zhu et al. [35] correlated increased coating delamination with the magnitude of polarization due to increased demand for cathodic reactants. Water diffusion coefficients were derived from EIS data to substantiate this claim. Leidheiser [40] observed increased blistering with increased levels of cathodic protection. Blistering can be alleviated by reducing the Mg pigment or polarizing the substrate to a lower corrosion potential.

6.4. Conclusions

Experiments were conducted to examine the feasibility of applying CPCP to coated metals by embedded sensors. This is the first known application of a reference electrode, embedded within a coating system, to impose cathodic protection. AA 2024-T3 was used as the sample substrate in these experiments, and the objective was to polarize this to a designated electrochemical potential by means of the embedded sensors. The goal is to achieve long-term polarization for effective corrosion mitigation of the substrate. Such a system may reduce or eliminate the requirements for active pigments. Reduced Mg pigment concentrations are explored, subsequently, for the Mg primer / AA 2024-T3 sacrificial coating system.

Au and Pt wire EEs were examined as corrosion potential monitoring devices to demonstrate their feasibility as corrosion potential feedback sensors. They were then combined with the Ag wire EREs to serve as the working electrodes for non-substrate EIS analysis. The final experiment applies these embedded sensors for controlled-potential cathodic protection of coated AA 2024-T3.

A continuous experiment would apply the controlled-potential at all times. Realistically, current is applied to reach the desired polarization followed by a rest period of seconds, minutes, or possibly hours. A period of 2 minutes was used in the experiments shown here. The results have shown that once a material is polarized, the current requirement to maintain this polarization is often small. The goal is to determine a period which effectively polarizes the material but with the minimal energy or current input. For the set-up used in this experiment, larger periods could be explored to examine the effect on current input.

6.5. References

[1] S. Egusay and N. Iwasawaz, Piezoelectric paints as one approach to smart structural materials with health-monitoring capabilities, Smart Materials and Structures, 7 (1998) 438-445.
[2] G. Park, H.H. Cudney and D.J. Inman, Impedance-based health monitoring of civil structural components, Journal of infrastructure systems, (2000) 153-160.
[3] C. Boller, Ways and options for aircraft structural health management, Smart Materials and Structures, 10 (2001) 432–440.
[4] H. Murayama, K. Kageyama, T. Kamita and H. Igawa, Structural health monitoring of a full-scale composite structure with fiber-optic sensors, Advance Composite Materials, 11 (2003) 287–297.
[5] Health Monitoring of Aerospace Structures - Smart Sensor Technologies and Signal Processing, John Wiley & Sons, Ltd, Munich, Germany, 2004.
[6] X.P. Qing, S.J. Beard, A. Kumar, T.K. Ooi and F.-K. Chang, Built-in sensor network for structural health monitoring of composite structure, Journal of Intelligent Materials and Structures, 18 (2007) 39-49.
[7] J.B. Ong, Z. You, J. Mills-Beale, E.L. Tan, B.D. Pereles and K.G. Ong, A wireless, passive embedded sensor for real-time monitoring of water content in civil engineering materials, IEEE Sensors Journal, 8 (2008) 2053-2058.

[8] V. Giurgiutiu, Structural Health Monitoring with Piezoelectric Wafer Active Sensors, Academic Press, Burlington, MA, 2008.
[9] F. Rajabipour and J. Weiss, Parameters affecting the measurements of embedded electrical sensors for concrete health monitoring applications, in: J.S. Popovics (Ed.) Health monitoring systems and sensors for assessing concrete, Curran Associates, Inc., Los Angeles, CA, 2008, pp. 7-22.
[10] I.S. Cole, P.A. Corrigan, G.C. Edwards, D. Followell, S. Galea, W. Ganther, B.R. Hinton, T. Ho, C.J. Lewis, T.H. Muster, D. Paterson, D.C. Price, D.A. Scott and P. Trathen, A sensor-based learning approach to prognostics in intelligent vehicle health monitoring, Materials Forum, 33 (2009) 27-35.
[11] Y. Yu, G. Qiao and J. Ou, Self-powered wireless corrosion monitoring sensors and networks, IEEE Sensors Journal, 10 (2010) 1901-1902.
[12] K. Diamanti and C. Soutis, Structural health monitoring techniques for aircraft composite structures, Progress in Aerospace Sciences, 46 (2010) 342–352.
[13] M.H. Parsa, S.R. Allahkaram and A.H. Ghobadi, Simulation of cathodic protection potential distributions on oil well casings, Journal of Petroleum Science and Engineering, 72 (2010) 215–219.
[14] D.A. Jones, Principles and Prevention of Corrosion, 2nd ed., Prentice Hall, Upper Saddle River, NJ, 1996.
[15] U.R. Evans, The Corrosion and Oxidation of Metals: Scientific Principles and Practical Applications, St. Martin's Press, New York, 1960.
[16] Cathodic protection of pipeline, in: Metallurgy & Material Engineering pp. Retrieved November 20, 2011 from http://met-engineering.blogspot.com/2009/2010/cathodic-protection-of-pipeline_2007.html.
[17] Q.L. Thu, G. Bonnet, C. Compere, H.L. Trong and S. Touzain, Modified wire beam electrode: A useful tool to evaluate compatibility between organic coatings and cathodic protection, Progress in Organic Coatings, 52 (2005) 118–125.
[18] M.C. Yan, J.Q. Wang, E.H. Han and W. Ke, Electrochemical measurements using combination microelectrode in crevice simulating disbonded of pipeline coatings under cathodic protection, Corrosion Engineering, Science and Technology, 42 (2007) 42-49.
[19] F.M. Song, Predicting the effect of soil seasonal change on stress corrosion cracking susceptibility of buried pipelines at high pH, Corrosion, 66 (2010) 1-14.
[20] Piping corrosion and corrosion protection, in, pp. Retrieved from November 20, 2011 from www.pipingguide.net/2010_2004_2001_archive.html.
[21] B.E. Merten, D. Battocchi, D.E. Tallman and G.P. Bierwagen, Embedded reference electrode for potential-monitoring of cathodic protective systems, Journal of the Electrochemical Society, 157 (2010) C244-C247.
[22] M.E. Nanna and G.P. Bierwagen, Mg-rich coatings: a new paradigm for Cr-free corrosion protection of Al aerospace alloys, Journal of Coatings Technology Research, 1 (2004) 69-80.
[23] D. Battocchi, A.M. Simoes, D.E. Tallman and G.P. Bierwagen, Electrochemical behaviour of a Mg-rich primer in the protection of Al alloys, Corrosion Science, 48 (2006) 1292–1306.
[24] D. Battocchi, A.M. Simoes, D.E. Tallman and G.P. Bierwagen, Comparison of testing solutions on the protection of Al-alloys using a Mg-rich primer, Corrosion Science, 48 (2006) 2226–2240.

[25] K.B. Oldham and J.C. Myland, Fundamentals of Electrochemical Science, Academic Principles, Inc., San Diego, CA, 1994.
[26] J. Kittel, N. Celati, M. Keddam and H. Takenouti, Influence of the coating–substrate interactions on the corrosion protection: characterisation by impedance spectroscopy of the inner and outer parts of a coating, Progress in Organic Coatings, 46 (2003) 135–147.
[27] J.N. Murray, Electrochemical test methods for evaluating organic coatings on metals: an update. Part II: single test parameter measurements, Progress in Organic Coatings, 31 (1997) 255–264.
[28] D. Loveday, P. Peterson and B. Rodgers, Evaluation of organic coatings with electrochemical Impedance Spectroscopy Part 1: Fundamentals of electrochemical impedance spectroscopy, in: JCT Coatings Tech, www.coatingstech.org, 2004, pp. 46-52.
[29] J. Kittel, N. Celati, M. Keddam and H. Takenouti, New methods for the study of organic coatings by EIS - New insights into attached and free films, Progress in Organic Coatings, 41 (2001) 93–98.
[30] C.S. Brossia and D.S. Dunn, Apparatus and method for detecting the degradation of a coating using embedded sensors, in: U.S.P. Office (Ed.) U.S. Patent 6,911,828 B1, 2005.
[31] A. Nogueira, X.R. Novoa and C. Perez, On the possibility of using embedded electrodes for the measurement of dielectric properties in organic coatings, Progress in Organic Coatings, 59 (2007) 186–191.
[32] A. Miszczyk and T. Schauer, Electrochemical approach to evaluate the interlayer adhesion of organic coatings, Progress in Organic Coatings, 52 (2005) 298–305.
[33] K. Allahar, Q. Su and G. Bierwagen, Non-substrate EIS monitoring of organic coatings with embedded electrodes, Progress in Organic Coatings, 67 (2010) 180–187.
[34] J. Zhang, K. Sun, X. Huang, J. Yin and S. Peng, Cathodic protection of aluminum hull ship, Chinese Journal of Oceanology and Limnology, 8 (1990) 257-262.
[35] C. Zhu, R. Xie, J. Xue and L. Song, Studies of the impedance models and water transport behaviors of cathodically polarized coating, Electrochimica Acta, 56 (2011) 5828–5835.
[36] H. Leidheiser Jr, W. Wang and L. Igetoft, The mechanism for the cathodic delamination of organic coatings from a metal surface, Progress in Organic Coatings, 11 (1983) 19-40.
[37] J.I. Skar and U. Steinsmo, Cathodic disbonding of paint films-transport of charge, Corrosion Science, 35 (1993) 1385-1389.
[38] P.A. Sørensen, K. Dam-Johansen, C.E. Weinell and S. Kiil, Cathodic delamination: Quantification of ionic transport rates along coating-steel interfaces, Progress in Organic Coatings, 67 (2010) 107-115.
[39] J. Leidheiser, Henry, A. Vertes, J.E. Roberts and R. Turoscy, Polymer/metal and polymer/ion interactions in protective coatings Hyperfine Interactions, 57 (1990) 1955-1962.
[40] H. Leidheiser and W. Wang, Some substrate and environmental influences on the cathodic delamination of organic coatings, Journal of Coatings Technology, 53 (1981) 77-84.

CHAPTER 7. CONCLUSIONS AND IMPACT OF THE ERE

A thin wire Ag/AgCl reference electrode was prepared using 25 μm as well as 50 μm Ag wire. A chemical oxidation method was applied using dilute $FeCl_3$. Two solution concentrations and two immersion times were explored in a preliminary experiment. SEM and EDX confirmed that a thin, 1 to 2 μm AgCl deposition formed on the Ag wire reference electrodes. The analysis showed superior results for 50 μm wires prepared by 30 second immersion in 0.1M $FeCl_3$. This method was adopted for much of the results provided here.

It was demonstrated that the wire reference electrodes could be embedded within two sacrificial coating systems to monitor their corrosion potential. This is the first report of a reference electrode which is embedded between organic coating layers for corrosion potential monitoring of the substrate health.

The ERE successfully monitored a Mg primer / AA 2024-T3 coating system for more than 600 days of exposure to constant immersion with DHS solution [1]. The interpretation of corrosion potential data was improved through the use of statistical analysis. Data more positive than -0.2 V vs ERE was omitted from the final presentation of the results. It is reported here that corrosion potentials recorded by an ERE are 0.1 to 0.2 V more positive than a standard SCE in solution. There is some indication that the ERE could be utilized as a coating $[Cl^-]$ sensor. The use of this electrode as a $[Cl^-]$ sensor for pipeline and concrete structures is reported [2-9].

A Zn primer / steel coating system was prepared with an ERE for corrosion potential monitoring. The amount of scatter was significantly larger than the Mg primer /

AA 2024-T3. A large percentage of unrealistic measurements were recorded. To test this the Mg-rich coating was formulated with nominal concentrations of Zn pigment and coated onto AA 2024-T3. The results seem to indicate that Zn disrupts the measurement by means of a short circuit. This is in part due to the Zn oxidation products and by-products, which are less dense than metallic Zn and much more conductive than Mg corrosion products. ERE corrosion potentials are 0.2 to 0.3 V more positive than a standard SCE in solution, although a larger data set is required to improve the confidence of these results.

The corrosion potential of Mg primer / AA 2024-T3 and Zn primer / steel was also monitored from within a B117 salt spray cabinet. This is the first report of *in-situ* corrosion potential measurements for a salt spray cabinet by a reference electrode embedded between the primer and topcoat.

The ERE was used for corrosion potential measurements in primers of varying thickness. There is some indication that thicker primer may undergo a longer cathodic protection activation period. Further development in this area may prove that the ERE is useful for obtaining corrosion potential information which is not possible by a conventional reference electrode exterior to the coating.

Potentiodynamic experiments showed that the ERE is very stable under applied potentials for the range of approximately -1.5 to 1.5 V vs SCE. This indicates that the ERE may be useful for corrosion potential feedback of impressed current cathodic protection (ICCP) or controlled potential cathodic protection (CPCP). Subsequently, the ERE was utilized to control for polarization experiments, intended to replicate CPCP applications. The polarization was achieved on coated AA 2024-T3 using a polarization of -0.95 V vs ERE [10]. Over-polarization, a common challenge for ICCP and CPCP [11-16], caused

blistering in many samples. A polarization of -0.75 or -0.85 V vs ERE may eliminate this effect by reducing the rates of hydrogen evolution. This is the first reported attempt for the cathodic polarization of an organic coatings system by a reference electrode, embedded between coating layers.

The ERE was utilized for the electrochemical analysis of a novel sacrificial coating system. This experiment provides a large amount of ERE data for coating systems with wide-ranging corrosion protection performance as well as protection mechanisms. The measurements included corrosion potential, low frequency impedance by electrochemical impedance spectroscopy (EIS), and noise resistance by the electrochemical noise method (ENM). Realistic and reproducible results were presented. Coating performance ranking by ERE was equivalent to characterization by standard SCE as well as visual analysis. This is the first report of a reference electrode, embedded within an organic coating system, utilized for the research and development new coating systems by common electrochemical techniques. ERE and saturated calomel electrode (SCE) standard configurations are fundamentally not equivalent and in some cases ERE trends were quite different from the SCE results. No standards exist for electrochemical characterizations from within a coating system; therefore, the data set requires further interpretation. Related reports have utilized inert materials as an embedded electrode for electrochemical characterization of organic coatings [17-28]. Corrosion potential results, measured by Au and Pt wire embedded electrodes (EE), are included in the present findings for comparison.

The novel coating system was also monitored by standard techniques, using a SCE and Pt mesh as reference and counter electrodes, respectively. Mixtures of lithium carbonate, magnesium nitrate, and Mg metal particulates were shown to provide corrosion

inhibition and cathodic protection for AA 2024-T3. To the knowledge of the author, this is the first experimentation with this combination of materials for corrosion protective coatings. Results of electrochemical characterization by EIS and ENM as well as visual analysis showed that these coatings maintained anti-corrosion and anti-blistering effects to a greater extent than a Mg-rich primer control following 1600 hours of exposure to B117 salt spray. The coatings were formulated a Mg pigment volume concentrations (PVC) less than 20. The results showed a short burst of cathodic protection at initial exposure times for Mg PVC as low as 6%. The results seem to suggest that both lithium carbonate and magnesium nitrate are necessary to observe this. Continued optimization of the proposed primer formulations offers the opportunity to design and implement unique cathodic protection plus corrosion inhibitor coating systems for use on aluminum.

When applied carefully, the Ag wire ERE presented here can be utilized for applications ranging from the characterization and ranking of experimental coating formulations coated on metal substrates to corrosion potential feedback for ICCP or CPCP. There is some indication that the latter has the potential for the ERE to control the polarization for a substrate plus organic coating system. Electrochemical characterization techniques which can be measured by means of the ERE include corrosion potential, EIS, and ENM. It is likely that potentiodynamic polarization measurements are possible, but results have not been shown here. Multiple replicates are suggested because the accuracy for these measurements, especially EIS, is likely sub-par compared common electrochemical techniques. When comparing ERE data to standard measurements by SCE or another reference electrode, it is important to remember that the two techniques use distinct experimental configurations. Therefore, they cannot be directly compared.

7.1. References

[1] B.E. Merten, D. Battocchi, D.E. Tallman and G.P. Bierwagen, Embedded reference electrode for potential-monitoring of cathodic protective systems, Journal of the Electrochemical Society, 157 (2010) C244-C247.
[2] G.S. Duffó and S.B. Farina, Development of an embeddable sensor to monitor the corrosion process of new and existing reinforced concrete structures, Construction and Building Materials, 23 (2009) 2746–2751.
[3] G.S. Duffó, S.B. Farina and C.M. Giordano, Characterization of solid embeddable reference electrodes for corrosion monitoring in reinforced concrete structures, Electrochimica Acta, 54 (2009) 1010-1020.
[4] R.-G. Du, R.-G. Hu, R.-S. Huang and C.-J. Lin, In situ measurement of Cl^- concentrations and pH at the reinforcing steel/concrete interface by combination sensors, Analytical Chemistry, 78 (2006) 3179-3185.
[5] M.A. Climent-Llorca, E. Viqueira-Pérez and M.M. López-Atalaya, Embeddable Ag/AgCl sensor for in-situ monitoring chloride contents in concrete, Cement and Concrete Research, 26 (1996) 1157-I 1161.
[6] M.F. Montemor, J.H. Alves, A.M. Simoes, J.C.S. Fernandes, Z. Lourenco, A.J.S. Costa, A.J. Appleton and M.G.S. Ferreira, Multiprobe chloride sensor for in situ monitoring of reinforced concrete structures, Cement & Concrete Composites, 28 (2006) 233–236.
[7] C.P. Atkins, J.D. Scantlebury, P.J. Nedwell and S.P. Blatch, Monitoring chloride concentrations in hardened cement pastes using ion selective electrodes, Cement and Concrete Research, 26 (1996) 319-324.
[8] C.P. Atkins, M.A. Carter and J.D. Scantlebury, Sources of error in using silver/silver chloride electrodes to monitor chloride activity in concrete, Cement and Concrete Research, 31 (2001) 1207– 1211.
[9] F.M. Song, S. Brossia, D. Dunn and N. Sridhar, New permanent reference electrode for protection of underground pipelines and storage tanks, Corrosion Engineering, Science and Technology, 40 (2005) 262-269.
[10] J. Zhang, K. Sun, X. Huang, J. Yin and S. Peng, Cathodic protection of aluminum hull ship, Chinese Journal of Oceanology and Limnology, 8 (1990) 257-262.
[11] C. Zhu, R. Xie, J. Xue and L. Song, Studies of the impedance models and water transport behaviors of cathodically polarized coating, Electrochimica Acta, 56 (2011) 5828–5835.
[12] H. Leidheiser Jr, W. Wang and L. Igetoft, The mechanism for the cathodic delamination of organic coatings from a metal surface, Progress in Organic Coatings, 11 (1983) 19-40.
[13] J.I. Skar and U. Steinsmo, Cathodic disbonding of paint films-transport of charge, Corrosion Science, 35 (1993) 1385-1389.
[14] P.A. Sørensen, K. Dam-Johansen, C.E. Weinell and S. Kiil, Cathodic delamination: Quantification of ionic transport rates along coating-steel interfaces, Progress in Organic Coatings, 67 (2010) 107-115.
[15] J. Leidheiser, Henry, A. Vertes, J.E. Roberts and R. Turoscy, Polymer/metal and polymer/ion interactions in protective coatings Hyperfine Interactions, 57 (1990) 1955-1962.

[16] H. Leidheiser and W. Wang, Some substrate and environmental influences on the cathodic delamination of organic coatings, Journal of Coatings Technology, 53 (1981) 77-84.
[17] J. Kittel, N. Celati, M. Keddam and H. Takenouti, New methods for the study of organic coatings by EIS - New insights into attached and free films, Progress in Organic Coatings, 41 (2001) 93–98.
[18] J. Kittel, N. Celati, M. Keddam and H. Takenouti, Influence of the coating–substrate interactions on the corrosion protection: characterisation by impedance spectroscopy of the inner and outer parts of a coating, Progress in Organic Coatings, 46 (2003) 135–147.
[19] A. Miszczyk and T. Schauer, Electrochemical approach to evaluate the interlayer adhesion of organic coatings, Progress in Organic Coatings, 52 (2005) 298–305.
[20] A. Nogueira, X.R. Novoa and C. Perez, On the possibility of using embedded electrodes for the measurement of dielectric properties in organic coatings, Progress in Organic Coatings, 59 (2007) 186–191.
[21] K. Allahar, Q. Su and G. Bierwagen, Non-substrate EIS monitoring of organic coatings with embedded electrodes, Progress in Organic Coatings, 67 (2010) 180–187.
[22] Q. Su, The application of embedded sensors for in-situ monitoring of protective coatings on metal substrates, in: Coatings and Polymeric Materials, North Dakota State University, Fargo, ND, 2008, pp. 259.
[23] K.N. Allahar, Q. Su, G.P. Bierwagen, D. Battocchi, V.J. Gelling and D. Tallman, Examination of the feasibility of the use of in-situ corrosion sensors in army vehicles, in: Tri-Service Corrosion Conference, 2005, pp. 1-11.
[24] K.N. Allahar, Q. Su, G.P. Bierwagen and D.-H. Lee, Monitoring of the AC-DC-AC degradation of organic coatings using embedded electrodes, Corrosion, 64 (2008) 773-787.
[25] K.N. Allahar, V. Upadhyay, G.P. Bierwagen and V.J. Gelling, Monitoring of a military vehicle coating under Prohesion exposure by embedded sensors, Progress in Organic Coatings, 65 (2009) 142–151.
[26] K.N. Allahar, Q. Su and G.P. Bierwagen, Electrochemical noise monitoring of the cathodic protection of Mg-rich primers, Corrosion, 66 (2010) 1-12.
[27] K.N. Allahar, B.R. Hinderliter, D.E. Tallman and G.P. Bierwagen, Water transport in multilayer organic coatings, Journal of the Electrochemical Society, 155 (2008) F201-F208.
[28] G.P. Bierwagen, K.N. Allahar, Q. Su and V.J. Gelling, Electrochemically characterizing the ac–dc–ac accelerated test method using embedded electrodes, Corrosion Science, 51 (2008) 95–101.

CHAPTER 8. FUTURE WORK

The ERE presents numerous opportunities for further development of the technique. These range from develop standard characterization techniques for research and develop to the implementation of controlled potential cathodic protection (CPCP) to various forms of structural health monitoring.

Corrosion potentials are the easiest electrochemical characterization method which can be performed. However, its use is not widespread. Murray [1] suggests many possible uses for this measurement. For instance, the breakpoint has been suggested to correlate to corrosion processes which are diffusion controlled. The breakpoint can be determine by using a log (time) plot for corrosion potentials. Based on the results ERE for electrochemical characterizations in Chapter 5, future work could be performed to determine if diffusion control is measured by the ERE.

The ERE can be classified as a microelectrode. Therefore, these measurements give novel electrochemical characterization of local electrochemistry within a coated metal system which could not be measured the standard global techniques. The wire beam electrode (WBE) is also used for local characterization [2-4]. The combination of the WBE with the electrochemical noise method (ENM) was recently reported by Tan [5]. A potential exists for a unique characterization method for combination of these techniques with the ERE.

The novel lithium carbonate, magnesium nitrate, and Mg metal primer presented here deserves further experimentation. Reports by Varma [6] and Visser and Hayes [7]

were combined to develop the idea for this primer system for AA 2024-T3. The results suggest multiple anti-corrosion mechanisms combine to provide long-lasting protection.

8.1. References

[1] J.N. Murray, Electrochemical test methods for evaluating organic coatings on metals: an update. Part II: single test parameter measurements, Progress in Organic Coatings, 31 (1997) 255–264.
[2] Y. Tan, Monitoring localized corrosion processes and estimating localized corrosion rates using a wire-beam electrode, Corrosion, 54 (1998) 403-413.
[3] J. Orozco, C. Fernández-Sánchez and C. Jiménez-Jorquera, Ultramicroelectrode array based sensors: A promising analytical tool for environmental monitoring, Sensors, 10 (2010) 475-490.
[4] Q.L. Thu, G. Bonnet, C. Compere, H.L. Trong and S. Touzain, Modified wire beam electrode: A useful tool to evaluate compatibility between organic coatings and cathodic protection, Progress in Organic Coatings, 52 (2005) 118–125.
[5] Y. Tan, Sensing localised corrosion by means of electrochemical noise detection and analysis, Sensors and Actuators B, 139 (2009) 688–698.
[6] P.C.R. Varma, B. Duffy and J. Cassidy, Influence of magnesium nitrate on the corrosion performance of sol-gel coated AA2024-T3 aluminium alloy, Surface & Coatings Technology, 204 (2009) 277-284.
[7] P. Visser and S.A. Hayes, Anti-corrosive coating composition, in: W.I.P. Organization (Ed.) WO 2010/112605 A1, 2010.